VNIVERSIDAD NACIONAL
AVTÓNOMA DE
MEXICO

UNIVERSIDAD NACIONAL AUTÓNOMA DE MÉXICO

PROGRAMA DE MAESTRÍA Y DOCTORADO EN INGENIERÍA

Modelos Dinámicos de Orden Fraccional Para la Simulación de Reactores

Fractional Order Dynamic Models for Reactors Simulation

T E S I S

QUE PARA OPTAR POR EL GRADO DE:

MAESTRO EN INGENIERÍA

ENERGÍA – SISTEMAS ENERGÉTICOS

P R E S E N T A :

MARCO ANTONIO POLO LABARRIOS

DIRECTORA:
DRA. CECILIA MARTÍN DEL CAMPO MÁRQUEZ

2012

JURADO ASIGNADO

Presidente: Dra. Martín Del Campo Márquez Cecilia

Secretario: Dr. Nuñez Carrera Alejandro

Vocal: Dr. Reinking Cejudo Arturo Guillermo

1er. Suplente: Dr. Chávez Mercado Carlos

2do. Suplente: Dr. Vázquez Rodríguez Rodolfo

Lugar o lugares donde se realizó la tesis:

UNIVERSIDAD NACIONAL AUTÓNOMA DE MÉXICO

TUTOR DE TESIS:

Cecilia Martín del Campo Márquez

_____

Angelita

Yaretzi

A la memoria de Lupita

AGRADECIMIENTOS

Agradezco el financiamiento otorgado por el Consejo Nacional de Ciencia y Tecnología (CONACYT). Al mismo tiempo, le estoy agradecido a mi asesora, la Dra. Cecilia Martín Del Campo Márquez, por haber aceptado colaborar conmigo en este trabajo.

Aprecio sinceramente las revisiones de la versión preliminar del trabajo que muy amablemente hicieron los doctores Alejandro Nuñez Carrera, Arturo G. Reinking Cejudo, Carlos Chávez Mercado y Rodolfo Vázquez Rodríguez, quienes además me permitieron visitarlos y me propusieron importantes mejoras en aspectos específicos del trabajo.

En particular, deseo expresar mi sincero agradecimiento al doctor Gilberto Espinosa-Paredes, no sólo por sus valiosas correcciones y recomendaciones, sino también por su amable disponibilidad para platicar conmigo sobre una gran variedad de temas en todo momento, lo cual me ayudó y motivó considerablemente a mejorar el trabajo. Asimismo, deseo agradecer al profesor Alejandro Vázquez-Rodríguez, quien aportó importantes comentarios y sugerencias al trabajo durante las diversas etapas de evaluación. También a mi hermano Saúl y mi amigo Erick con quienes he convivido todo este tiempo.

Como siempre, estoy eternamente agradecido con mi esposa Angela, mis padres Marco y María, mi hermano Cesar y su esposa Isela. Y con todas las personas que, en un momento u otro, han creído en mí. Lo último que me resta es manifestar que ha sido un honor y un placer llevar a cabo este trabajo.

Resumen

Tanto en el mundo natural como en el de la ciencia y en la tecnología el fenómeno de la difusión está presente en una gran cantidad de eventos. Para describir los procesos neutrónicos en sistemas nucleares se emplean teorías tan complejas como la teoría del transporte o teoría de difusión de neutrones, ambas descritas en el espacio y tiempo. Este tipo de aproximaciones son aplicadas para el diseño de reactores nucleares comerciales (ej. BWR, PWR, CANDU, etc.). Donde el detalle de la distribución neutrónica en espacio es fundamental para establecer la estrategia del quemado del combustible nuclear y realizar los análisis de transitorios e inestabilidades. No obstante, el reactor nuclear ha sido diseñado aplicando el modelo puntual de la cinética neutrónica, donde los fenómenos fundamentales de fisión, captura, dispersión, escape, en los componentes del núcleo del reactor como son la fuente, el combustible, elementos de control, etc., son aglutinados en dos términos relacionados con neutrones inmediatos y neutrones retardados debido a la concentración de los precursores. No obstante, la teoría de cinética puntual es tan simplificada que los efectos espaciales temporales no son del todo descritos de manera exacta, por lo cual se requiere hacer estudios de la dinámica de los procesos neutrónicos.

El motivo de este trabajo es mejorar las predicciones del modelo de difusión mediante la modificación de las leyes constitutivas, de tal manera que se permita ampliar el alcance y mejorar la teoría de difusión clásica. Respecto al alcance, puede describirse la evolución de un transitorio de neutrones en un reactor nuclear con una configuración altamente heterogénea, debida a la presencia de elementos fuertemente absorvedores de neutrones como las barras de control. Con el fin de mejorar la teoría de la difusión clásica, se hace la suposición de que el modelo de orden fraccional para la difusión de neutrones puede mejorar las predicciones y en algunos casos debe ser similar a la teoría de transporte.

Con estas ideas, Espinosa–Paredes et al. (2011) obtuvo un modelo reducido de la cinética de neutrones, el cual es un modelo de ecuaciones de la cinética neutrónica de orden fraccional (ECNF) de un reactor puntual. Este modelo fue empleado para la simulación del arranque de un

reactor del tipo PWR para dos casos de inserción de reactividad: 1) inserción de reactividad en pasos; 2) inserción de reactividad en rampa.

Este trabajo está estructurado de la siguiente manera: en el Capitulo 1 se presenta la introducción en la cual se establecen los antecedentes de difusión así como los antecedentes históricos del cálculo fraccional y los conceptos básicos de éste, también se presenta la forma generalizada de la ecuaciones diferenciales ordinarias y parciales para finalizar con los conceptos básicos de la difusión clásica y anómala. En el Capitulo 2 se presenta la teoría de la ecuación de Boltzmann o ecuación de transporte lineal así como la aproximación a la ecuación de difusión clásica, también se presentan las modificaciones realizadas a la ecuación de Fick, las cuales permiten describir los fenómenos de transporte anómalo. En el Capitulo 3 se presenta el desarrollo una nueva aproximación de la solución de la ecuación de Boltzmann dependiente del tiempo para un medio general, también se presenta el análisis de sensibilidad e incertidumbre del exponente de difusión anómala sobre el comportamiento del flujo neutrónico. Finalmente en el Capitulo 4 se presenta la simulación del arranque de un reactor del tipo PWR para los dos casos de inserción de reactividad: inserción de reactividad en pasos e inserción de reactividad en rampa, donde se utiliza el modelo de la ECNF.

Los resultados de este trabajo muestran que en los sistemas altamente heterogéneos así como en medios puramente absorbentes existen procesos sub-difusivos. El modelo desarrollado en el Capitulo 3 indica que el transporte de partículas o neutrones se lleva a cabo con una velocidad fraccional de la onda (adimensional) igual a $a_\gamma^* = 1/3^{\gamma/2}$, donde $a_\gamma = a_\gamma^* \sqrt{\upsilon^{1+\gamma} / D^{\gamma-1}}$ fue aplicada. De acuerdo con esta ecuación $a_\gamma^* = 1/\sqrt{3}$ cuando $\gamma = 1$, la cual corresponde a la velocidad obtenida con la ecuación del telegrafista hiperbólica. Entonces, más allá de su significado físico, se puede considerar como un parámetro de corrección para la predicción de la velocidad correcta para $c = 0$.

Abstract

In nature just as in science, the diffusion phenomenon is present in a variety of events. In order to describe the neutronic processes in nuclear systems, complex theories are employed such as transport theory or neutron diffusion theory; both are described in space and time. These kinds of approximations are applied for the design of commercial nuclear reactors (e.g. BWR, PWR, CANDU, among others), where the neutronic distribution detail in space is fundamental in order to establish the burn-up strategy of the nuclear fuel and to perform the transitory and instability analyses. However, nuclear reactors have been designed applying the neutron point kinetics model, where the phenomenon of fission, capture, dispersion and escape in the nuclear core components such as the source, fuel, and control elements, among others are agglutinated in two related terms with immediate neutrons and delayed neutrons due to the concentration of the precursors. Although, the point kinetic theory is so simplified that the spatial effect are not described.

The aim of this work is to improve the diffusion model predictions by modification of the constitutive laws, in order to extend and improve the classic diffusion theory. Regarding the extend, a neutron transitory evolution can be described in a nuclear reactor with a highly heterogeneous configuration, due to the presence of highly absorbing elements such as the control rods. In order to improve the classical diffusion theory, the supposition that the neutron diffusion fractional order model can improve the predictions and in some cases it must be similar to the transport theory.

With these ideas Espinosa–Paredes et al. (2011) obtained a reduced neutron kinetics model, which is an equations model of the neutron kinetics of fractional order (ECNF) of a point reactor. This model was employed for the simulation of a PWR start-up reactor for two cases of reactivity insertion: 1) reactivity insertion in steps; 2) reactivity insertion in ramp.

This work is structured as follows: chapter 1 presents the introduction and establishes the background of diffusion such as the historic background of the fractional calculus and its basic

concepts, also the generalized form of the ordinary differential and partial equations are presented. Chapter 2 presents the theory of the Boltzmann equation or lineal transport equation, also the classical diffusion equation approximation and the modifications performed by the Fick's equation, which allow describing the phenomena of anomalous transport. Chapter 3 presents the development of a new approximation of the solution of the Boltzmann equation, which depends on time for a general medium, also the sensibility and uncertainty analysis of the anomalous diffusion exponent on the neutronic flux behavior. Finally, chapter 4 presents the simulation of a PWR start-up for the two reactivity insertion cases: reactivity insertion in steps and reactivity insertion in ramp, where the ECNF model is used.

The results of this work show that in highly heterogeneous systems and in purely absorbent mediums, sub-diffusive processes are present. The model developed in chapter 3 shows that particle or neutron transport is performed at a wave fractional velocity (dimensionless) equal to $a_\gamma^* = 1/3^{\gamma/2}$, where $a_\gamma = a_\gamma^* \sqrt{\upsilon^{1+\gamma} / D^{\gamma-1}}$ was applied. According to this equation $a_\gamma^* = 1/\sqrt{3}$ when $\gamma = 1$, which corresponds to the obtained velocity with the hyperbolic telegrapher equation. Therefore, beyond the physical meaning, it can be considered as a parameter of correction for the correct velocity for $c = 0$.

Tabla de contenido

Índice de gráficas

Índice de tablas

Nomenclatura

La nomenclatura del presente trabajo es la siguiente:

Γ	*Función gamma*
D	*Coeficiente de difusión*
τ	*Duración de un paso*
$\langle\tau\rangle$	*Duración promedio*
P	*Distribución de probabilidad*
d_f	*Dimensión fractal*
d	*Dimensión del espacio euclidiano*
G	*Número de grupos de energía*
P_N	*Método de aproximación*
S_N	*Método de aproximación*
ψ	*Flujo angular*
υ	*Velocidad de la partícula*
n	*Densidad de partícula local, densidad neutrónica*
$\vec{r}$	*Vector de posición*
t	*Tiempo*
$\hat{\Omega}$	*Dirección del movimiento de la partícula*
Σ_t	*Sección eficaz total*
Σ_a	*Sección eficaz de absorción*
Σ_s	*Sección eficaz de dispersión*
Q	*Término fuente*
ϕ	*Flujo escalar*
$\vec{J}$	*Densidad de corriente*
$\bar{\mu}_0$	*Coseno medio del ángulo de dispersión*

Σ_{tr}	*Sección eficaz de transporte*
φ	*Función de distribución de la cantidad de difusión*
$\delta(x)$	*Delta de Dirac*
τ	*Tiempo de relajación*
$\langle x^2 \rangle$	*Desplazamiento cuadrático medio*
τ^{γ}	*Tiempo de relajación anómala*
D_{γ}	*Coeficiente de difusión anómalo*
λ_t	*Trayectoria libre media de transporte*
t_0	*Tiempo de simulación*
c	*Número medio de partículas emitidas por evento de colisión*
γ_0	*Valor inicial*
b	*Porcentaje de variación del número de Monte Carlo*
x_i	*Número relacionado con el método de Monte Carlo*
γ_i	*i-ésimo valor de exponente de difusión anómala*
a_{γ}^{*}	*Velocidad fraccional de la onda*
N	*Tamaño muestra*
$\overline{x}$	*Media*
s	*Desviación estándar*
ϕ / Q_0	*Flujo escalar adimensional*
S	*Término fuente*
β	*Fracción de neutrones retardados*
${}^{\gamma}\omega_{p,i}$	*Pesos de la convolución*
ρ_s	*Reactividad subcrítica*
r	*Velocidad de inserción de reactividad*
t_0	*Duración de elevación de la barra de control*
Λ	*Tiempo de generación de neutrones instantáneos*

C	*Densidad de precursores de neutrones retardados*
λ	*Constante de decaimiento*
l	*Tiempo de vida del neutrón*
q	*Fuente de neutrones*

Índices superiores

α	*Número complejo*
$m-,\ n-$	*Orden de la derivada*
γ_i, κ	*Orden fraccional de la derivada*
γ	*Exponente de difusión anómala*
$2/d_\omega$	*Representación del exponente de difusión anómala*

Índices inferiores

i	*Especie de un sistema de varios componentes*
j	*Especie de un sistema de varios componentes*
k	*Especie de un sistema de varios componentes*
0	*Condiciones iniciales*

Operaciones matemáticas

D^γ	*Operador diferencial de orden fraccional*
$\nabla\cdot$	*Divergencia*
∇	*Gradiente*
d/dt	*Operador diferencial*

Γ	*Función gamma*
Σ	*Suma de términos*
∂	*Operador derivada parcial*
∇^2	*Operador laplaciano*

Capítulo I

Introducción

Hoy en día, el concepto de difusión de partículas es una herramienta comúnmente utilizada para comprender el complejo comportamiento del movimiento promedio de partículas.

Las partículas experimentan colisiones elásticas (Duderstadt y Hamilton, 1976) con todos los núcleos, resultando como consecuencia una trayectoria neutrónica típica que consiste en una serie de elementos rectilíneos que unen entre sí los puntos (núcleos) donde el neutrón ha realizado colisiones de dispersión. Como se muestra en la siguiente figura:

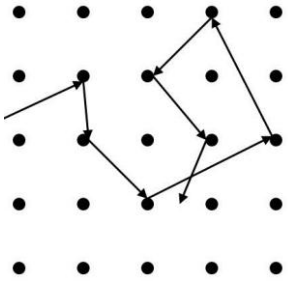

Figura 1.1. Dispersión elástica de partículas en un medio sólido.

Cuando se considera un gran número de partículas, hay siempre un desplazamiento neto desde regiones de mayor densidad neutrónica a otras de densidad menor. Este desplazamiento recibe el nombre de *difusión*

La mayoría de los estudios sobre reactores tratan el movimiento de neutrones como un proceso de difusión, donde se supone que el movimiento promedio de los neutrones tienden de regiones de alta a regiones de baja densidad neutrónica. El tratamiento del transporte de partículas como un proceso de difusión tiene una validez limitada debido a que los neutrones recorren una distancia relativamente grande entre interacciones. Por ejemplo, en un reactor de agua ligera

(LWR) la trayectoria libre media de los neutrones térmicos es típicamente alrededor de 1 cm, comparable con el diámetro del combustible, y alrededor de unos pocos centímetros para neutrones rápidos. Por lo que el modelo de difusión falla para predecir la distribución de neutrones en una varilla de combustible, donde la ecuación de transporte debe ser utilizada (Espinosa-Paredes et al., 2008).

El proceso de *difusión de neutrones* dentro de un reactor nuclear se lleva a cabo en un medio con una configuración jerárquica altamente heterogénea, como se ilustra en la Figura 1.2: donde Figura 1.2a representa el núcleo del reactor nuclear; la Figura 1.2b representa el ensamble de combustible, el cual es un arreglo de la celdas de combustible (cuatro celdas por cada ensamble para la mayoría de los BWR); la Figura 1.2c muestra el arreglo de barras de combustible. Normalmente, estas configuraciones (ensambles, arreglos y varillas) son periódicos con una anisotropía caracterizada por la geometría del arreglo nominal y se encuentran sumergidas dentro de un moderador (Todreas y Kazimi, 1990a, b).

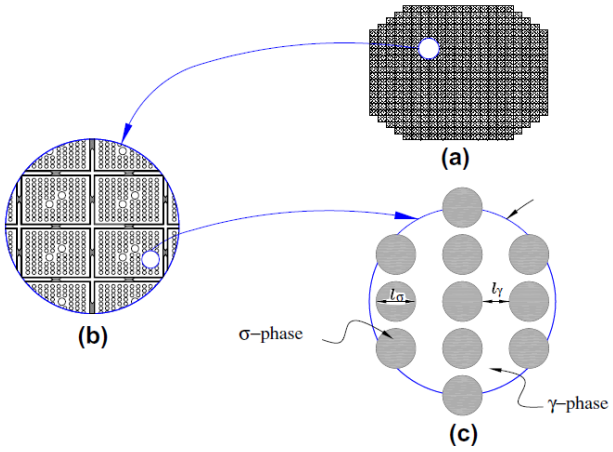

Figura 1.2. Longitudes características del sistema. (a) Núcleo del reactor nuclear; (b) Escala I: ensamble de combustible; Escala II: arreglo de varillas de combustible (Espinosa-Paredes et al., 2008).

La teoría de la difusión proporciona una descripción matemática estrictamente válida del flujo de neutrones cuando se cumplen las siguientes suposiciones (Stacey, 2001):

1) La absorción es mucho menos probable que la dispersión,

2) la variación espacial de la distribución de neutrones es lineal, y
3) proviene de la dispersión isotrópica.

La primera condición se satisface para la mayoría de los moderadores y en los materiales de las estructuras que se encuentran en un reactor, pero no para el combustible y elementos de control. La segunda condición se satisface en algunas trayectorias libres medias lejos de las fronteras y en medios homogéneos grandes con una fuente uniformemente distribuida. La tercera condición se cumple para la dispersión por núcleos de masa atómica grande.

Considerando un reactor nuclear de configuración altamente heterogénea (Figura 1.2), es decir, que las barras de combustible se encuentran dentro de un moderador cualquiera (se consideran solo dos materiales). Los neutrones rápidos que se forman dentro por fisión en el centro de las barras, alcanzan el moderador, donde van perdiendo energía gradualmente. Cuando a la proximidad de una barra llegan neutrones epitérmicos de energías cercanas a los valores de resonancia (Glasstone y Sensonske, 1968 Fig. 2.18), son absorbidos por núcleos de combustible, principalmente en las capas exteriores de la barra. Por consiguiente, de todos los neutrones epitérmicos que penetran en la barra de combustible, solamente son capturados los que poseen energías idénticas a los picos de resonancia o muy próximas. Todos los demás conservan una gran probabilidad de atravesar la barra, ya que las pérdidas energéticas que experimentan, por colisiones con los núcleos pesados de combustible son muy pequeñas. Al llegar nuevamente al moderador, los neutrones se moderan todavía más, pudiendo pasar por varios niveles energéticos de resonancias, antes de ser capturados, definitivamente, como neutrones térmicos.

Bajo estas consideraciones, los procesos de difusión de Fick presentan algunos fenómenos de difusión anómalos debido a la configuración altamente heterogénea en los reactores nucleares, específicamente, por la presencia de elementos altamente absorbentes de neutrones en las barras de combustible, en las barras de control y absorvedores químicos disueltos en el refrigerante. La dinámica de estos absorvedores cambia radicalmente la producción de energía local y cambia la re-distribución de los mismos elementos absorvedores, con frecuencia se requiere un tratamiento

más preciso del transporte de neutrones que el provisto por la teoría de la difusión clásica, la cual puede ser utilizada sin restricciones cuando la configuración altamente heterogénea en el reactor nuclear se sustituye por una mezcla homogeneizada utilizando un modelo promediado eficaz (Vázquez-Rodríguez et al. 2009).

Los elementos de control altamente absorbentes están representados en la teoría de difusión por las secciones eficaces, con lo que se reproduce una teoría de transporte para la tasa de absorciones. Sin embargo, el modelo promediado efectivo no corrige la dinámica de flujo de neutrones anómalos.

Por lo tanto, con la intensión de considerar algunos fenómenos de difusión anómalos debido a una configuración altamente heterogénea en los reactores nucleares, en este trabajo se propone un modelo de difusión fraccional como una ecuación constitutiva de la densidad de corriente neutrónica o de partícula. Este modelo puede ser aplicado cuando se tiene grandes variaciones de las secciones eficaces de los neutrones, debido a que estas variaciones impiden el uso correcto de la ecuación de difusión de neutrones clásica, y se deben a los elementos altamente absorvedores de neutrones en el combustible como son: las barras de control o boro inyectado en el refrigerante para forzar la parada del reactor.

La modificación de las leyes constitutivas propuestas en este trabajo permite ampliar el alcance y mejorar la teoría de difusión clásica. Respecto al alcance, puede describirse la evolución de un transitorio de neutrones en un reactor nuclear con una configuración altamente heterogénea, debida a la presencia de elementos fuertemente absorvedores de neutrones como las barras de control y venenos químicos introducidos en el refrigerante. Con el fin de mejorar la teoría de la difusión clásica, se hace la suposición de que el modelo de orden fraccional para la difusión de neutrones puede mejorar las predicciones y probablemente en algunos casos debe ser similar a la complicada teoría de transporte.

Con estas ideas, se obtiene un modelo reducido de la cinética de neutrones sobre la base de la teoría de la difusión de neutrones con una ley constitutiva fraccional usando todos los argumentos teóricos conocidos, esto se traduce en un modelo de ecuaciones de la cinética neutrónica de orden fraccional (ECNF) de un reactor puntual, el desarrollado fue presentado en el trabajo de Espinosa-Paredes et al. (2011).

En resumen, en muchos sistemas naturales observados, los procesos no siguen la ley de difusión de Fick. Un fenómeno de esta naturaleza se le conoce como difusión anómala. Algunos casos de difusión anómala ocurren debido a la configuración del sistema altamente heterogénea. En los reactores nucleares contrariamente a un proceso de difusión fickiano, la presencia de elementos de control altamente absorbentes puede inducir a la contracción del movimiento de los neutrones, donde el resultado es un proceso de difusión anómalo que no puede ser descrito con precisión cómo un proceso de difusión fickiano.

De muchos experimentos y consideraciones teóricas, se sabe que, en muchos casos de interés físico, los procesos de transporte difusivo son de naturaleza anómala (Havlin y Ben-Avraham, 1987; Bouchaud y Georges, 1990). Por esta razón la difusión anómala fraccional ha sido usada para describir los diferentes procesos de transporte; para describir el transporte en medios cristalinos ordenados (Havlin y Ben-Avraham, 1987); para describir el mecanismo estadístico que puede generar las leyes de difusión "*anómala*" (no Browniano) (Bouchaud y Georges, 1990); para el transporte de especies químicas en los sistemas de agua subterránea y el caudal del rio (Scher et al., 2002; Anderson y Meerschaert, 1998); en el procesos de difusión y reacción para obtener una descripción efectiva del medio y de la dinámica de concentración (Valdés-Parada et al., 2006); para obtener la ecuación de sub-difusión parabólica de un sistema unidimensional con una membrana delgada (Katarzyna y Lewandowska, 2009); y en ciencias nucleares para describir la dinámica de un reactor nuclear (Espinosa-Paredes et al., 2011a).

Como se puede ver hay muchos problemas interesantes a considerar desde el punto de vista de las Ecuaciones Diferenciales de Orden Fraccional (EDOF) los cuales pueden ser modelados, y

así comparar los nuevos con los viejos paradigmas para aplicar las mejoras en el modelado y la simulación de la nueva generación de reactores nucleares.

1.1 Antecedentes históricos del cálculo fraccional

El cálculo fraccional ha tenido una larga historia, datando desde 1695 cuando Leibniz discutió el significado de $D^{1/2} f(x)$ en una carta a L'Hopital. Leibniz escribió que su resultado era: "una aparente paradoja de la cual algún día se obtendrían consecuencias útiles". Muchos de los matemáticos distinguidos de generaciones posteriores han contribuido a esta teoría (Oldham y Spanier, 1974; Miller y Ross, 1993; Samko et al., 1993; Podlubny, 1999; Hilfer, 2000, etc), siendo estudiado principalmente para propósitos teóricos, pero durante las últimas décadas han aparecido muchas aplicaciones de esta rama de las matemáticas, debido a que el concepto de una derivada fraccional provee una herramienta útil para la descripción de varios procesos. Por ejemplo, se ha demostrado que los modelos de orden fraccional son más apropiados que los de orden entero para describir el estudio y la simulación en ciertos fenómenos como: trasporte de contaminantes (Guanhua et al., 2005), flujos neutrónicos (Espinosa-Paredes et al., 2008, 2011a), propagación en materiales porosos (Fellah et al., 2008), difusividad dinámica de las moléculas (Wu y Berland, 2008), entre otros tales como algoritmos genéticos, diseños y modelos termales, etc.

1.1.1 Conceptos básicos del cálculo de orden fraccional

Nuestra comprensión de la naturaleza se basa en el cálculo, que a su vez se basa en el concepto intuitivo de la derivada. Su poder descriptivo viene del hecho de que se analiza el comportamiento a escala lo suficientemente pequeña como para que sus propiedades cambian de forma lineal, evitando así las complejidades que surgen con escalas más grandes. El cálculo fraccional generaliza este concepto de orden entero a no entero. A pesar de que parece no tener aplicaciones importantes en la física fundamental, la investigación sobre este concepto básico podría ser útil en la comprensión de la naturaleza.

El cálculo fraccional es la rama de cálculo que generaliza la derivada de una función para que no sea de orden entero, permite cálculos como la derivación de una función de orden igual a $1/2$. A pesar de que "cálculo generalizado" sería una mejor opción, el nombre de "cálculo fraccional" se utiliza para denotar este tipo de derivadas.

La derivada de una función $f(x)$ es definida como

$$D^1 f(x) = \lim_{h\to 0} \frac{f(x+h) - f(x)}{h}. \tag{1.1}$$

Iterando esta operación se obtiene una expresión para $n-$ésima derivada de una función. Como puede verse fácilmente y demostrar por inducción, para cualquier número natural n,

$$D^n f(x) = \lim_{h\to 0} h^{-n} \sum_{m=0}^{n} (-1)^m \binom{n}{m} f(x+(n-m)h), \tag{1.2}$$

donde

$$\binom{n}{m} = \frac{n!}{m!(n-m)!}. \tag{1.3}$$

Al ver esta una expresión, la pregunta inmediata es si se puede generalizar para cualquier número n que no sea un entero, real o complejo. Hay algunas razones que nos hacen pensar así,

1. El hecho de que para cualquier número natural n, el cálculo de la $n-$ésima derivada es dado por una formula explicita (Ec. 1.2).
2. La generalización del factorial mediante la función gamma es

$$\binom{n}{m} = \frac{n!}{m!(n-m)!} = \frac{\Gamma(n+1)}{\Gamma(m+1)\Gamma(n-m+1)} \tag{1.4}$$

   la cual también es válida para valores no enteros.
3. La semejanza de la Ec. 1.2 a la fórmula del binomio

$$(a+b)^n = \sum_{m=0}^{n} \binom{n}{m} a^{n-m} b^m \tag{1.5}$$

la cual puede generalizarse para cualquier numero complejo α por

$$(a+b)^{\alpha}=\sum_{m=0}^{\infty}\frac{\Gamma(\alpha+1)}{n!\Gamma(\alpha-n+1)}a^{\alpha-n}b^{n} \tag{1.6}$$

que es convergente si

$$|b|<a\,. \tag{1.7}$$

Hay algunas propiedades deseables que podrían ser necesarias para la derivada fraccionaria,

1. Existencia y continuidad de la $m-$ésima derivada de la función, para cualquier m cuyo modulo es igual o menor que m.
2. Para $n=0$ el resultado debería ser la misma función; para valores enteros $n>0$ el resultado debería ser igual a la derivada ordinaria y para valores enteros $n<0$ debería ser igual a la integración ordinaria, sin tener en cuenta la constante de integración.
3. El producto de dos derivadas fraccionales como

$$D^{\alpha+\gamma}f(x)=D^{\alpha}D^{\gamma}f(x)\,. \tag{1.8}$$

4. Linealidad,

$$D^{\alpha}\left[af(x)+bg(x)\right]=aD^{\alpha}f(x)+bD^{\alpha}g(x)\,. \tag{1.9}$$

5. Permitir la expansión de Taylor de alguna otra manera.
6. Sus propiedades características deben ser conservada para la función exponencial

$$D^{\alpha}e^{x}=e^{x}\,. \tag{1.10}$$

1.1.2 Ecuaciones diferenciales de orden fraccional

En este trabajo se obtienen Ecuaciones Diferenciales de Orden Fraccional (EDOF) multi término de la forma general

$$D^{\gamma_n}x(t)+a_nD^{\gamma_{n-1}}x(t)+\cdots+a_2D^{\gamma_1}x(t)+a_1x(t)=u(t)\,, \tag{1.11}$$

donde D^{γ_i} es el operador diferencial de orden fraccional γ_i. Para solucionarla este tipo de ecuaciones se emplean diferentes definiciones del operador diferencial de orden fraccional, tales

como la derivada fraccional de Riemann-Lioville, derivada de Caputo, entre otros, tales como la derivada de Grünwald-Letnikov y la derivada de Riesz (Oldham y Spanier, 1974).

La definición de Riemann-Liouville de la derivada fraccional es (Cai y Liu, 2007);

$$ {}^{RL}D^{\alpha}\varphi(t)=\frac{d^{\alpha}\varphi(t)}{dt^{\alpha}}=\begin{cases}\dfrac{1}{\Gamma(m-\alpha)}\dfrac{d^{m}}{dt^{m}}\displaystyle\int_0^t\frac{\varphi(\tau)}{(t-\tau)^{\alpha+1-m}}d\tau, & 0\le m-1<\alpha<m\\ \dfrac{d^{m}\varphi(t)}{dt^{m}}, & \alpha=m\end{cases}, \tag{1.12} $$

donde m es un entero positivo y $\Gamma(m-\alpha)$ es la función gamma con argumento $m-\alpha$.

La derivada de Caputo de orden fraccional γ es definido como:

$$ D^{\gamma}\varphi(t)=\frac{d^{\gamma}\varphi(t)}{dt^{\gamma}}=\begin{cases}\dfrac{1}{\Gamma(m-\gamma)}\displaystyle\int_0^t\frac{\dfrac{d^{m}\varphi}{dt^{m}}(\tau)}{(t-\tau)^{\gamma+1-m}}d\tau, & 0\le m-1<\gamma<m\\ \dfrac{d^{m}\varphi(t)}{dt^{m}}, & \gamma=m\end{cases}. \tag{1.13} $$

La relación entre las derivadas fraccionales de Caputo y Riemann-Liouville es (Gorenflo et al., 2000)

$$ D^{\alpha}\varphi(t)={}_0D_t^{\alpha}\varphi(t)-\sum_{k=0}^{m-1}\frac{\dfrac{d^{m}\varphi(0^{+})}{dt^{m}}t^{k-\alpha}}{\Gamma(k-\alpha+1)},\quad 0\le m-1<\alpha<m. \tag{1.14} $$

La versión de Caputo dada por la Ec. (1.13) permite condiciones iniciales de la misma forma como para ecuaciones diferenciales de orden entero, mientras que la versión de Riemann-Liouville requiere condiciones iniciales cuyas derivadas deben estar específicamente en términos de integrales y derivadas fraccionales, lo cual es más complicado de determinar con respecto a la versión de Caputo.

Para más detalles de conceptos, propiedades y definiciones de las derivadas de orden fraccional, ver las referencias de Oldham y Spanier, 1974; Miller and Ross, 1993; Samko et al., 1993; Podlubny, 1999; Hilfer, 2000; Leszczynski y Ciesielski, 2001.

1.1.3 Difusión normal y anómala

La difusión es la propagación de las partículas moviéndose aleatoriamente de las regiones con mayor concentración a las regiones con menor concentración. La primera clase de procesos difusivos que ha sido reconocido históricamente y que hoy se conoce bajo el nombre de *difusión normal*, son los caracterizados por un crecimiento lineal con el tiempo del *desplazamiento cuadrático medio* (MSD, por sus siglas en ingles) de una partícula desde su punto de partida,

$$\left\langle x^2 \right\rangle = Dt\,. \tag{1.15}$$

En tiempos de escala largos, todos los procesos sub-difusivos normales muestran el mismo comportamiento, se observa en los detalles microscópicos que la dinámica de la partícula solo es relevante para la determinación del valor del *coeficiente de difusión* D.

La importancia y la generalidad del concepto de difusión normal fueron reconocidas en el siglo XIX. Uno de los primeros hitos fue el descubrimiento del movimiento browniano, en la difusión de las partículas suspendidas en un fluido, por el botánico escocés Robert Brown en 1827 (Brown, 1828). Se dio cuenta posteriormente de que los fenómenos aparentemente tan diferentes como la propagación de mosquitos infectados (Pearson, 1906) y la conducción de calor en los sólidos pueden ser descritos en términos de difusión normal.

La fuerza impulsora de la difusión no necesita diferencias en la concentración, también puede ocurrir por una diferencia de energía potencial. La conducción eléctrica en los metales es también, por lo general, un proceso normal de difusión, impulsada por las diferencias de potencial eléctrico (ya que las diferencias en la concentración de electrones violaría la neutralidad de carga) (Datta, 1995).

A pesar de que es un concepto muy general, la difusión normal no describe todos los fenómenos difusivos. Desde 1970, cada vez se encuentran más procesos en la naturaleza (Scher y Montroll, 1975), en donde el *desplazamiento cuadrático medio* de una escala de partículas como una potencia del tiempo es diferente a la unidad, es decir

$$\left\langle x^2 \right\rangle = Dt^{\gamma}, \quad \gamma \neq 1 \tag{1.16}$$

Como ejemplos, se incluyen los patrones de alimentación de algunos animales (Bartumeus et al., 2005), el comportamiento de los viajes humanos (Brockmann et al., 2006), y la difusión de la luz en una atmósfera nebulosa (Davis y Marshak, 1997). Este tipo de difusión que se ha denominado *anómala*, y puede ocurrir en dos variedades: *sub-difusión*, donde las partículas se propagan con un tiempo arbitrario más lento que la difusión normal ($\gamma < 1$); y *súper-difusión*, donde se propagan arbitrariamente más rápido ($\gamma > 1$, con una límite superior de $\gamma = 2$ para el movimiento balístico sin ningún tipo de dispersión).

Las c*aminatas aleatorias* son procesos estocásticos en donde las partículas se mueven en una secuencia de pasos dirigidos aleatoriamente. Las longitudes s de los pasos, y la duración τ de un paso se extraen de una distribución de probabilidad $P(s,\tau)$. (Por simplicidad, se supone una caminata aleatoria isotrópica, por lo que P es independiente de la dirección del paso). Para que un paseo aleatorio sea normal, la varianza del tamaño de paso $\left(Var(s) = \left\langle s^2 \right\rangle - \left\langle s \right\rangle^2\right)$ tiene que ser finita, así como la duración promedio $\left\langle \tau \right\rangle$. Entonces, de acuerdo con el teorema del límite central, el desplazamiento cuadrático medio después del tiempo t se aproximará a una distribución normal con varianza $\left(t/\left\langle \tau \right\rangle\right)Var(s)$. Esta es la razón de la similitud de todos los procesos difusivos mencionada anteriormente.

Si los requisitos para una caminata aleatoria normal son violados, la caminata aleatoria será anómala y la escala del desplazamiento cuadrático medio, en general, tienen una ley de potencia (Ec. 1.16) con $\gamma \neq 1$. Esto puede ocurrir de varias formas como lo presenta Weeks et al. (1996).

La *súper-difusión* ocurre si la distribución del tamaño de paso $P(s)$ tiene una cola pesada $\propto 1/s^{1+\kappa}$ para s grande, con $0<\kappa<2$. Si la duración $\tau=\upsilon s$ es simplemente proporcional al tamaño de paso (con velocidad constante υ) esto lleva a un comportamiento súper-difusivo con

$$\gamma=\max(3-\kappa,2) \tag{1.17}$$

Este tipo de caminata aleatorio anómala es llamada *caminata de Lévy*, después de que el matemático francés Paul Pierre Lévy. Alternativamente, uno podría dar cada paso con la misma duración τ_0, independiente de la longitud del paso, esta es llamada *vuelo de Lévy* que tiene un desplazamiento cuadrado medio divergente en cualquier tiempo $t>\tau_0$, y por lo tanto físicamente no realista.

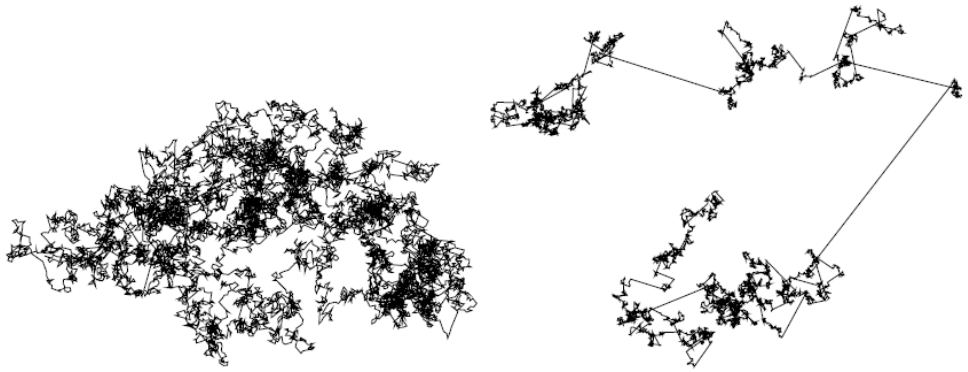

Figura 1.3. Dos caminatas aleatorias de 10^4 pasos cada una, se caracterizan por una ley de potencias de cola con distribución de tamaño de paso $P(s)=\kappa/s^{\kappa+1}$ para $s>1$, $P(s)=0$ en cualquier otro caso. La caminata izquierda es normal con un $\kappa=3$ (caminata browniana), mientras que el derecho tiene $\kappa=2/3$ el cual lo hace súper-difusivo (vuelo de Lévy).

La Figura 1.3 muestra dos esquemas de realizaciones de las leyes de potencia de cola de caminatas aleatorios de los cuales uno es normal y uno súper-difusivo. Se observa claramente que la cantidad de pasos individuales no juegan un papel preponderante en la difusión normal,

mientras que la súper-difusión está dominada por pasos largos individuales en todas las escalas de longitud.

Otra manera de romper con la difusión normal, es tener una distribución de tamaño de paso con una varianza finita, pero asociada con la duración de los pasos extraídas de una distribución con media infinita (ben-Avraham y Havlin, 2000). Esto lleva a un comportamiento sub-difusivo caracterizado por $\gamma < 1$. Efectivamente, esto sucede si la caminata aleatoria se realiza en un fractal: un objeto con escala invariante de dimensión fractal d_f no-entera incrustado en el espacio euclidiano de dimensión $d > d_f$. Las piezas del espacio euclidiano que no forman parte de los obstáculos fractales presentes para el caminador que está presente en todas las escalas de longitud y frena la difusión. El valor de $\gamma < 1$ es específico para cada fractal e independiente de la dimensión fractal (Verkrijging et al., 1980).

Capítulo II

Ecuación fraccional de Cattaneo

La ecuación de Boltzmann o ecuación de transporte lineal describe la densidad local de las partículas viajando en el medio con interacciones entre las partículas y el medio. La ecuación es una ecuación integro diferencial y la densidad local de las partículas depende de la posición, tiempo y de la velocidad (o alternativamente de la energía y dirección de movimiento) (Davison y Sykes, 1958; Bell y Gladstone, 1971; Pomraning, 1973; Duderstadt y Martin, 1979; Lewis y Miller, 1993).

La dependencia de la energía es usualmente modelada con la aproximación múltigrupo (también llamada aproximación múlti-energía), donde espacio-energía se divide en grupos discretos de energía. Así, esta aproximación se reduce al problema de una ecuación de transporte que depende de la energía con G ecuaciones monoenergéticas (donde G es el número de grupos de energía), las cuales se acoplan a través del término fuente (todas las transiciones entre los grupos de energía son debidas al término fuente). Sin embargo, el esfuerzo es enfocado en resolver la ecuación monoenergética de Boltzmann y especialmente encontrando la dependencia angular.

Hay varios métodos conocidos para manejar la dependencia angular de la ecuación de Boltzmann. Los más populares son las aproximaciones P_N (donde el flujo angular es descompuesto en series de Legendre), el método S_N (también llamado método de ordenada discreta donde el flujo escalar se descompone en varias direcciones discretas), y una familia de aproximaciones de difusión (Bell y Gladstone, 1971; Pomraning, 1973; Duderstadt y Martin, 1979; Lewis y Miller, 1993). Con las dos primeras aproximaciones se obtiene una solución exacta cuando $N \to \infty$.

La aproximación de difusión clásica (también llamada aproximación de Eddington) es desarrollada mediante la suposición de que la dependencia angular es isotrópica, o casi (alternativamente, puede ser desarrollada a partir de una derivación simple de la aproximación P_N con $N=1$). Naturalmente, la aproximación de difusión describe bien la densidad de partículas sólo cuando el medio es dominantemente dispersor isotrópico. Cuando esto no se cumple la aproximación clásica de difusión es inadecuada.

2.1 Antecedentes: definiciones y derivaciones básicas

La ecuación de transporte monoenergética lineal expresada en función del flujo neutrónico ψ puede escribirse como (por ejemplo, ver Duderstadt y Martin, 1979)

$$\begin{aligned}\frac{1}{\upsilon}\frac{\partial\psi\left(\vec{r},\hat{\Omega},t\right)}{\partial t}+\hat{\Omega}\cdot\vec{\nabla}\psi\left(\vec{r},\hat{\Omega},t\right)+\Sigma_t\left(\vec{r}\right)\psi\left(\vec{r},\hat{\Omega},t\right),\\ =\int_{4\pi}d\hat{\Omega}'\Sigma_s\left(\vec{r},\hat{\Omega}\cdot\hat{\Omega}'\right)\psi\left(\vec{r},\hat{\Omega}',t\right)+Q\left(\vec{r},\hat{\Omega},t\right)\end{aligned} \tag{2.1}$$

donde

$\psi\left(\vec{r},\hat{\Omega},t\right)=\upsilon n\left(\vec{r},\hat{\Omega},t\right)$: es el flujo angular ($\upsilon$ es la velocidad de la partícula y $n\left(\vec{r},\hat{\Omega}',t\right)$ es la densidad de partícula local), el cual depende de la posición $\vec{r}$, del tiempo t y de la dirección del movimiento de la partícula $\hat{\Omega}$,

$\Sigma_t\left(\vec{r}\right)=\Sigma_a\left(\vec{r}\right)+\Sigma_s\left(\vec{r}\right)$: es la sección eficaz total, la cual depende de la posición, donde $\Sigma_a\left(\vec{r}\right)$ es la sección eficaz de absorción y $\Sigma_s\left(\vec{r}\right)$ es la sección eficaz de dispersión $\left[\Sigma_s\left(\vec{r}\right)=\int_{4\pi}d\hat{\Omega}'\Sigma_s\left(\vec{r},\hat{\Omega}\cdot\hat{\Omega}'\right)\right]$,

$Q\left(\vec{r},\hat{\Omega},t\right)$: en el término fuente que puede describir ya sea las fuentes internas (como la fisión) o las fuentes externas.

Hay varias formas de derivar la ecuación de difusión de la ecuación de Boltzmann. La más directa es presentada aquí, la cual es crucial para entender la nueva aproximación más tarde. En primer lugar, integrando $\int_{4\pi} d\hat{\Omega}$ sobre la ecuación de Boltzmann, se obtiene

$$\frac{1}{\upsilon}\frac{\partial\phi(\vec{r},t)}{\partial t}+\vec{\nabla}\cdot\vec{J}(\vec{r},t)+\Sigma_a(\vec{r})\phi(\vec{r},t)=Q^{(0)}(\vec{r},t), \tag{2.2}$$

donde

$\phi(\vec{r},t)=\int_{4\pi}\psi(\vec{r},\hat{\Omega},t)d\hat{\Omega}$: es el momento cero del flujo angular $\psi(\vec{r},\hat{\Omega},t)$ llamado flujo escalar,

$\vec{J}(\vec{r},t)=\int_{4\pi}\psi(\vec{r},\hat{\Omega},t)\hat{\Omega}d\hat{\Omega}$: es el primer momento del flujo angular llamado densidad de corriente,

$Q^{(0)}(\vec{r},t)=\int_{4\pi}Q(\vec{r},\hat{\Omega},t)d\hat{\Omega}$.

La Ec. (2.2) es el momento cero de la ecuación de Boltzmann. Es una ecuación exacta y bien conocida como la ley de conservación. A continuación, integrando $\int_{4\pi}\hat{\Omega}d\hat{\Omega}$ sobre la ecuación de Boltzmann queda

$$\begin{aligned}\frac{1}{\upsilon}\frac{\partial\vec{J}(\vec{r},t)}{\partial t}+\vec{\nabla}\cdot\int_{4\pi}\hat{\Omega}\hat{\Omega}\psi(\vec{r},\hat{\Omega},t)d\hat{\Omega}+\Sigma_t(\vec{r})\vec{J}(\vec{r},t)&\\ =\bar{\mu}_0\Sigma_s(\vec{r})\vec{J}(\vec{r},t)+Q^{(1)}(\vec{r},t)&\end{aligned}, \tag{2.3}$$

donde $\bar{\mu}_0$ es el coseno medio del ángulo de dispersión definido por

$$\bar{\mu}_0=\left\langle\hat{\Omega}\cdot\hat{\Omega}'\right\rangle=\frac{1}{4\pi\Sigma_s(\vec{r})}\int_{4\pi}d\hat{\Omega}\int_{4\pi}d\hat{\Omega}'\hat{\Omega}\cdot\hat{\Omega}'\Sigma_s(\vec{r},\hat{\Omega}\cdot\hat{\Omega}') \tag{2.4}$$

y $Q^{(1)}(\vec{r},t)=\int_{4\pi}Q(\vec{r},\hat{\Omega},t)\hat{\Omega}d\hat{\Omega}$. Podemos ver que la Ec. (2.3) contiene un término de segundo momento del flujo angular. Hasta ahora, la derivación ha sido exacta. Es importante tener en cuenta que cada momento de la ecuación de Boltzmann contiene un momento del flujo angular

más alto. Así, con el fin de tener un número finito de ecuaciones, uno debe tener una aproximación adecuada para los otros momentos.

Como se dijo anteriormente, la aproximación de difusión describe el flujo de partículas en un medio isotrópico o en caso de que el medio sea casi isotrópico. La primera aproximación que se necesita hacer es asumir que el flujo angular puede ser escrito como la suma de los dos primeros momentos:

$$\psi\left(\vec{r},\hat{\Omega},t\right)\cong\frac{1}{4\pi}\phi\left(\vec{r},t\right)+\frac{3}{4\pi}\vec{J}\left(\vec{r},t\right)\cdot\hat{\Omega}, \tag{2.5}$$

asumiendo que $\phi\left(\vec{r},t\right)\gg\left|\vec{J}\left(\vec{r},t\right)\right|$. Si el flujo angular puede ser escrito de la forma de la Ec. (2.5), podemos aproximar el término que contiene el segundo momento del flujo angular en la Ec. (2.3) como

$$\vec{\nabla}\cdot\int_{4\pi}\hat{\Omega}\hat{\Omega}\psi\left(\vec{r},\hat{\Omega},t\right)d\hat{\Omega}\cong\frac{\vec{\nabla}\phi\left(\vec{r},t\right)}{3}. \tag{2.6}$$

En segundo lugar, se asume que la fuente de las partículas es isótropa, tal que $Q^{(1)}\left(\vec{r},t\right)=0$. Esta aproximación es necesaria para la obtención tanto de la ecuación de difusión como la ecuación aproximada de telégrafo. Sustituyendo la Ec. (2.6) en la Ec. (2.3) se obtiene la siguiente ecuación de aproximada:

$$\frac{3}{\upsilon}\frac{\partial\vec{J}\left(\vec{r},t\right)}{\partial t}+\vec{\nabla}\phi\left(\vec{r},t\right)+3\Sigma_{tr}\left(\vec{r}\right)\vec{J}\left(\vec{r},t\right)=0, \tag{2.7}$$

donde $\Sigma_{tr}\left(\vec{r}\right)\equiv\Sigma_t\left(\vec{r}\right)-\bar{\mu}_0\Sigma_s\left(\vec{r}\right)$ es llamada la sección eficaz de transporte y da una definición natural de la aproximación extendida (Bell et al., 1967). Cuando la sección eficaz de dispersión es isotrópica, se tiene $\Sigma_{tr}\left(\vec{r}\right)=\Sigma_t\left(\vec{r}\right)$. Las Ecs. (2.2) y (2.7) constituyen un conjunto cerrado de ecuaciones para el flujo escalar $\phi\left(\vec{r},t\right)$ y la densidad de corriente $\vec{J}\left(\vec{r},t\right)$. Las Ecs. (2.2) y (2.7) también son llamadas aproximación P_1.

Para un tratamiento completo de la distribución angular de la densidad de partículas, se puede utilizar la aproximación P_N. En esta aproximación, el flujo se descompone en una serie de Legendre para los problemas de una dimensión o en una serie de armónicos esféricos para el caso de una geometría general (multidimensionales). En una geometría general, la forma de la ecuación P_N puede ser complicada ($N>1$), incluso para una geometría en dos o tres dimensiones. La única excepción es el caso de $N=1$ (el caso de P_1), las dos ecuaciones que definen la aproximación P_1 para cualquier geometría son idénticas a las Ecs. (2.2) y (2.7) (Duderstadt y Martin, 1979).

Si la derivada del vector corriente de la partícula con respecto al tiempo es despreciable [es decir, $\left(1/\left|\vec{J}(\vec{r},t)\right|\right)\left(\partial\left|\vec{J}(\vec{r},t)\right|/\partial t\right) \ll \upsilon\Sigma_t(\vec{r})$], la Ec. (2.7) toma la forma de la ley de Fick (que da lugar a la aproximación de difusión):

$$\vec{J}(\vec{r},t) = -D(\vec{r})\vec{\nabla}\phi(\vec{r},t), \tag{2.8}$$

con un coeficiente de difusión $D(\vec{r}) \equiv 1/3\Sigma_t(\vec{r})$. Usamos $\Sigma_t(\vec{r})$ (un caso de dispersión isotrópica) por simplicidad. Ahora, reemplazamos $\Sigma_t(\vec{r})$ por $\Sigma_{tr}(\vec{r})$, para un caso de dispersión linealmente anisótropa. Sustituyendo la Ec. (2.8) en la Ec. (2.2) (la ley de conservación) se obtiene la ecuación de difusión:

$$\frac{1}{\upsilon}\frac{\partial\phi(\vec{r},t)}{\partial t} - \vec{\nabla}\cdot\left(D(\vec{r})\vec{\nabla}\phi(\vec{r},t)\right) + \Sigma_a\phi(\vec{r},t) = Q^{(0)}(\vec{r},t). \tag{2.9}$$

Esta ecuación es muy conocida en el análisis de los reactores nucleares, la cual, contiene los efectos más importantes que pueden ocurrir en la difusión de neutrones dentro de un reactor nuclear.

2.2 Generalización de la ecuación de Cattaneo para la descripción de un proceso de transporte anómalo

La ecuación de Cattaneo describe un proceso de difusión con velocidad finita de propagación, y fue generalizada por Comte y Metzler (1997) para describir un transporte anómalo, estudiando las propiedades de esta generalización en los regímenes de largo y corto tiempo.

Normalmente, la segunda ley de Fick es usada para describir procesos de difusión estándar, esta ley puede ser derivada por la combinación de una ecuación de continuidad:

$$\frac{\partial \varphi(x,t)}{\partial t} = -\frac{\partial \vec{J}(x,t)}{\partial x} \tag{2.10}$$

y una ecuación constitutiva (primera ley de fick):

$$\vec{J}(x,t) = -D\frac{\partial \varphi(x,t)}{\partial x} \tag{2.11}$$

donde, $J(x,t)$ denota el flujo, $\varphi(x,t)$ la función de distribución de la cantidad de difusión, y D la constante de difusión. Los operadores de derivada temporal y espacial son $\partial/\partial t$ y $\partial/\partial x$, respectivamente. Tomando el gradiente de la Ec. (2.11) e introduciéndolo el resultado en la Ec. (2.10), se llega a la ecuación de difusión (fenomenológica), o segunda ley de Fick (Crank, 1970)

$$\frac{\partial \varphi(x,t)}{\partial t} = D\frac{\partial^2 \varphi(x,t)}{\partial x^2} \tag{2.12}$$

asumiendo D constante. Con una distribución delta inicial $\varphi(x,0) = \delta(x)$, se encuentra la típica solución Gaussiana de la Ec. (2.12), es decir

$$\varphi(x,t) = \frac{1}{(4\pi Dt)^{1/2}} Exp\left(-\frac{x^2}{4Dt}\right). \tag{2.13}$$

Así, incluso para tiempos muy cortos, existe una cantidad de partículas difundidas a una gran distancia del origen. Por lo tanto, una propiedad intrínseca de la Ec. (2.12) es que emita a una velocidad infinita de propagación. Matemáticamente hablando, esto se debe a que la Ec. (2.12)

es una ecuación diferencial parcial parabólica. Desde el punto de vista físico, esta propiedad no es física.

Para superar la propagación infinitamente rápida, Cattaneo (1948) propuso una aproximación modificada (Cattaneo, 1948; Casas-Vázquez, 1996), la cual reemplaza la ecuación constitutiva (2.11) por

$$\vec{J}\left(\vec{r},t\right)+\tau\frac{\partial\vec{J}\left(\vec{r},t\right)}{\partial t}=-D\vec{\nabla}\varphi\left(\vec{r},t\right) \tag{2.14}$$

donde ahora el flujo se relaja, con tiempo constante τ característico dado. Combinando la Ec. (2.14) con la ecuación de continuidad (2.10), se llega a la llamada ecuación de Cattaneo (o ecuación de difusión modificada)

$$\frac{\partial\varphi\left(x,t\right)}{\partial t}+\tau\frac{\partial^2\varphi\left(x,t\right)}{\partial t^2}=D\frac{\partial^2\varphi\left(x,t\right)}{\partial x^2}, \tag{2.15}$$

con D y τ constante. Esta extensión de la Ec. (2.12) de difusión convierte la parábola en una ecuación hiperbólica. Consecuentemente, la velocidad de propagación es finita, la cual es $\upsilon=\left(D/\tau\right)^{1/2}$ (Nonnenmacher, 1980). Notar que en el límite de la difusión, $\tau\to 0$, se recupera la segunda ley de Fick con υ infinita. La Ec. (2.15) es del tipo onda amortiguada o del tipo ecuación del telegrafista.

La ecuación constitutiva de Cattaneo (Eq. 2.15) define un proceso de relajación de *primer orden*, que puede ser visto como una simple aproximación para modelar la dinámica de relajación realista.

Las aplicaciones de la ecuación de Cattaneo en las ciencias físicas son debido a su carácter hiperbólico, ampliamente difundido. Se incluyen tanto los casos de calor y del transporte de partículas, dado que la ecuación de Cattaneo es una generalización tanto de una ecuación de difusión del calor (*ley de Fourier*) y de una ecuación de difusión de partículas (*ley de Fick*). La ecuación de Cattaneo encuentra aplicaciones en termodinámica irreversible extendida (Casas-

Vázquez et al., 1996), en la transferencia de calor por convección en Bénard (Straughan, 1984; McTaggart y Lindsay, 1985), en modelos cosmológicos (Zakari and Jou, 1993), en las ondas de choque en conductores del calor rígido (Ruggeri et al., 1990), o en la teoría de la difusión en los sólidos cristalinos (Godoy y García-Colín, 1996). Por otro lado, puede ser explícitamente derivada de la ecuación de Boltzmann (Nonnenmacher , 1984) y por lo tanto es aplicada para generalizar las ecuaciones hidrodinámicas (Grmela y Teichmann, 1983; Velasco y García-Colín, 1991). El tiempo característico constante τ de la ecuación de Cattaneo se discutido por Kaminski (1990).

Sin embargo, en muchos experimentos y consideraciones teóricas se sabe que, en muchos casos de interés físico, los procesos difusivos de transporte son de naturaleza anómala (Havlin y Ben-Avraham, 1987; Bouchaud y Georges, 1990). En primer lugar, sobre todo, esta anomalía se manifiesta en un desplazamiento cuadrático medio (MSD, mean-square displacement) de la forma

$$\left\langle x^2 \right\rangle = Kt^{\gamma}, \tag{2.16}$$

el cual se desvía del comportamiento lineal estándar. El exponente γ, frecuentemente se escribe como $2/d_{\omega}$, es llamado exponente de difusión anómala. En este trabajo estudiamos los efectos de esta propiedad anómala en el comportamiento de las partículas.

De acuerdo con estas ideas, se sabe que los procesos de difusión anómala muestran diferentes comportamientos en el espacio y tiempo. Al considerar un sistema altamente heterogéneo, se toma en cuenta que el transporte de partículas tendrá un comportamiento irregular, es decir, que debido al cambio de medio de transporte en distancias cortas y a la presencia de regiones altamente absorbentes, el proceso de transporte de la partícula en el sistema no puede describirse mediante la ley de difusión de Fick (Ec. 2.9), y tampoco puede ser descrito con precisión por la ley de propagación del tipo Cattaneo (Ec. 2.14), a este proceso se le denomina difusión anómala. Para describir estos procesos, la versión de la ecuación constitutiva de orden fraccional del vector de densidad de corriente, es (Espinosa-Paredes et al., 2008):

$$\tau^{\gamma}\frac{\partial^{\gamma}\vec{J}(\vec{r},t)}{\partial t^{\gamma}}+\vec{J}(\vec{r},t)=-D_{\gamma}(\vec{r})\vec{\nabla}\varphi(\vec{r},t) \tag{2.17}$$

donde $\partial^{\gamma}/\partial t^{\gamma}$ es el operador diferencial de orden fraccional, definido por Riemann-Liouville (Oldham y Spannier, 1974), γ es el exponente de difusión anómalo, τ ($=1/\upsilon\Sigma_t=3D/\upsilon$) es el tiempo de relajación anómala y $D_{\gamma}(\vec{r})\equiv 1/3\Sigma_t(\vec{r})$ es el coeficiente de difusión anómalo. En el límite $\tau^{\gamma}\to 0$ se recupera la ley de Fick (Ec. 2.8), mientras que cuando $\gamma\to 1$ se obtiene la ecuación del tipo Cattaneo (Ec. 2.14).

Relación con la dinámica de los reactores nucleares

Como ya se mencionó anteriormente, los procesos de difusión normal en medios homogéneos son descritos por la relación de Einstein (Einstein, 1905), es decir, $\langle r^2(t)\rangle\propto t$, donde $\langle r^2(t)\rangle$ es el término cuadrado que se sustituye al tiempo t. Sin embargo, para los fines de este estudio la relación general es $\langle r^2(t)\rangle\propto t^{\gamma}$, la cual se refiere a procesos de difusión anómala.

Los procesos de difusión anómala muestran diferentes comportamientos en el espacio y tiempo. Al considerar un sistema nuclear altamente heterogéneo, se toma en cuenta que el transporte de neutrones tendrá un comportamiento irregular, es decir, que debido al cambio de medio de transporte en distancias cortas y a la presencia de regiones altamente absorbentes, el proceso nuclear del sistema no podrá describirse mediante la ley de difusión de Fick, y tampoco podrá ser descrito con precisión por la ley de propagación del tipo Vernotte, a este proceso se le denomina difusión anómala (Cattaneo, 1948).

Capítulo III

Ecuación del telegrafista de orden fraccional en el tiempo para la aproximación P1 de la ecuación de transporte

En esta sección se desarrolla una nueva aproximación de la solución de la ecuación dependiente del tiempo de Boltzmann, la cual incluye una ecuación constitutiva de orden fraccional para la densidad de corriente (con derivada en el tiempo de orden fraccional), para un medio general. Este desarrollo fue presentado en el trabajo de Espinosa-Paredes y Polo-Labarrios (2012a), el cual es incluido en el Anexo 1. También se presenta el análisis de sensibilidad e incertidumbre del exponente de difusión anómala en la ecuación del telegrafista de orden fraccional de la aproximación P1. Este análisis se llevó a cabo a través de la simulación Monte Carlo de tamaño de muestra superior a 65,000. El análisis de incertidumbre fue evaluado en un intervalo de confianza del 99% de la media para comprender el rango de los valores medios que pueden representar toda la población estadística de las variables de rendimiento, que en este caso es el flujo. Este análisis fue presentado en el trabajo de Espinosa-Paredes et al. (2012b), el cual es incluido en el Anexo 2.

3.1 Deducción de la ecuación del telegrafista de orden fraccional en el tiempo

Ahora, regresamos a las ecuaciones P_1, si se considera la derivada del vector corriente de la partícula con respecto al tiempo la Ec. (2.7) toma la forma de la Ec. (2.14), como

$$\tau \frac{\partial \vec{J}(\vec{r},t)}{\partial t} + \vec{J}(\vec{r},t) = -D(\vec{r})\vec{\nabla}\phi(\vec{r},t) \tag{3.1}$$

en esta teoría se pueden tener ondas rápidas llevando pequeñas cantidades de partículas y ondas a velocidades más pequeñas llevando grandes cantidades de partículas (Joseph y Preziosi, 1989).

Ahora, con las Ecs. (2.2) y (3.1), se obtiene la ecuación del telegrafista hiperbólica (Heizler, 2010):

$$\frac{\tau}{\upsilon}\frac{\partial^2\phi(\vec{r},t)}{\partial t^2}-D_\gamma\vec{\nabla}^2\phi(\vec{r},t)+\left(\tau\Sigma_a+\frac{1}{\upsilon}\right)\frac{\partial\phi(\vec{r},t)}{\partial t}+\Sigma_a\phi(\vec{r},t) = Q^{(0)}(\vec{r},t)+\tau\frac{\partial Q^{(0)}(\vec{r},t)}{\partial t} \tag{3.2}$$

donde τ es el tiempo de relajación y depende de las propiedades neutrónicas del material (García-Colín y Goldstein, 2003):

$$\tau=\frac{1}{\upsilon\ \Sigma_{tr}}=\frac{3\ D}{\upsilon}. \tag{3.3}$$

Se puede observar que la ecuación (3.2) contiene un término de segundo orden en el operador diferencial del término temporal y aparece la derivada respecto al tiempo del término fuente. Si $\tau\to 0$ se obtiene la ecuación típica de difusión dada por la Ec. (2.9), la cual es el modelo clásico de difusión, y es un modelo de primer orden.

En muchos sistemas naturales, se ha observado que los procesos de difusión no siguen la ley de difusión de Fick, a dichos procesos se les denomina como difusión anómala. Especialmente en el caso del sistema descrito en la Figura 1.1, algunos fenómenos de difusión anómala ocurren debido a la configuración altamente heterogénea del sistema. Contrariamente a los procesos de difusión Fickianos, la presencia de elementos de control altamente absorbentes puede inducir a la contracción espacial del movimiento de neutrones. El resultado es un proceso de difusión anómalo que no puede describirse exactamente como un proceso de difusión Fickiano. De acuerdo con estas ideas la versión de la ley constitutiva del vector corriente de la partícula es la Ec. (2.17), la cual es

$$\tau^\gamma\frac{\partial^\gamma\vec{J}(\vec{r},t)}{\partial t^\gamma}+\vec{J}(\vec{r},t)=-D_\gamma(\vec{r})\vec{\nabla}\phi(\vec{r},t), \tag{3.4}$$

donde el operador de derivada fraccional $\partial^\gamma / \partial t^\gamma$ se define en el sentido de Caputo (Oldham y Spanier, 1974), γ es el exponente de difusión anómalo y τ^γ es el tiempo de relajación anómalo y depende de las propiedades neutrónicas del material, el cual se define como:

$$\tau^\gamma = \frac{1}{\upsilon \Sigma_{tr}} = \frac{3D_\gamma}{\upsilon}. \tag{3.5}$$

Finalmente, con las Ecs. (2.2) y (3.4), obtenemos la ecuación de dispersión, como

$$\begin{aligned} \frac{\tau^\gamma}{\upsilon}\frac{\partial^{\gamma+1}\phi(\vec{r},t)}{\partial t^{\gamma+1}} - D\nabla^2\phi(\vec{r},t) + \tau^\gamma \Sigma_a \frac{\partial^\gamma \phi(\vec{r},t)}{\partial t^\gamma} + \frac{1}{\upsilon}\frac{\partial \phi(\vec{r},t)}{\partial t} \\ + \Sigma_a \phi(\vec{r},t) = Q^{(0)}(\vec{r},t) + \tau^\gamma \frac{\partial^\gamma Q^{(0)}(\vec{r},t)}{\partial t^\gamma} \end{aligned}. \tag{3.6}$$

Esta ecuación es llamada la ecuación del telegrafista de orden fraccional en el tiempo (ETFT) la cual describe la *dispersión de partículas* como el comportamiento de la densidad de partículas (*flux*) en un medio general. Cuando $\tau^\gamma \to 0$ se recupera la ecuación de difusión clásica (Ec. 2.9). Para $\tau^\gamma \neq 0$ y $\gamma \to 1$ se obtiene la ecuación del telegrafista hiperbólica (Ec. 3.2).

Un análisis de orden de magnitud indica que τ y τ^γ son de orden 10^{-5} o menor (Espinosa-Paredes et al., 2008), por lo que el término temporal $\tau\left(\partial \vec{J}(\vec{r},t)/\partial t\right)$ y el término $\tau^\gamma\left(\partial^\gamma \vec{J}(\vec{r},t)/\partial t^\gamma\right)$ son prácticamente despreciables, con lo cual las ecuaciones constitutivas del vector corriente de la partícula, dadas por la Ecs. (3.1) y (3.4) se simplifican a la Ec. (2.8) la cual es crucial para cerrar y obtener un conjunto completo de ecuaciones, y se puede observar claramente que la corriente de partículas se transporta de mayor a menor concentración de partículas.

Para demostrar las diferencias con otros modelos, se resuelve el problema de una placa de geometría infinita en una dimensión con una fuente independiente del tiempo ubicada en el centro ($x=0$), es decir, $Q(x)=Q_0\delta(x)$, cuyas condiciones iniciales son $\phi(x,0)=0$ y $\left(\partial\phi(x,t)/\partial t\right)\big|_{t=0}=0$, y condiciones de frontera dadas por $\lim_{x\to\infty}\phi(x,t)<\infty$ y $\lim_{x\to 0}\phi(x,t)$ es obtenida de la solución analítica de la ecuación de difusión clásica (Eq. 2.9). A este problema se le llamará en este trabajo "problema con fuente delta".

3.2 Solución numérica

En esta sección se presenta la solución del la Ec. (3.6), donde se utiliza el método de diferencias finitas para poner en forma discreta las derivadas de orden fraccional usando las aproximaciones de Caputo y Riemann-Liouville (Yang et al., 2008).

Para usar el método de integración temporal (de paso a paso en el tiempo) en el caso de derivadas fraccionales, es necesario el almacenamiento de todos los intervalos de tiempo anteriores. La dificultad en la solución de las ecuaciones diferenciales de orden fraccional (EDOF) es, sobre todo, cuando la aplicación requiere una solución en un intervalo de tiempo, porque las derivadas de orden fraccional temporales no son operadores locales. Esta propiedad llamada no local significa que el sistema no sólo depende de su estado actual, sino que también de los estados históricos a partir del momento inicial.

Entonces, la Ec. (3.6) para una placa infinita en una dimensión es dada por:

$$\frac{1}{\Sigma_t^{\gamma}\upsilon^{1+\gamma}}\frac{\partial^{1+\gamma}\phi(x,t)}{\partial t^{1+\gamma}}+\frac{1}{\upsilon}\frac{\partial\phi(x,t)}{\partial t}+\frac{\Sigma_a}{\Sigma_t^{\gamma}\upsilon^{\gamma}}\frac{\partial^{\gamma}\phi(x,t)}{\partial t^{\gamma}}+\Sigma_a\phi(x,t)-\frac{1}{3\Sigma_t}\frac{\partial^2\phi(x,t)}{\partial x^2}=Q_0\delta(x),\quad t\geq 0\ with\ 0<\gamma<1 \tag{3.7}$$

Las condiciones iniciales son elegidas simplemente como $\phi(x,0)=0$ y $\partial\phi(x,t=0)/\partial t=0$. Aquí el término $\partial^{\gamma}\phi(\vec{r},t)/\partial t^{\gamma}$ es la derivada de orden fraccional de Caputo, definido por (Podlubny, 1999):

$$\frac{\partial^{\gamma}\phi(x,t)}{\partial t^{\gamma}}=\frac{1}{\Gamma(1-\gamma)}\int_0^t (t-\eta)^{-\gamma}\frac{\partial\phi(x,\eta)}{\partial\eta}d\eta \tag{3.8}$$

y $\partial^{1+\gamma}\phi(\vec{r},t)/\partial t^{1+\gamma}$ es la derivada de orden fraccional de Riemann-Liouville (Meerschaert y Tadjeran, 2003):

$$\frac{\partial^{1+\gamma}\phi(x,t)}{\partial t^{1+\gamma}}=\frac{1}{\Gamma(2-\gamma)}\frac{\partial^2}{\partial t^2}\int_0^t \frac{\phi(x,\xi)}{(t-\xi)^{\gamma-1}}d\eta\,. \tag{3.9}$$

Para mayor estabilidad, se utiliza la formula de desplazamiento de Grünwald para aproximar la derivada fraccional en el tiempo (Meerschaert y Tadjeran, 2003).

El algoritmo fraccional para la aproximación numérica es presentado en el Apéndice A.

Para resolver la Ec. (3.7), se considera que la dimensión espacial está en términos de la trayectoria libre media de transporte. Por lo que la Ec. (3.7) puede re-escribirse como:

$$\frac{\partial^{1+\gamma}\phi(x,t)}{\partial {t_0}^{1+\gamma}}+\frac{\partial\phi(x,t)}{\partial t_0}+(1-c)\frac{\partial^{\gamma}\phi(x,t)}{\partial {t_0}^{\gamma}}+(1-c)\phi(x,t)-\frac{1}{3}\frac{\partial^2\phi(x,t)}{\partial {\lambda_t}^2}=Q_0\delta(x),\quad t_0\geq 0 \tag{3.10}$$

donde los números adimensionales usados son: $\lambda_t=x\Sigma_t$ y $t_0=t\upsilon\Sigma_t$. El número medio de partículas emitidas por evento de colisión es dado por:

$$c=\frac{\Sigma_s}{\Sigma_t}=\frac{\Sigma_s}{\Sigma_a+\Sigma_s} \tag{3.11}$$

y la condición de frontera es obtenida de la aproximación de la difusión clásica:

$$x(0,t)=\frac{Q_0}{4}\sqrt{\frac{3}{(1-c)}}\left[erfc\left(-\sqrt{(1-c)t_0}\right)-erfc\left(\sqrt{(1-c)t_0}\right)\right]. \tag{3.12}$$

Ahora, sustituyendo las ecuaciones del Apéndice A, Ecs. (A3) – (A5) en la Ec. (3.10), y re-arreglando términos, se obtiene una ecuación que puede ser solucionada explícitamente para ϕ_i^{j+1}:

$$\phi_i^{j+1} = \frac{d}{(1+a+b)}\phi_{i-1}^{j} - \frac{(c+2d-a-b+g_1)}{(1+a+b)}\phi_i^{j} + \frac{d}{(1+a+b)}\phi_{i+1}^{j} - \frac{g_2}{(1+a+b)}\phi_i^{j-1} - \frac{b}{(1+a+b)}\sigma_j\left(\phi_i^{1}-\phi_i^{0}\right) - \frac{1}{(1+a+b)}\sum_{k=3}^{j+1} g_k \phi_i^{j-k+1} - \frac{b}{(1+a+b)}\sum_{k=1}^{j-1}\sigma_k\left(\phi_i^{j+1-k}-\phi_i^{j-k}\right) \tag{3.13}$$

donde $a=\tau^{\gamma}$, $b=\frac{\tau(1-c)}{\Gamma(2-\gamma)}$, $c=\tau^{1+\gamma}(1-c)$, $d=\frac{\tau^{1+\gamma}}{3h^2}$, y $\sigma_k=(k+1)^{1-\gamma}-k^{1-\gamma}$ para $k=0,1,2,\ldots,j-1$.

Para geometrías de 2 y 3 dimensiones la aplicabilidad sería sencilla, la complejidad numérica se incrementaría considerablemente debido al efecto memoria, es decir, los cuatro últimos términos del lado derecho de la Ec. (3.13), los cuales representan la diferencia con respecto a la ecuación de difusión clásica.

3.3 Análisis de sensibilidad e incertidumbre de la ETFT

El análisis de sensibilidad e incertidumbre del exponente de difusión anómala de ETFT mediante la simulación Monte Carlo fue realizada con diferentes tamaños de muestras, la más grande fue de 65,536. El método de Monte Carlo ha sido ampliamente utilizado para el análisis de la incertidumbre (Badar et al., 1993; Rochman et al, 2011; Espinosa-Paredes et al., 2012a). La simulación de Monte Carlo fue usada por Badar et al. (1993) para determinar las incertidumbres de los parámetros térmicos en el diseño de intercambiadores de calor. Rochman utilizó este método en la propagación de incertidumbre en los datos nucleares, en este trabajo se aplicó la simulación Monte Carlo para evaluar la sensibilidad y la incertidumbre de la ecuación de la cinética neutrónica de orden fraccional para un reactor puntual, esto fue publicado en Espinosa-Paredes et al., (2012a).

Implementación de la simulación Monte Carlo

La metodología del Método de Montecarlo es presentada en el Apéndice 2, a continuación se muestra cómo se implementó.

Para analizar los efectos de γ en el comportamiento de la ETFT, se implementó la simulación Monte Carlo en la solución numérica de la ETFT a través de la siguiente expresión:

$$\gamma_i = \gamma_0 + b \times x_i, \qquad i = 1, 2, 3, ..., N \tag{3.14}$$

donde γ_i es el *i*-ésimo valor de exponente de difusión anómala, γ_0 es un valor inicial menor que uno y mayor que cero, b es el porcentaje de variación del número de Monte Carlo el cual es constante y x_i es el numero relacionado con el método de Monte Carlo. Entonces, γ_i es calculado para cada valor de x_i (con $i = 1, 2, 3, ..., N$), el cual es usado como dato de entrada en la simulación numérica de la ETFT.

Para analizar los efectos del exponente de difusión anómala (γ) es necesario una dinámica de experimentos numéricos, donde la variación con respecto al tiempo del flujo escalar es importante. Con la intensión de analizar los efectos de γ en el flujo escalar se considera un problema con una fuente delta para tres diferentes tipos de medio (Espinosa-Paredes y Polo-Labarrios, 2012): 1) *medio puramente absorbente* ($c = 0$); 2) *medio heterogéneo* ($c = 0.65$); y 3) medio altamente dispersante ($c = 0.99$), donde c es calculado con la Ec. (3.11), siendo el heterogéneo un medio parcialmente dispersor y absorbente. También se consideraron diferentes tiempo: *tiempos muy cortos* (t_0, donde $t_0 \equiv t\upsilon\Sigma_t$); *tiempo cortos* ($2t_0$); y *tiempos muy largos* ($6t_0$). Para cada tipo de medio y tiempo, el flujo escalar es presentado en términos de la trayectoria libre media de transporte ($\lambda_t = x\Sigma_t$) para diferentes valores. Con estas consideraciones se llevó a cabo el análisis de sensibilidad e incertidumbre.

3.4 Resultados y discusiones

Los resultados de ETFT son comparados con la ecuación de Boltzmann para el caso de una placa infinita en una dimensión con una fuente en el centro, para dicha comparación se consideraron dos tipos de medio: (1) medio puramente absorbente ($c=0$), y (2) medio altamente dispersivo ($c=0.99$). En Anexo 1 se presenta el artículo publicado donde se comparó con otros modelos propuestos anteriormente y adicionalmente se consideró un medio heterogéneo ($c=0.65$).

La ecuación de transporte lineal monoenergética o ecuación de Boltzmann monoenergética es:

$$\frac{1}{\upsilon}\frac{\partial\psi\left(\vec{r},\hat{\Omega},t\right)}{\partial t}+\hat{\Omega}\cdot\vec{\nabla}\psi\left(\vec{r},\hat{\Omega},t\right)+\Sigma_t\left(\vec{r}\right)\psi\left(\vec{r},\hat{\Omega},t\right)=\int_{4\pi}d\hat{\Omega}'\Sigma_s\left(\vec{r},\hat{\Omega}\cdot\hat{\Omega}'\right)\psi\left(\vec{r},\hat{\Omega},t\right)+Q\left(\vec{r},\hat{\Omega},t\right) \tag{3.15}$$

y la solución exacta del problema con fuente delta en el plano es:

$$\phi_{exact}\left(x,t\right)=\frac{Q_0}{2}\left[E_1\left(\left|x\right|\Sigma_a\right)-E_1\left(\upsilon\Sigma_a t\right)\right]H\left(t-\frac{\left|x\right|}{\upsilon}\right), \tag{3.16a}$$

$$\phi\left(x,t\right)=\frac{\sqrt{15}\Sigma_t\upsilon Q_0}{2}\int_0^t e^{-5(\upsilon/2)\Sigma_t u}\cdot I_0\left[5\frac{\upsilon}{2}-\Sigma_t\sqrt{u^2-\frac{3}{5}\frac{\left|x\right|^2}{\upsilon^2}}\right]\cdot H\left(u-\sqrt{\frac{3}{5}}\frac{\left|x\right|}{\upsilon}\right)du$$
$$-\frac{Q_0}{2}\sqrt{\frac{27}{5}}e^{-5(\upsilon/2)\Sigma_t t}\cdot I_0\left[5\frac{\upsilon}{2}\Sigma_t\sqrt{t^2-\frac{3}{5}\frac{\left|x\right|^2}{\upsilon}}\right]\cdot H\left(t-\sqrt{\frac{3}{5}}\frac{\left|x\right|}{\upsilon}\right) \tag{3.16b}$$

donde la Ec. (3.16a) es para $c=0$ y la Ec. (3.16b) es para $c\approx 1$ (Ecs. 56 y 58, respectivamente en Heizler 2010).

3.4.1 Discusión de resultados

Después de haber realizado pruebas para diferentes valores de gamma, se encontró que el valor de γ =0.6 ofrecía una mejor aproximación.

La Figura 3.1 muestra la comparación de la aproximación ETFT desarrollado en este trabajo con la solución exacta de la ecuación de Boltzmann (EB). Se graficó el flujo escalar y nótese que la escala no es la misma en todas las gráficas.

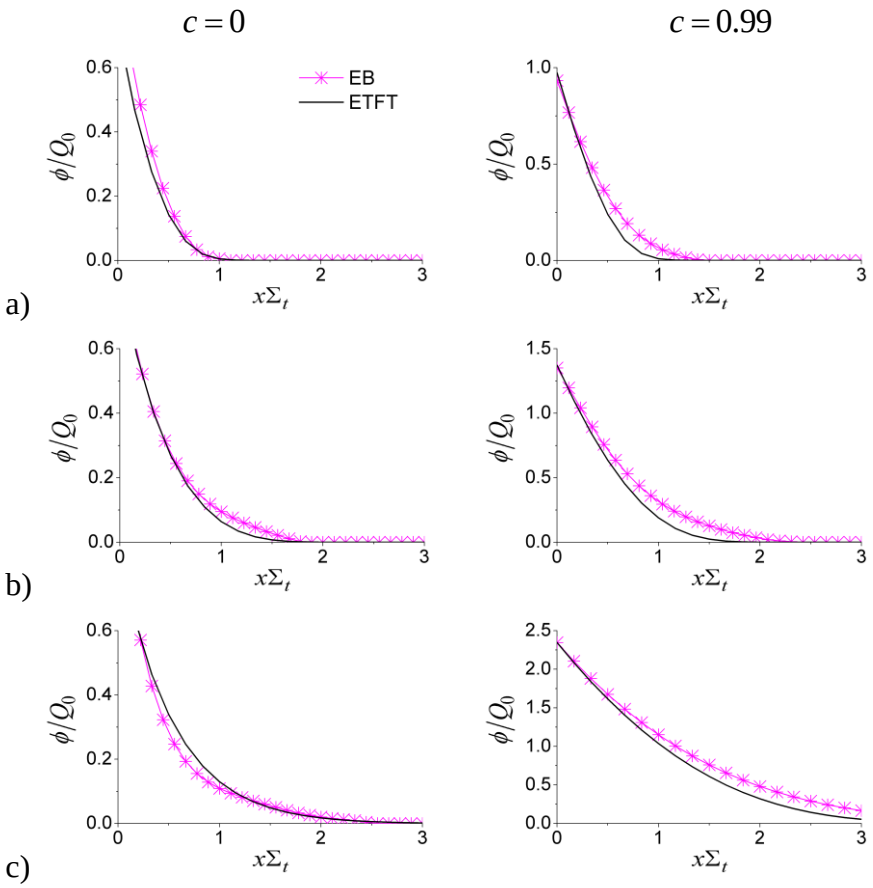

Figura 3.1. Flujo escalar para un problema con fuente delta para un medio puramente absorbente ($c = 0$) y para un medio altamente dispersor ($c = 0.99$). La solución exacta para la Ecuación de Boltzmann (EB) dada por la Ec. (3.16), y la aproximación de este trabajo es la ecuación del telegrafista de orden fraccional en el tiempo (ETFT) dada por la Ec. (3.13). El EDA es $\gamma = 0.6$; a) tiempos muy cotos (t_0); b) tiempos cortos ($2t_0$); y c) tiempos muy largos ($6t_0$); donde $t_0 \equiv t\upsilon\Sigma_t$.

Como se muestra en la Figura 3.1, dos casos fueron considerados para la comparación de resultados: (1) medio puramente absorbente ($c = 0$), y (2) medio altamente dispersor ($c = 0.99$).

La comparación de resultados se muestran para tiempos muy cortos (t_0; dónde $t_0 \equiv t\upsilon\Sigma_t$), tiempos cortos ($2t_0$), y tiempos muy largos ($6t_0$). A continuación se discuten las principales características de la aproximación ETFT:

1) Medio puramente absorbente ($c = 0$). Para tiempos muy cortos, la aproximación ETFT muestra que la partícula está avanzando con una velocidad cercana a la velocidad real, mostrada por EB (solución exacta de la Ecuación de Boltzmann) donde las diferencias son despreciables para todos los casos.

2) Medio altamente dispersor ($c \approx 1$). En este caso, para todos los tiempos la ETFT sub-predice ligeramente el comportamiento con respecto a la solución exacta de EB.

En términos generales, y como se puede observar en los resultados, la ETFT ofrece una buena aproximación para EB cuando el medio es puramente absorbente, en donde las aproximaciones comparadas en el Anexo 1 son menos precisas. La interpretación física de este comportamiento es que en el medio hay procesos sub-difusivos que están mejor representados por el modelo desarrollado en este trabajo. En un medio altamente dispersor los procesos de sub-difusión (ver sección 1.1.3) no son predominantes y la ETFT sub-predice ligeramente el flujo en los fenómenos de propagación pero sigue la misma tendencia que la EB.

Las aproximaciones ETFT así como otros modelos propuestos anteriormente y presentados en el Anexo 1 son más fáciles de resolver que la ecuación de Boltzmann. Sin embargo, la ETFT es crucial donde los fenómenos son sub-difusivos, además, tiene un enfoque más amplio y requiere un menor número de cálculos.

Con el fin de mejorar el comportamiento de la ETFT en un medio heterogéneo ($c = 0.65$), y en un medio altamente dispersor ($c \approx 1$), se realizó el experimento numérico incluyendo el coeficiente de difusión asintótica (Ec. 25 en Heizler, 2010). Los resultados obtenidos son presentados en el Anexo 1, los cuales muestran que ETFT con el coeficiente de difusión

asintótica presenta un comportamiento significativamente distinto al de la solución EB para todos los casos que se muestran, es decir, para tiempos muy cortos, tiempos cortos y tiempos largos.

La ecuación del telegrafista de orden fraccional en el tiempo de la aproximación P_1 para la ecuación de transporte predice que la velocidad fraccional de la onda (adimensional) es $a_\gamma^* = 1/3^{\gamma/2}$ donde $a_\gamma = a_\gamma^* \sqrt{\upsilon^{1+\gamma} / D^{\gamma-1}}$ fue aplicada. De acuerdo con esta ecuación $a_\gamma^* = 1/\sqrt{3}$ cuando $\gamma = 1$, la cual corresponde a la velocidad obtenida con la ecuación del telegrafista hiperbólica. Entonces, más allá de su significado físico, se puede considerar como un parámetro de corrección para la predicción de la correcta velocidad del neutrón para $c = 0$.

3.4.2 Desviación estándar relativa (RSD, por sus siglas en ingles)

Los principales resultados del análisis de sensibilidad e incertidumbre son presentados en el Anexo 2, sin embargo aquí se mencionan brevemente.

El análisis de sensibilidad e incertidumbre del exponente de difusión anómala (EDA) en la ETFT se realizo mediante la simulación Monte Carlo con un tamaño muestra (N) optimo, donde el valor del RSD es prácticamente constante e independiente del tamaño de la muestra. Para lo cual se usaron tres tipos de muestras (N_1, N_2 y N_3) que contenían diferentes tipos de números generados al azar, los cuales fueron obtenidos con el paso 1 y validados con el paso 2 de la metodología presentada en el Apéndice B de este trabajo.

La Figura 3.2 (Figura 1 del Anexo 2) presenta un grafica esquemática que muestra los valores expresados en porcentajes del RSD de la muestras N_1, N_2 y N_3. El RSD se calculó según la siguiente expresión:

$$\mathrm{RSD} = \frac{s}{\overline{x}} \times 100 \tag{3.17}$$

donde s es la desviación estándar y $\bar{x}$ es la media. Considerar el RSD permite establecer el tamaño óptimo de la simulación N. El tamaño óptimo de N es obtenido cuando el valor del RSD deja de variar con respecto al tamaño de la simulación N. En la Figura 3.2, se puede observar que para un tamaño de la simulación N (N_1, N_2 y N_3) más pequeño que 5,000 el RSD varia de manera considerable e impredeciblemente; para $N = 10{,}000$; 15,000 y 20,000 las variaciones del valor del RSD decrecen y tienden al valor de 10%. Para N más grande que 50,000 los valores del RSD son prácticamente constantes e independientes del tamaño de la muestra. Sin embargo, el tamaño óptimo N de simulación usado en este trabajo fue de 65,000. El valor del RSD para γ fue el mismo para cada tiempo de simulación como se esperaba, debido a que para cada tiempo el numero aleatorio que le corresponden es el mismo.

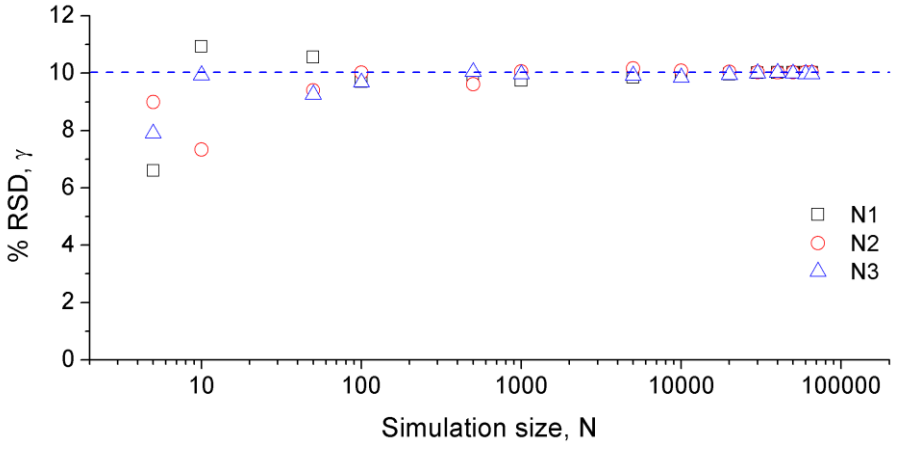

Figura 3.2. Desviación estándar relativa (RSD) para γ como una función del tamaño de simulación N. la línea punteada horizontal al 10% es la referencia para γ.

3.4.3 Exponente de difusión anómala en el comportamiento de ETFT

Los resultados de la influencia del EDA en las características de respuesta de ETFT evaluados a partir de la simulación Monte Carlo para *medios puramente absorbentes* son mostrados en la Figura 3.3 (Figura 3 del Anexo 2), los cuales fueron obtenidos con un tamaño de simulación de 65,000 para cada tiempo de simulación: para *tiempo muy cortos* (t_0), *tiempos cortos* ($2t_0$) y

para *tiempos muy largos* ($6t_0$), y para diferentes valores de λ_t los cuales varían en cada caso de acuerdo al comportamiento de flujo escalar.

En la Figura 3.3 se puede observar la influencia del exponente de difusión anómala (γ) sobre el flujo escalar adimensional (ϕ/Q_0) en el problema con fuente delta, el cual es de la siguiente manera: a) Para *tiempos muy cortos* (t_0): en $\lambda_t = 0.25$ se nota una correlación positiva estadísticamente significativa entre estos dos parámetros, y en $\lambda_t = 0.5$ y 1.0 se nota una correlación negativa estadísticamente significativa entre estos dos parámetros; b) Para *tiempos cortos* ($2t_0$); en $\lambda_t = 0.5$ y 1.0 se observa una correlación positiva entre estos dos parámetros, y en $\lambda_t = 1.5$ se nota una correlación negativa estadísticamente significativa entre estos dos parámetros; y c) Para *tiempos muy largos* ($6t_0$): en $\lambda_t = 0.5,\ 1.0,\ 2.0$, se nota una correlación positiva estadísticamente significativa entre estos dos parámetros.

Los resultados de la influencia del EDA en las características de respuesta de ETFT también fueron evaluados a partir de la simulación Monte Carlo para *medios heterogéneos* ($c = 0.65$) y para *medios altamente dispersores* ($c \approx 1$) (Figuras 4 y 5 del Anexo 2), para todos los casos, es decir, para $t_0,\ 2t_0$ y $6t_0$. Los resultados cualitativos obtenidos tienen las mismas características que se observaron en un *medio puramente absorbente* (Figura 3.3). Sin embargo, la diferencia entre ellos es su rango de variación el cual es presentado en las Tablas 1 – 3 del Anexo 2.

3.4.4 Análisis de sensibilidad

Se utilizaron los limites de confianza del 99% (LC99) o intervalos de confianza del 99% (IC99) de la media para entender la sensibilidad del sistema a los cambios del EDA (γ). Estos fueron calculados usando la siguiente formula estándar (Bevington and Robinson, 2003):

$$LC99 = t_{(n-1)} \cdot \frac{s}{\sqrt{N}} \tag{3.18}$$

$$IC99 = \bar{x} \pm t_{(n-1)} \cdot \frac{s}{\sqrt{N}} \tag{3.19}$$

donde s es la desviación estándar, $\bar{x}$ es la media, N es el tamaño de la simulación usada y t es el valor critico t de Student para los grados requeridos de libertad.

Los resultados (mostrados en las Tablas 1 – 3 del Anexo 2) muestran como los valores medios de la población estadística del exponente de difusión anómala (γ) en la ETFT pueden estar localizados en intervalos de confianza del 99% (o 1% de significancia). De esta forma, hay una confianza del 99% que el valor de γ este dentro del intervalo de 0.59932 – 0.60053, con lo que el flujo escalar adimensional (ϕ / Q_0) podría estar entre el intervalo mostrado en las Tablas 1 – 3 del Anexo 2 para *medios puramente absorbentes* ($c = 0$), *medios heterogéneos* ($c = 0.65$), y para *medios altamente dispersantes* ($c \approx 1$), respectivamente. Por ejemplo, para un *medio puramente absorbente* ($c = 0$) en la Tabla 1: para los valores de γ dentro del intervalo de 0.59932 – 0.60053, el flujo escalar adimensional (ϕ / Q_0) podría estar entre 0.14259 – 0.14261 en $\lambda_t = 0.5$, para *tiempos muy cortos* (t_0); y así sucesivamente para cada condición analizada.

El análisis de sensibilidad se llevo a cabo a través de la regresión polinomial lineal, cuadrática y cubica de los datos simulados, sin embargo sólo se presentan los resultados obtenidos mediante la regresión cúbica (Tablas 4 – 6 del Anexo 2) usando el EDA (γ) como variable predictora. Estos resultados muestran una correlación estadísticamente válida para flujo escalar adimensional (ϕ / Q_0).

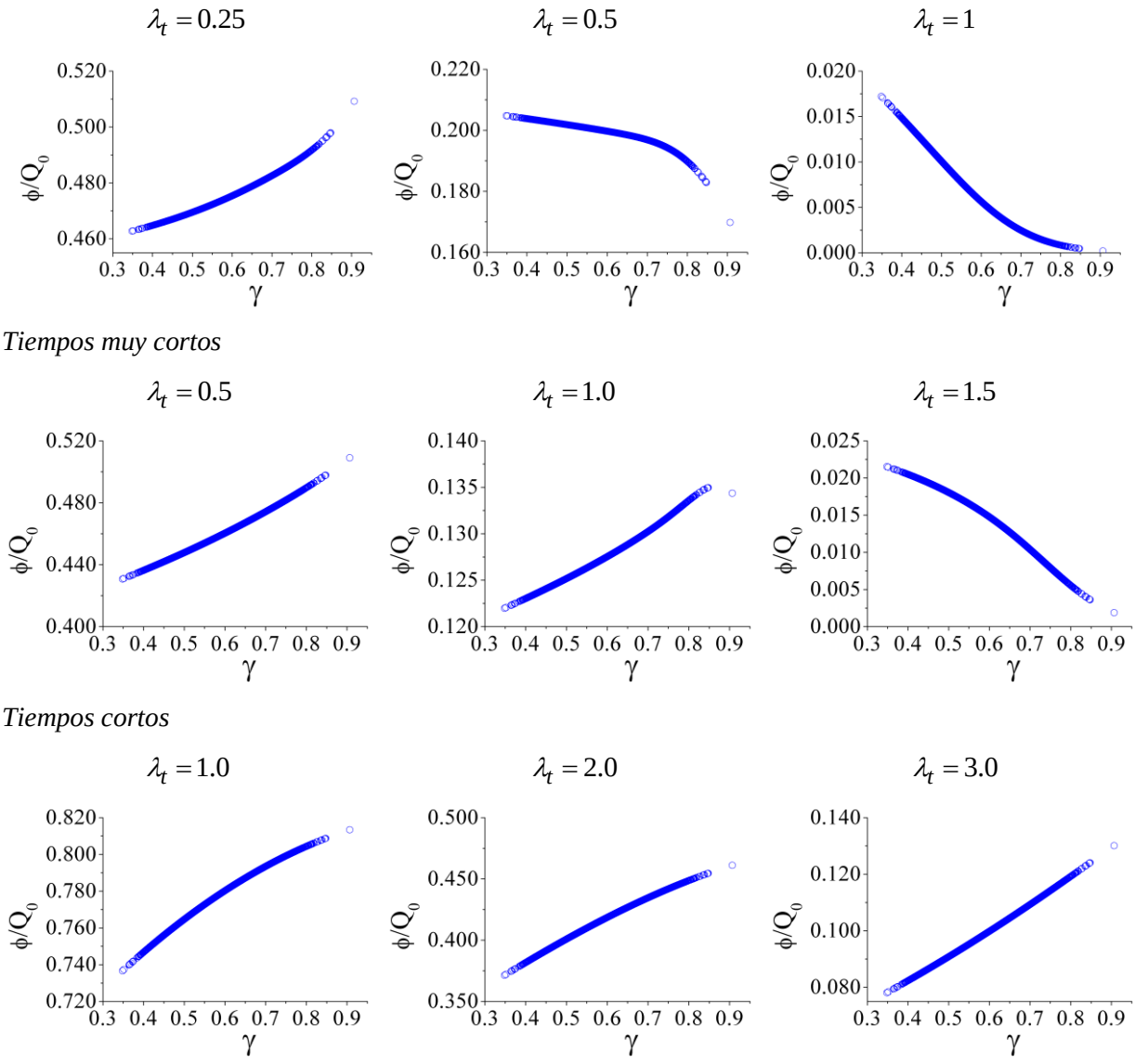

Tiempos muy cortos

Tiempos cortos

Tiempos muy largos

Figura 3.3. Medio heterogéneo ($c = 0.65$): Influencia del exponente de difusión anómala (γ) sobre el flujo escalar en un problema de fuente delta para *tiempos muy cortos* (t_0), *tiempos cortos* ($2t_0$), y *tiempos muy largos* ($6t_0$).

3.4.5 Análisis de incertidumbre

Para este análisis, los resultados son resumidos en la Tablas 7 – 9 del Anexo 2: para *medios puramente absorbentes* ($c = 0$), *medios heterogéneos* ($c = 0.65$), y *medios altamente dispersores* ($c \approx 1$), respectivamente. Para cada medio y tiempo característico de simulación, en cada caso se seleccionaron tres diferentes valores de λ_t de acuerdo al comportamiento del flujo escalar adimensional (ϕ / Q_0), como se puede observar en la Figura 2 del Anexo 2.

La explicación de estas tablas es mostrada con el siguiente ejemplo: en la Tabla 8 del Anexo 2 se observa que con el 10% de variación en el exponente de difusión anómala (γ) el flujo escalar adimensional (ϕ / Q_0) en $\lambda_t = 1.5$ varia alrededor de 15.82% para tiempos cortos. Es importante señalar que de acuerdo con los resultaos reportados en estas tablas la máxima variación observada es de alrededor del 39.36% en $\lambda_t = 1.0$ para *medios altamente dispersores* ($c \approx 1$) y *tiempos muy cortos* (Tabla 9 del Anexo 2), por otro lado en ese mismo valor de λ_t y para *tiempos muy cortos* en los tres tipos de medios se observa una variación del mismo orden, mientras que la mínima variación es de alrededor del 0.49% observada en $\lambda_t = 0.5$ para *medios puramente absorbentes* ($c = 0$) y tiempos muy cortos (Tabla 7 del Anexo 2).

Capítulo IV

Ecuación de la cinética neutrónica de orden fraccional de un reactor puntual

Las ecuaciones de cinética neutrónica puntual clásica (ECNC) de un reactor son uno de los modelos más importantes de la ingeniería nuclear, a través de éstas es posible determinar el comportamiento de la densidad neutrónica de una forma simple durante la variación de la reactividad en el tiempo, y ha sido objeto de incontables estudios y aplicaciones para entender la dinámica neutrónica y sus efectos, así como el desarrollo de diferentes métodos para su solución (Chao and Attard, 1985; Aboanber, 2003; Kinard and Allen, 2003; Chen et al., 2006; Li et al., 2007; Zhang et al., 2008; Palma et al., 2009; Li et al., 2010; Espinosa-Paredes et al., 2011).

La difusión de neutrones a través de un material es el resultado de las interacciones nucleares del sistema. En el análisis de un reactor, se asume que los neutrones no chocan entre ellos. Esto es válido porque la densidad de neutrones es mucho menor que la densidad atómica del medio. Debido a que las colisiones son casi constantes, los neutrones en el medio viajan en zig-zag. Cuando se considera un número grande de neutrones se asume que son monoenergéticos, y hay un movimiento global de neutrones de una región de alta densidad neutrónica a una de baja. Esta es la razón de porqué la ley de Fick de difusión normal es aplicada para definir la variación neta del flujo de neutrones. Sin embargo, se considera que un reactor nuclear es un sistema altamente heterogéneo debido al cambio de medio de transporte en distancias cortas y a la presencia de regiones altamente absorbentes, como ya se mencionó anteriormente. Considerando estas ideas se tiene un proceso de difusión anómalo, el cual muestra diferentes comportamientos en el espacio y tiempo. Por esta razón el proceso de transporte de neutrones en un sistema nuclear no puede describirse de manera exacta mediante la ley de difusión de Fick (Ec. 3.9) y tampoco puede ser descrito con precisión por la ley de propagación del tipo Cattaneo (Ec. 3.14).

Bajo estas consideraciones, en el trabajo de Espinosa-Paredes et al. (2011) se presenta el desarrollo de un modelo matemático el cual describe la dinámica del transporte de neutrones aplicando una ley constitutiva de orden fraccional para la densidad de corriente neutrónica (Ec 2.17). Este trabajo es presentado en el Anexo 6. El modelo desarrollado será empleado para la simulación del arranque de un reactor del tipo PWR para dos caso de inserción de reactividad: 1) inserción de reactividad en pasos; 2) inserción de reactividad en rampa.

Para la aplicación (1) el análisis numérico del comportamiento de la densidad neutrónica cuando se incrementa la potencia del reactor nuclear durante la puesta en marcha de un PWR, en el cual la inserción de reactividad es paso a paso, donde se considera una fuente de neutrones externa definida como constante de un estado inicial estable subcrítico conocido. Mientras que para la aplicación (2) se presenta el comportamiento de la variación de la densidad neutrónica cuando la potencia del reactor nuclear aumenta, donde se analiza el caso de aumento de potencia del reactor nuclear cuando se arranca en frío, el cual es un proceso de inserción de reactividad mediante el levantamiento de las barras de control de forma discontinua. Se considera que hay un tiempo de relajación asociado con una rápida variación en el flujo de neutrones y su interpretación física del orden fraccional está relacionada con los efectos no-fickianos desde el punto de vista de la ecuación de difusión de neutrones.

4.1 Ecuación de la cinética neutrónica de orden fraccional (ECNF) de un reactor puntual

Al considerar un sistema nuclear altamente heterogéneo, se toma en cuenta que el transporte de neutrones tendrá un comportamiento irregular debido al cambio de medio de transporte en distancias cortas y a la presencia de regiones altamente absorbentes. Para considerar estas anomalías del sistema de transporte de neutrones, en el trabajo de Espinosa-Paredes et al. (2011) se desarrolló una ecuación de dispersión del flujo neutrónico basada en la ecuación de la ecuación de difusión dada por la Ec. (3.6), como

$$\begin{aligned}&\frac{\tau^{\gamma}}{\upsilon}\frac{\partial^{\gamma+1}\phi(\vec{r},t)}{\partial t^{\gamma+1}}+\frac{1}{\upsilon}\frac{\partial\phi(\vec{r},t)}{\partial t}+\tau^{\gamma}\Sigma_a\frac{\partial^{\gamma}\phi(\vec{r},t)}{\partial t^{\gamma}}\\&+\Sigma_a\phi(\vec{r},t)-D\vec{\nabla}^2\phi(\vec{r},t)=S(\vec{r},t)+\tau^{\gamma}\frac{\partial^{\gamma}S(\vec{r},t)}{\partial t^{\gamma}}\end{aligned},\quad t\geq 0, \tag{4.1}$$

que es la ecuación del telegrafista de orden fraccional en el tiempo para describir la difusión anómala. Donde $S(\vec{r},t)$ es el término fuente y en este caso se considera que depende del tiempo, el cual para neutrones de un grupo de energía, es dado por (Glasstone and Sesonske, 1981)

$$S(\vec{r},t)=(1-\beta)k_{\infty}\Sigma_{a\gamma}\phi_{\gamma}(\vec{r},t)+\sum_{i=1}^{m}\lambda_i\hat{C}_i(\vec{r},t) \tag{4.2}$$

donde β es la fracción de neutrones retardados, k_{∞} es el coeficiente de multiplicación infinita, λ_i constante de decaimiento del precursor y C_i es la concentración de precursores. En esta ecuación el primer término de lado derecho representa la producción de neutrones instantáneos, mientras que el segundo término es la variación total de la formación de neutrones de precursores retardados.

Aplicando todos los conceptos y fundamentos conocidos en la Ec. (4.1) de la manera análoga como se obtiene el modelo de la ECNC (Glasstone y Sesonske, 1981; Lamarsh y Baratta, 2001) se obtiene la ecuación de la cinética neutrónica de orden fraccional (ECNF) para un reactor puntual, de la forma

$$\begin{aligned}&\tau^{\gamma}\frac{d^{\gamma+1}n(t)}{dt^{\gamma+1}}+\tau^{\gamma}\left[\frac{1}{l}+\frac{(1-\beta)}{\Lambda}\right]\frac{d^{\gamma}n(t)}{dt^{\gamma}}+\frac{dn(t)}{dt}\\&=\frac{\rho-\beta}{\Lambda}n(t)+\sum_{i=1}^{m}\lambda_i C_i+\tau^{\gamma}\sum_{i=1}^{m}\left(\lambda_i\frac{d^{\gamma}C_i}{dt^{\gamma}}\right)\end{aligned}. \tag{4.3}$$

donde n es la densidad neutrónica, l es el tiempo de vida del neutrón, ρ es la reactividad y Λ es tiempo de generación del neutrón. Cuando $\tau^{\gamma}\to 0$, se recupera la ecuación clásica, es decir,

$$\frac{dn(t)}{dt}=\frac{\rho-\beta}{\Lambda}n(t)+\sum_{i=1}^{m}\lambda_i C_i \tag{4.4}$$

La diferencia entre las Ecs. (4.3) y (4.4), es que la Ec. (4.3) tiene tres términos adicionales respecto de la ecuación clásica: 1) $\frac{d^{\gamma+1}n(t)}{dt^{\gamma+1}}$, 2) $\frac{d^{\gamma}n(t)}{dt^{\gamma}}$ y 3) $\frac{d^{\gamma}C_i}{dt^{\gamma}}$. El significado físico de estos término es que para valores de $0<\gamma<1$, hay procesos sub-difusivos, el primero y el tercero tienen relevancia para cambios rápidos en la potencia neutrónica, mientras que el segundo término tiene especial relevancia cuando los cambios en la potencia neutrónica son pequeños.

La velocidad neta de formación de neutrones de precursor retardados del grupo *i*-ésimo está dada por

$$\frac{dC_i(t)}{dt}=\frac{\beta_i}{\Lambda}n(t)-\lambda_i C_i \tag{4.5}$$

Esta ecuación fue derivada considerando que

$$\frac{d\hat{C}_i(\vec{r},t)}{dt}=\beta_i k_\infty \Sigma_a \phi(\vec{r},t)-\lambda_i \hat{C}_i(\vec{r},t) \tag{4.6}$$

donde, el primero y el segundo término de la derecha son la rapidez de formación de precursores y el decaimiento radioactivo del *i*-ésimo grupo, respectivamente. En esta ecuación β representa la fracción de neutrones retardados. Para mayores detalles sobre el procedimiento en el Anexo 6 se presenta el trabajo de Espinosa-Paredes et al. (2011).

4.2 Solución de la ECNF

La aproximación numérica de la solución del modelo de la ECNF fue obtenida aplicando el algoritmo para resolver ecuaciones diferenciales ordinarias de orden fraccional múlti-términos (EDOF) propuesto por Edwards et al. (2002) el cual es presentado en el Apéndice C, el método consiste en representar la ecuación diferencial de orden fraccional como un sistema de ecuaciones diferenciales de orden fraccional.

Considerando un grupo de neutrones retardados la ecuación de la cinética neutrónica de un reactor puntual y las condiciones iniciales son dadas por:

Ecuación de la cinética neutrónica fraccional de un reactor puntual

$$\tau^{\gamma}\frac{d^{\gamma+1}n}{dt^{\gamma+1}}+\tau^{\gamma}\left[\frac{1}{l}+\frac{(1-\beta)}{\Lambda}\right]\frac{d^{\gamma}n}{dt^{\gamma}}+\frac{dn}{dt}=\frac{\rho-\beta}{\Lambda}n+\lambda C+\tau^{\gamma}\lambda\frac{d^{\gamma}C}{dt^{\gamma}}, \tag{4.7}$$

$$n=n_0, \qquad \text{at} \qquad t=0. \tag{4.8}$$

Concentración de precursores

$$\frac{dC}{dt}=\frac{\beta}{\Lambda}n-\lambda C, \tag{4.9}$$

$$C=C_0=\frac{\beta}{\Lambda\lambda}n_0, \qquad \text{at} \qquad t=0. \tag{4.10}$$

Para simplificar la notación se usa el operador diferencial D en lugar de d/dt. Entonces, el sistema de ecuaciones puede ser escrito como:

Ecuación de la cinética neutrónica fraccional de un reactor puntual

$$D^{\gamma+1}n+a_3Dn+a_2D^{\gamma}n+a_1n=b_2D^{\gamma}C+b_1C, \qquad 0<\gamma\leq 1 \tag{4.11}$$

Concentración de precursores

$$DC+b_2C=a_0n \tag{4.12}$$

donde los coeficientes de las ecuaciones anteriores son:

$$a_0=\frac{\beta}{\Lambda} \tag{4.13}$$

$$a_1=-\frac{1}{\tau^{\gamma}}\left(\frac{\rho-\beta}{\Lambda}\right) \tag{4.14}$$

$$a_2=\left[\frac{1}{l}+\frac{(1-\beta)}{\Lambda}\right] \tag{4.15}$$

$$a_3=\frac{1}{\tau^{\gamma}} \tag{4.16}$$

$$b_1=\frac{\lambda}{\tau^{\gamma}} \tag{4.17}$$

$$b_2 = \lambda \tag{4.18}$$

Para seguir el procedimiento dado por Edwards et al. (2002), se define un cambio de variable con respecto al problema original:

Ecuación de la cinética neutrónica fraccional de un reactor puntual

$$x_1(t) = n(t) \tag{4.19}$$

$$x_2(t) = D^{\gamma} n(t) = D^{\gamma} x_1(t) \tag{4.20}$$

$$x_3(t) = Dn(t) = Dx_1(t) \tag{4.21}$$

$$x_4(t) = D^{\gamma} Dn(t) = D^{\gamma+1} n(t) = D^{\gamma} x_3(t) \tag{4.22}$$

Concentración de precursores

$$y_1(t) = C(t) \tag{4.23}$$

$$y_2(t) = D^{\gamma} C(t) = D^{\gamma} y_1(t) \tag{4.24}$$

$$y_3(t) = DC(t) = Dy_1(t) \tag{4.25}$$

el cual en forma matricial es

$$\begin{pmatrix} D^{\gamma} & 0 & 0 & 0 & 0 \\ D & 0 & 0 & 0 & 0 \\ 0 & 0 & D^{\gamma} & 0 & 0 \\ 0 & 0 & 0 & D^{\gamma} & 0 \\ 0 & 0 & 0 & D & 0 \end{pmatrix} \begin{pmatrix} x_1 \\ x_2 \\ x_3 \\ y_1 \\ y_2 \end{pmatrix} = \begin{pmatrix} x_2 \\ x_3 \\ x_4 \\ y_2 \\ y_3 \end{pmatrix} \tag{4.26}$$

donde

$$x_4 = -\sum_{j=1}^{3} a_j x_j + \sum_{j=1}^{2} b_j y_j \tag{4.27}$$

$$y_3 = a_0 x_1 - b_2 y_1 \tag{4.28}$$

Los coeficientes x_4 y y_3 se obtuvieron sustituyendo las Ecs. (4.20) – (4.22) y las Ecs. (4.24) y (4.25), en las Ecs. (4.11) y (4.12), respectivamente.

Para la forma de la derivada fraccional se aplica el método de Diethelm (Diethelm 1997a, 1977b), el cual es definido como:

$$D^{\gamma}x = \frac{1}{{}^{\gamma}\Gamma_i}\left(\sum_{p=0}^{i} {}^{\gamma}\omega_{p,i}x_{i-p} + \frac{x_0}{\gamma}\right) \tag{4.29}$$

Aquí ${}^{\gamma}\Gamma_i = (ih)^{\gamma}\,\Gamma(-\gamma)$, donde $\Gamma(-\gamma)$ es la función gamma cuyo argumento es $-\gamma$; x_0 es la condición inicial, y ${}^{\gamma}\omega_{p,0},\ldots,{}^{\gamma}\omega_{p,i}$ son los pesos de la convolución definidos como:

$${}^{\gamma}\omega_{p,i} = \begin{cases} -1 & , \quad for \quad p=0 \\ 2p^{1-\gamma} - (\kappa-1)^{1-\gamma} - (\kappa+1)^{1-\gamma} & , \quad for \quad p=1,2,\cdots,i-1. \\ (\gamma-1)\,p^{\gamma} - (p-1)^{1-\gamma} + p^{1-\gamma} & , \quad for \quad p=i \end{cases} \tag{4.30}$$

Entonces, se aplica la Ec. (4.29) con $x = x_1$ para la forma discreta de la Ec. (4.21), se obtiene:

$$D^{\gamma}x_{1,i} = \frac{1}{{}^{\gamma}\Gamma_i}\left(\sum_{p=0}^{i} {}^{\gamma}\omega_{p,i}x_{1,i-p} + \frac{x_{1,0}}{\gamma}\right) \tag{4.31}$$

De acuerdo con el método de Edward et al. (2002) se considera que

$$S_{1,i} = \sum_{p=1}^{i} {}^{\gamma}\omega_{p,i}x_{1,i-p} + \frac{x_{1,0}}{\gamma} \tag{4.32}$$

Ahora, sustituyendo la Ec. (4.32) en la Ec. (4.31):

$$D^{\gamma}x_{1,i} = \frac{1}{{}^{\gamma}\Gamma_i}\left({}^{\gamma}\omega_{0,i}x_{1,i} + S_{1,i}\right) \tag{4.33}$$

En esta ecuación se puede observar que

$$\sum_{p=0}^{i} {}^{\gamma}\omega_{p,i}x_{1,i-p} - \sum_{p=1}^{i} {}^{\gamma}\omega_{p,i}x_{1,i-p} = {}^{\gamma}\omega_{0,i}x_{1,i} \tag{4.34}$$

De acuerdo con la Ec. (4.20) $D^{\gamma}x_{1,i} = x_{2,i}$; entonces, la Ec. (4.33) puede re-escribirse como:

$$x_{2,i} = \frac{1}{{}^{\gamma}\Gamma_i}\left({}^{\gamma}\omega_{0,i}x_{1,i} + S_{1,i}\right) \tag{4.35}$$

Entonces, despejando $S_{1,i}$:

$$S_{1,i} = {}^{\gamma}\Gamma_i x_{2,i} - {}^{\gamma}\omega_{0,i} x_{1,i} \tag{4.36}$$

Combinando las Ecs. (4.32) y (4.35), se obtiene

$${}^{\gamma}\Gamma_i x_{2,i} - {}^{\gamma}\omega_{0,i} x_{1,i} = \sum_{p=1}^{i} {}^{\gamma}\omega_{p,i} x_{1,i-p} + \frac{x_{1,0}}{\gamma} \tag{4.37}$$

Para la forma discreta de la Ec. (4.21) se usa la regla del trapecio:

$$x_{1,i} = x_{1,i-1} + \frac{h}{2}\left(x_{3,i} + x_{3,i-1}\right) \tag{4.38}$$

Ahora, se procede de manera similar como en la forma discreta de la Ec. (4.20), entonces

$$S_{2,i} = x_{1,i-1} + \frac{h}{2} x_{3,i-1} \tag{4.39}$$

Sustituyendo la Ec. (4.39) en la Ec. (4.38), se tiene:

$$x_{1,i} = S_{2,i} + \frac{h}{2} x_{3,i} \tag{4.40}$$

Despejando $S_{2,i}$:

$$S_{2,i} = x_{1,i} - \frac{h}{2} x_{3,i} \tag{4.41}$$

Combinando las Ecs. (4.39) y (4.41), se obtiene:

$$x_{1,i} - \frac{h}{2} x_{3,i} = x_{1,i-1} + \frac{h}{2} x_{3,i-1} \tag{4.42}$$

Se procede de manera similar para obtener la forma discreta de las Ecs. (4.22), (4.24) y (4.25):

$${}^{\gamma}\Gamma_i\left(b_1 y_{1,i} + b_2 y_{2,i}\right) - {}^{\gamma}\Gamma_i\left(a_1 x_{1,i} + a_2 x_{2,i}\right) - \left({}^{\gamma}\Gamma_i a_3 + {}^{\kappa}\omega_{0,i}\right) x_{3,i} = \sum_{p=1}^{i} {}^{\gamma}\omega_{p,i} x_{3,i-p} + \frac{x_{3,0}}{\gamma} \tag{4.43}$$

$$\left({}^{\gamma}\Gamma_i\right) y_{2,i} - {}^{\gamma}\omega_{0,i} y_{1,i} = \sum_{p=1}^{i} {}^{\gamma}\omega_{p,i} y_{1,i-p} + \frac{y_{1,0}}{\gamma} \tag{4.44}$$

$$y_{1,i}\left(1 - \frac{b_2 h}{2}\right) - \frac{a_0 h}{2} x_{1,i} = y_{1,i-1} + \frac{h}{2}\left[a_0 x_{1,i-1} - b_2 y_{1,i-1}\right] \tag{4.45}$$

respectivamente. Ahora, con las Ecs. (4.37), (4.42), (4.43) – (4.45) se construye la forma matricial:

$$\begin{pmatrix} -{}^{\gamma}\omega_{0,i} & {}^{\gamma}\Gamma_i & 0 & 0 & 0 \\ 1 & 0 & -h/2 & 0 & 0 \\ -{}^{\gamma}\Gamma_i a_1 & -{}^{\gamma}\Gamma_i a_2 & -({}^{\gamma}\Gamma_i a_2 + {}^{\gamma}\omega_{0,i}) & {}^{\gamma}\Gamma_i b_1 & {}^{\gamma}\Gamma_i b_2 \\ 0 & 0 & 0 & -{}^{\gamma}\omega_{0,i} & {}^{\gamma}\Gamma_i \\ -(a_0 h)/2 & 0 & 0 & 1-(b_2 h)/2 & 0 \end{pmatrix} \begin{pmatrix} x_{1,i} \\ x_{2,i} \\ x_{3,i} \\ y_{1,i} \\ y_{2,i} \end{pmatrix} = \begin{pmatrix} S_{1,i} \\ S_{2,i} \\ S_{3,i} \\ R_{1,i} \\ R_{2,i} \end{pmatrix} \tag{4.46}$$

donde

$$S_{1,i} = \sum_{p=1}^{i} {}^{\gamma}\omega_{p,i} x_{1,i-p} + \frac{x_{1,0}}{\gamma} \tag{4.47}$$

$$S_{2,i} = x_{1,i-1} + \frac{h}{2} x_{3,i-1} \tag{4.48}$$

$$S_{3,i} = \sum_{p=1}^{i} {}^{\gamma}\omega_{p,i} x_{3,i-p} + \frac{x_{3,0}}{\gamma} \tag{4.49}$$

$$R_{1,i} = \sum_{p=1}^{i} {}^{\gamma}\omega_{p,i} y_{1,i-p} + \frac{y_{1,0}}{\gamma} \tag{4.50}$$

$$R_{2,i} = y_{1,i-1} + \frac{h}{2}\left[a_0 x_{1,i-1} - b_2 y_{1,i-1} \right] \tag{4.51}$$

4.3 Aplicaciones de la ECNF

Durante la puesta en marcha de un reactor nuevo o recargado, se debe prestar atención cuidadosa al problema de control, con el fin de evitar la posibilidad de un accidente. En los reactores de alto flujo y que se ha añadido un exceso de reactividad, el período del reactor puede ser muy pequeño durante el inicio. Si se permite que continúe, ya sea por un fallo mecánico o del operador, a través de la etapa de la criticidad por neutrones instantáneos, la energía superará muy rápidamente el nivel normal de operación y las consecuencias podrían ser graves. La puesta en marcha del reactor requiere una atención especial, ya que el nivel de neutrones puede ser tan bajo que podrían ser inciertas las indicaciones de los instrumentos de medida habituales. En este caso, una condición de máxima importancia es que las barras de control no se pueden mover, hasta que el flujo de neutrones sea lo suficientemente grande como para ser detectado. Este flujo

de neutrones detectable puede provenir de la fisión espontánea o una fuente de neutrones especial introducida en el reactor. Incluso en estas circunstancias, existe la posibilidad de que el reactor alcance la criticidad por neutrones del sistema en un intervalo de tiempo corto; esta situación se puede evitar regulando cuidadosamente la velocidad de ascenso de la reactividad, es decir, la velocidad de movimiento de las barras de control durante el proceso de inicio (Glasstone y Sesonske, 1981).

4.3.1 Análisis numérico del arranque de un PWR con la ECNF: inserción de reactividad en pasos

Actualmente, el método básico de seguimiento crítico es la extrapolación, y el método de *inverse count rate* se utiliza ampliamente en los reactores del tipo PWR. Debido a que no hay solución analítica para la ECNC con una fuente externa en subcrítico, aún se sigue utilizando la fórmula tradicional sub-crítica (Hetrick, 1993): $n(t \to \infty) = q_0 \Lambda / \rho_0$ (donde $n(t)$ es la densidad de neutrones en el caso $t \to \infty$, q_0 es la fuente de neutrones externa de densidad emitida por segundo, Λ es el tiempo de generación de neutrones instantáneos, y ρ_0 es el valor inicial de reactividad debida a la barra de control retirada), lo que demuestra que la sub-criticidad necesita un tiempo más largo para que el reactor alcance el estado estacionario. En realidad, cuando se lleva a cabo el arranque físico de un reactor y se retiran las barras de control para extrapolar al estado crítico se usa la fórmula sub-crítica tradicional, incluso si la reactividad añadida es igual a 1/3 del valor de extrapolación, los fenómenos de súper-criticidad a veces pueden ocurrir accidentalmente (Li et al., 2010). Frecuentemente en la práctica se tiene que a partir del apagado a fondo, la varianza de la densidad neutrónica se incrementa varios órdenes de magnitud. Al final de los pasos iniciales durante el arranque del reactor, el valor de la densidad de neutrones casi alcanza un valor estable, pero es tan pequeño que puede ser considerado como cero. Durante este proceso, el método de extrapolación se utiliza para encontrar el punto crítico. Además, después de algunos pasos, especialmente cuando el reactor está cerca de ser crítico por retardados, la densidad de neutrones llega a un nivel alto y no puede ser tomada como cero. En este momento la fórmula sub-crítica tradicional no es aplicable más. Por otro lado, Chen (1997)

ilustra algunos ejemplos sobre accidentes por criticidad, que se producen si se utiliza la cuenta del detector de neutrones para extrapolar a estado crítico mediante la fórmula sub-crítica tradicional. De acuerdo con esas ideas, Li et al. (2010) propone una nueva solución para la multiplicación de neutrones mediante la ECNC con un grupo de neutrones retardados.

El principal objetivo de esta sección es analizar los efectos del exponente de difusión anómala (γ) y el tiempo de relajación anómalo sobre el comportamiento de la densidad neutrónica durante la puesta en marcha de un PWR, y la relación entre la respuesta de la densidad neutrónica y la reactividad insertada paso a paso. Este análisis se presentó en el trabajo de Polo-Labarrios y Espinosa-Paredes (2012b) el cual se presenta en el Anexo 3.

Formulación matemática fraccional

El sistema de ECNF con un grupo de neutrones de precursores retardados dado por las Ecs. 4.7 – 4.10, al considerar una fuente neutrónica externa y sus condiciones iniciales, quedan como:

Ecuación de la cinética neutrónica de orden fraccional de un reactor puntual

$$\tau^{\gamma}\frac{d^{1+\gamma}n(t)}{dt^{1+\gamma}}+\frac{dn(t)}{dt}+\tau^{\gamma}\left[\frac{1}{l}+\frac{(1-\beta)}{\Lambda}\right]\frac{d^{\gamma}n(t)}{dt^{\gamma}} \quad , \quad 0<\gamma<1 \tag{4.52}$$
$$=\frac{\rho-\beta}{\Lambda}n(t)+\tau^{\gamma}\lambda\frac{d^{\gamma}C(t)}{dt^{\gamma}}+\lambda C(t)+q$$

$$\rho_0=-\frac{q\Lambda}{n_0} \tag{4.53}$$

$$\left.\frac{d^{\gamma}n(t)}{dt^{\gamma}}\right|_{t=0}=0 \tag{4.54}$$

$$\left.\frac{d^{\gamma+1}n(t)}{dt^{\gamma+1}}\right|_{t=0}=0 \tag{4.55}$$

Concentración de precursores

$$\frac{dC(t)}{dt}=\frac{\beta}{\Lambda}n(t)-\lambda C(t) \tag{4.56}$$

$$C(0) = \frac{\beta}{\Lambda\lambda} n_0 \tag{4.57}$$

$$\left.\frac{d^{\gamma} C(t)}{dt^{\gamma}}\right|_{t=0} = 0 \tag{4.58}$$

Para obtener la solución de la ECNF se procede de manera similar que en la sección anterior. Por lo que la representación matricial de la solución de las Ecs. (4.52) y (4.56) es:

$$\begin{pmatrix} -{}^{\gamma}\omega_{0,i} & {}^{\gamma}\Gamma_i & 0 & 0 & 0 \\ 1 & 0 & -h/2 & 0 & 0 \\ -{}^{\gamma}\Gamma_i a_1 & -{}^{\gamma}\Gamma_i a_2 & -({}^{\gamma}\Gamma_i a_2 + {}^{\gamma}\omega_{0,i}) & {}^{\gamma}\Gamma_i b_1 & {}^{\gamma}\Gamma_i b_2 \\ 0 & 0 & 0 & -{}^{\gamma}\omega_{0,i} & {}^{\gamma}\Gamma_i \\ -(a_0 h)/2 & 0 & 0 & 1-(b_2 h)/2 & 0 \end{pmatrix} \begin{pmatrix} x_{1,i} \\ x_{2,i} \\ x_{3,i} \\ y_{1,i} \\ y_{2,i} \end{pmatrix} = \begin{pmatrix} S_{1,i} \\ S_{2,i} \\ S_{3,i} \\ R_{1,i} \\ R_{2,i} \end{pmatrix} \tag{4.59}$$

donde

$$S_{1,i} = \sum_{p=1}^{i} {}^{\gamma}\omega_{p,i}\, x_{1,i-p} + \frac{x_{1,0}}{\gamma} \tag{4.60}$$

$$S_{2,i} = x_{1,i-1} + \frac{h}{2} x_{3,i-1} \tag{4.61}$$

$$S_{3,i} = \sum_{p=1}^{i} {}^{\gamma}\omega_{p,i}\, x_{3,i-p} + \frac{x_{3,0}}{\kappa} - {}^{\gamma}\Gamma_i d \tag{4.62}$$

$$R_{1,i} = \sum_{p=1}^{i} {}^{\gamma}\omega_{p,i}\, y_{1,i-p} + \frac{y_{1,0}}{\gamma} \tag{4.63}$$

$$R_{2,i} = y_{1,i-1} + \frac{h}{2}\left[a_0 x_{1,i-1} - b_2 y_{1,i-1}\right] \tag{4.64}$$

4.3.2 Análisis numérico del arranque de un PWR con la ECNF: inserción de reactividad en rampa

La reactividad es una de las propiedades más importantes en un reactor nuclear debido a que está directamente relacionado con el control del reactor. La reactividad se inserta básicamente cuando las barras de control son elevadas, en la práctica cada paso del levantamiento de las barras de control es un paso de introducción de reactividad lineal en un cierto período de tiempo. Sin embargo, las barras de control se levantan de forma discontinua, y cuando está cerca de la criticidad la longitud de cada paso tiene un intervalo de tiempo el cual permite que el transitorio dure lo suficiente para que el reactor pueda llegar a la criticidad de una manera lenta y segura. Por otro lado, la eyección o retirada descontrolada de las barras de control es el tipo más común de iniciador de un accidente de inserción de reactividad, este es un evento que ha sido el tema de trabajos anteriores (por ejemplo: Duderstadt y Hamilton, 1976; Glasstone y Sesonske, 1981; Stacey, 2001; Zhang et al., 2008; Palma et al., 2009; etc.).

El objetivo de esta sección es analizar los efectos del exponente de difusión anómala (γ) y el tiempo de relajación anómalo (τ^{γ}) en el comportamiento de la densidad neutrónica durante el arranque de un reactor nuclear de potencia, y la relación de la respuesta de la densidad neutrónica con la velocidad y duración del levantamiento de las barras de control.

Durante el arranque en frio, el reactor se encuentra en estado subcrítico y la fuente externa de neutrones no puede ser despreciada. En este caso la temperatura promedio del núcleo del reactor es menor, así como la potencia añadida, por lo que el efecto de retroalimentación de temperatura puede ser despreciado. De acuerdo con estas ideas, recientemente Zhang et al. (2008) y Palma et al. (2009), desarrollaron soluciones analíticas para el cálculo de la densidad neutrónica a partir de un conjunto de aproximaciones físicas y matemáticas, estas soluciones son presentadas en el Anexo 4. Sus formulaciones fueron basadas en las ECNC, en donde se considera una fuente de neutrones externa y la inserción de reactividad es variable en el tiempo y representada por:

$$\rho(t)=\begin{cases}\rho_s+rt, & (0\le t<t_o)\\ \rho_s+rt_0 & (t\ge t_o)\end{cases} \tag{4.65}$$

Donde ρ es la reactividad; ρ_s es la reactividad subcrítica; r es la velocidad de inserción de reactividad; t es el tiempo; t_0 es la duración de elevación de la barra de control. El resto de los parámetros han sido descritos anteriormente.

Formulación matemática fraccional

En este caso la ecuación de cinética neutrónica de orden fraccional (ECNF) con un grupo de precursores de neutrones retardados tiene la forma de las Ecs. 4.52 y 4.56, y sus condiciones iniciales son iguales a excepción de la Ec. 4.53, la cual en este caso es:

$$n(0)=\frac{q\Lambda}{\rho_s}\,. \tag{4.66}$$

Este análisis se presentó en el trabajo de Polo-Labarrios y Espinosa-Paredes (2012c) el cual se presenta en el Anexo 4.

Solución numérica fraccional

La solución numérica de la aproximación ECNF es igual que la obtenida en el caso anterior, es decir, es dada por las Ecs. 4.59 – 4.64. La diferencia principal entre ambos casos es que la perturbación de reactividad como una función del tiempo es introducida usando la Ec. (4.65), la cual es consistente con la solución numérica fraccional, presentada en este trabajo.

4.3.3 Análisis de sensibilidad e incertidumbre de la ECNF con inserción de reactividad en rampa

Se realizo el análisis de sensibilidad e incertidumbre del exponente de difusión anómala sobre el comportamiento de la densidad neutrónica obtenido con la ecuación de cinética neutrónica de orden fraccional (ECNF) de un reactor puntual, los resultados son presentados de manera extensa en el Anexo 5. Este análisis se ejecutó a través de la simulación Monte Carlo con un

tamaño de muestra superior a 65,000; el tamaño de 50,000 fue considerado como válido para aplicaciones de rutina. La sensibilidad se evaluó en términos de intervalos de confianza del 99% de la media para comprender el rango de los valores medios que pueden representar toda la población estadística de las variables de rendimiento. El análisis de regresión con un exponente de difusión anómala como la variable predictora mostró una relación cuadrática estadísticamente válida de la densidad neutrónica y la concentración de neutrones retardados.

Los parámetros usados en este estudio para realizar el análisis de sensibilidad e incertidumbre de acuerdo a su contribución relativa en la ECNF son: densidad neutrónica (n) y la densidad de precursores de neutrones retardados (C), considerando un solo grupo. Los resultados de este análisis se presentaron en el trabajo de Espinosa-Paredes et al. (2012a) el cual se presenta en el Anexo 5.

4.4 Resultados de las simulaciones

Para analizar los efectos del exponente de difusión anómala (γ) y el tiempo de relajación anómala (τ^{γ}) en el comportamiento de la densidad neutrónica en cada uno de los casos presentados anteriormente, las soluciones del modelo numérico en forma matricial (Ecs. 4.46 – 4.51, y las Ecs. 4.59 – 4.64) fueron implementadas en el programa de computadora comercial MATLAB®, donde se empleó el método de eliminación gausiana para invertir el sistema matricial dado por la Ec. (4.46).

4.4.1 Comparación entre las ECNC y las ECNF

Para observar las diferencias entre los modelos de ECNC y ECNF se utilizaron los parámetros obtenidos de Kinard y Allen (2004):

$\beta = \sum_{i=1}^{6} \beta_i = 0.007$, $\lambda = \dfrac{\beta}{\sum_{i=1}^{6} \beta_i / \lambda_i} = 0.0810958\, s^{-1}$, $\Lambda = 0.002\, s$ y $l = 0.00024\, s$, donde β_i y λ_i son presentados en la Tabla 4.1, y el valor del parámetro l fue obtenida de Glasstone y Sesonske (1981).

Las condiciones iniciales son:

$$x_{1,0} = n_0 = 1$$
$$x_{2,0} = 0$$
$$x_{3,0} = 0$$
$$y_{1,0} = C_0 = 43.1588$$
$$y_{2,0} = n0$$

donde $C_0 = \beta n_0 / \Lambda\lambda$.

Tabla 4.1. Fracción de neutrones retardados y constantes de decaimiento (Kinard y Allen, 2004).

	β_i	$\lambda_i \left(s^{-1}\right)$
Grupo 1	0.000266	0.0127
Grupo 2	0.001491	0.0317
Grupo 3	0.001316	0.1550
Grupo 4	0.002849	0.3110
Grupo 5	0.008960	1.4000
Grupo 6	0.000182	3.8700

Para observar el comportamiento de la densidad neutrónica con cambios de reactividad utilizando el modelo fraccional se utilizaron diferentes valores del exponente de difusión anómala. El experimento numérico se realizó con tres valores de reactividad:

- Caso 1: $\rho = 0.002$ (reactividad supercrítica)
- Caso 2: $\rho = 0$ (reactividad critica)
- Caso 3: $\rho = -0.002$ (reactividad subcrítica)

Los valores del exponente de difusión anómala son $\gamma = 0.99, 0.95, 0.9$ y están asociados a un tiempo de relajación anómalo igual a $\tau^{\gamma} = 10^{-5}\ s$.

Los resultados muestran que existen diferencias entre los comportamientos descritos por los modelos clásico y fraccional. Estas comparaciones permiten establecer la importancia de los términos adicionales que se tienen en el modelo fraccional (ECNF).

En los tres experimentos numéricos se observa que a medida que el valor del exponente de difusión anómalo disminuye, el valor de la densidad neutrónica también, es decir, el modelo de la ECNF sub-predice el comportamiento de la densidad neutrónica descrito por la ECNC.

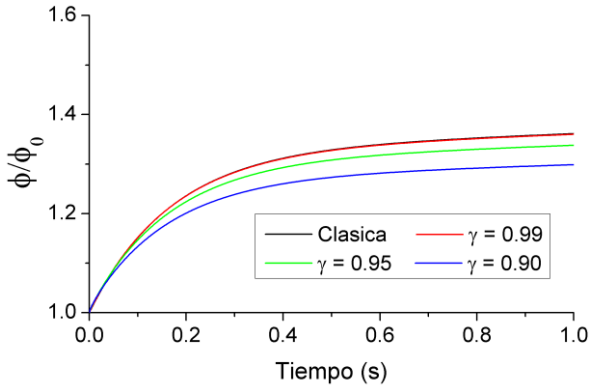

Figura 4.1. Comparación del comportamiento de la densidad neutrónica para las ECNF y ECNC, con $\rho = 0.002$.

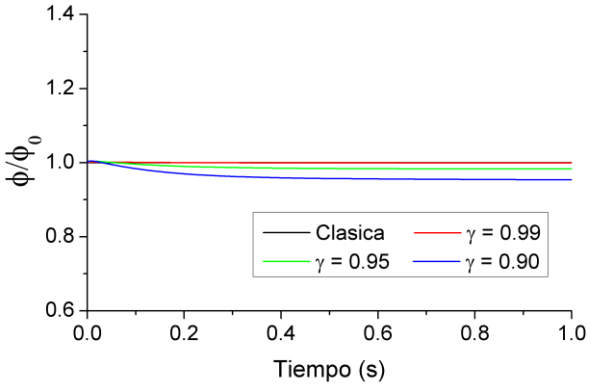

Figura 4.2. Comparación del comportamiento de la densidad neutrónica para las ECNF y ECNC, con $\rho = 0$.

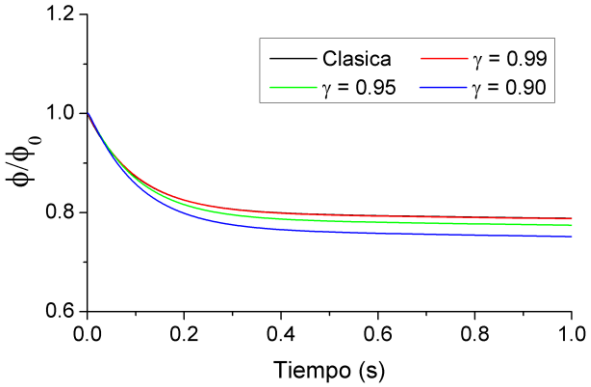

Figura 4.3. Comparación del comportamiento de la densidad neutrónica para las ECNF y ECNC, con $\rho = -0.002$.

4.4.2 Resultados de la simulación con inserción de reactividad en pasos

Para analizar los efectos del tiempo de relajación anómala (τ^{γ}) en el comportamiento de la densidad neutrónica durante el proceso de arranque de un reactor del tipo PWR con inserción de reactividad en pasos, se usaron las Ecs. (4.59) – (4.64) y la solución numérica de la formula subcrítica tradicional (presentada en el Anexo 3) para aplicar al mismo problema estudiado por Li et al. (2010). Los resultados del modelo numérico de la ECNF son comparados con la solución numérica de la ECNC

Parámetros

Los parámetros nucleares usados fueron obtenidos de Li et al. (2010), los cuales son: $\lambda = 0.0774\, s^{-1}$, $\beta = 0.0065$, $\Lambda = 10^{-4}\, s$ y $q = 1\times10^{8}\ neutrones/m^3 s$ los cuales corresponden a un reactor nuclear de agua presurizada con ^{235}U como material fisil, y el valor del parámetro $l = 0.00024\, s$ fue obtenido de Glasstone and Sesonske (1981).

Los valores de subcríticidad fueron tomados de Li et al. (2010). Asume que, antes del cambio repentino en la reactividad ocurrida en $t_1 = 0$, la cuenta inicial del detector de neutrones es igual al (n_0). Entonces el calor inicial subcrítico y la densidad de precursores de neutrones retardados puede ser obtenida usando $\rho_0 = -q\Lambda / n_0$ y $C_0 = \beta n_0 / \lambda\Lambda$, respectivamente. De acuerdo con los resultado mostrados por Li et al. (2010), el valor inicial subcrítico es $\rho_0 = -100\, mk$, cuando se extrae la barra de control por primera vez al tiempo $t_1 = 0$ el valor subcrítico insertado es $\rho_1 = -10\, mk$, después de esperar $100\, s$ (t_2) la barra de control es extraída por segunda ocasión y el valor subcrítico insertado es $\rho_2 = -5\, mk$, así sucesivamente, entonces a $t_3 = 200\, s$ el valor subcrítico es $\rho_3 = -2.5\, mk$, a $t_4 = 300\, s$ el valor subcrítico insertado es $\rho_4 = -1.25\, mk$, en $t_5 = 420\, s$ el valor subcrítico insertado es $\rho_5 = -1\, mk$, finalmente en $t_6 = 600\, s$ el valor subcrítico insertado es $\rho_6 = -0.75\, mk$.

El experimento numérico se ejecutó para los valores del tiempo de relajación anómala de: $\tau^{\gamma} = 0.01$, 0.001, y 0.0025 *s*; y los valores del exponente de difusión anómala de: $\gamma = 0.6$, 0.8 y 0.999.

Experimentos numéricos

Las Figuras 4.4 y 4.5 muestran los principales resultados obtenidos del experimento numérico (EN), los cuales presentan las características del incremento de la densidad neutrónica durante el proceso de arranque del reactor nuclear, fueron hechas usando las ECNF (Espinosa-Paredes et

al., 2011a) y las ECNC para comparar las diferencias entre estos dos modelos. Para analizar los efectos del exponente de difusión anómala, así como el tiempo de relajación anómalo sobre el incremento de la densidad neutrónica durante el proceso de arranque del reactor, se realizaron dos tipos de figuras: primero, con el tiempo de relajación fijo se usaron diferentes valores del exponente de difusión anómala; segundo, con el valor del exponente de difusión anómala se usaron diferentes valores del tiempo de relajación anómala. Adicionalmente en todos los casos se analizaron dos rangos de simulación; (a) todo el rango de simulación; y (b) el rango de simulación de 500 a 700 s. Así, los casos analizados fueron:

EN1. Se realizaron tres experimentos (Figuras 1 – 3 del Anexo 3); cada una fue realizada con un valor fijo del tiempo de relajación anómalo y diferentes valores del exponente de difusión anómala.

EN2. Se realizaron tres experimentos (Figuras 4 – 6 del Anexo 3); cada una se realizó con diferentes valores del tiempo de relajación anómalo y un valor fijo del exponente de difusión anómala.

Resultados y discusiones

Los resultados de ambos experimentos son presentados y discutidos en el Anexo 3 de manera amplia, sin embargo, debido a su similitud sólo se presentará un caso de cada experimento numérico en esta sección.

La Figura 4.4 muestra los resultados numéricos de la ECNF con los valores del exponente de difusión anómala iguales a $\gamma = 0.999, 0.8, 0.6$, y un valor de tiempo de relajación anómalo igual a $\tau^{\gamma} = 0.0025$, y la comparación con el resultado obtenido con la ECNC. El comportamiento transitorio fue analizado considerado el rango de tiempo de 0 a 700 *s* y un zoom de 500 a 700 *s*.

En la Figura 4.4a, se puede observar que el comportamiento de la densidad neutrónica descrito por ECNF con $\tau^{\gamma} = 0.0025$, para $\gamma = 0.999$ es igual al comportamiento descrito por ECNC, mientras que para $\gamma = 0.8$ y 0.6 el comportamiento de la densidad neutrónica descrito por la ECNF sobre-predice el comportamiento descrito por ECNC. Sin embargo, las diferencias entre los valores de la densidad nuclear descritos por ambos modelos son pequeñas, incluso los valores son casi iguales en todo el rango de simulación. En el zoom mostrado en la Figura 4.4b, se puede observar que los valores de la densidad neutrónica alrededor de 600 *s* descritos por ECNF con $\gamma = 0.8$ y 0.6 son muy similares entre ellos antes y después de la inserción de la reactividad; mientras que la diferencia de estos dos valores con el comportamiento descrito por ECNC son muy pequeños antes y después de la inserción de la reactividad.

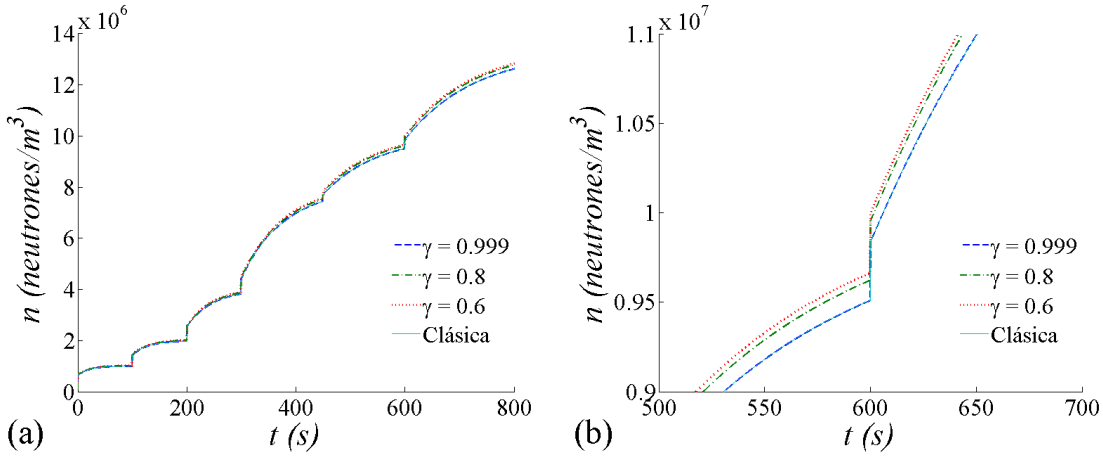

Figura 4.4. Comportamiento de la densidad neutrónica después de insertar la reactividad en pasos en un núcleo subcrítico. Con un tiempo de relajación anómalo en común igual a $\tau^{\gamma} = 0.0025$, para diferentes valores del exponente de difusión anómala ($\gamma = 0.999, 0.8, 0.6$). (a) Rango total del tiempo de simulación; (b) zoom en el rango de simulación de 500 a 700 s.

En términos generales, se puede observar que las diferencias entre el comportamiento de la densidad nuclear descrita por ECNF y ECNC son pequeñas (Figuras 1 – 3 del Anexo 3), sin

embargo, el comportamiento de la densidad nuclear descrito por ECNF sobre-predice el comportamiento descrito por ECNC. Es importante mencionar que cuando $\gamma = 0.999$ el comportamiento de la densidad nuclear es igual para cualquier valor del tiempo de relajación anómala, mientras que para $\gamma = 0.8, 0.6$ el comportamiento de la densidad nuclear cambia para cada valor de τ^{γ}.

EN 2:

La Figura 4.5 muestra los resultados de la simulación numérica usando la aproximación ECNF con el valor fijo del exponente de difusión anómala igual a $\gamma = 0.8$ y diferentes valores del tiempo de relajación anómala iguales a $\tau^{\gamma} = 0.0025$, 0.005 y 0.01, también se muestra el resultado obtenido con ECNC. El comportamiento transitorio fue analizado considerando dos rangos de tiempo: (a) de 0 a 700 s, y (b) de 500 a 700 *s*.

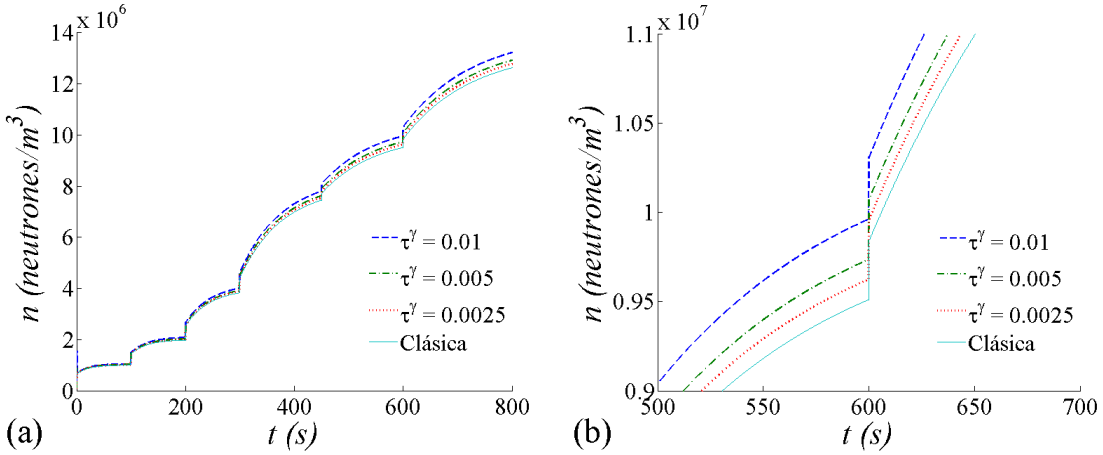

Figura 4.5. Comportamiento de la densidad neutrónica después de insertar la reactividad en pasos en un núcleo subcrítico. Con diferentes valores del tiempo de relajación anómalo ($\tau^{\gamma} = 0.0025, 0.005, 0.01$), para un valor en común del exponente de difusión anómala $\gamma = 0.8$. (a) Rango total del tiempo de simulación; (b) zoom en el rango de simulación de 500 a 700 s.

En la Figura 4.5a, se puede observar que las diferencias del comportamiento de la densidad nuclear descrito por la aproximación ECNF con $\gamma = 0.8$ y $\tau^{\gamma} = 0.0025$, 0.005 0.01 y el comportamiento descrito por ECNC son pequeños, incluso casi iguales hasta los 200 *s*, después de este punto el comportamiento descrito por la aproximación ECNF sobre-predice el comportamiento descrito por ECNC, incluso las diferencias se incrementan más en cada paso de inserción de reactividad. De manera más detallada: el comportamiento descrito por la aproximación ECNF con $\tau^{\gamma} = 0.0025$ es más grande que el comportamiento descrito por ECNC; el comportamiento descrito por ECNF con $\tau^{\gamma} = 0.005$ es más grande que el comportamiento descrito por ECNF con $\tau^{\gamma} = 0.0025$; y finalmente, el comportamiento descrito por ECNF con $\tau^{\gamma} = 0.01$ es más grande que todos los demás.

En el zoom mostrado en la Figura 4.5b, se puede observar que a los 600 *s* la reactividad es insertada, por lo que, se puede observar que los valores de la densidad nuclear obtenidos con la aproximación ECNF con $\gamma = 0.8$ para $\tau^{\gamma} = 0.0025$ y 0.005, al final del paso de inserción de reactividad anterior son más grandes que el valor de la densidad nuclear dada por ECNC, pero menor que el valor de la densidad nuclear obtenido con ECNC. Con ECNF para $\tau^{\gamma} = 0.01$ el valor de la densidad nuclear obtenida al final del paso de inserción de reactividad anterior es incluso mayor que el valor de la densidad nuclear obtenido con ECNC después de la inserción de reactividad.

En términos generales, en las Figuras 4 – 6 del Anexo 3 se puede observar que las diferencias entre los valores del comportamiento de la densidad nuclear descrito por ECNF y ECNC son pequeños, sin embargo, el comportamiento de la densidad nuclear descrito por ECNF sobre-predice el comportamiento descrito por ECNC. Es importante mencionar que cuando el valor del exponente de difusión anómala es $\gamma = 0.999$ el comportamiento de la densidad nuclear es igual para cualquier valor del tiempo de relajación anómala, mientras que para $\gamma = 0.8$, 0.6 el comportamiento de la densidad nuclear cambia para cada valor de τ^{γ}, incluso el valor de la

densidad nuclear incrementa al incrementar el valor del tiempo de relajación anómala para cada valor de γ.

La comparación de los resultados obtenidos por la aproximación ECNF y la aproximación numérica de las ecuaciones de la cinética neutrónica clásica de un reactor puntual, muestran que las diferencias son muy pequeñas; incluso cuando $\gamma = 0.999$ no hay diferencias para ningún valor de τ^{γ}.

La interpretación física de este comportamiento en la densidad nuclear del reactor es que existen procesos sub-difusivos, es decir, el movimiento de las partículas tiene un tiempo de relajación o tiempo de retraso el cual es considerado por la aproximación ECNF. Estos efectos contribuyen en cada inicio de paso de inserción de reactividad, los cuales pueden ser cruciales durante el arranque de un reactor nuclear, por lo tanto no son despreciables. En el Capítulo 3 se encontró que en un medio heterogéneo la velocidad media de la partícula es $3^{-\gamma/2}$ para $\gamma < 1$. Por esta razón el número de neutrones que se escapan de reactor decrece, y en consecuencia la densidad nuclear incrementa en este proceso de arranque.

4.4.3 Resultados de la simulación con inserción de reactividad en rampa

Con el fin de analizar los efectos de exponente de difusión anómala (γ) y el tiempo de relajación (τ) (aproximación ECNF) en el comportamiento de la densidad neutrónica durante el arranque de un reactor nuclear de potencia, se aplicó el mismo problema de estudio dado por Zhang et al., (2008) y Palma et al. (2009), es decir, que el valor de la reactividad insertada depende de la velocidad de inserción de reactividad (r), la reactividad subcrítica (ρ_s) y de la duración de extracción de cada barra de control (t_0). La solución numérica de la aproximación ECNF fue comparada con la solución analítica de Zhang et al. (2008).

Parámetros nucleares

Los parámetros nucleares usados en este trabajo fueron obtenidos del trabajo de Palma et al. (2009) los cuales son: $\lambda = 0.001 s^{-1}$, $\beta = 0.0075$, $\Lambda = 0.0015 s$ y $q = 10^8\ n's/cm^3 s$, el valor del parámetro $l = 0.00024 s$ fue obtenido de Glasstone y Sesonske (1981). Los valores subcríticos usados son -6 y $-10\ pcm$, se consideran dos tipos de velocidad de extracción de la barra de control, que son $10\ pcm/s$ y $40\ pcm/s$. Dos valores de la duración de extracción de la barra de control, que son 5 s y 10 s. el tiempo de relajación anómala es $\tau^{\gamma} = 10^{-5} s$; el exponente de difusión anómala toma los valores de $\gamma = 0.99, 0.9, 0.8, 0.6, 0.3$.

Experimentos numéricos

Las Figuras 4.6 y 4.7 muestran los principales resultados obtenidos por los experimentos numéricos (EN), los otros resultados son presentados en el Anexo 4. Los casos analizados fueron:

EN-1.

Comparación con la solución analítica (Zhang et al., 2008) usando $\rho_s = -6\ pcm$, $r = 10\ pcm/s$ y $t_0 = 5 s$ (Figura 1 del Anexo 4).

EN-2.

Efectos de la velocidad de extracción de la barra de control ($r = 10\ pcm/s$, $r = 40\ pcm/s$) usando una duración de extracción de barra igual a $t_0 = 5 s$, y una reactividad subcrítica de $\rho_s = -6\ pcm$ en la respuesta de la densidad neutrónica, para $\gamma = 0.99, 0.9, 0.6, 0.3$ (Figura 2 del Anexo 4).

EN-3.

Efectos de la duración de extracción de la barra de control ($t_0 = 5\,s$ and $t_0 = 10\,s$) usando un valor de velocidad de extracción igual a $r = 10\,pcm/s$ y una reactividad subcrítica de $\rho_s = -6\,pcm$ en la respuesta de la densidad neutrónica, para $\gamma = 0.99, 0.9, 0.6, 0.3$ (Figura 3 del Anexo 4).

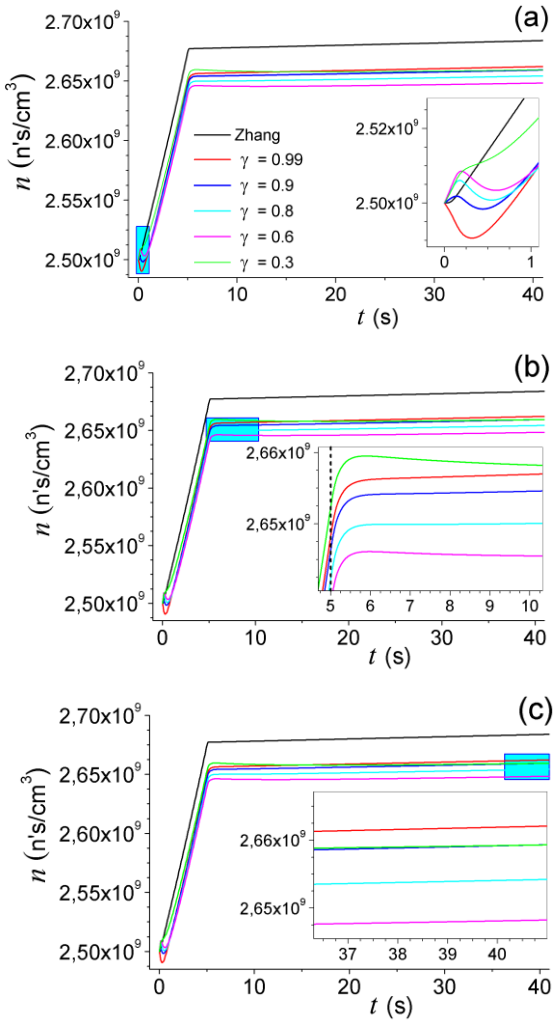

Figura 4.6. Comparación de la respuesta de la densidad neutrónica entre ECNC y ECNF, con $r = 10\,pcm/s$, $\rho_s = -6\,pcm$ y $t_0 = 5\,s$. El área sombreada representa diferentes aproximaciones para tiempos de escala pequeños: a) Inicio del arranque; b) después de haber levantado las barras de control; y c) después de un tiempo de simulación largo.

EN-4.

Efectos en la densidad neutrónica cuando la reactividad subcrítica es $\rho_s = -10\ pcm$, los valores de la duración de extracción de la barra de control son $t_0 = 1\,s$ y $t_0 = 4\,s$ y los valores de la velocidad de extracción de la barra de control son $r = 40\ pcm/s$ y $r = 10\ pcm/s$, respectivamente, para $\gamma = 0.99, 0.9, 0.6, 0.3$ (Figura 4 del Anexo 4).

Análisis de resultados

En esta sección presentamos y discutimos EN-1 y EN-4, los cuales se muestran en las Figuras 4.6 y 4.7, respectivamente. Sus análisis y discusiones son los siguientes:

EN 1.

Los resultados mostrados en la Figura 4.6 son la solución numérica de la aproximación ECNF con diferentes valores del exponente de difusión anómala (γ) y la solución analítica de ECNC obtenida por Zhang et al. (2008). El comportamiento transitorio fue analizado considerando tres escalas de tiempo pequeñas: (a) cuando comienza el arranque; (b) después de haber levantado la barra de control; y (c) al final del tiempo de simulación.

En términos generales, los resultados muestran que el comportamiento descrito por la aproximación ECNF sub-predice el comportamiento descrito por ECNC después del levantamiento de las barras de control, cuya diferencia entre estos dos modelos es de aproximadamente del orden de $2.4\times10^7\ \ n's/cm^3$, prácticamente para todos los valores de γ (Figura 4.6a).

Para tiempos de escala pequeños se observa un retraso en el comportamiento de la densidad neutrónica debido al tiempo de relajación anómalo (este retraso es diferente para cada valor de γ), a continuación se describe:

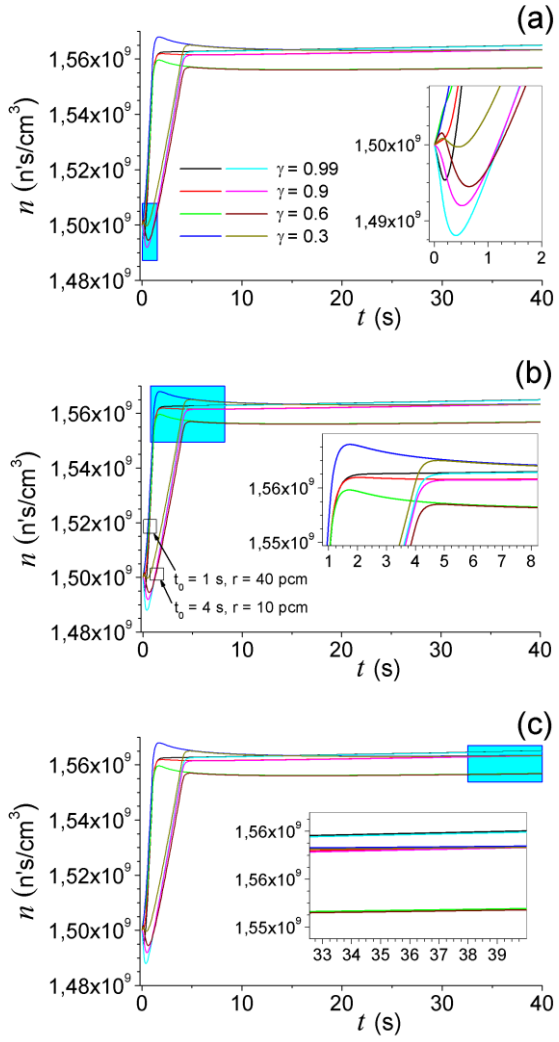

Figura 4.7. Efectos en la respuesta de la densidad neutrónica cuando la reactividad subcrítica es $\rho_s = -10\ pcm$, la duración de levantamiento de las barras de control es $t_0 = 1\,s$ y $t_0 = 4\,s$ y la velocidad de levantamiento de las barras de control es $r = 40\ pcm/s$ y $r = 10\ pcm/s$, respectivamente. El área sombreada representa diferentes aproximaciones para tiempos de escala pequeños: a) Inicio del arranque; b) después de haber levantado las barras de control; y c) después de un tiempo de simulación largo.

- Cuando $\gamma = 0.99$ la aproximación ECNF tiene el siguiente comportamiento: la Figura 4.6a muestra un zoom (área sombreada) en el rango de tiempo de 0 a 1 *s*. En este rango la densidad neutrónica decrece debido a la existencia de procesos sub-difusivos los cuales

impiden el libre movimiento de los neutrones, por lo que el movimiento de los neutrones es retrasado, en consecuencia la densidad neutrónica decrece. Físicamente este comportamiento se debe a que las varillas de control no están lo suficientemente extraídas, por lo que muchos de los neutrones generados por la fuente y por los procesos de fisión son absorbidos. La densidad neutrónica alcanza un mínimo local aproximadamente a los 0.25 *s*, y este es menor que el valor inicial de la densidad neutrónica ($n_0 = 2.5\times10^9\ n\acute{}s/cm^3 s$). Después de $t = 1\,s$ la densidad neutrónica comienza a incrementar debido a que se absorben mucho menos neutrones por las varillas de control y la generación de éstos es mayor. Después de haber levantado las barras de control, a los 5 *s* (zoom en la Figura 4.6b) los efectos en el tiempo de relajación sobre el comportamiento de la densidad neutrónica aún son importantes respecto a la descripción obtenida con ECNC. Es interesante observar que cuando la varilla de control se detuvo (a los 5 *s*) la densidad neutrónica continúa incrementando suavemente. Finalmente, en la Figura 4.6c se muestra aparentemente el estado estacionario de ECNF el cual es más pequeño que el obtenido con ECNC, como se mencionó anteriormente.

- Para $\gamma = 0.9$, 0.8, y 0.6, el comportamiento de la densidad neutrónica descrito por ECNF es mostrado en las Figuras 4.6a, b, y c. En los primeros instantes (menores a 0.2 *s*, en la Figura 4.6a) la densidad neutrónica se incrementa, se observa que sobre-predice el comportamiento descrito por ECNC. Mientras se levantan las barras de control la densidad neutrónica alcanza un máximo aproximadamente en 0.2 *s*, posteriormente hay un cambio en las tendencias observadas, cuya magnitud es debida al valor de γ, es decir, cuando decrece γ, los efectos de retraso en la densidad neutrónica son menores. La interpretación física es que cuando se incrementa el valor de γ, también aumentan los efectos de absorción, pero el valor de la densidad neutrónica no llega a ser menor que el valor de la densidad neutrónica inicial ($n_0 = 2.5\times10^9\ n\acute{}s/cm^3 s$). Es importante notar que este comportamiento es debido a que la producción de neutrones por la fuente externa ($q = 10^8\ n\acute{}s/cm^3 s$) y el levantamiento de las barras de control comienzan al mismo tiempo, entonces la densidad neutrónica se

incrementa pero la capacidad de absorción de las barras de control es mayor que la capacidad de multiplicación neutrónica, por lo que la densidad neutrónica decrece suavemente. Sin embargo, cuando las varillas de control están lo suficientemente levantadas, la densidad neutrónica comienza a incrementarse. Para $\gamma = 0.8$, y 0.6 (zoom en las Figuras 4.6 b y c) el comportamiento es similar al obtenido con $\gamma = 0.99$, sin embargo, la densidad neutrónica es más pequeña. Este comportamiento no se observa con ECNC debido a que los efectos de absorción retardada por la presencia de las barras de control no son considerados.

- Para $\gamma = 0.3$ (zoom en la Figura 4.6a), se puede observar que la densidad neutrónica incrementa continuamente hasta que el comportamiento descrito por ECNF y ECNC se interceptan aproximadamente en $n = 2.51 \times 10^9 \; n's/cm^3$, lo cual indica que bajo estas condiciones, ambas aproximaciones tienen la misma predicción. Antes de este punto el comportamiento de ECNF sobre-predice el comportamiento de ECNC, y después de este punto se puede observar que lo sub-predice. Como se discutió anteriormente; antes de este punto la multiplicación de los neutrón es más grande que los efectos de absorción, y después de este tiempo se frena la generación de neutrones (cambian en la tendencia) pero continúa, y sigue siendo mayor que los efectos de absorción. La Figura 4.6b muestra que aproximadamente a los 5.5 *s* los efectos de absorción son menores que los observados para otros valores de $\gamma \neq 0.3$ Después de un tiempo de simulación largo (Figura 4.6c) le densidad neutrónica tiene los mismos valores de la densidad neutrónica que con $\gamma = 0.9$.

En términos generales, los resultados muestran que los efectos del tiempo de relajación anómalo sobre el valor de la densidad neutrónica alcanzado después de haber levantado las barras de control son menores, y los efectos de exponente de difusión anómala son relevantes al comienzo y final del levantamiento de las barras.

EN 4.

Los resultados son mostrados en la Figura 4.7. El comportamiento del transitorio fue analizado considerando tres escales de tiempo pequeñas: (a) cuando el arranque está comenzando; (b) después de haber levantado las barras de control; y (c) al final del tiempo de simulación.

Este EN fue realizado con $\rho_s = -10\ pcm$ en lugar de $\rho_s = -6 pcm$, para observar mejor los efectos sub-difusivos debido a la velocidad y la duración del levantamiento de las barras de control.

En este EN para una velocidad de levantamiento de barras de control igual a $r = 10\ pcm/s$ la duración de levantamiento es mayor que para la velocidad de $r = 40\ pcm/s$, pero al final de ambos procesos la reactividad total insertada es la misma. De acuerdo con esto, en el zoom de la Figura 4.7a se observa que, para $r = 40\ pcm/s$ y $t_0 = 1\ s$ con los valores del exponente de difusión anómala iguales a $\gamma = 0.99,\ 0.9,\ 0.6,\ 0.3$ la aproximación ECNF presenta un comportamiento de la densidad neutrónica similar al obtenido con los valores de $r = 10\ pcm/s$ y $t_0 = 4\ s$ pero la magnitud obtenida en el primer caso es mayor, es decir, en ambos casos se presentan los mismos efectos físicos de absorción. En el zoom de la Figura 4.7b, se puede ver que el comportamiento de la densidad neutrónica con $r = 40\ pcm/s$ y $t_0 = 1\ s$ para cada valor correspondiente de γ, se alcanzan valores más grandes que con $r = 10\ pcm/s$ y $t_0 = 4\ s$. En la Figura 4.7c se observa que para escalas de tiempo grandes, se alcanza un aparente estado estacionario, cuyas diferencias se deben al valor de γ.

En términos generales, para grandes escalas de tiempo se puede observar que cuando las varillas fueron levantadas, el incremento de la densidad neutrónica no es igual al valor del estado estacionario obtenido con ECNC con respecto a ECNF. Para escalas de tiempo cortas la aproximación de ECNF presenta procesos sub-difusivos caracterizados por las absorciones y dispersiones cuyas magnitudes dependen del valor de γ.

4.4.4 Resultados del análisis de sensibilidad e incertidumbre de la ECNF con inserción de reactividad en rampa

Para analizar la dinámica del (EDA) se realizaron experimentos numéricos, los cuales son necesarios cuando la variación de la densidad neutrónica y la concentración de precursores de neutrones retardados son importantes con respecto al tiempo. Por lo tanto, durante la simulación de arranque de un reactor con inserción de reactividad en rampa se realizó el análisis de sensibilidad e incertidumbre, considerando diferentes tiempos de simulación los cuales son: 1 *s*, 3 *s*, 5 *s* y 20 *s*. Para cada tiempo se presenta la respuesta de la densidad neutrónica con respecto al EDA en las Figuras 4 y 5 del Anexo 5, en donde los parámetros usados para realizar el análisis de sensibilidad e incertidumbre de acuerdo a su contribución relativa en la ECNF son: densidad neutrónica (n) y la densidad de precursores de neutrones retardados (C), considerando un solo grupo. El comportamiento de la potencia neutrónica es aproximadamente cuadrático con respecto al EDA y se puede observar que cuando el EDA se incrementa, la densidad neutrónica decrece y viceversa. Mientras que el comportamiento de la concentración de precursores de neutrones retardados como una función del EDA es aproximadamente de segundo orden, la tendencia de la concentración de precursores de neutrones retardados con el EDA es similar a la densidad neutrónica. Es decir, cuando el EDA incrementa, la concentración de precursores de neutrones retardados decrece y viceversa.

Mediante el análisis del RSD de los valores expresados en porcentajes de los principales parámetros de la ECNF (γ, n, y C) tomados a diferentes tiempos transcurridos de simulación (1 *s*, 3 *s*, 5 *s* y 20 *s*) de arranque del reactor nuclear, se puede observar que para un tamaño de simulación N más grande que 50,000 (y superior a 65,000), el valor del RSD se hace prácticamente constante e independiente del tamaño de simulación. Sin embargo, el tamaño óptimo N usado en este trabajo fue 50,000 (Figuras 1 – 3 del Anexo 5).

Análisis de sensibilidad

Los resultados de la Tabla 1 del Anexo 5 muestran cómo los valores medios de la población estadística de los parámetros en la ECNF pueden estar localizados (en 99% de confianza o 1% de significancia) en los intervalos respectivos de nivel de confianza del 99%, la muestra de los

valores iniciales son $\gamma_0 = 0.63$, $n = 2.5 \times 10^9 n\acute{}s / cm^3$ y $C = 1.25 \times 10^{13} n\acute{}s / cm^3$. De esta forma, hay un 99% de confianza de que el EDA (γ) esté en cualquier lugar dentro del intervalo de 0.629 – 0.630.

También se realizó un análisis de sensibilidad de los datos simulados (Tabla 2 del Anexo 5) usando las regresiones lineal y polinomial, utilizando el exponente de difusión anómala (γ) como la variable predictora. Los resultados mostraron correlaciones cuadráticas estadísticamente válidas para la densidad neutrónica y para la concentración de los precursores.

Análisis de incertidumbre

Los resultados de este análisis son resumidos en la Tabla 3 del Anexo 5, en la cual se muestran los porcentajes de variación de los valores de la densidad neutrónica (n) y de la concentración de precursores (C) que se obtienen al variar en 1% el valor del exponente de difusión anómala (γ).

Conclusiones

Este trabajo se centra en observar el comportamiento en espacio y tiempo de los procesos de difusión anómala, considerando un sistema nuclear altamente heterogéneo, donde se considera que el transporte de neutrones tiene un comportamiento irregular, el cual se debe al cambio de medio de transporte en distancias cortas y a la presencia de regiones altamente absorbentes. Por esta razón el proceso nuclear del sistema no puede describirse correctamente mediante la ley de difusión de Fick, y tampoco puede ser descrito con precisión por la ley de propagación del tipo Cattaneo.

Por lo que, para describir estos procesos, primeramente se desarrolló una aproximación de la ecuación de Boltzmann que considere los efectos de difusión anómala, la cual fue obtenida utilizando la ecuación constitutiva de orden fraccional del vector densidad de corriente para un medio general (Ec. 2.17), que al combinarla con la ley de conservación que gobierna la colisión de las partículas y los procesos de reacción (Ec. 2.2), se obtiene la ecuación del telegrafista de orden fraccional en el tiempo de la aproximación P_1 de Boltzmann.

La ecuación se resolvió de manera numérica considerando diferencias finitas de orden fraccional con esquema explícito y la implementación se realizó en MATLAB©. De los resultados obtenidos destacan los siguientes: con el modelo desarrollado se describe una velocidad de la onda igual a $3^{-\gamma/2}$ para $\gamma<1$, y también se encontró que este modelo ofrece la mejor estimación para un medio puramente absorbente donde la mayoría de las aproximaciones desarrolladas anteriormente fallan (Figura 3.1).

Debido a la poca información respecto al tema de la difusión anómala, el uso de este modelo está limitado por el valor del exponente de difusión anómala (γ). Por lo que para saber qué efectos tiene este parámetro en el comportamiento descrito por el modelo desarrollado, se

realizó un análisis de sensibilidad e incertidumbre sobre el exponente de difusión anómala en la ETFT, el cual se llevó a cabo con la simulación Monte Carlo. Donde la sensibilidad fue evaluada para intervalos de confianza del 99% del valor medio, para comprender el rango de los valores medios que pueden representar toda la población estadística de las variables; y así mismo se observó de qué manera la incertidumbre se propaga.

Para observar los efectos sub-difusivos en la dinámica del transporte de neutrones dentro de un reactor nuclear se utilizó la ecuación de la cinética neutrónica para un reactor puntual, el desarrollo de este modelo fue presentado en el trabajo de Espinosa-Paredes et al. (2011). Este modelo se empleó para la simulación del arranque de un reactor del tipo PWR para dos casos de inserción de reactividad: 1) inserción de reactividad en pasos; e 2) inserción de reactividad en rampa, en este último se realizó un análisis de sensibilidad e incertidumbre sobre los efectos del coeficiente de difusión anómala sobre el comportamiento de la densidad neutrónica y la concentración de precursores. En estos casos la solución numérica fue obtenida aplicando el método propuesto por Edwards et al. (2002).

En el primer caso sobre el PWR, en el cual la inserción de reactividad es paso a paso, el principal resultado de este caso fue que el tiempo de relajación anómalo se asocia con una rápida variación en el flujo de neutrones debido a la naturaleza sub-difusiva la cual es una función del tiempo de relajación anómala, es decir, la generación y fuga de neutrones en el reactor tiene un tiempo de retardo.

El caso de inserción de reactividad en rampa se analizó el caso de aumento de potencia del reactor nuclear cuando se arranca en frío. Los principales resultados fueron: 1) las ecuaciones de la cinética neutrónica clásica (ECNC) sobre-predice la densidad neutrónica obtenida con la aproximación de la cinética neutrónica de orden fraccional (ECNF); para tiempos de escala cortos durante el levantamiento de las barras de control y una rápida inserción de reactividad la aproximación ECNF predice una mayor multiplicación neutrónica, lo que puede causar un disparo de potencia del reactor.

En el caso de inserción de reactividad en rampa se evaluó la sensibilidad e incertidumbre del exponente de difusión anómala en la ECNF de un reactor puntual. Donde mediante el análisis de regresión con el EDA como la variable predictora, mostró una relación cuadrática estadísticamente válida para la densidad neutrónica y la concentración de neutrones retardados

Los resultados de este trabajo muestran que en los sistemas altamente heterogéneos, así como en medios puramente absorbentes existen procesos sub-difusivos. Los cuales durante el arranque de un reactor nuclear son relevantes, bebido a que durante la puesta en marcha de un reactor nuevo o recargado, se debe prestar atención cuidadosa al problema de control, con el fin de evitar la posibilidad de un accidente. Por lo que, es importante la relación del nivel de densidad neutrónica y su razón de cambio con la velocidad de inserción de reactividad para un arranque seguro.

Apéndices

Apéndice A

Método de diferencias finitas para derivadas de orden fraccional

En esta sección se presenta el esquema de solución numérica fraccional para ecuaciones diferenciales ordinarias de orden fraccional. El cual es un método de diferencias finitas que utiliza la forma discreta de la aproximación de Caputo para la derivada fraccional de orden $0<\alpha<1$, cuya definición es (Podlubny, 1999):

$$\frac{\partial^{\alpha}u(x,t)}{\partial t^{\alpha}}=\frac{1}{\Gamma(1-\alpha)}\int_0^t(t-\eta)^{-\alpha}\frac{\partial u(x,\eta)}{\partial \eta}d\eta \qquad \text{(A-1)}$$

Para $1<\beta<2$, se emplea la aproximación de Riemann-Liouville, cuya definición es (Podlubny, 1999):

$$\frac{\partial^{\beta}u(x,t)}{\partial t^{\beta}}=\frac{1}{\Gamma(2-\beta)}\frac{\partial^2}{\partial t^2}\int_0^t\frac{u(x,\xi)}{(t-\xi)^{\beta-1}}d\xi \qquad \text{(A-2)}$$

Se asume que la solución de la EDOF es lo suficientemente suave. Para la estabilidad se utiliza la formula de Grünwald de desplazamiento para aproximar la derivada fraccional de Riemann-Liouville (Ec. 2) (Meerschaert y Tadjeran, 2003).

Para establecer el esquema de la aproximación numérica, se tiene que $t_j=j\theta\ \ (j=0,1,2,\ldots,m)$ es el tiempo de integración, con $0\le t_j\le T$ y $\theta=\frac{T}{m}$; para el mayeo de la dirección espacial se tiene que $h=\frac{L}{n}>0$ y $x_i=ih\ \ (i=0,1,2,\ldots,n)$.

Por lo tanto, se emplean las siguientes aproximaciones para las derivadas en el tiempo de orden fraccional y entero que se usarán en este trabajo (Yang et. al, 2008; Podlubny, 1999; Meerschaert and Tadjeran, 2003; Case et. al, 1953):

$$\frac{\partial^{\gamma}\phi(x,t)}{\partial t^{\gamma}} = \frac{\theta^{1-\gamma}}{\Gamma(2-\gamma)}\sum_{k=0}^{j}\frac{\phi(x_i,t_{j+1-k})-\phi(x_i,t_{j-k})}{\theta}\left[(k+1)^{1-\gamma}-k^{1-\gamma}\right]+\mathbf{O}(\theta) \qquad \text{(A-3)}$$

$$\frac{\partial\phi(x,t)}{\partial t} = \frac{\phi(x_i,t_{j+1})-\phi(x_i,t_j)}{\theta}+\mathbf{O}(\theta) \qquad \text{(A-4)}$$

Para la aproximación de la derivada de orden fraccional de Riemann-Liouville $\partial^{\beta}u(x,t)/\partial t^{\beta}$, como ya se mencionó anteriormente, se usa la fórmula de Grünwald de desplazamiento (Meerschaert and Tadjeran, 2003):

$$\frac{\partial^{\alpha}\phi(x,t)}{\partial t^{\alpha}} = \frac{1}{\theta^{\alpha}}\sum_{k=0}^{j+1}g_k\phi(x_i,t_{j-k+1})+\mathbf{O}(\theta+h) \qquad \text{(A-5)}$$

donde $\alpha = 1+\gamma$, y g_k son los pesos de Grünwald normalizados, definidos como

$$g_0 = 1 \quad \text{and} \quad g_k = (-1)^k\frac{(\alpha)(\alpha-1)\cdots(\alpha-k+1)}{k!} \quad \text{for} \quad k = 1,2,3,\ldots \qquad \text{(A-6)}$$

Notar que los pesos normalizados sólo dependen del exponente de difusión anómala y del índice k.

Apéndice B

Método de Monte Carlo

El método de Monte Carlo se basa en el muestreo del vector de parámetros de entrada en una secuencia aleatoria, se ejecuta el código computacional del modelo del sistema para cada muestra del vector para obtener una muestra estadística correspondiente a las variable de salida del vector, posteriormente se estiman las características de estas variables de salida usando las muestras generadas. Una de las ventajas del método de Monte Carlo es que todos los métodos estadísticos estándar y las pruebas se pueden utilizar para estimar la distribución de las variables de salida, así como para evaluar cualquier hipótesis. Esto hace que sea el método más sencillo y potente disponible en la literatura científica para hacer frente a un análisis de sensibilidad y la propagación de la incertidumbre en los modelos complejos. Aunque existen ecuaciones para estos procesos de propagación de errores (Bevington y Robinson, 2003), estas ecuaciones son aproximadas (Verma, 2005), y su uso en la evaluación de los modelos complejos es muy engorroso. Estas consideraciones hacen al método de Monte Carlo mucho más adecuado para el estudio de simulación actual.

Metodología

La metodología de simulación de Monte Carlo puede ser implementada de acuerdo con los siguientes pasos (Espinosa-Paredes et al., 2010):

Paso 1. Se generan números aleatorios uniformemente distribuidos en el espacio $(0,1)$, es decir, muestras de una distribución uniforme $U(0,1)$: Esta distribución fue simulada usando el algoritmo de Marsenne Twister de Matsumoto y Nishimura (1998), el cual es un generador ampliamente utilizado con un periodo muy de largo $\left(2^{19937}-1\right)$. Con lo que los flujos necesarios de números aleatorios independientes e idénticamente distribuidos $\left(IID\,U(0,1)\right)$ de 64 bits fueron generados.

Paso 2. Se prueban los números aleatorios para ver si se parecen a una distribución idéntica e independiente $IID\,U(0,1)$ de variantes aleatorias: Cada secuencia fue probada de aleatoriedad usando el método gráfico de dos y tres dimensiones Marsaglia (1968). Los datos simulados claramente llenan el espacio $(0,1)$ como lo requiere esta prueba de aleatoriedad de dos y tres dimensiones. Otra prueba de aleatoriedad también se aplica, la cual comprueba la cantidad de números individuales que son repetidos en la secuencia dada de números aleatorios, y si tales números repetidos son pocos, los números aleatorios simulados pueden usarse de manera segura para futuras aplicaciones. En promedio, sólo alrededor de 1 de 100,000 números de una secuencia individual de $IID\,U(0,1)$ se repitió.

Paso 3. Convertir los números aleatorios en datos con una distribución normal $N(0,1)$: para esto el método polar de Marsaglia y Bray (1964) fue empleado. Dos corrientes paralelas de números aleatorios (R1 y R2) fueron utilizados para la generación de un conjunto de datos con distribución $IID\,N(0,1)$. La normalidad de los datos simulados fue examinada gráficamente. Prácticamente no se encontraron números repetidos en las pruebas con más de 100,000 números en las muestras de datos aleatorios normales. Por lo tanto, los datos fueron considerados como de alta calidad para representar una distribución normal, y por lo tanto podrían utilizarse de forma segura para futuras aplicaciones. Los hemos utilizado aquí para la comprensión de la sensibilidad y el análisis de la incertidumbre del exponente de difusión anómala en las ecuaciones de difusión y en ECNF.

Paso 4. Se realiza el análisis de sensibilidad y de incertidumbre del exponente de difusión anómala en las ecuaciones de difusión y en la ECNF: se utilizaron estos datos aleatorios normales $IID\,N(0,1)$ para la evaluación las relaciones de sensibilidad entre exponente de difusión anómala con la densidad de partículas (en el caso de la ecuación de difusión); y con la densidad de neutrones instantáneos y con la densidad de neutrones de precursores retardados (en caso de ECNF).

Apéndice C

Ecuaciones diferenciales ordinarias de orden fraccional múlti-términos

En esta sección se presenta el procedimiento del método para la solución de una ecuación diferencial ordinaria de orden fraccional (EDOF) múlti-términos propuesto por Edwards et al. (2002), la cual es una aproximación numérica que se calcula reduciendo el problema (EDOF) a un sistema de ecuaciones diferenciales ordinarias y fraccionales, cada una cercana al primer orden (Edwards et al., 2002).

El enfoque del método es para resolver una ecuación diferencial lineal múlti-términos y de alto orden, de la forma general

$$\sum_{i=0}^{n} b_i D^{\alpha_i} y(t) = g(t), \qquad b_i \in \mathbb{R}, \qquad b_n \neq 0, \qquad \alpha_i \geq 0, \qquad \text{(C-1)}$$

como un sistema de ecuaciones diferenciales ordinarias y fraccionales de orden ≤ 1. Se asume, por conveniencia, que $i > j \Rightarrow \alpha_i > \alpha_j$.

Derivada fraccional

En esta aplicación se utiliza el desarrollo convencional que Caputo propone (Caputo, 1976) en su versión de derivada fraccional, en lugar de la versión de Riemann-Liouville. Así, D_*^q denota el operador de derivada fraccional de orden $q \in \mathbb{N}$ el cual es denotado y definido por Gorenflo et al. (Gorenfo, F. Mainardi, 1997), como

$$D_*^q := J^{m-q} y^m(t),$$

donde m es un entero definido por la relación $m-1 < q < m$ y J^μ es el operador integral fraccional,

$$J^\mu g(t) = \frac{1}{\Gamma(\mu)} \int_0^t (t-u)^{\mu-1} g(u)\, du.$$

La razón de esta preferencia es por que cuando el operador fraccional es la Ec. (C-1) como una derivada fraccional de Caputo, con las condiciones apropiadas en la función $g(u)$ y con los valores iniciales $y^i(0) = y_0^i,\ i = 0,\ldots,m-1$ especificados, el sistema tendría una solución única. Si se interpreta el operador diferencial fraccional como derivada fraccional de Riemann-Liouville, se tendría que especificar las condiciones iniciales en términos de las integrales fraccionales y sus derivadas. Las condiciones iniciales requeridas por la definición de Caputo coinciden con los estados físicos conocidos, y estos conducen a la preferencia de elegir la definición de Caputo.

El resultado del análisis básico de existencia y unicidad de la solución de una ecuación diferencial fraccional se dan en Oldham y Spanier (1999), Podlubny (1999) y Samko et al. (1993). Para las ecuaciones definidas en términos del operador diferencial fraccional de Caputo se encuentra una discusión adicional en las publicaciones recientes de Diethelm y Ford (Diethelm y Ford, 2001, 2002a,b).

Forma discreta de la derivada fraccional

Hay diferentes métodos con variantes en forma discreta de una derivada, tanto entera como de orden fraccional. Sin embargo, para facilitar el procedimiento Edwards et al., (2002) elige un método simple tal que presente puntos importantes y no se confunda con otros detalles matemáticos.

Para la solución de una ecuación diferencial de primer orden, el método propuesto por Edwards et al., (2002) usa la regla del trapecio, la cual es

$$Dy = f \Rightarrow y_i = y_{i-1} + \frac{1}{2}h\left(f_i + f_{i-1}\right).$$

Para la forma discreta de una derivada fraccional, usa el método de Diethelm, definido como

$$D^{\alpha}y = \frac{1}{{}_{\alpha}\gamma_i}\left(\sum_{k=0}^{i} {}_{\alpha}\omega_{k,i}\, y_{i-k} + \frac{y_0}{\alpha}\right) \qquad \text{(C-2)}$$

donde

$$ {}^{\alpha}\gamma_i = (ih)^{\alpha}\,\Gamma(-\alpha), \tag{C-3} $$

y ${}^{\alpha}\omega_{k,0},\ldots,{}^{\alpha}\omega_{k,i}$ son los términos de *convolución pesada* derivados del hecho de que el operador fraccional es definido en términos de una integral de convolución, y se definen como:

$$ \begin{aligned} {}^{\alpha}\omega_{0,i} &= -1 && ; \quad k = 0 \\ {}^{\alpha}\omega_{k,i} &= 2k^{1-\alpha} - (k-1)^{1-\alpha} - (k+1)^{1-\alpha} && ; \quad k = 1,\ldots,i-1 \\ {}^{\alpha}\omega_{0,i} &= (\alpha-1)k^{\alpha} - (k-1)^{1-\alpha} - k^{1-\alpha} && ; \quad k = i \end{aligned} \tag{C-4} $$

Solución de una Ecuación Lineal General Múlti-Términos

Se considera una EDOF lineal general múlti-términos de la forma

$$ \sum_{s=0}^{p} c_s D^{\beta_s} y = f\,, \tag{C-5} $$

donde $0 \le \beta_0 < \beta_r < \beta_{r+1} < \beta_p$, $c_p = 1$, $c_s \in \mathbb{R}$. Notar que no es necesario que el orden mayor de β_p sea entero. Sin embargo, se estima que todos los números como los iniciales de la Ec. (C-5) (sí es necesario con coeficiente cero) no se originan o generan así como las condiciones iniciales. Para enfatizar la solución de una ecuación así, se reúnen todos los órdenes en cada intervalo $(j, j+1]$, $j \in \mathbb{Z}^+ = \mathbb{N} \cup \{0\}$ y entonces se usará la forma:

$$ b_{0,0}y + \sum_{j=0}^{m}\sum_{r=1}^{n_j} b_{r,j} D^{j+\alpha_{r,j}} y = f\,, \tag{C-6} $$

donde, para $j = 1,\ldots,m-1$ se tiene $0 < \alpha_{1,j} < \alpha_{2,j} < \cdots < \alpha_{n_j,j} = 1$ y $0 < \alpha_{1,m} < \alpha_{2,m} < \cdots < \alpha_{n_m,m} \le 1$ y $b_{i,j} \in \mathbb{R}$. También $n_0 + \cdots + n_m = p$ y se hace $p_k = \sum_{j=0}^{k-1} n_j$.

Entonces la Ec. (C-6) se re-escribe como un sistema:

$$
\begin{aligned}
{}^{1}Y &= y, \\
{}^{2}Y &= D^{\alpha_{i,0}} y, \\
&\vdots \\
{}^{1+n_0}Y &= Dy, \\
{}^{2+n_0}Y &= D^{\alpha_{i,1}} Dy, \\
&\vdots \\
{}^{p+1}Y &= D^{\alpha_{n_m,m}} D^{m-1} y,
\end{aligned}
$$

el cuál en forma matricial es

$$
\mathscr{D}\, y = \begin{pmatrix} \mathscr{D}_1 & 0 & \cdots & 0 \\ \vdots & \ddots & \ddots & \vdots \\ 0 & \cdots & \cdots & \mathscr{D}_m \end{pmatrix} \begin{pmatrix} {}^{1}Y \\ \vdots \\ {}^{1+n_0}Y \\ \vdots \\ {}^{p}Y \end{pmatrix} = \begin{pmatrix} {}^{2}Y \\ \vdots \\ {}^{2+n_0}Y \\ \vdots \\ f - \sum_{k=0}^{p-1} c_k \, {}^{k}Y \end{pmatrix},
$$

donde para $k = 1, \ldots, m-1, \mathscr{D}_k$ es una matriz de operadores diferenciales de n_k por n_k, de la forma:

$$
\begin{pmatrix} D^{\alpha_{1,k}} & 0 & \cdots & 0 \\ D^{\alpha_{2,k}} & 0 & \cdots & 0 \\ \vdots & \ddots & \ddots & \vdots \\ D & 0 & \cdots & 0 \end{pmatrix}.
$$

La expresión correspondiente para mantener $k = m$, se tiene: *caso 1* para $\alpha_{n_m,m} = 1$, y el *caso 2* para $\alpha_{n_m,m} \neq 1$, se tiene

$$
\mathscr{D}_m = \begin{pmatrix} D^{\alpha_{1,m}} & 0 & \cdots & 0 \\ D^{\alpha_{2,m}} & 0 & \cdots & 0 \\ \vdots & \ddots & \ddots & \vdots \\ D^{\alpha_{n_m,m}} & 0 & \cdots & 0 \end{pmatrix}.
$$

Al poner en forma discreta la derivada en $\mathscr{D}$ se produce $\bar{\mathscr{D}}$. La matriz $\bar{\mathscr{D}}$ consiste de bloques de matrices cuadradas $\bar{\mathscr{D}}_k$ a lo largo de la diagonal la cual es la forma discreta análoga de $\bar{\mathscr{D}}_k$ para $k = 1,\ldots,m-1$. El grupo de matrices del renglón inferior en las matrices $\bar{\mathscr{D}}_{m,1},\ldots,\bar{\mathscr{D}}_{m,m}$.

Así, se escribe el sistema en forma discreta como

$$\bar{\mathscr{D}} Y_i = S_i, \tag{C-7}$$

donde

$$\bar{\mathscr{D}} = \begin{pmatrix} \bar{\mathscr{D}}_1 & 0 & \cdots & \cdots & \cdots & 0 \\ 0 & \bar{\mathscr{D}}_2 & 0 & \ddots & \ddots & \vdots \\ \vdots & \ddots & \ddots & \ddots & \ddots & \vdots \\ 0 & \ddots & \ddots & 0 & \bar{\mathscr{D}}_{m-1} & 0 \\ \bar{\mathscr{D}}_{m,1} & \cdots & \cdots & \cdots & \cdots & \bar{\mathscr{D}}_{m,m} \end{pmatrix}, \tag{C-8}$$

y

$$\bar{\mathscr{D}}_k = \begin{pmatrix} -{}^{1,k}\omega_{0,i} & {}^{1,k}\gamma_i & 0 & \cdots & \cdots & 0 \\ -{}^{2,k}\omega_{0,i} & 0 & {}^{2,k}\gamma_i & 0 & \ddots & \vdots \\ \vdots & \ddots & \ddots & \ddots & \ddots & \vdots \\ -{}^{n_k-1,k}\omega_{0,i} & 0 & \cdots & 0 & {}^{n_k-1,k}\gamma_i & 0 \\ 1 & 0 & \cdots & \cdots & 0 & -\dfrac{h}{2} \end{pmatrix},$$

y por consiguiente implica que se tenga:

$${}^{k}\bar{Y}_i = \begin{pmatrix} {}^{1-p_k}Y_i \\ \vdots \\ {}^{p_{k-1}}Y_i \end{pmatrix},$$

$${}^{k}\bar{S}_i = \begin{pmatrix} {}^{1-p_k}S_i \\ \vdots \\ {}^{p_{k-1}}S_i \end{pmatrix},$$

donde

$$ {}^{j+p_k}S_i = \sum_{r=0}^{i-1} {}^{j+p_k}\omega_{i-r,\,j+p_k\beta-(k-1)}\,{}^{1+p_k}Y_r + \frac{{}^{1+p_k}Y_0}{{}^{j+p_k}\beta}; \quad j=1,\ldots,n_k-1, $$

$$ {}^{p_{k+1}}S_i = {}^{1+p_k}Y_{i-1} + \frac{h}{2}\,{}^{p_{k-1}}Y_{i-1}. $$

Poniendo en forma discreta para $k=m$ (*caso 1*), y agrupando términos semejantes se obtiene la primera fila n_m-1 de $\bar{\mathcal{D}}_{m,m}$ como

$$ \begin{pmatrix} -{}^{1,k}\omega_{0,i} & {}^{1,k}\gamma_i & 0 & \cdots & 0 \\ -{}^{2,k}\omega_{0,i} & 0 & {}^{2,k}\gamma_i & 0 & \vdots \\ \vdots & \ddots & \ddots & \ddots & \vdots \\ -{}^{n_k-1,k}\omega_{0,i} & 0 & {}^{n_k-1,k}\gamma_i & \cdots & 0 \end{pmatrix}. $$

Análogamente, para el último renglón con $\alpha_{n_m,m}\neq 1$ (*caso2*), se tiene

$$ D^{\alpha_{n_m},m}\,{}^{1+p_m}Y_i = f - \sum_{s=1}^{p} c_{s-1}\,{}^{s}Y_i\,. \tag{C-9} $$

La cual, en forma discreta es:

$$ \frac{1}{{}^{n_m,m}\gamma_i}\left(\sum_{k=0}^{i} {}^{n_m,m}\omega_{i,k}\,{}^{1+p_m}Y_{i-k} + \frac{{}^{1+p_m}Y_0}{\alpha_{n_m,m}}\right) = f_i - \sum_{s=1}^{p} c_{s-1}\,{}^{s}Y_i\,. \tag{C-10} $$

Re-ordenando la Ec. (C-10), queda:

$$ -{}^{n_m,m}\omega_{i,0}\,{}^{1+p_m}Y_i + {}^{n_m,m}\gamma_i \sum_{s=1}^{p} c_{s-1}\,{}^{s}Y_i = {}^{n_m,m}S_i\,, \tag{C-11} $$

donde

$$ {}^{n_m,m}S_i = {}^{n_m,m}\gamma_i\, f_i - \sum_{k=0}^{i-1} {}^{n_m,m}\omega_{i,k}\,{}^{1+p_m}Y_{i-k} - \frac{{}^{1+p_m}Y_0}{\alpha_{n_m,m}}\,. \tag{C-12} $$

Entonces para $k=1,\ldots,m-1$, las entradas para $\bar{\mathscr{D}}_{m,k}$ son cero para el primer renglón n_m-1, y el último renglón para $\bar{\mathscr{D}}_{m,1}$ es dado por:

$$\left({}^{n_m,m}\gamma_i c_0 \cdots {}^{n_m,m}\gamma_i c_{n_0}\right), \tag{C-13}$$

el último renglón de $\bar{\mathscr{D}}_{m,k}$ para $k=2,\ldots,m-1$, es

$$\left({}^{n_m,m}\gamma_i c_{p_k+1} \cdots {}^{n_m,m}\gamma_i c_{p_k+1}\right), \tag{C-14}$$

y la última fila de $\bar{\mathscr{D}}_{m,m}$ es dada por:

$$\left({}^{n_m,m}\gamma_i c_{p_m+1} - {}^{n_m,m}\omega_{i,0} \cdots {}^{n_m,m}\gamma_i c_p\right). \tag{C-15}$$

En el caso donde $\alpha_{n_m,m}=1$, se tiene:

$$D^{1+p_m}Y = f - \sum_{s=1}^{p} c_{s-1}\,{}^{s}Y \quad , \tag{C-16}$$

la cual, en forma discreta es:

$${}^{1+p_m}Y_i = {}^{1+p_m}Y_{i-1} + \frac{h}{2}\left(f_i + f_{i-1} - \sum_{s=1}^{p} c_{s-1}\,{}^{s}\left(Y_i + Y_{i-1}\right)\right). \tag{C-17}$$

Re-ordenando términos, se obtiene:

$${}^{1+p_m}Y_i + \frac{h}{2}\sum_{s=1}^{p} c_{s-1}\,{}^{s}Y_i = {}^{n_m,m}S_i, \tag{C-18}$$

donde

$${}^{n_m,m}S_i = {}^{1+p_m}Y_{i-1} + F_i - \frac{h}{2}\sum_{s=1}^{p} c_{s-1}\,{}^{s}Y_{i-1}\,. \tag{C-19}$$

Entonces, para $k=1,\ldots,m-1$, las entradas para $\bar{\mathscr{D}}_{m,k}$ son cero para el primer renglón n_m-1, y el último renglón para $\bar{\mathscr{D}}_{m,1}$ es dado por

$$\left(\frac{h}{2}c_0 \cdots \frac{h}{2}c_{n_0}\right), \tag{C-20}$$

y $\bar{\mathscr{D}}_{m,k}$ para $k = 2,\ldots,m-1$ es:

$$\left(\frac{h}{2}c_{p_k+1} \cdots \frac{h}{2}c_{p_k+1}\right), \tag{C-21}$$

y el último renglón de $\bar{\mathscr{D}}_{m,m}$ es dado por:

$$\left(1+\frac{h}{2}c_{p_m+1}\frac{h}{2}c_{p_m+2} \cdots \frac{h}{2}c_{p}\right), \tag{C-22}$$

Anexo 1

Time-Fractional Telegrapher's Equation (P1) Approximation for the Transport Equation

X-7 11-58N

NUCLEAR SCIENCE AND ENGINEERING: 171, 1–7 (2012)

Technical Note

Time-Fractional Telegrapher's Equation (P_1) Approximation for the Transport Equation

Gilberto Espinosa-Paredes*

Universidad Autónoma Metropolitana-Iztapalapa
Área de Ingeniería en Recursos Energéticos
Av. San Rafael Atlixco 186, Col. Vicentina, México D.F. 09340, México

and

Marco Antonio Polo-Labarrios

Universidad Autónoma Metropolitana-Iztapalapa
Área de Ingeniería en Recursos Energéticos
Av. San Rafael Atlixco 186, Col. Vicentina, México D.F. 09340, México
and
Universidad Nacional Autónoma de México, Facultad de Ingeniería
Departamento de Sistemas Energéticos, Av. Universidad 3000
Universidad Nacional Autónoma de México Coyoacán, México D.F. 04510, México

Received August 13, 2011
Accepted November 29, 2011

Abstract—*In this paper we develop a new approximation from the solution of the time-dependent Boltzmann equation, which includes a fractional constitutive equation of the neutron current density, for a general medium. The fractional constitutive equation in combination with the conservation law that governs the particle collision and reaction processes (P_1) approximation for the transport equation gives a time-fractional telegrapher's equation (TFTE). The wave velocity found with this approximation is $3^{-\gamma/2}$ for $\gamma < 1$. The numerical results are compared with the exact solution and Heizler's approximation. We found that the TFTE gives the best estimate for a purely absorbing medium, where most approximations fail. The asymptotic diffusion coefficient was applied for a heterogeneous medium, and the results show that the behavior of the TFTE improves.*

I. INTRODUCTION

Nowadays, the particle diffusion concept is a tool commonly used to understand the complex behavior of the neutrons' average motion. Most reactor studies treat the neutron motion as a diffusion process, where it is assumed that neutrons in averaged motion tend to diffuse from regions of high neutron density to those of low neutron density. The diffusion theory provides a strictly valid mathematical description of the neutron flux when the following assumptions are satisfied: (a) absorption much less likely than scattering, (b) linear spatial variation of the neutron distribution, and (c) isotropic scattering in its derivation.[1]

In time-dependent problems, the diffusion equation fails to describe the front of streaming generating from a source, even for a highly scattering medium, due to the parabolic nature of the diffusion equation (infinite particle velocity). The P_1 approximation for the Boltzmann equation, which yields the telegrapher's equation, replaces this feature of an infinite velocity with a wrong finite velocity (given by $v/\sqrt{3}$) (Ref. 2).

In a recent paper, Heizler[2] presented a version of the asymptotic telegrapher's equation approximation to describe the local density of particles traveling inside a medium with interactions between the particles and the

*E-mail: gepe@xanum.uam.mx

medium, using the full equations of the P_1 approximation modifying the approximate equation to the current vector ($\vec{J}$).

In this paper we develop a new approximation from the solution of the time-dependent Boltzmann equation, which includes a fractional constitutive equation of the particle current density. This approximation, called the time-fractional telegrapher's equation (TFTE) in this work, can be applied where large variations on neutron cross sections normally preclude the use of the classical particle diffusion equation, specifically, in the presence of strong neutron absorbers in the fuel, control rods, and coolant when boron is injected to force shutdown of the reactor.

II. PRELIMINARIES: ANOMALOUS DIFFUSION

Anomalous diffusion has been known since Richardson's treatise[3] on turbulent diffusion in 1926. Within transport theory it has been studied since the late 1960s. In particular, its theoretical investigation was instigated by Scher and Montroll in their description of dispersive transport in amorphous semiconductors, a system where the traditional methods failed.[4] The notion of anomalous subdiffusion generalizes the property of mean square displacement proportionality to time, typical of Brownian motion, to the power law $\langle r^2 \rangle \sim t^{\gamma}$, with an exponent $0 < \gamma < 1$. Subdiffusion characterizes systems where various physical factors impede the free random walk of particles.[5,6]

One of the pertinent utilities for the description of anomalous diffusion is the continuous-time random walk model.[5,6] According to that model, the molecules are trapped so that the probability of performing a jump depends on the time elapsing since the last jump, i.e., the age of the molecule. Actually, the molecule is released from its trap due to some changes in its environment rather than changes in the molecule itself. Introduction of a waiting time distribution of this type resulted in integrodifferential memory operators, known as fractional derivatives.

The TFTE developed in this work to describe the behavior of the particle density (flux) for a general medium is based in these ideas.

III. DERIVING THE TFTE APPROXIMATION

The fractional constitutive equation of the current density vector is given by[7]

$$\tau^{\gamma} \frac{\partial^{\gamma} \vec{J}}{\partial t^{\gamma}} + \vec{J} = -D \nabla \phi \ , \qquad (1)$$

where

$\partial^{\gamma}/\partial t^{\gamma}$ = fractional derivative operator

γ = anomalous diffusion exponent

$\tau (= 1/v\Sigma_t = 3D/v)$ = relaxation time

$D(\vec{r}) = 1/3\Sigma_t(\vec{r})$ = diffusion coefficient.

For the obtaining of γ we explored the analysis of the neutronic power signals of a nuclear power plant using detrended fluctuation analysis[8] (DFA), which is a method based on the random walk theory that has been applied to neutronic power signals of Forsmark stability benchmark.[9] DFA is a scaling method commonly used for detecting long-range correlation in nonstationary time series. The scale coefficient obtained with the DFA method can be interpreted as an anomalous diffusion exponent using the Grünwald-Letnikov formula.[10] The preliminary results show that the anomalous diffusion exponents using these ideas are among the values used in our work, whose physical interpretations are the Brownian motion and dominant periodic fluctuation. The Forsmark nuclear power plant presents superdiffusive (known in the literature as enhanced diffusivity) and subdiffusive phenomena.[9]

The conservation law that governs the particle collision and reaction processes is given by

$$\frac{1}{v} \frac{\partial \phi(\vec{r},t)}{\partial t} + \vec{\nabla} \cdot \vec{J}(\vec{r},t) + \Sigma_a(\vec{r}) \phi(\vec{r},t) = Q^{(0)}(\vec{r},t) \ , \qquad (2)$$

where $Q^{(0)}$ is the source term. Substituting Eq. (1) into Eq. (2) yields the TFTE approximation for the anomalous diffusion approximation as

$$\frac{\tau^{\gamma}}{v} \frac{\partial^{1+\gamma} \phi(\vec{r},t)}{\partial t^{1+\gamma}} + \frac{1}{v} \frac{\partial \phi(\vec{r},t)}{\partial t} + \tau^{\gamma} \Sigma_a \frac{\partial^{\gamma} \phi(\vec{r},t)}{\partial t^{\gamma}} + \Sigma_a \phi(\vec{r},t) - D \vec{\nabla}^2 \phi(\vec{r},t) = Q^{(0)}(\vec{r},t) \ , \quad t \geq 0 \ . \qquad (3)$$

The terms related with a time-dependent source $[\partial Q^{(0)}(\vec{r},t)/\partial t$ and $\partial^{\gamma} Q^{(0)}(\vec{r},t)/\partial t^{\gamma}]$ are not considered in this study.

To demonstrate the difference with other models, we introduce a one-dimensional infinite-slab problem with a time-independent delta source in the middle (at $x = 0$); i.e., $Q(x) = Q_0 \delta(x)$. The initial conditions are $\phi(x,0) = 0$ and $(\partial \phi(x,t)/\partial t)|_{t=0} = 0$, the boundary conditions are given by $\lim_{x \to \infty} \phi(x,t) < \infty$, and $\lim_{x \to 0} \phi(x,t)$ is obtained from the analytical solution of the classic diffusion equation [Eq. (9)].

IV. FRACTIONAL NUMERICAL SOLUTION

In this section, we present the scheme of fractional numerical solution of Eq. (3). A finite difference method is used for the discretized form of the time fractional derivative with Caputo's approximation.[11]

Using time-stepping methods in the fractional case requires the storage of all previous time steps. The difficulty in solving fractional differential equations is particularly where the application requires a solution over a long interval, because fractional derivatives are nonlocal operators. The so-called nonlocal property means that the next state of a system depends not only on its current state but also on the historical states, starting from the initial time.

Then, Eq. (3) for one dimension in slab infinity geometry is given by

$$\frac{1}{\Sigma_t^{\gamma} v^{1+\gamma}} \frac{\partial^{1+\gamma}\phi(x,t)}{\partial t^{1+\gamma}} + \frac{1}{v}\frac{\partial\phi(x,t)}{\partial t} + \frac{\Sigma_a}{\Sigma_t^{\gamma} v^{\gamma}} \frac{\partial^{\gamma}\phi(x,t)}{\partial t^{\gamma}} + \Sigma_a\phi(x,t) - \frac{1}{3\Sigma_t}\frac{\partial^2\phi(x,t)}{\partial x^2} = Q_{\circ}\delta(x) \ , \quad t \geq 0 \text{ with } 0 < \gamma < 1 \ . \tag{4}$$

The initial conditions are chosen simply as $\phi(x,0) = 0$ and $\partial\phi(x, t=0)/\partial t = 0$. Here, $\partial^{\gamma}\phi(\vec{r},t)/\partial t^{\gamma}$ is the Caputo fractional order derivative, defined by[12]

$$\frac{\partial^{\gamma}\phi(x,t)}{\partial t^{\gamma}} = \frac{1}{\Gamma(1-\gamma)}\int_0^t (t-\eta)^{-\gamma}\frac{\partial\phi(x,\eta)}{\partial\eta}\,d\eta \ , \tag{5}$$

and $\partial^{1+\gamma}\phi(\vec{r},t)/\partial t^{1+\gamma}$ is the Riemann-Liouville fractional order derivative[13]:

$$\frac{\partial^{1+\gamma}\phi(x,t)}{\partial t^{1+\gamma}} = \frac{1}{\Gamma(2-\gamma)}\frac{\partial^2}{\partial t^2}\int_{\circ}^t \frac{\phi(x,\xi)}{(t-\xi)^{\gamma-1}}\,d\eta \ . \tag{6}$$

For stability, a shifted Grünwald formula is used to approximate the time-fractional derivative.[13] The fractional algorithm for numerical approximation is presented in the Appendix.

To solve Eq. (4), we consider that the space dimension is in terms of the transport mean free path. Then, Eq. (4) can be rewritten as

$$\frac{\partial^{1+\gamma}\phi(x,t)}{\partial t_0^{1+\gamma}} + \frac{\partial\phi(x,t)}{\partial t_{\circ}} + (1-c)\frac{\partial^{\gamma}\phi(x,t)}{\partial t_0^{\gamma}} + (1-c)\phi(x,t) - \frac{1}{3}\frac{\partial^2\phi(x,t)}{\partial\lambda_t^2} = Q_{\circ}\delta(x) \ , \quad t_{\circ} \geq 0 \ , \tag{7}$$

where dimensionless numbers used are $\lambda_t = x\Sigma_t$ and $t_0 = t v\Sigma_t$ (being $t_0 = nt$ for $n \in \mathbb{R}_+$). The mean number of secondary particles emitted per collision event is given by

$$c = \frac{\Sigma_s}{\Sigma_t} = \frac{\Sigma_s}{\Sigma_a + \Sigma_s} \ , \tag{8}$$

and the boundary condition is obtained from classical diffusion approximation:

$$x(0,t) = \frac{Q_{\circ}}{4}\sqrt{\frac{3}{(1-c)}}\left[\operatorname{erfc}(-\sqrt{(1-c)t_0}) - \operatorname{erfc}(\sqrt{(1-c)t_0})\right] \ . \tag{9}$$

Now, substituting Eqs. (A.1) through (A.4) into Eq. (7), and rearranging terms, we obtain an equation than can be explicitly solved for ϕ_i^{j+1}:

$$\begin{aligned}\phi_i^{j+1} = {} & \frac{d}{(1+a+b)}\phi_{i-1}^{j} - \frac{(c+2d-a-b+g_1)}{(1+a+b)}\phi_i^{j} + \frac{d}{(1+a+b)}\phi_{i+1}^{j} - \frac{g_2}{(1+a+b)}\phi_i^{j-1} \\ & - \frac{b}{(1+a+b)}\sigma_j(\phi_i^1 - \phi_i^0) - \frac{1}{(1+a+b)} \times \sum_{k=3}^{j+1} g_k\phi_i^{j-k+1} - \frac{b}{(1+a+b)} \times \sum_{k=1}^{j-1}\sigma_k(\phi_i^{j+1-k} - \phi_i^{j-k}) \ ,\end{aligned} \tag{10}$$

where

$$a = \tau^{\gamma} \ ,$$

$$b = \frac{\tau(1-c)}{\Gamma(2-\gamma)} \ ,$$

$$c = \tau^{1+\gamma}(1-c) \ ,$$

$$d = \frac{\tau^{1+\gamma}}{3h^2} \ ,$$

and

$$\sigma_k = (k+1)^{1-\gamma} - k^{1-\gamma} \ , \quad k = 0,1,2,\ldots,j-1 \ .$$

For two- and three-dimensional geometries, the applicability would be straightforward; however, the numerical complexity of the solution would increment considerably due to the memory effect, i.e., the last four terms on the right side of Eq. (10), which represent the difference with respect to the classical diffusion integer order equation.

V. COMPARISON WITH PREVIOUS WORKS

The results of TFTE are compared with the Boltzmann equation and Heizler's approximation for the case of the plane source problem.

V.A. Exact Solution of the Boltzmann Equation

The monoenergetic linear transport equation or monoenergetic Boltzmann equation is

$$\frac{1}{v}\frac{\partial\psi(\vec{r},\hat{\Omega},t)}{\partial t} + \hat{\Omega}\cdot\vec{\nabla}\psi(\vec{r},\hat{\Omega},t) + \Sigma_t(\vec{r})\psi(\vec{r},\hat{\Omega},t) = \int_{4\pi} d\hat{\Omega}'\Sigma_s(\vec{r},\hat{\Omega}\cdot\hat{\Omega}')\psi(\vec{r},\hat{\Omega},t) + Q(\vec{r},\hat{\Omega},t) \ , \tag{11}$$

and the exact Boltzmann solution of the plane source problem is

$$\phi_{\text{exact}}(x,t) = \frac{Q_0}{2}[E_1(|x|\Sigma_a) - E_1(v\Sigma_a t)]H\left(t - \frac{|x|}{v}\right) \ , \tag{12a}$$

$$\phi(x,t) = \frac{\sqrt{15}\Sigma_t v Q_0}{2}\int_0^t e^{-5(w'/2)\Sigma_t u}\cdot I_0\left[5\frac{v}{2} - \Sigma_t\sqrt{u^2 - \frac{3}{5}\frac{|x|^2}{v^2}}\right]\cdot H\left(u - \sqrt{\frac{3}{5}}\frac{|x|}{v}\right)du$$

$$- \frac{Q_0}{2}\sqrt{\frac{27}{5}}e^{-5(w'/2)\Sigma_t t}\cdot I_0\left[5\frac{v}{2}\Sigma_t\sqrt{t^2 - \frac{3}{5}\frac{|x|^2}{v}}\right]\cdot H\left(t - \sqrt{\frac{3}{5}}\frac{|x|}{v}\right) \ , \tag{12b}$$

where Eq. (12a) is for $c = 0$ and Eq. (12b) is for $c = 1$ [Eqs. (56) and (58), respectively, from Ref. 2].

V.B. Asymptotic Diffusion Equation

The asymptotic diffusion equation is obtained combining Eq. (3) with the modified Fick's law:

$$J(x) = -D(c,\Sigma_t)\cdot\frac{\partial\phi(x)}{\partial x} \ . \tag{13}$$

The modified diffusion coefficient depends on the properties of the medium (c), instead of the constant classical diffusion coefficient $D = 1/3\Sigma_t$:

$$D(c,\Sigma_t) = \frac{1-c}{\chi_0^2(c)\Sigma_t} = D_0(c)\frac{1}{\Sigma_t} \ . \tag{14}$$

Solving the asymptotic diffusion (AD) equation with a plane source gives this solution[2,14]

$$\phi_{AD} = \frac{Q_0}{2}\frac{1}{\chi_0(c)D_0(c)}e^{-\chi_0(c)\Sigma_t|x|}$$

$$= \frac{Q_0}{2}\frac{\chi_0(c)}{1-c}e^{-\chi_0(c)\Sigma_t|x|} \ . \tag{15}$$

V.C. Heizler's Approximation

The asymptotic telegrapher's equation proposed by Heizler[2] is obtained by combining Eq. (3) with the following approximation:

$$\frac{A}{v}\frac{\partial J(x,t)}{\partial t} + \frac{\partial\phi(x,t)}{\partial x} + B\Sigma_t J(x,t) = 0 \ . \tag{16}$$

The analytical solution of the asymptotic telegrapher's equation is given by Heizler[2]:

$$\phi(x,t) = \frac{B(c)\Sigma_t v Q_0}{2\sqrt{A(c)}}\int_0^t e^{-(w/2)(\Sigma_a + (B(c)/A(c))\Sigma_t)u}$$

$$\times I_0\left[\frac{v}{2}\left(\Sigma_a - \frac{B(c)}{A(c)}\Sigma_t\right)\sqrt{u^2 - A(c)\frac{|x|^2}{v^2}}\right]$$

$$\times H\left(u - \sqrt{A(c)}\frac{|x|}{v}\right)du \ . \tag{17}$$

In this equation the parameters A and B are functions of c, given by Eqs. (25) and (54) from Ref. 2.

VI. DISCUSSION

Figure 1 shows a comparison of the TFTE approximation developed in this work with the exact solution of the Boltzmann equation (BE), the AD equation, and the asymptotic telegrapher's equation, in this work called Heizler's approximation (denoted HE). As shown in Fig. 1, three cases were considered for comparison: (a) purely absorbing medium ($c = 0$), (b) a heterogeneous medium ($c = 0.65$), and (c) a highly scattering medium ($c \approx 1$). Shown for the three cases are the results for a very short time ($t = t_0$; where $t_0 = tv\Sigma_t$), a short time ($t = 2t_0$), and a very long time ($t = 6t_0$). The main features of the TFTE approximation are as follows:

1. *purely absorbing medium* ($c = 0$): For the very short time, the TFTE is advancing with a velocity that is close to the real particle velocity, shown by the BE (exact solution), where the differences are negligible, whereas the HE describes the real particle velocity only in the wave front. For the short time, the TFTE behavior is similar to that described by the BE; i.e., our approximation is closer to the exact solution than are the HE and AD. For the very long time, the HE tends to the AD, where both fail, and once again the TFTE has the best approximation.

2. *heterogeneous medium* ($c = 0.65$): In this case the TFTE was compared with the HE and AD; the BE is shown just for the two limit cases. For the very short time, the TFTE underpredicts the particle behavior with respect to the HE and AD approximations. For the short time, at $x\Sigma_t \approx 0.5$ the three models intersect, and afterward the trend of the TFTE underpredicts the behavior with respect to the HE and AD. For the very long time, the intersection occurs at $x\Sigma_t \approx 1$, and afterward the trends follow the same pattern as for the short time. When the approximations intersect, physically it means that the particles from these solutions have the same velocity at this exact point.

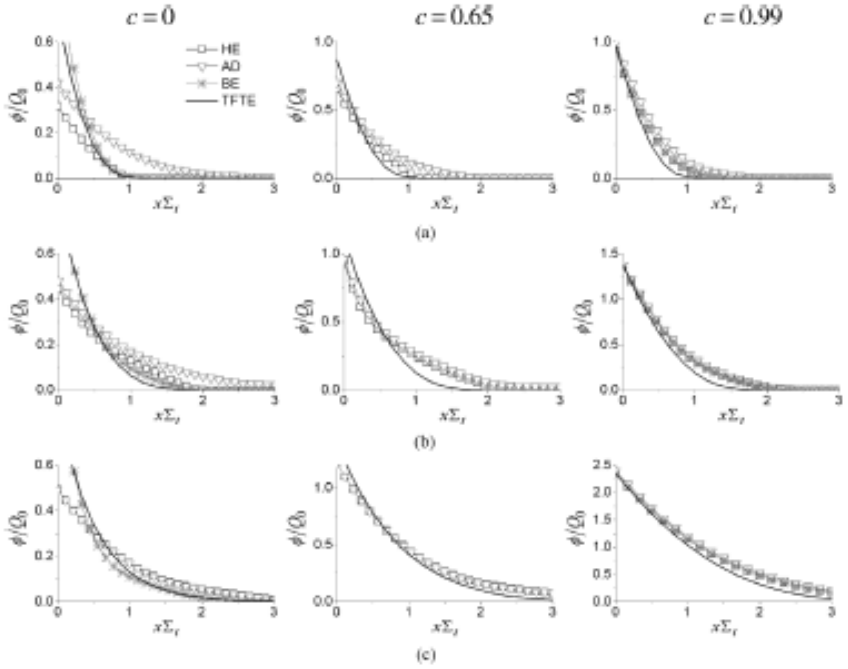

Fig. 1. Scalar flux to a delta source problem for a purely absorbing medium ($c = 0$), for a heterogeneous medium ($c = 0.65$), and for a highly scattering medium ($c = 0.99$). The HE is given by Eq. (17), the AD is given by Eq. (15), the exact solution of the BE is obtained using Eq. (12), and the TFTE is given by Eq. (10). The anomalous diffusion exponent $\gamma = 0.6$. (a) Very short time ($t = t_0$), (b) short time ($t = 2t_0$), and (c) very long time ($t = 6t_0$), where $t_0 = (tv\Sigma_t)^{-1}$.

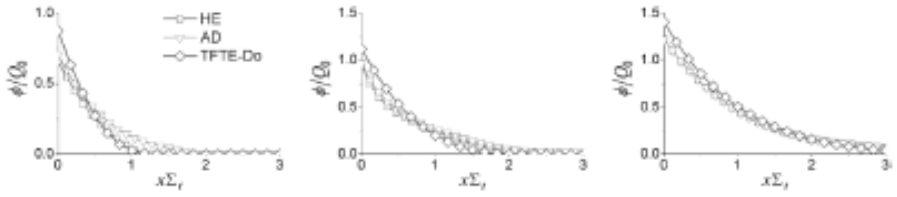

Fig. 2. Scalar flux to a delta source problem for a heterogeneous medium ($c = 0.65$). The HE is given by Eq. (17), the AD is given by Eq. (15), and the TFTE-D_0 is given by the TFTE considering the asymptotic diffusion exponent D_0 [Eq. (25), Ref. 2]. The anomalous diffusion exponent $\gamma = 0.6$. (a) very short time ($t = t_0$), (b) short time ($t = 2t_0$), and (c) very long time ($t = 6t_0$), where $t_0 = (v\Sigma_t)^{-1}$.

3. *highly scattering medium or almost isotropic medium* ($c \approx 1$): In this case, for all the times the TFTE underpredicts the behavior with respect to the exact solution (BE). It can be observed that for an isotropic medium, the HE behavior is closer to that of the BE, and the AD fails at the very short time.

In general terms, and as can be observed in the results, the TFTE gives the best approximation to the BE when the medium is purely absorbing, where the approximations given by HE and AD fail. The physical interpretation of this behavior is that in the medium there are subdiffusive processes that are better represented by the model developed in this work. In the heterogeneous medium, the models describe different behaviors and there is an intersection among them; after the intersection point the TFTE underpredicts the particle velocity with respect to the HE and AD. We can infer that the subdiffusive process are dominant for the heterogeneous medium where the TFTE gives a better approximation with respect to the HE and AD, as was demonstrated with results obtained for the purely absorbing medium. In the highly scattering medium, the subdiffusive processes are not predominant and the TFTE underpredicts the propagation phenomena, following the same trend of the BE, and the HE is the better approximation, which means that the correction introduced by Heizler in the propagation velocity is correct in this case.

The TFTE, HE, and AD approximations are simpler to solve than the BE. However, the TFTE is crucial where the phenomena are subdiffusive, and furthermore, it has a wider approach and requires fewer calculations; the HE can be applied for highly scattering media, where the subdiffusive processes are negligible. The difficulty of the HE approximation is obtaining the coefficients for its solution[2]; however, once obtained, the HE can be used in a straightforward way.

To improve the behavior of the TFTE in a heterogeneous medium ($c = 0.65$) and a highly scattering medium ($c \approx 1$), we performed a numerical experiment including the asymptotic diffusion coefficient [Eq. (25), Ref. 2]. The results obtained show that for $c = 0$, the asymptotic diffusion coefficient fails for all cases, i.e., for very short times, short times, and long times. For $c = 0.65$, the TFTE model improves for all cases, as shown in Fig. 2, where the TFTE-D_0 indicates the behavior with asymptotic diffusion coefficient approximation. For very short times this improvement is substantial; however, for short and long times a slight improvement can be appreciated, which indicates that the TFTE considering the asymptotic diffusion exponent is not the best option with respect to the HE and AD models. For $c = 0.99$ changes cannot be perceived a priori, due that when c tends to 1 the asymptotic diffusion coefficient tends to 1/3, which is approximately the same solution yielded without the asymptotic diffusion coefficient.

The TFTE (P_1) approximation for the transport equation predicted that the wave fractional velocity (dimensionless) is $a_\gamma^* = 1/3^{\gamma/2}$ where $a_\gamma = a_\gamma^* \sqrt{v^{1+\gamma}/D^{\gamma-1}}$ was applied. According to this equation $a_\gamma^* = 1/\sqrt{3}$ when $\gamma = 1$, which corresponds to the classical telegrapher's equation. On the other hand, it can be observed that a_γ^* increases for $\gamma < 1$. Then, beyond its physical meaning, γ can be considered as a correction parameter for the prediction of the correct velocity for $c = 0$.

VII. CONCLUSIONS

In this paper we developed the TFTE. The wave velocity found with this approximation is $3^{-\gamma/2}$ for $\gamma < 1$. We found that the TFTE gives the best estimate for a purely absorbing medium, where most approximations fail (Fig. 1). The asymptotic diffusion coefficient was applied for a heterogeneous medium and results show that the behavior of the TFTE improves (Fig. 2).

APPENDIX

To establish the numerical approximation scheme, let $t_j = j\tau (j = 0,1,2,\ldots,m)$ be the integration time

$0 \le t_j \le T, \tau = T/m, h = L/n > 0$ is the grid in space direction, $x_i = ih (i = 0, 1, 2, \ldots, n)$.

We take the following finite difference approximations for the time-fractional derivatives that appeared in Eq. (7) (Refs. 11 through 14):

$$\frac{\partial^\gamma \phi(x,t)}{\partial t^\gamma} = \frac{\tau^{1-\gamma}}{\Gamma(2-\gamma)} \sum_{k=0}^{j} \frac{\phi(x_i, t_{j+1-k}) - \phi(x_i, t_{j-k})}{\tau} \times [(k+1)^{1-\gamma} - k^{1-\gamma}] + \mathbf{O}(\tau) \ , \quad \text{(A.1)}$$

$$\frac{\partial \phi(x,t)}{\partial t} = \frac{\phi(x_i, t_{j+1}) - \phi(x_i, t_j)}{\tau} + \mathbf{O}(\tau) \ , \quad \text{(A.2)}$$

and

$$\frac{\partial^2 \phi(x,t)}{\partial x^2} = \frac{\phi(x_{i-1}, t_j) - 2\phi(x_i, t_j) + \phi(x_{i+1}, t_j)}{h^2} + \mathbf{O}(h) \ . \quad \text{(A.3)}$$

For the approximation of the Riemann-Liouville fractional order derivative $\partial^{1+\gamma}\phi(x,t)/\partial t^{1+\gamma}$, we use the shifted Grünwald formula[13]:

$$\frac{\partial^\alpha \phi(x,t)}{\partial t^\alpha} = \frac{1}{\tau^\alpha} \sum_{k=0}^{j+1} g_k \phi(x_i, t_{j-k+1}) + \mathbf{O}(\tau + h) \ , \quad \text{(A.4)}$$

where $\alpha = 1 + \gamma$, and the normalized Grünwald weights are defined by

$$g_0 = 1 \text{ and } g_k = (-1)^k \frac{(\alpha)(\alpha-1)\cdots(\alpha-k+1)}{k!} \quad \text{for } k = 1, 2, 3, \ldots \ . \quad \text{(A.5)}$$

Note that these normalized weights depend only on the order and the index k.

ACKNOWLEDGMENTS

Both authors would like to thank to E.-G. Espinosa-Martínez for collaborating in the development of this work. Additionally, we would like to thank the two anonymous reviewers for their thorough revision of the text. The first author is grateful for the financial support through a scholarship from the Consejo Nacional de Ciencia y Tecnología (CONACyT) for the Master's Graduate Studies in Engineering Program of the Universidad Nacional Autónoma de México, and special thanks to Laboratory of the Severe Accidents in Nuclear Reactors of the Universidad Autónoma Metropolitana-Iztapalapa, which conducted this research.

REFERENCES

1. W. M. STACEY, *Nuclear Reactor Physics*, Wiley-VCH (2004).

2. S. HEIZLER, "Asymptotic Telegrapher's Equation (P_1) Approximation for the Transport Equation," *Nucl. Sci. Eng.*, **166**, 17 (2010).

3. L. F. RICHARDSON, "Atmospheric Diffusion Shown on a Distance-Neighbour Graph," *Proc. Roy. Soc. London, Ser. A*, **110**, 709 (1926).

4. H. SCHER and E. W. MONTROLL, "Anomalous Transit-Time Dispersion in Amorphous Solid," *Phys. Rev. B*, **12**, 2455 (1975).

5. J. KLAFTER, G. ZUMOFEN, and M. F. SHLESINGER, in *The Physics of Complex Systems*, F. MALLAMACE and H. E. STANLEY, Eds., Amsterdam (1997).

6. R. METZLER and J. KLAFTER, "The Random Walk's Guide to Anomalous Diffusion: A Fractional Dynamics Approach," *Phys. Rep.*, **339**, 1 (2000).

7. G. ESPINOSA-PAREDES, J. B. MORALES-SANDOVAL, R. VÁZQUEZ-RODRÍGUEZ, and E. G. ESPINOSA-MARTÍNEZ, "Constitutive Laws for the Neutron Density Current," *Ann. Nucl. Energy*, **35**, 1963 (2008).

8. C. K. PENG, S. V. BULDYREV, S. HAVLIN, M. SIMONS, H. E. STANLEY, and L. A. GOLDBERGER, "Mosaic Organization of DNA Nucleotides," *Phys. Rev. E*, **49**, 1686 (1994).

9. G. ESPINOSA-PAREDES, J. ALVAREZ-RAMÍREZ, and A. VÁZQUEZ, "Detecting Long-Range Correlation with Detrended Fluctuation Analysis: Application to BWR Stability," *Ann. Nucl. Energy*, **33**, *16*, 1308 (2006).

10. E. RODRIGUEZ, C. ECHEVERRIA, and J. ALVAREZ-RAMIREZ, "**1/f** $^\alpha$ Fractal Noise Generation from Grünwald-Letnikov Formula," *Chaos, Sol. Fract.*, **39**, 882 (2009).

11. Q. YANG, I. TURNER, and F. LIU, "Analytical and Numerical Solutions for the Time and Space-Symmetric Fractional Diffusion Equation," *Proc. 4th Biennial Computational Techniques and Applications Conf.* (CTAC 2008), Canberra, Australia, July 13–16, 2008.

12. I. PODLUBNY, *Fractional Differential Equations*, Academic Press, New York (1999).

13. M. M. MEERSCHAERT and C. TADJERAN, "Finite Difference Approximations for Fractional Advection-Dispersion Flow Equations," *J. Comput. Appl. Math.*, **172**, 65 (2003).

14. Y. ZHANG, "A Finite Method for Fractional Partial Differential Equation," *Appl. Math. Comput.*, **215**, 524 (2009).

Anexo 2

Sensitivity and Uncertainty Analysis of the Time-Fractional Telegrapher´s Equation for Neutron Motion

*Manuscript
Click here to view linked References

Sensitivity and Uncertainty Analysis of the Time-Fractional Telegrapher´s Equation for Neutron Motion

G. Espinosa-Paredes*, M.-A. Polo-Labarrios**, A. Vázquez-Rodríguez

Área de Ingeniería en Recursos Energéticos, Universidad Autónoma Metropolitana-Iztapalapa, Av. San Rafael Atlixco 186, Col. Vicentina, 09340 México D.F., MÉXICO

* Corresponding author gepe@xanum.uam.mx

** Master's Graduate Studies in Engineering Program of the Universidad Nacional Autónoma de México.

Manuscript to be submitted to: *Progress in Nuclear Energy*

April 13, 2012

Total number of pages	23
Total number of figures	5
Total number of tables	9

Abstract

In this paper the sensitivity and uncertainty of the anomalous diffusion exponent (ADE) in the Time-Fractional Telegrapher's Equation (P1) Approximation, is presented. This analysis was carried out through Monte Carlo simulations of sizes up to 65 000, and the size of 50 000 was considered as valid for routine applications. The sensitivity was evaluated in terms of 99% confidence intervals of the mean to understand the range of mean values that may represent the entire statistical population of performance variables. The uncertainties were propagated as follows: for 10% change in the ADE, the responses for flux scalar changed by 39.36% (most greater variation) for highly scattering medium, and the least variation of only about 0.49% was found for purely absorbing medium.

Keywords: Telegrapher's Equation with Monte Carlo Simulation; Anomalous Diffusion Exponent; Sensitivity and Uncertainty Analysis.

1. Introduction

The phenomena of anomalous diffusion have been observed in numerous physical and biological systems (Klafter and Sokolov, 2005; Povstenko, 2005; Langlands, 2006; Tan et al., 2007). The notion of anomalous sub-diffusion generalizes the property of mean square displacement proportionality to time, typical of Brownian motion, to the power law $\langle r^2 \rangle \sim t^{\gamma}$ with an exponent $0 < \gamma < 1$. Sub-diffusion characterizes systems where various physical factors impede the free random walk of particles (Klafter, 1997; Metzler and Klafter, 2000). The anomalous diffusion has been known since Richardson's treatise on turbulent diffusion in 1926 (Richardson, 1926). Within transport theory it has been studied since the late 1960s. In particular, its theoretical investigation was instigated by Scher and Montroll in their description of dispersive transport in amorphous semiconductors, a system where the traditional methods proved to fail (Scher and Montroll, 1975).

The last five decades have witnessed the intensive study of the neutrons distribution in a reactor with both numerical and analytical techniques. Normally, Fick's law is adopted as basic model for the description and understand the complex behaviour of the neutrons motion. Most reactor studies treat the neutron motion as a diffusion process, where one assumes that neutrons in average tend to diffuse from regions of high neutron density to low neutron density. However, the validity of using this law has been questioned extensively. It is due that the Fick' law provides a strictly valid mathematical description of the neutron flux when the following assumptions are satisfied: 1) Absorption much less likely than scattering, 2) Linear spatial variation of the neutron distribution, and 3) Isotropic scattering in its derivation (Stacey, 2004). But the main reason is that this diffusive law implies an infinity velocity of propagation. This

property is unphysical from a physical point of view. In order to consider a finite velocity of propagation or describe the phenomena of anomalous diffusion, several new constitutive models have been introduced. For example, the widely used Cattaneo model, the fractional Fick's law which is written in terms of space and/or time fractional derivatives and lead to obtain the space and/or time fractional diffusion equation (Chaves, 1998; Paradisi et al., 2001; Jiang et al., 2000). The Cattaneo model was used by Heizler in the P_1 approximation for the Boltzmann equation, which yields to the Telegrapher's equation, and replaces the feature of an infinite velocity with a wrong finite velocity (given by $\upsilon/\sqrt{3}$) (Heizler, 2010). Recently Espinosa-Paredes and Polo-Labarrios used a fractional Fick's law, which is written in terms of time fractional derivatives and lead to the fractional model that describe anomalous diffusion process, this model is the Time-Fractional Telegrapher's Equation (TFTE) given by (Espinosa-Paredes and Polo-Labarrios, 2012a):

$$\frac{\tau^{\gamma}}{\upsilon}\frac{\partial^{1+\gamma}\phi(\vec{r},t)}{\partial t^{1+\gamma}}+\frac{1}{\upsilon}\frac{\partial\phi(\vec{r},t)}{\partial t}+\tau^{\gamma}\Sigma_a\frac{\partial^{\gamma}\phi(\vec{r},t)}{\partial t^{\gamma}} \quad , \; t\geq 0. \qquad (1)$$
$$+\Sigma_a\phi(\vec{r},t)-D\vec{\nabla}^2\phi(\vec{r},t)=Q^{(0)}(\vec{r},t)$$

where $\partial^{\gamma+1}/\partial t^{\gamma+1}$ and $\partial^{\gamma}/\partial t^{\gamma}$ are the fractional derivative operators, γ is the anomalous diffusion exponent (ADE) of the fractional differential equation, τ $(=1/\upsilon\Sigma_t)$ is the relaxation time, υ is the neutron velocity, $D(\vec{r})\equiv 1/3\Sigma_t(\vec{r})$ is the diffusion coefficient, and $Q^{(0)}(\vec{r},t)$ is the source term. The sum of macroscopic cross section for absorption (Σ_a) and scattering (Σ_s) is represented by Σ_t. In this approximation the propagation velocity of the neutrons predicted is a power law equal to $1/3^{\gamma/2}$ for $0<\gamma<1$. The TFTE give the best estimate for purely absorbing

medium (Espinosa-Paredes and Polo-Labarrios, 2012a). The derivation of the TFTE approximation and its initials conditions are presented in Appendix A.

The main problem of the TFTE is a method for determination the fractional order (ADE) of the partial differential equation. However, with the statistical treatment of the neutronic data of the nuclear power plant, the ADE can be estimated (Espinosa-Paredes et al., 2008). However, the lack of knowledge on the ADE limits the use of the TFTE.

This paper presents an ADE sensitivity and uncertainty analysis of TFTE from Monte Carlo simulations for simulation sizes up to 60 000. The Monte Carlo method has been widely used for uncertainty analysis (Badar et al., 1993; Rochman et al., 2011; Espinosa-Paredes et al., 2012b). The Monte Carlo simulation for determining uncertainties of the thermal parameters in design of heat exchangers was discussed by Badar et al. (1993), Rochman et al. (2011) used this method in nuclear data uncertainty propagation, and Espinosa-Paredes et al. (2012b) applied the Monte Carlo simulation to evaluate the sensitivity and uncertainty of the fractional neutron point kinetics equations.

2. Preliminaries

The Monte Carlo method is based on sampling the vector of the input parameters in a random sequence, running the system model computer code for each sample of that vector to get a corresponding statistical sample of the vector of the output variables, and then estimating the characteristics of these output variables using the output samples. One of the benefits of the Monte Carlo method is that we may use all standard statistical methods and tests to estimate

distributions of the output variables as well as to evaluate any hypothesis. This makes it the most straightforward and powerful method available in the scientific literature to deal with sensitivity analysis and uncertainty propagation in complex models. Although there equation for such error propagation process, these equations are, in fact an approximate and their use in the evaluation of complex models are highly cumbersome (Bevington and Robinson, 2003). These considerations make the Monte Carlo approach much more amenable for the present simulation study.

3. Methodology

The Monte Carlo simulation methodology can be implemented are the following steps (Espinosa-Paredes et al., 2012b):

Step 1. Generating random numbers uniformly distributed in space (0, 1), i.e., samples from a uniform U(0, 1) distribution (where theory mean is 0 and theory deviation standard is 1): The Mersenne Twister algorithm of Matsumoto and Nishimura was employed (Matsumoto et al., 1998), which is a widely used generator with a very long (2^{19937}-1) period. Thus, the necessary streams of independent and identically distributed random numbers (IID U(0, 1)) of 64 bits were generated.

Step 2. Testing of the random numbers if they resemble independent and identically distributed IID U(0, 1) random variants: The simulated data clearly filled the (0, 1) space as required by this randomness test in both two- and three-dimensions. On the average, only around 1 number out of 100 000 numbers in individual streams of IID U(0, 1) was repeated. Because the simulations

sizes were only up to 65 000, practically no repeated numbers were encountered in the entire chain, which made the Monte Carlo method fully valid for this application.

Step 3. Converting the random numbers to continuous random variants for a normal distribution N(0, 1): The polar method of Marsaglia and Bray was chosen for the present application (Marsaglia and Bray, 1964). Two parallel streams of random numbers (R_1 and R_2) were used for generating one set of IID N(0, 1) normal random variants. Practically no repeated-numbers were found in tests with 100 000 numbers in these sets of random normal variants. Therefore, the data was considered as high quality to represent a normal distribution and could, therefore, be safely used for further applications.

Step 4. To analyse the effect of the γ on the TFTE behaviour, the Monte Carlo simulation was implemented in the numerical solution of TFTE (See Fractional numerical solution, and Sec. 5 of implementation).

Step 5. Sensitivity and uncertainty analysis of ADE in the TFTE equations: These IID N(0,1) normal random variants for the evaluation of the sensitivity relationships of ADE with flux scalar were used.

4. Fractional Numerical Solution

The numerical approximation of the solution of the Eq. (1) model was solved by Espinosa-Paredes and Polo-Labarrios (2012a), applying a finite difference method (FDM) used for the

discretized form of the time fractional derivative with Caputo's approximation (Yang et al., 2008), which can be explicitly solved for ϕ_i^{j+1}:

$$\phi_i^{j+1} = -\frac{d}{(1+a+b)}\phi_{i-1}^{j} - \frac{(d+2e-a-b+g_1)}{(1+a+b)}\phi_i^{j} + \frac{e}{(1+a+b)}\phi_{i+1}^{j} - \frac{g_2}{(1+a+b)}\phi_i^{j-1} - \frac{b}{(1+a+b)}\sigma_j\left(\phi_i^{1}-\phi_i^{0}\right) - \frac{1}{(1+a+b)}\sum_{k=3}^{j+1} g_k\phi_i^{j-k+1} - \frac{b}{(1+a+b)}\sum_{k=1}^{j-1}\sigma_k\left(\phi_i^{j+1-k}-\phi_i^{j-k}\right) \quad (2)$$

where $a=\tau^{\gamma}$, $b=\frac{\tau(1-c)}{\Gamma(2-\gamma)}$, $d=\tau^{1+\gamma}(1-c)$, $e=\frac{\tau^{1+\gamma}}{3h^2}$, $g_k=(-1)^k\frac{(\alpha)(\alpha-1)\cdots(\alpha-k+1)}{k!}$

(with $\alpha=1+\gamma$), $\sigma_k=(k+1)^{1-\gamma}-k^{1-\gamma}$ for $k=0,1,2,\ldots,j-1$.

The fundamentals on fractional numerical solution for TFTE are present in Appendix B.

5. Implementation of Monte Carlo Simulation

To analyse the effect of the γ on the TFTE behaviour, the Monte Carlo simulation was implemented in the numerical solution of TFTE through the following expression:

$$\gamma_i = \gamma_0 + b\times x_i, \qquad i=1,2,3,\ldots,N \quad (3)$$

where γ_i is the *i*-th value of the ADE, γ_0 is an initial value less than one and greater than zero, b is the percent change in the ADE which is constant and x_i is the number related to the Monte Carlo method. Then, γ_i is calculated for each x_i value (with $i=1,2,3,\ldots,N$), which is used as the input data of TFTE numerical simulation.

To analyze the ADE (γ) are necessary dynamic numerical experiments where variations with respect to time of the scalar flux is important. In order to analyze the γ effect in scalar flux we

consider a delta source problem for three different kinds of medium (Espinosa-Paredes and Polo-Labarrios, 2012a): 1) *purely absorbing medium* ($c=0$), 2) *heterogeneous medium* ($c=0.65$), and 3) *highly scattering medium* ($c\approx 1$), for different times: *very short time* ($T=t_0$; where $t_0 \equiv t\upsilon\Sigma_t$), *short time* ($T=2t_0$), and *very long time* ($T=6t_0$). For each medium and time, the scalar flux is presented for different transport mean free path ($\lambda_t = x\Sigma_t$) values, as can be observed in Figure 2 the scalar flux have different behavior for each kind of medium and simulation time, in this sense λ_t values were selected for case shown in this Figure. With these considerations, the sensitivity and uncertainty analysis is carried out.

6. Results and Discussions

6.1 Relative standard deviation (RSD)

The aim of this section is to determine the optimal size sample (N) where RSD is practically constant and independent of the simulation size. To difference of the work of Espinosa-Paredes et al. (2012b), in this work we used three random numbers (N1, N2, N3) generated with three different seeds obtained with the **step 1** and validate with **step 2** of the methodology presented previously in Sec. 3 of this work.

Figure 1 presents a schematic plot showing RSD values expressed in percentages for γ for N1, N2, and N3. The RSD was calculated according to the following expression (Bevington and Robinson, 2003):

$$\text{RSD} = \frac{s}{\bar{x}} \times 100 \tag{4}$$

where s in the standard deviation and $\bar{x}$ is the mean. Consideration of the RSD allows us to establish the optimal simulation size N. The optimal value of N is obtained when the value of RSD becomes practically invariable with respect to the simulation size N. In Figure 1, it can be observed that for simulation size N (N1, N2, and N3) smaller than 5 000, the RSD varies considerably and unpredictably; for N =10 000, 15 000 and 20 000 the variations in the values of RSD tend to decrease. For N greater than 50 000, the values of RSD became practically constant and independent of the simulation size. Therefore, the optimal simulation size N used in this work was 65 000. The value of RSD for γ were the same for each time simulation as expected, due that for each time the correspondent random numbers are the same.

6.2 Anomalous diffusion exponent on TFTE behaviour

The results of the influence of ADE on the TFTE response characteristics evaluated from the Monte Carlo simulation for *purely absorbing medium* ($c=0$), *heterogeneous medium* ($c=0.65$), and *highly scattering medium* ($c\approx 1$) are shown in Figures 3, 4 and 5, respectively, which were obtained with the simulation size of 65 000, for each simulation time, for *very short times* ($T=t_0$), *short times* ($T=2t_0$), and *very long times* ($T=6t_0$), and for different values of λ_t.

In Figure 3 can be observed the influence of ADE (γ) on scalar flux dimensionless (ϕ/Q_0) in a delta source problem, is as follow: a) For *very short times* ($T=t_0$): at $\lambda_t=0.25$ can be observed that the behavior of the scalar flux is approximately quadratic with respect to the ADE, and it note a statistically significant positive correlation between these two parameters; and at $\lambda_t=0.5$, and 1.0 note a statistically significant negative correlation between these two parameters,

and it can be observed that the behavior of the scalar flux is approximately quadratic with respect to the ADE, too.

b) For *short times* ($T = 2t_0$): at $\lambda_\tau = 0.5,$ and 1.0 note a statistically significant positive correlation between these two parameters, and it can be observed that the behavior of the scalar flux is approximately quadratic and cubic with respect to the ADE, respectively; and at $\lambda_\tau = 1.5$ can be observed that the behavior of the scalar flux is approximately cubic with respect to the ADE, and note a statistically significant negative correlation between these two parameters; c) For *very long times* ($T = 6t_0$): at $\lambda_\tau = 0.5, 1.0, 2.0$, note a statistically significant positive correlation between these two parameters, and it can be observed that the behavior of the scalar flux is approximately quadratic with respect to the ADE in all cases.

The results of the influence of ADE on the TFTE response characteristics evaluated from the Monte Carlo simulation for *heterogeneous medium* ($c = 0.65$), for *very short times* ($T = t_0$), *short times* ($T = 2t_0$), and *very long times* ($T = 6t_0$) the same qualitative results was observed respect to *purely absorbing medium*, this can be observed in Figure 4. In the case *Highly scattering medium* ($c \approx 1$), for all the cases, i.e., for $T = t_0$, $T = 2t_0$, $T = 6t_0$, the same qualitative results were observed respect to *purely absorbing medium* and *heterogeneous medium*, this can be observed in Figure 5. However, the difference among them is their range of variation which is presented on Tables 1–3.

6.3 Sensitivity analysis

We used the 99% confidence limits ($CL99$) or 99% confidence intervals ($CI99$) of the mean to understand the sensitivity of the system to changes in ADE (γ). These were calculated using the standard formulae as follows (Bevington and Robinson, 2003):

$$CL99 = t_{(n-1)} \cdot \frac{s}{\sqrt{n}} \tag{5}$$

$$CI99 = \overline{x} \pm t_{(n-1)} \cdot \frac{s}{\sqrt{n}} \tag{6}$$

where s is the standard deviation, $\overline{x}$ is the mean value, n is the simulation size used and t is the Student t critical value for the required degrees of freedom.

The results (Tables 1–3) show how the statistical population mean values of the ADE (γ_0) in TFTE would be localized within these respective intervals of 99% confidence level (or 1% significance). Thus, there is 99% confidence that if γ were anywhere between the interval of 0.59932 – 0.60053, the flux scalar dimensionless (ϕ/Q_0) would be between the interval shown in the Table 1–3 for *purely absorbing medium* ($c = 0$), *heterogeneous medium* ($c = 0.65$), and *highly scattering medium* ($c \approx 1$), respectively. For example for *purely absorbing medium* ($c = 0$) in Table 1: for γ interval of 0.59932 – 0.60053, the flux scalar dimensionless (ϕ/Q_0) would be between 0.14259 – 0.14261 at $\lambda_t = 0.50$, and *very short times* ($T = t_0$); so for each condition analysed. Sensitivity analysis was also carried out through cubic and polynomial regressions on the simulated data (Table 4–6) using the anomalous diffusion exponent (γ) as the predictor variable. The results showed statistically valid cubic correlations for scalar flux.

6.4 Uncertainty analysis

For this analysis, the results are summarized in Tables 7–9: for *purely absorbing medium* ($c = 0$), *heterogeneous medium* ($c = 0.65$), and *highly scattering medium* ($c \approx 1$), respectively. For each characteristic medium and simulation time, were selected three different λ_t values according to the behaviour of the flux scalar dimensionless (ϕ/Q_0) in each case, as was observed (Figure 2). The interpretation of these tables is shown with the following example: Table 8 shows that with 10% variation in the ADE (γ), the flux scalar dimensionless (ϕ/Q_0) at $\lambda_t = 1.5$ varied about 15.82% for short times. It is important to point according to the results reported in these tables that the greatest variation of only about 39.36% was observed at $\lambda_t = 1.0$ for *highly scattering medium* ($c \approx 1$) and very short times (Table 9), and the least variation of only about 0.49% was found at $\lambda_t = 0.5$ for *purely absorbing medium* ($c = 0$) and very short times (Table 7).

7. Conclusions

The sensitivity and uncertainty analysis of ADE (fractional order of differential equation) in the time-fractional telegrapher´s equation (TFTE) was performed with the Monte Carlo simulations. The following results were obtained:

(1) The optimal simulation size N found in this work was 50 000 when the RSD values were practically constant and independent of the simulation size up to 65 000 (Figure 1).

(2) The influence of ADE on flux scalar dimensionless from the Monte Carlo simulation was graphically obtained (Figures 3, 4 and 5).

(3) The sensitivity was evaluated in terms of 99% confidence intervals of the mean to understand the range of mean values that may represent the entire statistical population of performance variables (Table 1–3). The regression analysis with anomalous diffusion

exponent (γ) as the predictor variable showed statistically valid cubic correlation for scalar flux (Table 4–6).

(4) The uncertainties were propagated as follows (Tables 7–9): for 10% change in the ADE (γ), the responses for flux scalar changed by 39.36% (greatest variation) at $\lambda_\gamma = 1.0$ for *highly scattering medium* ($c \approx 1$) and *very short times* (Table 9), and the least variation of only about 0.49% was found at $\lambda_\gamma = 0.5$ for *purely absorbing medium* ($c = 0$) and also for *very short times* (Table 7).

Appendix A

The fractional constitutive equation of the current density vector is given by Espinosa-Paredes et al. (2008)

$$\tau^\gamma \frac{\partial^\gamma \vec{J}}{\partial t^\gamma} + \vec{J} = -D\nabla\phi \tag{A.1}$$

where $\partial^\gamma / \partial t^\gamma$ is the fractional derivative operator, γ is the anomalous diffusion exponent, τ $(= 1/\upsilon\Sigma_t = 3D/\upsilon)$ is the relaxation time, and $D(\vec{r}) \equiv 1/3\Sigma_t(\vec{r})$ is the diffusion coefficient.

The conservation law that governs the particle collision and reaction processes is given by

$$\frac{1}{\upsilon}\frac{\partial\phi(\vec{r},t)}{\partial t} + \vec{\nabla}\cdot\vec{J}(\vec{r},t) + \Sigma_a(\vec{r})\phi(\vec{r},t) = Q^{(0)}(\vec{r},t) \tag{A.2}$$

where $Q^{(0)}$ is the source term.

Substituting Eq. (A.1) into Eq. (A.2) yields the TFTE approximation for the anomalous diffusion approximation as (Espinosa-Paredes and Polo-Labarrios, 2012a)

$$\frac{\tau^{\gamma}}{\upsilon}\frac{\partial^{1+\gamma}\phi(\vec{r},t)}{\partial t^{1+\gamma}}+\frac{1}{\upsilon}\frac{\partial\phi(\vec{r},t)}{\partial t}+\tau^{\gamma}\Sigma_a\frac{\partial^{\gamma}\phi(\vec{r},t)}{\partial t^{\gamma}} \quad , \; t\geq 0. \tag{A.3}$$
$$+\Sigma_a\phi(\vec{r},t)-D\vec{\nabla}^2\phi(\vec{r},t)=Q^{(0)}(\vec{r},t)$$

Where the terms related with a time-dependent source ($\partial Q^{(0)}(\vec{r},t)/\partial t$ and $\partial^{\gamma} Q^{(0)}(\vec{r},t)/\partial t^{\gamma}$) were not considered. Then, the Eq. (A.3) applied to a one-dimensional infinite-slab problem with a time-independent delta source in the middle (at $x=0$), i.e., $Q(x)=Q_0\delta(x)$ (Heizler, 2010), whose initial conditions are $\phi(x,0)=0$ and $\left(\partial\phi(x,t)/\partial t\right)\big|_{t=0}=0$, and the boundary conditions are given by $\lim_{x\to\infty}\phi(x,t)<\infty$ and $\lim_{x\to 0}\phi(x,t)$ is obtained of classical diffusion approximation which is (Espinosa-Paredes and Polo-Labarrios, 2012a):

$$x(0,t)=\frac{Q_0}{4}\sqrt{\frac{3}{(1-c)}}\left[erfc\left(-\sqrt{(1-c)t_0}\right)-erfc\left(\sqrt{(1-c)t_0}\right)\right] \tag{A.4}$$

Under these considerations the Eq. (A.3) took the form:

$$\frac{1}{\Sigma_t^{\gamma}\upsilon^{1+\gamma}}\frac{\partial^{1+\gamma}\phi(x,t)}{\partial t^{1+\gamma}}+\frac{1}{\upsilon}\frac{\partial\phi(x,t)}{\partial t}+\frac{\Sigma_a}{\Sigma_t^{\gamma}\upsilon^{\gamma}}\frac{\partial^{\gamma}\phi(x,t)}{\partial t^{\gamma}} \quad , \; t\geq 0 \; with \; 0<\gamma<1 \tag{A.5}$$
$$+\Sigma_a\phi(x,t)-\frac{1}{3\Sigma_t}\frac{\partial^2\phi(x,t)}{\partial x^2}=Q_0\delta(x)$$

Here $\partial^{\gamma}\phi(\vec{r},t)/\partial t^{\gamma}$ is Caputo fractional order derivative, defined by (Podlubny, 1999):

$$\frac{\partial^{\gamma}\phi(x,t)}{\partial t^{\gamma}}=\frac{1}{\Gamma(1-\gamma)}\int_0^t(t-\eta)^{-\gamma}\frac{\partial\phi(x,\eta)}{\partial\eta}d\eta \tag{A.6}$$

and $\partial^{1+\gamma}\phi(\vec{r},t)/\partial t^{1+\gamma}$ is Riemann–Liouville fractional order derivative (Meerschaert and Tadjeran, 2003):

$$\frac{\partial^{1+\gamma}\phi(x,t)}{\partial t^{1+\gamma}}=\frac{1}{\Gamma(2-\gamma)}\frac{\partial^2}{\partial t^2}\int_0^t\frac{\phi(x,\xi)}{(t-\xi)^{\gamma-1}}d\eta \tag{A.7}$$

To solving the Eq. (A.5) we considering that the space dimension is in terms of the transport mean free path. Then, the Eq. (A.5) can be re-write as (Espinosa-Paredes and Polo-Labarrios, 2012a)

$$\frac{\partial^{1+\gamma}\phi(x,t)}{\partial t_0^{1+\gamma}}+\frac{\partial\phi(x,t)}{\partial t_0}+(1-c)\frac{\partial^{\gamma}\phi(x,t)}{\partial t_0^{\gamma}}+(1-c)\phi(x,t)-\frac{1}{3}\frac{\partial^2\phi(x,t)}{\partial\lambda_t^{2}}=Q_0\delta(x)\ ,\ t_0\geq 0 \quad \text{(A.8)}$$

where dimensionless number used are: $\lambda_t = x\Sigma_t$ and $t_0 = t/\upsilon\Sigma_t$ (being $t_0 = nt$ for $n\in\mathbb{R}_+$).

The mean number of secondary particles emitted per collision event,

$$c=\frac{\Sigma_s}{\Sigma_t}=\frac{\Sigma_s}{\Sigma_a+\Sigma_s} \quad \text{(A.9)}$$

Where substituting Eqs. (B.1) to (B.4) into the Eq. (A.8), and rearranging terms is obtained Eq. (2).

Appendix B

To establish the numerical approximation scheme, let $t_j = j\tau\ (j=0,1,2,\ldots,m)$ be the integration time $0\leq t_j\leq T$, $\tau=\frac{T}{m}$, $h=\frac{L}{n}>0$ is the grid in space direction, $x_i = ih\ (i=0,1,2,\ldots,n)$.

We take the following finite differences approximations for time fractional derivatives appeared in Eq. (A.8) (Yang et al., 2008; Podlubny, 1999; Meerschaert and Tadjeran, 2003):

$$\frac{\partial^{\gamma}\phi(x,t)}{\partial t^{\gamma}}=\frac{\tau^{1-\gamma}}{\Gamma(2-\gamma)}\sum_{k=0}^{j}\frac{\phi(x_i,t_{j+1-k})-\phi(x_i,t_{j-k})}{\tau}\left[(k+1)^{1-\gamma}-k^{1-\gamma}\right]+\mathbf{O}(\tau), \quad \text{(B.1)}$$

$$\frac{\partial\phi(x,t)}{\partial t}=\frac{\phi(x_i,t_{j+1})-\phi(x_i,t_j)}{\tau}+\mathbf{O}(\tau) \quad \text{(B.2)}$$

$$\frac{\partial^2\phi(x,t)}{\partial x^2}=\frac{\phi(x_{i-1},t_j)-2\phi(x_i,t_j)+\phi(x_{i+1},t_j)}{h^2}+\mathbf{O}(h) \quad \text{(B.3)}$$

For the approximation of Riemann–Liouville fractional order derivative $\partial^{1+\gamma}\phi(x,t)/\partial t^{1+\gamma}$, we use the shifted Grünwald formula (Meerschaert and Tadjeran, 2003):

$$\frac{\partial^{\alpha}\phi(x,t)}{\partial t^{\alpha}} = \frac{1}{\tau^{\alpha}}\sum_{k=0}^{J+1} g_k \phi(x_1, t_{J-k+1}) + \mathbf{O}(\tau + h) \tag{B.4}$$

where $\alpha = 1+\gamma$, and the normalized Grünwald weights are defined by

$$g_0 = 1 \text{ and } g_k = (-1)^k \frac{(\alpha)(\alpha-1)\cdots(\alpha-k+1)}{k!} \text{ for } k = 1,2,3,\ldots \tag{B.5}$$

Note that these normalized weights only depend on the order and the index k.

References

Badar, A.M., Zubair, M.S., Sheiki, A., 1993. Uncertainty analysis of heat-exchanger thermal design using the Monte Carlo simulation technique, Energy 18, 859.

Bevington, P.R., Robinson, D.K., 2003. Data reduction and error analysis for the physical sciences. Mc Graw Hill, Boston.

Chaves, A.S., 1998. A fractional diffusion equation to describe Lévy flights. Phys. Lett. A 239, 13.

Espinosa-Paredes, G., Morales-Sandoval, J.B., Vázquez-Rodríguez, R., Espinosa-Martínez, E.-G., 2008. Constitutive laws for the neutron density current. Ann Nucl Energy 35, 1963.

Espinosa-Paredes, G., Polo-Labarrios, M.-A., 2012a. Time-fractional telegrapher equation (P1) approximation for the transport equation. Nucl Sci Eng 171. In press.

Espinosa-Paredes, G., Polo-Labarrios, M.-A., Díaz-Gonzáles, L., Vázquez-Rodríguez, A., Espinosa-Martínez, E.-G., 2012b. Sensitivity and uncertainty analysis of the fractional neutron point kinetics equations. Ann Nucl Energy 42, 169.

Heizler, S.I., 2010. Asymptotic Telegrapher's Equation (P1) Approximation for the Transport Equation. Nucl Sci Eng 166, 17.

Jiang, X.Y., Xu, M.Y., Qi, H.T., 2000. The fractional diffusion model with an absorption term and modified Fick's law for non-Local transport processes. Nonlinear Anal. RWA 11, 262.

Klafter, J., Sokolov, I.M., 2005. Anomalous diffusion spreads its wings. Phys. Word 18, 29.

Klafter, J., Zumofen, G., Shlesinger, M.F., 1997. The Physics of Complex Systems ed. F Mallamace and H E Stanley, Amsterdam.

Langlands, T.A.M., 2006. Solution of a modified fractional diffusion equation. Physica A 367, 136.

Marsaglia, G., Bray, T.A., 1964. A convenient method for generating normal variables, SIAM Rev. 6, 260.

Meerschaert, M.M., Tadjeran, C., 2003. Finite difference approximations for fractional advection–dispersion flow equations. J. Comput. Appl. Math. 172, 65.

Matsumoto, M., Nishimura, T., Twister, M., 1998. A 623-dimensionally equidistributed uniform pseudorandom number generator. ACM Trans. Modell. Comput. Sim. 8, 3.

Meerschaert, M.M., Tadjeran, C., 2003. Finite difference approximations for fractional advection–dispersion flow equations. J. Comput. Appl. Math. 172, 65.

Metzler, R., Klafter, J., 2000. The Random Walk's Guide to Anomalous Diffusion: A Fractional Dynamics Approach, Phys. Rep. 339, 1.

Paradisi, P., Cesari, R., Mainardi, F., Tampieri, F., 2001. The fractional Fick's law for non-local transport process. Physica A 293, 130.

Podlubny, I., 1999. Fractional Differential Equations. Academic Press, New York.

Povstenko, Y.Z., 2005. Fractional heat conduction equation and associated thermal stress. J. Therm. Stresses 28, 83.

Richardson, L.F., 1926. Atmospheric Diffusion Shown on a Distance-Neighbour Graph, Proceeding of the Royal Society of London, Series A 110, 709.

Rochman, D., Koning, A.J., van der Marck, S.C., Hogenbirk, A., Sciolla, C.M., 2011. Nuclear data uncertainty propagation: Perturbation vs. Monte Carlo. Ann Nucl Energy 38, 942.

Scher, H., Montroll, E.W., 1975. Anomalous Transit-time Dispersion in Amorphous Solid. Phys. Rev. B 12, 2455.

Stacey, W.M., 2004. Nuclear Reactor Physics. Wiley-VCH.

Tan, W.C., Fu, C.Q., Fu, C.J., Xie, W.J., Cheng, H., 2007. An anomalous subdiffusion model for calcium spark in cardiac myocytes. Appl. Phys. Lett. 91, 183901-1.

Yang, Qianquian, Turner, Ian, Liu, Fawang, 2008. Analytical and numerical solutions for the time and space-symmetric fractional diffusion equation. In: ANZIAM Journal: Proceedings of the 4th Biennial Computational Techniques and Applications Conference (CTAC2008), Australian National University, Canberra, 13- 16 July.

*Highlights (for review)

Research Highlights

- The Time-Fractional Telegrapher´s Equation for neutron motion is numerically studied
- The sensitivity and uncertainties was carryout for the fractional coefficient
- This analysis was carried out through Monte Carlo simulations of sizes up to 65,000
- Uncertainties was propagated for 10% change in the fractional coefficient
- Greater variation found for neutron flux was of 39.36% for highly scattering medium
- Least variation found for neutron flux was of 0.49% for purely absorbing medium.

Figure

Figure Caption

Figure 1. Relative standard deviation (RSD) for γ as a function of the simulation size N. The horizontal dashed line at 10% is the reference line for γ.

Figure 2. Scalar flux to a delta source problem for a purely absorbing medium ($c=0$), for heterogeneous medium ($c=0.65$), and for a highly scattering medium ($c=0.99$). The Time-Fractional Telegrapher's Equation (TFTE) given by Eq. (1). The anomalous diffusion exponent $\gamma=0.6$; a) very short time ($T=t_0$), b) short time ($T=2t_0$), and c) very long times ($T=6t_0$); where $t_0 \equiv tv\Sigma_t$.

Figure 3. *Purely absorbing medium* ($c=0$): Influence of anomalous diffusion exponent (γ) on scalar flux in a source problem for *very short times* ($T=t_0$), *short times* ($T=2t_0$), and *very long times* ($T=6t_0$).

Figure 4. *Heterogeneous medium* ($c=0.65$): Influence of anomalous diffusion exponent (γ) on scalar flux in a source problem for *very short times* ($T=t_0$), *short times* ($T=2t_0$), and *very long times* ($T=6t_0$).

Figure 5. *Highly scattering medium* ($c\approx 1$): Influence of anomalous diffusion exponent (γ) on scalar flux in a source problem for *very short times* ($T=t_0$), *short times* ($T=2t_0$), and *very long times* ($T=6t_0$).

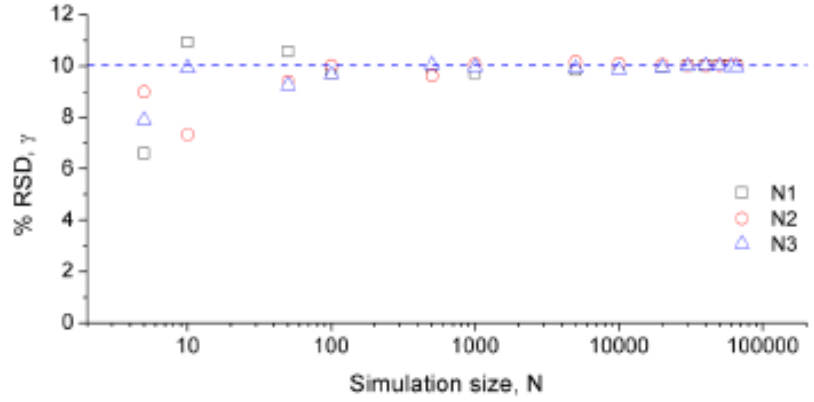
% RSD, y
Simulation size, N
N1
N2
N3
0
2
4
6
8
10
12
10
100
1000
10000
100000

Figure 1.

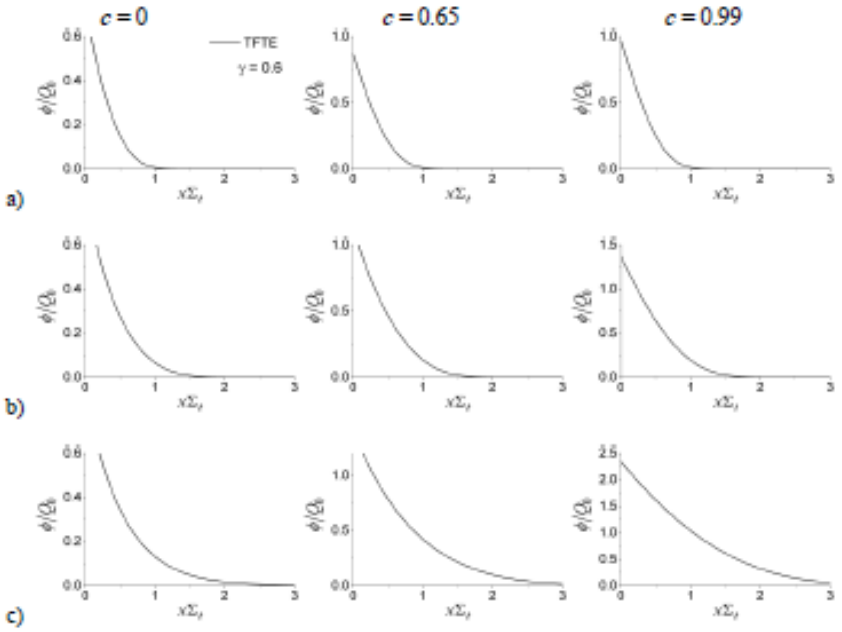

Figure 2.

3

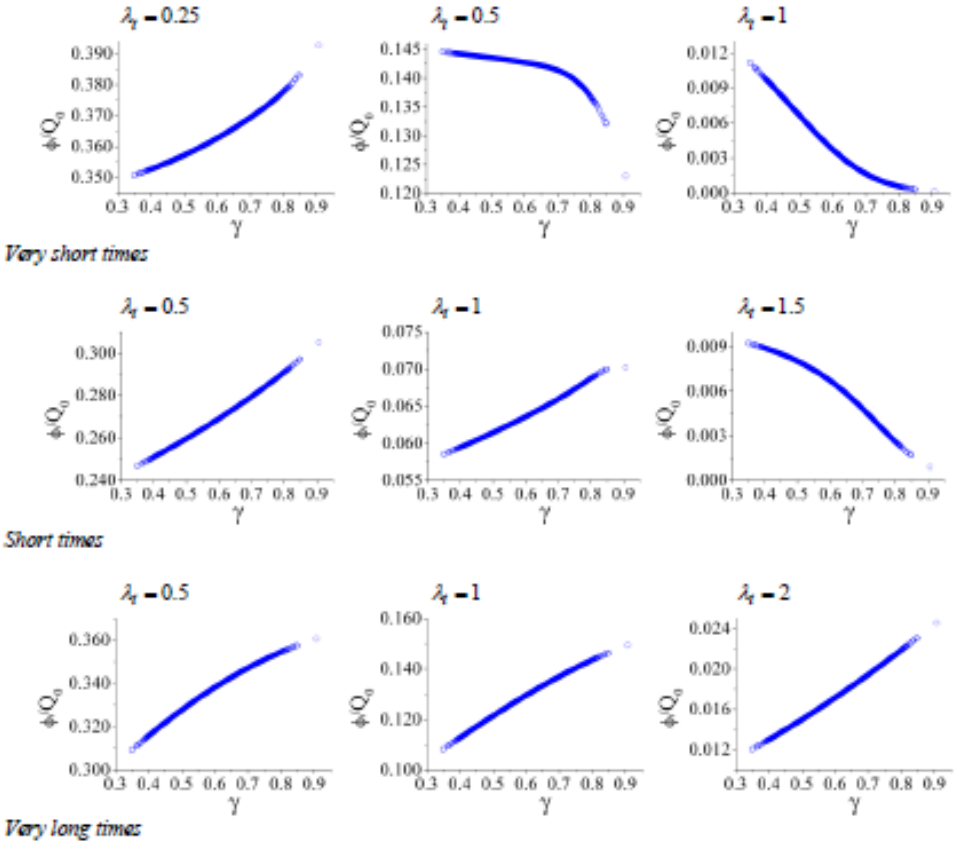
$\lambda_t = 0.25$
$\lambda_t = 0.5$
$\lambda_t = 1$
ϕ/Q_0
γ
Very short times
$\lambda_t = 0.5$
$\lambda_t = 1$
$\lambda_t = 1.5$
Short times
$\lambda_t = 0.5$
$\lambda_t = 1$
$\lambda_t = 2$
Very long times

Figure 3.

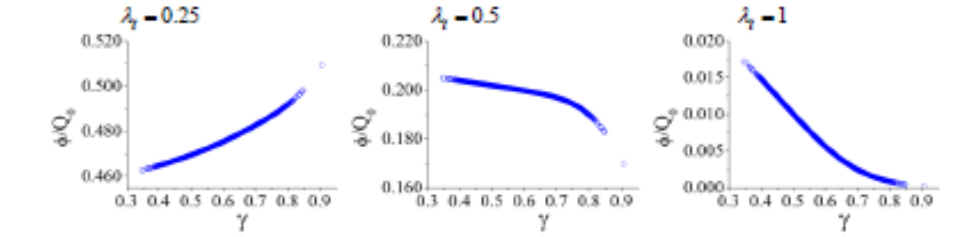

Very short times

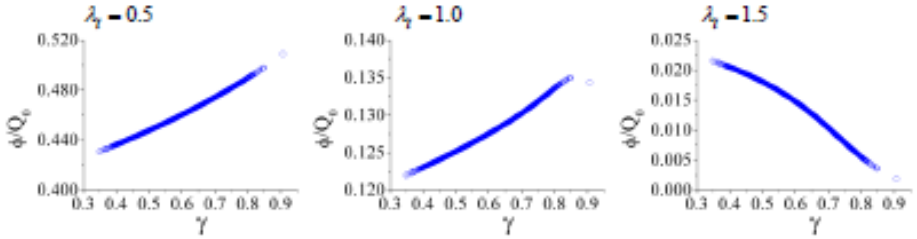

Short times

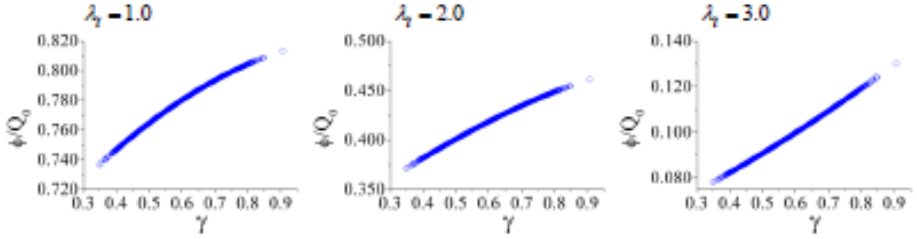

Very long times

Figure 4.

5

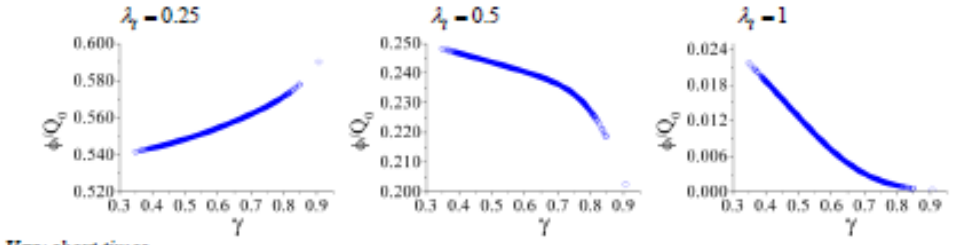

Very short times

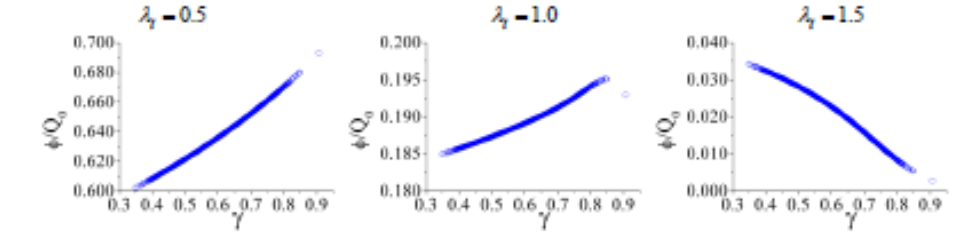

Short times

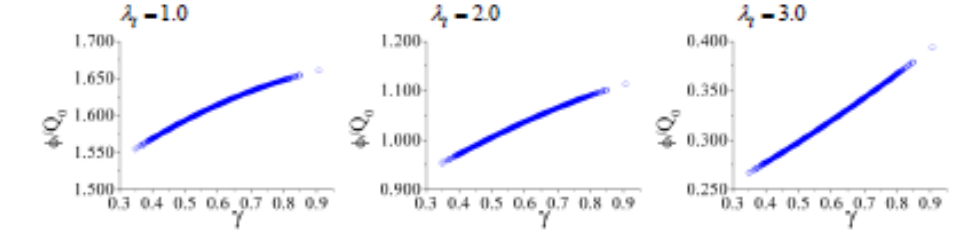

Very long times

Figure 5.

Table

Table Caption

Table 1. Sensitivity analysis through 99% confidence intervals of the mean (CI99), for $c = 0$.

Table 2. Sensitivity analysis through 99% confidence intervals of the mean (CI99), for $c = 0.65$.

Table 3. Sensitivity analysis through 99% confidence intervals of the mean (CI99), for $c \approx 1$.

Table 4. Regression analysis (γ is the predictor variable) in very short times ($T = t_0$), short times ($T = 2t_0$) and very long times ($T = 6t_0$), for *purely absorbing medium* ($c = 0$).

Table 5. Regression analysis (γ is the predictor variable) in very short times ($T = t_0$), short times ($T = 2t_0$) and very long times ($T = 6t_0$), for *heterogeneous medium* ($c = 0.65$).

Table 6. Regression analysis (γ is the predictor variable) in very short times ($T = t_0$), short times ($T = 2t_0$) and very long times ($T = 6t_0$), for *high scattering medium* ($c = 0.99$).

Table 7. Uncertainty estimates on important parameters evaluated in terms of the RSD, for *purely absorbing medium* ($c = 0$).

Table 8. Uncertainty estimates on important parameters evaluated in terms of the RSD, for *heterogeneous medium* ($c = 0.65$).

Table 9. Uncertainty estimates on important parameters evaluated in terms of the RSD, for *highly scattering medium* ($c \approx 1$).

γ	λ_t	ϕ/Q_0 Very short times	ϕ/Q_0 Short times	ϕ/Q_0 Very long times
	0.25	0.36282 – 0.36290		
	0.50	0.14259 – 0.14261	0.269190 – 0.269310	0.337749 – 0.337867
0.59932 – 0.60053	1.00	0.00386 – 0.00389	0.063590 – 0.063620	0.129321 – 0.129415
	1.50		0.00659 – 0.00662	
	2.00			0.017146 – 0.017173

Table 1.

γ	λ_t	ϕ/Q_0 Very short times	ϕ/Q_0 Short times	ϕ/Q_0 Very long times
	0.25	0.475552 – 0.475632		
	0.50	0.199558 – 0.199590	0.460464 – 0.460624,	
	1.00	0.005856 – 0.005903	0.127568 – 0.127599	0.779682 – 0.779857
0.59932 – 0.60053	1.50		0.014551 – 0.014598	
	2.00			0.418080 – 0.418284
	3.00			0.099798 – 0.099910

Table 2.

γ	λ_f	ϕ/Q_0 Very short times	ϕ/Q_0 Short times	ϕ/Q_0 Very long times
0.59932 – 0.60053	0.25	0.554589 – 0.554671		
	0.50	0.240244 – 0.240289	0.636222 – 0.636407	
	1.00	0.007329 – 0.007388	0.189173 – 0.189197	1.613641 – 1.61388
	1.50		0.022455 – 0.022530	
	2.0			1.035939 – 1.036301
	3.0			0.319535 – 0.320007

Table 3.

Dependent variable	Cubic regression quality parameter (R^3)	Regression equation
$T-t_0$ $\left.\frac{\phi}{Q}\right\|_{\lambda_t=0.25}$	0.999952	$\phi/Q_0 = (0.337691 \pm 0.000039) + (0.039488 \pm 0.000195)\cdot\gamma$ $-(0.024112 \pm 0.000327)\cdot\gamma^2 + (0.046010 \pm 0.000181)\cdot\gamma^3$
$T-t_0$ $\left.\frac{\phi}{Q}\right\|_{\lambda_t=0.5}$	0.991289	$\phi/Q_0 = (0.1844240 \pm 0.0001007) - (0.2140185 \pm 0.0005091)\cdot\gamma$ $+(0.3803261 \pm 0.0008526)\cdot\gamma^2 - (0.2323753 \pm 0.0004729)\cdot\gamma^3$
$T-t_0$ $\left.\frac{\phi}{Q}\right\|_{\lambda_t=1}$	0.999918	$\phi/Q_0 = (0.0167464 \pm 0.0000208) + (0.0093441 \pm 0.0001054)\cdot\gamma$ $-(0.0966771 \pm 0.0001765)\cdot\gamma^2 + (0.0749473 \pm 0.0000979)\cdot\gamma^3$
$T-2t_0$ $\left.\frac{\phi}{Q}\right\|_{\lambda_t=0.5}$	0.999999	$\phi/Q_0 = (0.2194747 \pm 0.0000044) + (0.0777595 \pm 0.0000221)\cdot\gamma$ $-(0.0106015 \pm 0.0000369)\cdot\gamma^2 + (0.0313784 \pm 0.0000205)\cdot\gamma^3$
$T-2t_0$ $\left.\frac{\phi}{Q}\right\|_{\lambda_t=1}$	0.999963	$\phi/Q_0 = (0.0509574 \pm 0.0000126) + (0.0257072 \pm 0.0000635)\cdot\gamma$ $-(0.0180973 \pm 0.0001063)\cdot\gamma^2 + (0.0171108 \pm 0.0000589)\cdot\gamma^3$
$T-2t_0$ $\left.\frac{\phi}{Q}\right\|_{\lambda_t=1.5}$	0.999812	$\phi/Q_0 = (0.0056851 \pm 0.0000203) + (0.0211793 \pm 0.0001025)\cdot\gamma$ $-(0.0352995 \pm 0.0001717)\cdot\gamma^2 + (0.0047192 \pm 0.0000952)\cdot\gamma^3$
$T-6t_0$ $\left.\frac{\phi}{Q}\right\|_{\lambda_t=0.5}$	0.9999999	$\phi/Q_0 = (0.2548347 \pm 0.0000006) + (0.1771183 \pm 0.0000029)\cdot\gamma$ $-(0.0583924 \pm 0.0000050)\cdot\gamma^2 - (0.0092502 \pm 0.0000028)\cdot\gamma^3$

$T-6r_0$ $\left.\frac{\phi}{Q}\right\|_{\lambda_r=1}$	0.999999	$\phi/Q_0 = (0.0761548 \pm 0.0000010) + (0.0901988 \pm 0.0000050)\cdot\gamma$ $+(0.0138198 \pm 0.0000084)\cdot\gamma^2 - (0.0266309 \pm 0.0000047)\cdot\gamma^3$
$T-6r_0$ $\left.\frac{\phi}{Q}\right\|_{\lambda_r=2}$	0.99999986	$\phi/Q_0 = (0.0066824 \pm 0.0000007) + (0.0125163 \pm 0.0000038)\cdot\gamma$ $+(0.0084798 \pm 0.0000063)\cdot\gamma^2 - (0.0005135 \pm 0.0000035)\cdot\gamma^3$

Table 4.

Dependent variable	Cubic regression quality parameter (R^3)	Regression equation
$T-t_0$ $\left.\frac{\phi}{Q}\right\|_{\lambda_t=0.25}$	0.994599	$\phi/Q_0=(0.4503695\pm0.0004430)+(0.0353836\pm0.0022403)\cdot\gamma$ $-(0.0181723\pm0.0037522)\cdot\gamma^2+(0.0476598\pm0.0020812)\cdot\gamma^3$
$T-t_0$ $\left.\frac{\phi}{Q}\right\|_{\lambda_t=0.5}$	0.963238	$\phi/Q_0=(0.2613885\pm0.0004601)-(0.2944069\pm0.0023269)\cdot\gamma$ $+(0.5042947\pm0.0038972)\cdot\gamma^2-(0.3080434\pm0.0021617)\cdot\gamma^3$
$T-t_0$ $\left.\frac{\phi}{Q}\right\|_{\lambda_t=1}$	0.999890	$\phi/Q_0=(0.0271717\pm0.0000368)+(0.0065005\pm0.0001863)\cdot\gamma$ $-(0.1356567\pm0.0003120)\cdot\gamma^2+(0.1084534\pm0.0001731)\cdot\gamma^3$
$T-2t_0$ $\left.\frac{\phi}{Q}\right\|_{\lambda_t=0.5}$	0.999999	$\phi/Q_0=(0.3961041\pm0.0000077)+(0.0972871\pm0.0000391)\cdot\gamma$ $-(0.0084876\pm0.0000654)\cdot\gamma^2+(0.0411838\pm0.0000363)\cdot\gamma^3$
$T-2t_0$ $\left.\frac{\phi}{Q}\right\|_{\lambda_t=1}$	0.999907	$\phi/Q_0=(0.1126271\pm0.0000224)+(0.0351072\pm0.0001133)\cdot\gamma$ $-(0.0346362\pm0.0001897)\cdot\gamma^2+(0.0291617\pm0.0001052)\cdot\gamma^3$
$T-2t_0$ $\left.\frac{\phi}{Q}\right\|_{\lambda_t=1.5}$	0.999861	$\phi/Q_0=(0.0158128\pm0.0000414)+(0.0414246\pm0.0002092)\cdot\gamma$ $-(0.0829853\pm0.0003504)\cdot\gamma^2+(0.0183320\pm0.0001944)\cdot\gamma^3$
$T-6t_0$ $\left.\frac{\phi}{Q}\right\|_{\lambda_t=1}$	0.99999999	$\phi/Q_0=(0.6526773\pm0.0000010)+(0.2794384\pm0.0000052)\cdot\gamma$ $-(0.1088688\pm0.0000087)\cdot\gamma^2-(0.0043780\pm0.0000048)\cdot\gamma^3$

$T-6t_0$ $\frac{\phi}{Q}\Big\vert_{\lambda_1=2}$	0.99999999	$\phi/Q_0 = (0.2966565 \pm 0.0000011) + (0.2204588 \pm 0.0000056)\cdot\gamma$ $-(0.0014449 \pm 0.0000094)\cdot\gamma^2 - (0.0458948 \pm 0.0000052)\cdot\gamma^3$
$T-6t_0$ $\frac{\phi}{Q}\Big\vert_{\lambda_1=3}$	0.9999999	$\phi/Q_0 = (0.0538044 \pm 0.0000028) + (0.0601381 \pm 0.0000142)\cdot\gamma$ $+(0.0287819 \pm 0.0000239)\cdot\gamma^2 - (0.0022109 \pm 0.0000132)\cdot\gamma^3$

Table 5.

Dependent variable	Cubic regression quality parameter (R^3)	Regression equation
$T-t_0$ $\left.\frac{\phi}{Q}\right\|_{\lambda_t=0.25}$	0.999913	$\phi/Q_0 = (0.5307448 \pm 0.0000576) + (0.0272725 \pm 0.0002912)\cdot\gamma$ $-(0.0056789 \pm 0.0004877)\cdot\gamma^2 + (0.0431085 \pm 0.0002705)\cdot\gamma^3$
$T-t_0$ $\left.\frac{\phi}{Q}\right\|_{\lambda_t=0.5}$	0.997662	$\phi/Q_0 = (0.3168781 \pm 0.0001669) - (0.3514261 \pm 0.0008442)\cdot\gamma$ $+(0.5903494 \pm 0.0014140)\cdot\gamma^2 - (0.3614239 \pm 0.0007843)\cdot\gamma^3$
$T-t_0$ $\left.\frac{\phi}{Q}\right\|_{\lambda_t=1}$	0.999925	$\phi/Q_0 = (0.0351922 \pm 0.0000382) + (0.0030672 \pm 0.0001934)\cdot\gamma$ $-(0.1626154 \pm 0.0003239)\cdot\gamma^2 + (0.1323653 \pm 0.0001796)\cdot\gamma^3$
$T-2t_0$ $\left.\frac{\phi}{Q}\right\|_{\lambda_t=0.5}$	0.999999	$\phi/Q_0 = (0.5631329 \pm 0.0000105) + (0.1074734 \pm 0.0000533)\cdot\gamma$ $-(0.0049645 \pm 0.0000892)\cdot\gamma^2 + (0.0472519 \pm 0.0000495)\cdot\gamma^3$
$T-2t_0$ $\left.\frac{\phi}{Q}\right\|_{\lambda_t=1}$	0.999704	$\phi/Q_0 = (0.1767072 \pm 0.0000310) + (0.0338538 \pm 0.0001568)\cdot\gamma$ $-(0.0415682 \pm 0.0002627)\cdot\gamma^2 + (0.0327286 \pm 0.0001457)\cdot\gamma^3$
$T-2t_0$ $\left.\frac{\phi}{Q}\right\|_{\lambda_t=1.5}$	0.999883	$\phi/Q_0 = (0.0272003 \pm 0.0000610) + (0.0599577 \pm 0.0003088)\cdot\gamma$ $-(0.1339729 \pm 0.0005172)\cdot\gamma^2 + (0.0360803 \pm 0.0002869)\cdot\gamma^3$
$T-6t_0$ $\left.\frac{\phi}{Q}\right\|_{\lambda_t=1}$	0.99999999	$\phi/Q_0 = (1.4391319 \pm 0.0000015) + (0.3864721 \pm 0.0000077)\cdot\gamma$ $+(-0.1578140 \pm 0.0000129)\cdot\gamma^2 + (0.0006495 \pm 0.0000072)\cdot\gamma^3$

$T-6t_0$ $\left.\frac{\phi}{Q}\right\|_{\lambda_1=2}$	0.99999999	$\phi/Q_0=(0.8200692\pm0.0000010)+(0.3987726\pm0.0000053)\cdot\gamma$ $+(-0.0235248\pm0.0000009)\cdot\gamma^2+(-0.0657819\pm0.0000049)\cdot\gamma^3$
$T-6t_0$ $\left.\frac{\phi}{Q}\right\|_{\lambda_1=3}$	0.99999993	$\phi/Q_0=(0.2056608\pm0.0000052)+(0.1568797\pm0.0000256)\cdot\gamma$ $+(0.0533967\pm0.0000444)\cdot\gamma^2+(0.0030717\pm0.0000246)\cdot\gamma^3$

Table 6.

λ_t	γ (%)	ϕ/Q_0 (%) Very short times	ϕ/Q_0 (%) Short times	ϕ/Q_0 (%) Very long times
0.25	10	1.01		
0.5	10	0.49	2.32	1.73
1.0	10	39.01	2.14	3.62
1.5	10		14.72	
2.0	10			7.76

Table 7.

λ_t	γ (%)	ϕ/Q_0 (%) Very short times	ϕ/Q_0 (%) Short times	ϕ/Q_0 (%) Very long times
0.25	10	0.83		
0.5	10	0.78	1.72	
1.0	10	39.24	1.19	1.11
1.5	10		15.82	
2.0	10			2.43
3.0	10			5.56

Table 8.

λ_t	γ (%)	ϕ/Q_0 (%) Very short times	ϕ/Q_0 (%) Short times	ϕ/Q_0 (%) Very long times
0.25	10	0.73		
0.5	10	0.95	1.45	
1.0	10	39.36	0.63	0.74
1.5	10		16.49	
2.0	10			1.74
3.0	10			4.22

Table 9.

Anexo 3

Numerical Analysis of Start-up PWR with Fractional

Neutron Point Kinetic Equation

Numerical Analysis of Start-up PWR with Fractional Neutron Point Kinetic Equation

M.-A. Polo-Labarrios [a,b], G. Espinosa-Paredes [b,*]

[a] Departamento de Sistemas Energéticos, Facultad de Ingeniería, Universidad Nacional Autónoma de México, Av. Universidad 3000, Universidad Nacional Autónoma de México Coyoacán, México, D.F., 04510, MÉXICO.

[b,*] Área de Ingeniería en Recursos Energéticos, Universidad Autónoma Metropolitana-Iztapalapa, Av. San Rafael Atlixco 186, Col. Vicentina, 09340 México D.F., MÉXICO.

Paper to be submitted to ***Progress in Nuclear Energy***

February 9, 2012

*Corresponding author: gepe@xanum.uam.mx

Abstract

In this paper we present the numerical analysis of the neutron density behavior when the nuclear reactor power is increased during start-up of a PWR. The fractional neutron point kinetic (FNPK) equation with one-group delayed neutron precursor and external neutron source was used for this analysis. It is considered that there is a relaxation time associated with a rapid variation in the neutron flux and this effect is considered with the FNPK which have a physical interpretation of the fractional order is related with the sub-diffusive process, i.e., non-Fickian effects from the neutron diffusion equation point of view. In order to steady of the relaxation time effects during start-up of a PWR, a numerical analysis with FNPK is carried out, which it is assumed that during the *i*-th step of control rod withdrawal the way of reactivity insertion is step to step, where the neutron source strength was defines as a constant in terms of a known initial stable subcriticality and the neutron signal from a steady state condition. The results of the FNPK were compared with the classical neutron point kinetics (CNPK), for different values of the anomalous relaxation time.

KEYWORDS: Fractional Neutronic Point Kinetic; Reactor Cold Start-Up; Fractional Calculus; Nuclear Reactor Dynamics; PWR.

1. Introduction

During the startup of the new or reloaded reactor, should be given careful attention to the problem of control, in order to avoid the possibility of an accident. In the high flux reactors and that have added an excess reactivity; the reactor period can become very small during the startup. If allowed to continue, either by mechanical or operator failure, through the stage of criticality by prompt neutron, power very quickly exceed the normal operating level, and the consequences could be serious. The reactor startup requires special attention, since the neutron level can be so low as to make uncertain the indications of the usual measuring instruments. In this case, a condition of utmost importance is that the control bars are not be moved, until the neutron flux is large enough to be detected. This detectable neutron flux can come from spontaneous fission or a special neutron source introduced into the reactor. Even under these circumstances, there is the possibility that the reactor reaches the criticality by prompt neutron in a short time interval; this situation can be avoided by carefully regulating the rate of ascent of the reactivity, i.e. the speed of movement of control rods during the startup process (Glasstone and Sesonske, 1981).

A reactor is initially started up from a cold condition by withdrawing control rods until the reactor is slightly subcritical, thus producing an exponentially increasing neutron population on a very long period. As the neutron population increases, the fission heating and thus the reactor temperature increase. This increase in temperature produces a decrease in reactivity (almost all reactors are designed to have a negative temperature coefficient) that would cause the neutron population to decrease and the reactor to shut down if the control rods were not withdrawn further to maintain an increasing neutron population. The total amount of feedback reactivity that must be offset by control rod withdrawal during the course of the startup to operating power level is known as the temperature defect (Stacey, 2001). However, during the physical startup process,

the supercritical accident occurs easily due the blind zone of neutron detector and the great change of neutron density. Possibly, the accident results are more severe than those happened under the normal operation condition, because the reactor power increases so rapidly without temperature feedback that the automatic safety system does not have enough time to work (Li et al., 2010).

The classical neutron point kinetics (CNPK) equations are one of the most important reduced models of nuclear engineering, through them it is possible to determine the flux behaviour in a very simple way given a certain reactivity variation during the time, and have been the subject of countless studies and applications to understand the neutron dynamics and its effects, such as developed of different method for their solution (Chao and Attard, 1985; Ratemi and Eshabo, 1998; Aboanber, 2003; Kinard and Allen, 2003; Chen et al., 2006; Li et al., 2007; Zhang et al., 2008; Palma et al., 2009; Li et al., 2010; Espinosa-Paredes et al., 2011a, b).

Nowadays, the basic critical monitoring method is extrapolation, and the *inverse count rate* method is widely used in PWR. Due there is no analytical solution for the CNPK with a strange source at subcritical, still uses the traditional subcritical formula (Hetrick, 1993): $n(t\to\infty)=q_0\Lambda/\rho_0$ (where $n(t)$ is the neutron density in the case $t\to\infty$; q_0 is the strength neutron source density emitted in per second; Λ is one generation average lifetime of instantaneous neutron; and ρ_0 is the initial value of reactivity due to control rod withdraw), which shows that the subcriticality need the longer time for the reactor reaches steady state. Actually, when we carry out the physical startup of reactor and withdraw control rods to extrapolate to critical state by the traditional subcritical formula, even if reactivity added is equal

to 1/3 of the extrapolation value, the phenomena of supercriticality sometimes may happen accidentally (Li et al., 2010). It is often the case in practice that from the shutdown depth to the delayed critical the variance of the neutron density spans several orders of magnitude. At the end of the initial steps during the startup of reactor, the value of the neutron density almost reaches a stable value, but it is as small as to be considered as zero. During this process the extrapolation method is used to find the critical point. In addition, after some steps, especially when the reactor is close to delayed critical, the neutron density reaches to a high level and cannot be taken as zero. At this time the traditional subcritical formula is not applicable any more. In the other hand, Chen (1997) illustrates some example about critical accident, which occur if we used the count of neutron detector to extrapolate to critical state by the traditional subcritical formula. According with those ideas, Li et al. (2010) proposed a new solution of neutron multiplication for the CNPK with one group delayed neutron.

In a recent paper, Espinosa-Paredes et al. (2011a) proposed a fractional neutronic point kinetic (FNPK) equation with one-group of delayed neutron in order to describe the dynamic behavior in a nuclear reactor. The physical interpretation of this model is that the fractional order is related with non-Fickian effects (Espinosa-Paredes and Polo-Labarrios, 2011) from the neutron diffusion equation point of view, their model considered that there is a relaxation time associated with a rapid variation in the neutron flux due to the fast variation of reactivity.

The main goal of this work is to analyze the effect of the anomalous diffusion coefficient (κ) and the anomalous relaxation time (τ^{κ}) on the behavior of the neutron density during the start-up of PWR, and the relationships of the neutron density response with reactivity added step by step.

2. Dynamics of startup of PWR reactor

2.1 Preliminaries

During cold start-up, the reactor is in sub-critical state and the external neutron source cannot be neglected. In this case the average temperature of reactor core is lower and power added is smaller, so the temperature feedback effect can be neglected. The CNPK with one-group of delayed neutron is given by (Duderstadt and Hamilton, 1976)

$$\frac{dn(t)}{dt} = \frac{\rho-\beta}{\Lambda}n(t)+\lambda C(t)+q \tag{1}$$

$$\frac{dC(t)}{dt} = \frac{\beta}{\Lambda}n(t)-\lambda C(t) \tag{2}$$

In these equations $n(t)$ is the neutron density; ρ is the reactivity; β is the total fraction of delayed neutron; Λ is one generation average lifetime of instantaneous neutron; λ is decay constant of delayed neutron precursor; $C(t)$ is the delayed neutron precursor density; q is the strength neutron source density emitted in per second, which we shall call the source term and in this work this term is considered independent of time; t is the time.

When the rector power is steady state, all time derivatives are equal to zero, so from de Eqs. (1) and (2) we obtain the initial conditions $C_0 = n_0\beta/\lambda\Lambda$ and $\rho_0 = -\Lambda q/n_0$, where n_0 is the initial count of neutron detector which is equal to the initial value of neutron density, and ρ_0 is the subcritical reactivity initial value. For operation at low power, for instance, at startup the contributions of the neutron source must be explicitly taken into account and high power levels this term is practically neglected.

2.2 Extrapolation method

During the process of reactor startup, the extrapolation method is used to find the critical point. As it is known, neutron detectors are located in the shield water tank and the number of thermal neutrons leaked from the reactor core to the shield water tank is very small. The pulse count per second detected by neutron detectors is given by: $N = s\eta n v$, where ε is the attenuation factor, which denotes the ratio of the neutron density where detector is located to the average thermal neutron density in the core; v average thermal neutron speed; η is the neutron sensitivity of the detector, which denotes pulse count of the detector per second induced by unit thermal neutron density. In order to guarantee the safety of reactor, the following rules for the critical extrapolation should be obeyed (Li at al., 2010): 1) at subcritical state, the positive reactivity should be added step by step and from $1/3$ *to* $1/2$ of the extrapolation value, 2) while the reactor is close to the critical, in order to prevent supercritical accidents, it should wait more than two minutes each time after inserting the reactivity.

3. Fractional mathematical formulation

The fractional neutron point kinetic (FNPK) approximation developed by Espinosa-Paredes et al. (2011a) with one-group of neutron delayed precursors which considered an external source and initial conditions taken from a known initial steady state are given by:

Fractional neutron point-kinetic

$$\begin{aligned} &\tau^{\kappa}\frac{d^{1+\kappa}n(t)}{dt^{1+\kappa}}+\frac{dn(t)}{dt}+\tau^{\kappa}\left[\frac{1}{l}+\frac{(1-\beta)}{\Lambda}\right]\frac{d^{\kappa}n(t)}{dt^{\kappa}} \\ &=\frac{\rho-\beta}{\Lambda}n(t)+\tau^{\kappa}\lambda\frac{d^{\kappa}C(t)}{dt^{\kappa}}+\lambda C(t)+q \end{aligned}, \quad 0<\kappa<1 \qquad (3)$$

$$\rho_0 = -\frac{q\Lambda}{n_0} \tag{4}$$

$$\left.\frac{d^{\kappa} n(t)}{dt^{\kappa}}\right|_{t=0} = 0 \tag{5}$$

$$\left.\frac{d^{1+\kappa} n(t)}{dt^{1+\kappa}}\right|_{t=0} = 0 \tag{6}$$

Precursor concentration

$$\frac{dC(t)}{dt} = \frac{\beta}{\Lambda} n(t) - \lambda C(t) \tag{7}$$

$$C(0) = \frac{\beta}{\Lambda\lambda} n_0 \tag{8}$$

$$\left.\frac{d^{\kappa} C(t)}{dt^{\kappa}}\right|_{t=0} = 0 \tag{9}$$

In Eq. (3) τ is the relaxation time and τ^{κ} is denominated as anomalous relaxation time, κ is the order of the differential operator known as the anomalous diffusion coefficient (for sub-diffusion process: $0<\kappa<1$; while that for super-diffusion process: $1<\kappa<2$), l is the prompt-neutron lifetime for finite media, the other parameters were defined previously.

For estimating the anomalous diffusion coefficient (κ), the Detrended Fluctuation Analysis (DFA) method can be applied to the neutronic signal of the average power range monitor of the Nuclear Power Plant (Espinosa-Paredes et al., 2006).

3.1 Fractional numerical solution

The numerical approximation of the solution of the FNPK approximation was obtained applying the numerical solution of linear multi-term fractional differential equations as a system of equations given by Edwards et al. (2002). The FNPK approximation can be represented as a multi-term and higher-order linear fractional differential equation, which is calculated by reduction of the problem to a system of Ordinary and Fractional Differential Equations (OFDE).

3.1.1 Linear multi-term fractional equations

In order to solve the FNPK approximation we use numerical algorithm given by Edwards et al. (2002). Additional, in order to simplify notation used the differential operator D instead of d/dt. Then, equations system can be re-written as linear multi-term fractional form:

Fractional point kinetics

$$D^{\kappa+1}n + a_3 Dn + a_2 D^{\kappa} n + a_1 n = b_2 D^{\kappa} C + b_1 C + d, \qquad 0 < \kappa < 1 \tag{10}$$

Precursor concentration

$$DC + b_2 C = a_0 n \tag{11}$$

where the coefficients the above equations are:

$$a_0 = \frac{\beta}{\Lambda} \tag{12}$$

$$a_1 = -\frac{\rho - \beta}{\tau^{\kappa}\Lambda} \tag{13}$$

$$a_2 = \frac{1}{l} - \frac{(1-\beta)}{\Lambda} \tag{14}$$

$$a_3 = \frac{1}{\tau^{\kappa}} \tag{15}$$

$$b_1 = \frac{\lambda}{\tau^\kappa} \tag{16}$$

$$b_2 = \lambda \tag{17}$$

$$d = \frac{q}{\tau^\kappa} \tag{18}$$

3.1.2 Reduction of the problem to a system of OFDE each of the order at most unity

In this section we convert the problem into an OFDE system, each one with an order at the most of the unity. Following the procedure given by Edwards et al. (2002), we define a change of variables regarding the original problem:

Fractional neutron point kinetics

$$x_1(t) = n(t) \tag{19}$$

$$x_2(t) = D^\kappa n(t) = D^\kappa x_1(t) \tag{20}$$

$$x_3(t) = Dn(t) = Dx_1(t) \tag{21}$$

$$x_4(t) = D^\kappa Dn(t) = D^{\kappa+1} n(t) = D^\kappa x_3(t) \tag{22}$$

Precursor concentration

$$y_1(t) = C(t) \tag{23}$$

$$y_2(t) = D^\kappa C(t) = D^\kappa y_1(t) \tag{24}$$

$$y_3(t) = DC(t) = Dy_1(t) \tag{25}$$

The mathematical expressions given by Eqs. (19)-(25), can be expressed in a matrix form as follows:

$$\begin{pmatrix} D^{\kappa} & 0 & 0 & 0 & 0 \\ D & 0 & 0 & 0 & 0 \\ 0 & 0 & D^{\kappa} & 0 & 0 \\ 0 & 0 & 0 & D^{\kappa} & 0 \\ 0 & 0 & 0 & D & 0 \end{pmatrix} \begin{pmatrix} x_1 \\ x_2 \\ x_3 \\ y_1 \\ y_2 \end{pmatrix} = \begin{pmatrix} x_2 \\ x_3 \\ x_4 \\ y_2 \\ y_3 \end{pmatrix} \tag{26}$$

where

$$x_4 = -\sum_{j=1}^{3} a_j x_j + \sum_{j=1}^{2} b_j y_j + d \tag{27}$$

$$y_3 = a_0 x_1 - b_2 y_1 \tag{28}$$

The term x_4 were obtained by substitution the Eqs. (19)-(21) into Eq. (22), while y_3 was obtained by substituting Eqs. (19) and (23) into Eqs. (25).

3.1.3 Discretize form of the fractional derivatives

In order to discretize the fractional derivative, Edwards et al. (2002) used the Diethelm´s method (Diethelm 1997a, b), which is defined as:

$$D^{\kappa} x = \frac{1}{{}^{\kappa}\gamma_i} \left(\sum_{p=0}^{i} {}^{\kappa}\omega_{p,i} x_{i-p} + \frac{x_0}{\kappa} \right) \tag{29}$$

Here ${}^{\kappa}\gamma_i = (ih)^{\kappa} \Gamma(-\kappa)$, where $\Gamma(-\kappa)$ is the gamma function whose argument is $-\kappa$; x_0 is the initial condition, and ${}^{\kappa}\omega_{p,0}, \cdots, {}^{\kappa}\omega_{p,i}$ are convolution weights defined as:

$${}^{\kappa}\omega_{p,i} = \begin{cases} -1 & , \quad for \quad p = 0 \\ 2p^{1-\kappa} - (\kappa-1)^{1-\kappa} - (\kappa+1)^{1-\kappa} & , \quad for \quad p = 1,2,\cdots,i-1 \\ (\kappa-1)p^{\kappa} - (p-1)^{1-\kappa} + p^{1-\kappa} & , \quad for \quad p = i \end{cases} \tag{30}$$

In order to discretize Eq. (10), we apply Eq. (19) with $x = x_1$;

$$D^{\kappa}x_{1,j} = \frac{1}{{}^{\kappa}\gamma_i}\left(\sum_{p=0}^{i} {}^{\kappa}\omega_{p,j}x_{1,j-p} + \frac{x_{1,0}}{\kappa}\right) \tag{31}$$

The Edwards´s et al. (2002) method considers that

$$S_{1,j} = \sum_{p=1}^{i} {}^{\kappa}\omega_{p,j}x_{1,j-p} + \frac{x_{1,0}}{\kappa} \tag{32}$$

Now, substituting Eq. (32) into Eq. (31):

$$D^{\kappa}x_{1,j} = \frac{1}{{}^{\kappa}\gamma_i}\left({}^{\kappa}\omega_{0,j}x_{1,j} + S_{1,j}\right) \tag{33}$$

In this equation can be observed that

$$\sum_{p=0}^{i} {}^{\kappa}\omega_{p,j}x_{1,j-p} - \sum_{p=1}^{i} {}^{\kappa}\omega_{p,j}x_{1,j-p} = {}^{\kappa}\omega_{0,j}x_{1,j} \tag{34}$$

As $D^{\kappa}x_{1,j} = x_{2,j}$ at Eq. (20), we get:

$$x_{2,j} = \frac{1}{{}^{\kappa}\gamma_i}\left({}^{\kappa}\omega_{0,j}x_{1,j} + S_{1,j}\right) \tag{35}$$

Now, solving for $S_{1,j}$:

$$S_{1,j} = {}^{\kappa}\gamma_i x_{2,j} - {}^{\kappa}\omega_{0,j}x_{1,j} \tag{36}$$

Combine Eqs. (36) and (32), we obtain

$${}^{\kappa}\gamma_i x_{2,j} - {}^{\kappa}\omega_{0,j}x_{1,j} = \sum_{p=1}^{i} {}^{\kappa}\omega_{p,j}x_{1,j-p} + \frac{x_{1,0}}{\kappa} \tag{37}$$

To discretize Eq. (21) we use the trapezium rule:

$$x_{1,j} = x_{1,j-1} + \frac{h}{2}\left(x_{3,j} + x_{3,j-1}\right) \tag{38}$$

Now, we proceed in similar form regarding procedure used in Eq. (19), i.e.

$$S_{2,l} = x_{1,l-1} + \frac{h}{2} x_{3,l-1} \tag{39}$$

Substituting Eq. (39) into Eq. (38), we have:

$$x_{1,l} = S_{2,l} + \frac{h}{2} x_{3,l} \tag{40}$$

here, solving for $S_{2,l}$:

$$S_{2,l} = x_{1,l} - \frac{h}{2} x_{3,l} \tag{41}$$

Now, combining Eqns. (38) and (41), we have

$$x_{1,l} - \frac{h}{2} x_{3,l} = x_{1,l-1} + \frac{h}{2} x_{3,l-1} \tag{42}$$

Then, the discretize form of the Eqs. (22), (24) and (25) are given by:

$$\begin{aligned} {}^{\kappa}\gamma_l \left(b_1 y_{1,l} + b_2 y_{2,l}\right) - {}^{\kappa}\gamma_l \left(a_1 x_{1,l} + a_2 x_{2,l}\right) - \left({}^{\kappa}\gamma_l a_3 + {}^{\kappa}\omega_{0,l}\right) x_{3,l} \\ - \sum_{p=1}^{l} {}^{\kappa}\omega_{p,l} x_{3,l-p} + \frac{x_{3,0}}{\kappa} - {}^{\kappa}\gamma_l d \end{aligned} \tag{43}$$

$$\left({}^{\kappa}\gamma_l\right) y_{2,l} - {}^{\kappa}\omega_{0,l} y_{1,l} = \sum_{p=1}^{l} {}^{\kappa}\omega_{p,l} y_{1,l-p} + \frac{y_{1,0}}{\kappa} \tag{44}$$

$$y_{1,l}\left(1 - \frac{b_2 h}{2}\right) - \frac{a_0 h}{2} x_{1,l} = y_{1,l-1} + \frac{h}{2}\left[a_0 x_{1,l-1} - b_2 y_{1,l-1}\right] \tag{45}$$

Eqs. (37), (42) and (43)-(45) represent the discretize form of the OFDE set for FNPK approximation. These equations in matrix form are:

$$\begin{pmatrix} -{}^{\kappa}\omega_{0,l} & {}^{\kappa}\gamma_l & 0 & 0 & 0 \\ 1 & 0 & -h/2 & 0 & 0 \\ -{}^{\kappa}\gamma_l a_1 & -{}^{\kappa}\gamma_l a_2 & -({}^{\kappa}\gamma_l a_2 + {}^{\kappa}\omega_{0,l}) & {}^{\kappa}\gamma_l b_1 & {}^{\kappa}\gamma_l b_2 \\ 0 & 0 & 0 & -{}^{\kappa}\omega_{0,l} & {}^{\kappa}\gamma_l \\ -(a_0 h)/2 & 0 & 0 & 1-(b_2 h)/2 & 0 \end{pmatrix} \begin{pmatrix} x_{1,l} \\ x_{2,l} \\ x_{3,l} \\ y_{1,l} \\ y_{2,l} \end{pmatrix} = \begin{pmatrix} S_{1,l} \\ S_{2,l} \\ S_{3,l} \\ R_{1,l} \\ R_{2,l} \end{pmatrix} \tag{46}$$

where

$$S_{1,i} = \sum_{p=1}^{i} \kappa \omega_{p,i} x_{1,i-p} + \frac{x_{1,0}}{\kappa} \tag{47}$$

$$S_{2,i} = x_{1,i-1} + \frac{h}{2} x_{3,i-1} \tag{48}$$

$$S_{3,i} = \sum_{p=1}^{i} \kappa \omega_{p,i} x_{3,i-p} + \frac{x_{3,0}}{\kappa} - \kappa \gamma_i d \tag{49}$$

$$R_{1,i} = \sum_{p=1}^{i} \kappa \omega_{p,i} y_{1,i-p} + \frac{y_{1,0}}{\kappa} \tag{50}$$

$$R_{2,i} = y_{1,i-1} + \frac{h}{2}\left[a_0 x_{1,i-1} - b_2 y_{1,i-1} \right] \tag{51}$$

In a recently paper, Espinosa-Paredes, et al. (2011b), performed the sensitivity and uncertainty analysis about anomalous diffusion coefficient (κ) as predictor variable in FNPK with the Monte Carlo simulation. According with this authors the sensitivity was evaluated in terms of the 99% confidence, these authors found that for 1% change in the κ, the responses for the neutron density changed 0.017% for short times, and 0.012% for long times, additionally, they found that the influence of κ on the neutron density follows a quadratic correlations negative.

The classical point neutron kinetics equations (Eqs. 1 and 2), also were solved using the numerical approximation with explicit temporal integration method, i.e.:

$$\frac{n_{i+1} - n_i}{\Delta t} = \frac{\rho_i - \beta}{\Lambda} n_i + \lambda C_i + q \tag{52}$$

$$\frac{C_{i+1} - C_i}{\Delta t} = \frac{\beta}{\Lambda} n_i - \lambda C_i \tag{53}$$

where $\Delta t = t_{i+1} - t_i$, $n_i = n(t_i)$, $C_i = C(t_i)$, $\rho_i = \rho(t_i)$ and t_i is time lapsed at i-th iteration.

4. Simulations

In order to analyze the effect of the anomalous relaxation time (τ^{κ}) on the behavior of the neutron density during start-up process of PWR reactor, we used Eqs. (46) to (51) and the numerical solution of traditional subcritical formula given by Eqs, (1) and (2) to apply the same problem studied given by Li et al. (2010). The results of the FNPK numerical model are compared with numerical solution of the CNPK. The numerical models presented in this work (fractional, and classical solution) were implemented in a commercial computer program MATLAB®.

4.1 Nuclear parameters

The nuclear parameters used in this work were obtained from Li et al. (2010) which are: $\lambda = 0.0774 s^{-1}$, $\beta = 0.0065$, $\Lambda = 10^{-4} s$ and $q = 1\times10^{8}\ neutrones/m^{3}s$ whose correspond to a pressurized-water reactor with ^{235}U as fissile material, and the value of the parameter $l = 0.00024 s$ was obtained from Glasstone and Sesonske (1981).

The sub-criticality values used were taken from Li et al. (2010). It is assumed that, before the sudden change in reactivity occurred at $t_1 = 0$, the initial count of neutron detector is equal to the initial value of neutron density (n_0). Then the initial sub-critical value and delayed neutron precursor density can be obtained using $\rho_0 = -q\Lambda/n_0$ and $C_0 = \beta n_0/\lambda\Lambda$, respectively. According with the results shown by Li et al. (2010), the initial sub-critical value is $\rho_0 = -100\, mk$, when withdraw the control rod for the first time at $t_1 = 0$ the sub-critical value added is $\rho_1 = -10\, mk$, after waiting $100 s$ (t_2) the control rod is withdraw for second time and

the sub-critical value added is $\rho_2 = -5\,mk$, and so on, then at $t_3 = 200\,s$ the sub-critical value added is $\rho_3 = -2.5\,mk$, at $t_4 = 300\,s$ the sub-critical value added is $\rho_4 = -1.25\,mk$, at $t_5 = 420\,s$ the sub-critical value added is $\rho_5 = -1\,mk$, finally at $t_6 = 600\,s$ the sub-critical value added is $\rho_6 = -0.75\,mk$.

The numerical experimental were carried out for anomalous relaxation time values of: $\tau^{\kappa} = 0.01$, 0.001, and 0.0025 s; and the anomalous diffusion coefficient values of: $\kappa = 0.6$, 0.8 and 0.999.

4.2 Numerical experiments

The Figures 1-6 shows the results obtained of the numerical experiments (NE), which present the characteristics of the neutron density increase during the reactor startup process, they were made using the FNPK equation of approximation (Espinosa-Paredes et al., 2011a) and CNPK to compare the differences between these two models. In order to analyzed the effects of the anomalous diffusion coefficient such as anomalous relaxation time on the neutron density increase during reactor startup process, we realized two kind of figures: firth, with fixed anomalous relaxation time are used different anomalous diffusion coefficients; second, with anomalous diffusion coefficients fixed using different values of anomalous relaxation time. Addition in all cases we analyze two range of simulation: (a) all range of simulation; and (b) the range of simulation from 500 to 700 s. Thus, the cases analysed were:

NE1. were realized three experiments (Figures 1-3); each one was realized with a fixed value of anomalous relaxation time and different values of anomalous diffusion coefficient.

NE2. were realized three experiments (Figures 4-6); each one was realized with different values of anomalous relaxation time values and a fixed value of anomalous diffusion coefficient.

4.3 Results and discussions

NE 1.

Figure 1 shows the results of numerical solution of the FNPK approximation with anomalous diffusion coefficient values equal to $\kappa = 0.999$, 0.8, 0.6, and a fixed anomalous relaxation time equal to $\tau^{\kappa} = 0.0025$, and the comparison with the result obtained by CNPK. The transient behavior was analyzed considering the time range from 0 to 700 s and a zoom from 500 to 700 s. In Figure 1a, can be observed that the nuclear density behavior described by FNPK with $\tau^{\kappa} = 0.0025$, for $\kappa = 0.999$ is equal to behavior described by CNPK, while for $\kappa = 0.8$ and 0.6 the nuclear density behavior described by FNPK over-predicted the behavior described by CNPK. However, the differences between values of nuclear density described by both models are small, even the values are almost equal in all range of simulation. In zoom shown in Figure 1b, can be observed that the values of nuclear density around 600 s described by FNPK with $\kappa = 0.8$ and 0.6 are very similar between them before and after of reactivity insertion, while the difference between nuclear density behavior described by FNPK with these two values and the behavior described by CNPK are small before and after of reactivity insertion, too.

Figure 2 shows the results of numerical solution of the FNPK approximation with $\kappa = 0.999$, 0.8, 0.6 and $\tau^{\kappa} = 0.005$, and the result obtained by CNPK. The transient behavior was analyzed considering the time range from 0 to 700 s and a zoom from 500 to 700 s.

In Figure 2a can be observed that the nuclear density behavior described by FNPK with $\tau^{\kappa}=0.005$, for $\kappa=0.999$ is equal to behavior described by CNPK as in the previous case, while the behavior described by FNPK for $\kappa=0.8$ and 0.6 on-predicted the behavior described by CNPK, but the behavior described by FNPK with $\kappa=0.6$ is greater than behavior described by FNPK with $\kappa=0.8$. The differences between the values of nuclear density described by both models are small until 300 s, after of this point the differences increase constantly. In zoom shown in Figure 2b, can be observed that at 600 s the reactivity is insert, then, the value of nuclear density described by FNPK with $\kappa=0.6$ at end of step of reactivity insertion previous, is very similar at nuclear density value given by CNPK after of reactivity insertion but less, while the value of FNPK with $\kappa=0.8$ is less than nuclear density value given by CNPK after of reactivity insertion.

Figure 3 shows the results of numerical solution of the FNPK approximation with $\kappa=0.999$, 0.8, 0.6 and $\tau^{\kappa}=0.001$, and the result obtained by CNPK. The transient behavior was analyzed considering the time range from 0 to 700 s and a zoom from 500 to 700 s.

In Figure 3a, can be observed that the nuclear density behavior described by FNPK for $\kappa=0.999$ is equal to behavior described by CNPK as in previous cases, while the behavior described by FNPK with $\kappa=0.8$ and 0.6 on-predicted the behavior described by CNPK, but the behavior described by FNPK with $\kappa=0.6$ is greater than behavior described by FNPK with $\kappa=0.8$. The differences between the values of nuclear density described by both models are very small until 200 s, after of this point the differences increase more in each step of reactivity insertion. In zoom shown in Figure 3b, can be observed that at 600 s the reactivity is inserting, then, the values of

nuclear density described by FNPK with $\kappa = 0.6$ and 0.8 at end of step of reactivity insertion previous, are greater than nuclear density value given by CNPK after of reactivity insertion.

In general terms, can be observed that the different between nuclear density behavior described by FNPK and CNPK are small (Figures 1-3), therefore, the nuclear density behavior described by the FNPK over-predicted the behavior described by the CNPK. Is important mentioned that when $\kappa = 0.999$ the nuclear density behavior is same for any value of anomalous relaxation time, while for $\kappa = 0.8$, 0.6 the nuclear density behavior change for each τ^{κ} value.

NE 2:

Figure 4 shows the results of numerical solution using FNPK approximation with fixed value of anomalous diffusion coefficient equal to $\kappa = 0.999$ and different values of anomalous relaxation time which are $\tau^{\kappa} = 0.0025$, 0.005 and 0.01, and the result obtained by CNPK. The transient behavior was analyzed considering two time range: (a) from 0 to 700 s, and (b) from 500 to 700 s.

Figure 4a, can be observed that the nuclear density behaviors described by FNPK approximation for $\kappa = 0.999$ and $\tau^{\kappa} = 0.0025$, 0.005, 0.01 are equal to behavior described by CNPK. This can be corroborated in Figure 4b, which shows a zoom in time range from 500 to 700, where can be observed that the values of nuclear density behavior described by FNPK with values of κ and τ^{κ}, mentioned above, are equal to nuclear density behavior described by CNPK.

Figure 5 shows the results of numerical solution using FNPK approximation with fixed value of anomalous diffusion coefficient equal to $\kappa = 0.8$ and different values of anomalous relaxation time which are $\tau^{\kappa} = 0.0025$, 0.005 and 0.01, and the result obtained by CNPK. The transient behavior was analyzed considering two time range: (a) from 0 to 700 s, and (b) from 500 to 700 s.

In Figure 5a, can be observed that the differences of the nuclear density behavior described by FNPK approximation with $\kappa = 0.8$ and $\tau^{\kappa} = 0.0025$, 0.005 0.01 and the behavior described by CNPK are small, even almost equal until 200 s, after from this point the behavior described by FNPK over-predicted the behavior described by CNPK, even the differences increase more in each step of reactivity insertion. In more detailed: the behavior described by FNPK with $\tau^{\kappa} = 0.0025$ is greater than behavior described by CNPK; the behavior described by FNPK with $\tau^{\kappa} = 0.005$ is greater than behavior described by FNPK with $\tau^{\kappa} = 0.0025$; and finally, the behavior described by FNPK with $\tau^{\kappa} = 0.01$ is greater than all of them. In zoom shown in Figure 5b, can be observed that at 600 s the reactivity is inserting, then, can be observed that the values of nuclear density obtained by FNPK with $\kappa = 0.8$ and for $\tau^{\kappa} = 0.0025$ and 0.005, in the end of step of reactivity insertion previous are greater than nuclear density value given by CNPK, but less than the value of nuclear density obtained with CNPK after of reactivity insertion, with FNPK for $\tau^{\kappa} = 0.01$ the value of the nuclear density obtained in the end of step of reactivity insertion previous is even greater than the value of the nuclear density obtained by CNPK after of reactivity insertion.

Figure 6 shows the results of numerical solution using FNPK approximation with fixed value of anomalous diffusion coefficient equal to $\kappa = 0.6$ and different values of anomalous relaxation time which are $\tau^{\kappa} = 0.0025$, 0.005 and 0.01, and the result obtained by CNPK. The transient behavior was analyzed considering again two time range: (a) from 0 to 700 s, and (b) from 500 to 700 s.

Figure 6a, can be observed that the differences of the nuclear density behavior described by FNPK approximation with $\kappa = 0.6$ and $\tau^{\kappa} = 0.0025$, 0.005 0.01 and the behavior described by CNPK are small, even almost equal until 200 s, after from this point the behavior described by FNPK over-predicted the behavior described by CNPK, as in the previous case, and the differences increase more and more in each step of reactivity insertion. In more detailed: the behavior described by FNPK with $\tau^{\kappa} = 0.0025$ is greater than behavior described by CNPK; the behavior described by FNPK with $\tau^{\kappa} = 0.005$ is greater than behavior described by FNPK with $\tau^{\kappa} = 0.0025$; and similarly as previous case, finally the behavior described by FNPK with $\tau^{\kappa} = 0.01$ is greater than all of them. In zoom shown in Figure 6b, as was mentioned above at 600 s the reactivity is inserting, and can be observed that the values of nuclear density described by FNPK for $\tau^{\kappa} = 0.0025$ in the end of step of reactivity insertion previous is greater than nuclear density value given by CNPK but less than the value of nuclear density obtained with CNPK after of reactivity insertion, for FNPK with $\tau^{\kappa} = 0.005$ the value of the nuclear density obtained in the end of step of reactivity insertion previous is almost equal to the value of the nuclear density obtained by CNPK after of reactivity insertion but less, and finally, for FNPK with $\tau^{\kappa} = 0.01$ the value of the nuclear density obtained in the end of step of reactivity insertion

previous is greater than the value of the nuclear density obtained by CNPK after of reactivity insertion.

In general terms, in Figures 4-6 can be observed that the different between nuclear density behavior described by FNPK and CNPK are small, therefore, the nuclear density behavior described by the FNPK over-predicted the behavior described by the CNPK. Is important mentioned that when $\kappa = 0.999$ the nuclear density behavior is same for any value of anomalous relaxation time, while for $\kappa = 0.8$, 0.6 the nuclear density behavior change for each τ^{κ} value, even the value of the nuclear density increases by increasing the value of anomalous relaxation time for each value of κ.

The comparison between results obtained by FNPK developed by Espinosa-Paredes et al., (2011b), and the numerical approximation of the classical neutronic point kinetics, shows that the differences are small, even when $\kappa = 0.999$ there is no difference for any value of τ^{κ}.

The physical interpretation of this behavior is that in the nuclear reactor there are sub-diffusive processes, i.e., the movement of the particles have a time delay or relaxation time which are considered by FNPK. This effects contribute in each begin step of reactivity insertion, which can be crucial during start-up of a nuclear reactor, due that this effect is not neglected. Espinosa-Paredes and Polo-Labarrios (2011) found that in heterogeneous medium the particle velocity is $3^{-\kappa/2}$ for $\kappa < 1$. For this reason the number of neutrons that leak from reactor decreases, and in consequence the neutron density increases in this start-up process.

5. Conclusion

The behavior of the variation of neutron density when the nuclear reactor power is increased using the fractional neutron point kinetic (FNPK) equation was numerically analyzed in this work. The numerical results show that the relaxation time is associated with a rapid variation in the neutron flux due to sub-diffusive nature which is a function of the anomalous relaxation time, i.e., the generation and leak of the neutrons in the reactor have a delayed time, which was approximated in this work with the FNPK equation.

The relationship of the neutron density level and its chance rate with the speed of reactivity insertion is very important for the startup safety, because if the reactor power increases so rapidly there is not temperature feedback and the automatic safety system does not have enough time to act. According the numerical results we found that:

(1) At the end of the initial steps during the startup of reactor, the value of the neutron density almost reaches a stable value; even the different between nuclear density behavior described by FNPK and CNPK are very small until 200 s, after from this point the behavior described by FNPK over-predicted the behavior described by CNPK, and the differences increase more and more in each step of reactivity insertion (e.g., Figure 1).

(2) The nuclear density behavior described by the FNPK over-predicted the behavior described by the CNPK. But with $\kappa = 0.999$ and for any value of anomalous relaxation time the nuclear density behavior is same to behavior described by CNPK (Figure 4), while for $\kappa = 0.8$, 0.6 the nuclear density behavior change for each τ^{κ} value, even the

value of the nuclear density increases by increasing the value of anomalous relaxation time for each value of κ (Figure 3).

Acknowledgment

First Author is grateful for the financial support through a scholarship from the Consejo Nacional de Ciencia y Tecnología (CONACyT) for the Master's Graduate Studies in Engineering Program of the Universidad Nacional Autónoma de México, and special thanks to Laboratory of the Severe Accidents in Nuclear Reactors of the Universidad Autónoma Metropolitana-Iztapalapa, where was developed this work.

References

Aboanber, A.E., 2003. Analytical solution of the point kinetics equations by exponential mode analysis. Progress in Nuclear Energy 42, 179–197.

Chao, Y., Attard, A., 1985. A Resolution of the Stiffness Problem of Reactor Kinetics. Nuclear Science and Engineering 90, 40-46.

Chen, X.Y., 1997. Divergence phenomena of critical extrapolation curve of control rods rising during physical start-up of PWR: the cause and mechanism. Nuclear Power Engineering 18 (6), 496–499 (in Chinese).

Chen, W.Z., Kuang, B., Guo, L.F., Chen Z.Y., Zhu, B., 2006. New analysis of prompt supercritical process with temperature feedback. Nuclear Engineering and Design 236, 1326–1329.

Diethelm, K., 1997a. An algorithm for the numerical solution of differential equations of fractional order. Electronic Transactions on Numerical Analysis 5, 1–6.

Diethelm, K., 1997b. Numerical approximation of finite-part integrals with generalized compound quadrature formulae. IMA Journal of Numerical Analysis 17, 479–493.

Duderstadt, J.J., Hamilton, L.J., 1976. Nuclear Reactor Analysis, Jhon Wiley and Sons, New York, United States of America.

Edwards, J.T., Ford, N.J., Simpson, A.C., 2002. The numerical solution of linear multiterm fractional differential equations. Journal of Computational and Applied Mathematics 148, 401–418.

Espinosa-Paredes, G., Álvarez-Ramírez, J., Vázquez, A., 2006. Detecting long-range correlation with detrended fluctuation analysis: Application to BWR stability. Annals of Nuclear Energy 33, 1308–1313.

Espinosa-Paredes, G., Polo-Labarrios, M.-A., 2011. Time-Fractional Telegrapher's Equation (P1) Approximation for the Transport Equation. Nuclear Science and Engineering. (Accepted for publication).

Espinosa-Paredes, G., Polo-Labarrios, M.-A., Espinosa-Martínez, E.-G., del Valle-Gallegos, E., 2011a. Fractional neutron point kinetics equations for nuclear reactor dynamics. Annals of Nuclear Energy 38, 307-330.

Espinosa-Paredes, G., Polo-Labarrios, M.-A., Díaz-González, L., Vázquez-Rodríguez, A., Espinosa-Martínez, E.-G., 2011b. Sensitivity and Uncertainty Analysis of the Fractional Neutron Point Kinetics Equations. Annals of Nuclear Energy.

Glasstone, S., Sesonske, A., 1981. Nuclear Reactor Engineering, Third ed. VNR, New York, United States of America.

Hetrick, D.L., 1993. Dynamics of Nuclear Reactor. American Nuclear Society, Jbc., Illinois, USA, ISBN 0-89448-453-2, pp. 164–167.

Kinard, M., Allen, E.J., 2003. Efficient numerical solution of the point kinetics equations in nuclear reactors dynamics. Annals of Nuclear Energy 31, 1039-1051.

Li, H., Chen, W., Zhang, F., Chen, Z., 2010. A new formula of neutron multiplication during startup of PWR. Progress in Nuclear Energy 52, 321-326.

Li, H., Chen, W., Zhang, F., Luo, L., 2007. Approximate solutions of point kinetics equations with one delayed neutron group and temperature feedback during delayed supercritical process. Annals of Nuclear Energy 34, 521–526.

Palma, D.A.P., Martínez, A.S., Gonçalves, A.C. 2009. Analytical solution of point kinetics equations for linear reactivity variation during the start-up of a nuclear reactor. Annals of Nuclear Energy 36, 1469-1471.

Ratemi,W.M., Eshabo, A.E., 1998. New form of the in-hour equation and its universal ABC-values for different reactor types. Annals of Nuclear Energy 25, 377–386.

Stacey, W.M., 2001. Nuclear Reactor Physics. John Wiley and Sons, INC, New York, United States of America.

Zhang, F., Chen, W.Z., Gui, X.W., 2008. Analytic method study of point-reactor kinetic equation when cold start-up. Annals of Nuclear Energy 35, 746-749.

Figures

Figure 1. Neutron density behavior after inserting step reactivity into a subcritical core. With a fixed anomalous relaxation time $\tau^{\kappa} = 0.0025$, for different anomalous diffusion coefficient values ($\kappa = 0.6, 0.8, 0.999$). (a) Full range of the simulation time; (b) zoom in the simulation range from $500\,s$ to $700\,s$.

Figure 2. Neutron density behavior after inserting step reactivity into a subcritical core. With a fixed anomalous relaxation time $\tau^{\kappa} = 0.005$, for different anomalous diffusion coefficient values ($\kappa = 0.3, 0.6, 0.8, 0.999$). (a) Full range of the simulation time; (b) zoom in the simulation range from $500\,s$ to $700\,s$.

Figure 3. Neutron density behavior after inserting step reactivity into a subcritical core. With a fixed anomalous relaxation time $\tau^{\kappa} = 0.01$, for different anomalous diffusion coefficient values ($\kappa = 0.3, 0.6, 0.8, 0.999$). (a) Full range of the simulation time; (b) zoom in the simulation range from $500\,s$ to $700\,s$.

Figure 4. Neutron density behavior after inserting step reactivity into a subcritical core. With different anomalous relaxation time values ($\tau^{\kappa} = 0.01$, 0.005, and 0.0025), for a fixed anomalous diffusion coefficient $\kappa = 0.999$. (a) Full range of the simulation time; (b) zoom in the simulation range from $500\,s$ to $700\,s$.

Figure 5. Neutron density behavior after inserting step reactivity into a subcritical core. With different anomalous relaxation time values ($\tau^{\kappa} = 0.01$, 0.005, and 0.0025), for a fixed anomalous diffusion coefficient $\kappa = 0.8$. (a) Full range of the simulation time; (b) zoom in the simulation range from $500\,s$ to $700\,s$.

Figure 6. Neutron density behavior after inserting step reactivity into a subcritical core. With different anomalous relaxation time values ($\tau^{\kappa} = 0.01$, 0.005, and 0.0025), for a fixed anomalous diffusion coefficient $\kappa = 0.6$. (a) Full range of the simulation time; (b) zoom in the simulation range from $500\,s$ to $700\,s$.

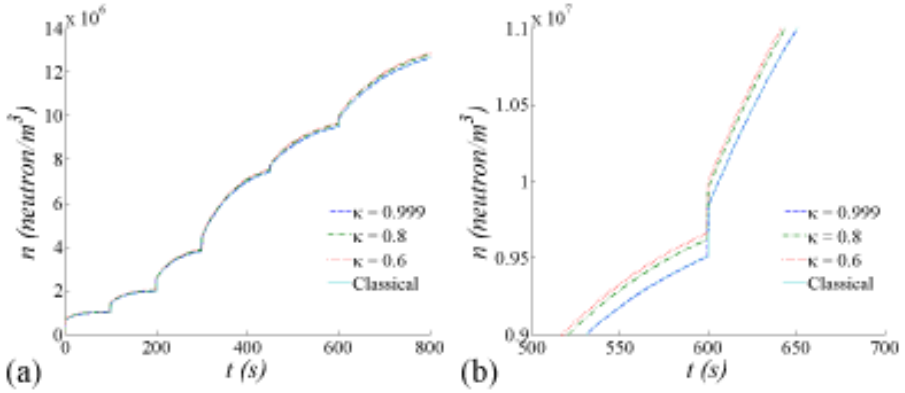
x 10^6
n (neutron/m^3)
t (s)
κ = 0.999
κ = 0.8
κ = 0.6
Classical
(a)
x 10^7
n (neutron/m^3)
t (s)
κ = 0.999
κ = 0.8
κ = 0.6
Classical
(b)

Figure 1

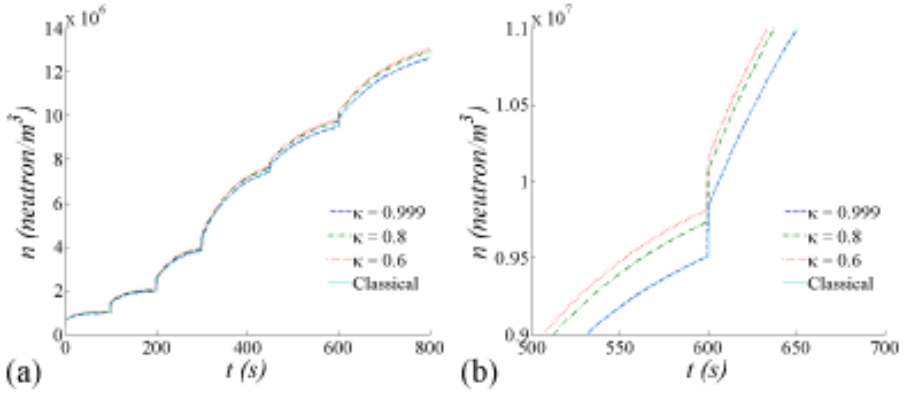
X 10^6
n (neutron/m^3)
t (s)
κ = 0.999
κ = 0.8
κ = 0.6
Classical
(a)
X 10^7
n (neutron/m^3)
t (s)
κ = 0.999
κ = 0.8
κ = 0.6
Classical
(b)

Figure 2

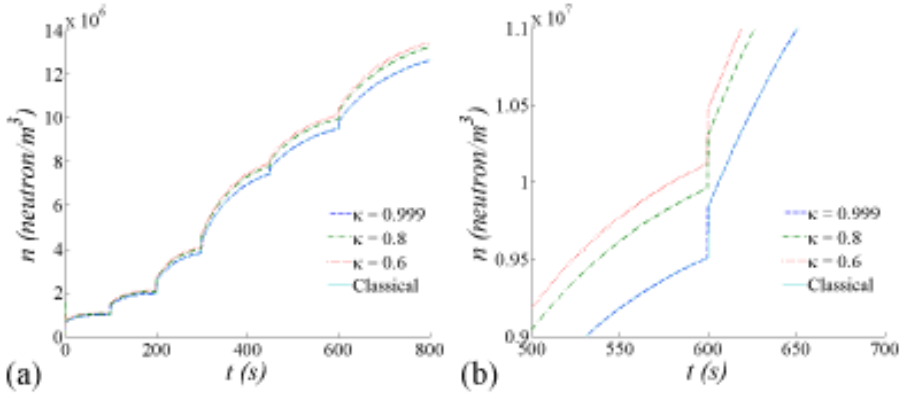
x 10^6
n (neutron/m^3)
t (s)
(a)
κ = 0.999
κ = 0.8
κ = 0.6
Classical
x 10^7
n (neutron/m^3)
t (s)
(b)
κ = 0.999
κ = 0.8
κ = 0.6
Classical

Figure 3

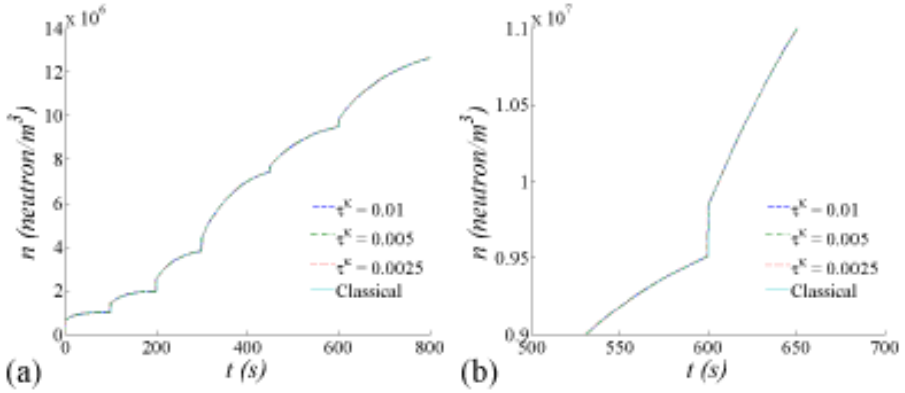
X 10^6
n (neutron/m^3)
t (s)
(a)
τ^K = 0.01
τ^K = 0.005
τ^K = 0.0025
Classical
X 10^7
n (neutron/m^3)
t (s)
(b)
τ^K = 0.01
τ^K = 0.005
τ^K = 0.0025
Classical

Figure 4

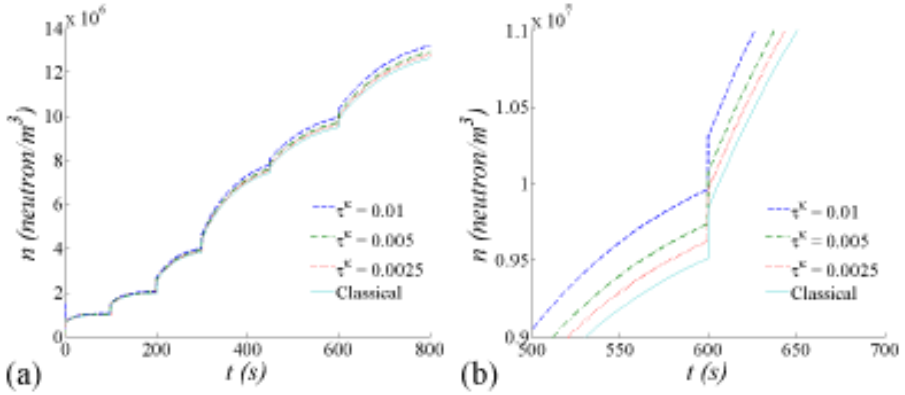
x 10^6
n (neutron/m^3)
t (s)
(a)
τ^K = 0.01
τ^K = 0.005
τ^K = 0.0025
Classical
x 10^7
n (neutron/m^3)
t (s)
(b)
τ^K = 0.01
τ^K = 0.005
τ^K = 0.0025
Classical

Figure 5

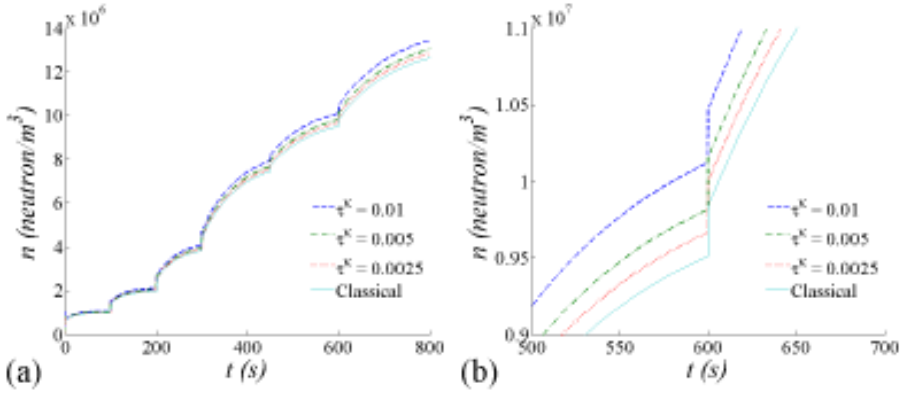
X 10^6
n (neutron/m^3)
t (s)
(a)
ε^K = 0.01
ε^K = 0.005
ε^K = 0.0025
Classical
X 10^7
n (neutron/m^3)
t (s)
(b)
ε^K = 0.01
ε^K = 0.005
ε^K = 0.0025
Classical

Figure 6

Anexo 4

Application of the fractional neutron point kinetic equation: Start-up of a nuclear reactor

Annals of Nuclear Energy 46 (2012) 37–42

Contents lists available at SciVerse ScienceDirect

Annals of Nuclear Energy

journal homepage: www.elsevier.com/locate/anucene

Application of the fractional neutron point kinetic equation: Start-up of a nuclear reactor

M.-A. Polo-Labarrios [a,b], G. Espinosa-Paredes [a,*]

[a] Área de Ingeniería en Recursos Energéticos, Universidad Autónoma Metropolitana-Iztapalapa, Av. San Rafael Atlixco 186, Col. Vicentina, 09340 México D.F., Mexico
[b] Departamento de Sistemas Energéticos, Facultad de Ingeniería, Universidad Nacional Autónoma de México, Av. Universidad 3000, Universidad Nacional Autónoma de México Coyoacán, 04510 México D.F., Mexico

ARTICLE INFO

Article history:
Received 4 December 2011
Accepted 14 March 2012

Keywords:
Fractional neutron point kinetic
Reactor start-up
Fractional calculus
Nuclear reactor dynamics

ABSTRACT

In this paper we present the behavior of the variation of neutron density when the nuclear reactor power is increased using the fractional neutron point kinetic (FNPK) equation with a single-group of delayed neutron precursor. It is considered that there is a relaxation time associated with a rapid variation in the neutron flux and its physical interpretation of the fractional order is related with non-Fickian effects from the neutron diffusion equation point of view. We analyzed the case of increase the nuclear reactor power when reactor is cold start-up which is a process of inserting reactivity by lifting control rods discontinuously. The results show that for short time scales of the start-up the neutronic density behavior with FNPK shows sub-diffusive effects whose absorption are government by control rods velocity. For large times scale, the results shows that the classical equation of the neutron point kinetics over predicted the neutron density regarding to FNPK.

1. Introduction

The classical neutron point kinetics (CNPK) equations are one of the most important reduced models of nuclear engineering, and they have been the subject of countless studies and applications to understand the neutron dynamics and its effects.

The reactivity is one of the most important properties in a nuclear reactor due that it is directly related to the control of the reactor. The reactivity is basically inserted when the control rods are lifted, in practice each step of the lifting of the control rods is a step introducing linear reactivity in a certain period of time. However the control rods are lifted discontinuously, and when near to criticality the length of each step is a time interval which allows the duration of a transitory so that the reactor can reach criticality in a slow and safety way. However, uncontrolled control rods withdrawal or ejection is the most common type of initiator for a reactivity insertion accident, thus is has been an event that has been the topic previous works (e.g., Duderstadt and Hamilton, 1976; Glasstone and Sesonske, 1981; Stacey, 2001; Zhang et al., 2008; Palma et al., 2009; etc).

In a recent paper, Espinosa-Paredes et al. (2011b) proposed a fractional neutron point kinetic (FNPK) equation with a group of delayed neutron in order to describe the dynamic behavior in a nuclear reactor. The physical interpretation of this model is that the fractional order is related with non-Fickian effects (Espinosa-Paredes and Polo-Labarrios, 2011) from the neutron diffusion equation point of view, their model considered that there is a relaxation time associated with a rapid variation in the neutron flux due to the fast variation of reactivity.

In a recently paper, Espinosa-Paredes et al. (2011a), performed the sensitivity and uncertainty analysis of γ in FNPK with the Monte Carlo simulation. According with this authors the sensitivity was evaluated in terms of the 99% confidence, these authors found that for 1% change in the γ, the responses for the neutron density changed 0.017% for short times, and 0.012% for long times.

The main goal of this work is to analyze the effect of the anomalous diffusion coefficient (γ) and the relaxation time on the behavior of the neutron density during the start-up of a nuclear power reactor, and the relationships of the neutron density response with the speed of the lifting of the control rods and its duration.

2. Preliminaries

During cold start-up, the reactor is in sub-critical state and the external neutron source cannot be neglected. In this case the average temperature of reactor core is lower and power added is smaller, so the temperature feedback effect can be neglected. According with these ideas, in recent papers, Zhang et al. (2008) and Palma et al. (2009) developed analytical solutions for the calculation of neutron density from a set of physics and mathematics approximations. Their mathematical formulation was based in the classical formulation:

* Corresponding author.
E-mail address: gepe@xanum.uam.mx (G. Espinosa-Paredes).

0306-4549/$ - see front matter © 2012 Elsevier Ltd. All rights reserved.
http://dx.doi.org/10.1016/j.anucene.2012.03.015

$$\frac{dn(t)}{dt} = \frac{\rho(t)-\beta}{\Lambda} n(t) + \lambda C(t) + q \tag{1}$$

$$\frac{dC(t)}{dt} = \frac{\beta}{\Lambda} n(t) - \lambda C(t) \tag{2}$$

Furthermore, these authors considered a reactivity insertion that is variable in time and represented by:

$$\rho(t) = \begin{cases} \rho_i + rt, & (0 \leqslant t < t_0) \\ \rho_i + rt_0 & (t \geqslant t_0) \end{cases} \tag{3}$$

In these equations $n(t)$ is the neutron density; $\rho(t)$ is the reactivity; β is the total fraction of delayed neutron; Λ is one generation average lifetime of instantaneous neutron; λ is decay constant of delayed neutron precursor; $C(t)$ is the delayed neutron precursor density; q is the external neutron source intensity; ρ_i is sub-critical reactivity; r is the inserted reactivity velocity; t is the time; t_0 is the duration of each lifting control rods.

Both authors (Zhang et al., 2008 and Palma et al., 2009) neglected the term $\Lambda d^2 n(t)/dt^2$, this term is important for large changes in neutron density in extremely short time scales. On their methods of solution, additionally also adopted the prompt jump approximations and considers constant external source. For neutron density when a linear insertion of reactivity occurs, Zhang et al. (2008) proposed the following expression:

$$n(t) = \begin{cases} \frac{\beta q + q\Lambda}{\beta + \rho_i \Lambda - rt}, & 0 \leqslant t < t_0 \\ \frac{q\Lambda}{\rho_i - rt_0}\left[1 - e^{\frac{\Lambda\rho_i + r\Lambda}{\beta + \rho_i \Lambda - rt_0}(t-t_0)}\right] + \frac{\beta q + q\rho_i}{\beta + \rho_i \Lambda} e^{\frac{\beta + \rho_i \Lambda - rt_0}{\Lambda}(t-t_0)}, & t \geqslant t_0 \end{cases} \tag{4}$$

and Palma et al. (2009) proposed an alternative solution:

$$n(t) = \begin{cases} A_1 \frac{e^{-\lambda}}{(-\lambda t_0)^{k_1+k_2}}\left[\Gamma(k_1 + \lambda k_2, \lambda(k_2 + t)) + A_2\right], & 0 \leqslant t < t_0 \\ -\frac{q}{\rho_i + rt_0} + A_0 e^{-\lambda(t-t_0)}, & t \geqslant t_0 \end{cases} \tag{5}$$

whose main feature is the used of the incomplete gamma function ($\Gamma(a,x)$). For more detailed of this models are presented in the works of these authors.

3. Fractional mathematical formulation

The fractional neutron point kinetic (FNPK) model developed by Espinosa-Paredes et al. (2011b) equations with one-group of neutron delayed precursors and initial conditions are given by:

Fractional neutron point-kinetic

$$\begin{aligned} &\tau^{\gamma} \frac{d^{1+\gamma} n(t)}{dt^{1+\gamma}} + \frac{dn(t)}{dt} + \tau^{\gamma}\left[\frac{1}{l} + \frac{(1-\beta)}{\Lambda}\right]\frac{d^{\gamma} n(t)}{dt^{\gamma}}, \quad 0 < \gamma \leqslant 2 \\ &= \frac{\rho(t)-\beta}{\Lambda} n(t) + \tau^{\gamma} \lambda \frac{d^{\gamma} C(t)}{dt^{\gamma}} + \lambda C(t) + q \end{aligned} \tag{6}$$

$$n(0) = \frac{q\Lambda}{\rho_i} \tag{7}$$

$$\left.\frac{d^{\gamma} n(t)}{dt^{\gamma}}\right|_{t=0} = 0 \tag{8}$$

$$\left.\frac{d^{1+\gamma} n(t)}{dt^{1+\gamma}}\right|_{t=0} = 0 \tag{9}$$

Precursor concentration

$$\frac{dC(t)}{dt} = \frac{\beta}{\Lambda} n(t) - \lambda C(t) \tag{10}$$

$$C(0) = \frac{\beta}{\Lambda\lambda} n_0 \tag{11}$$

$$\left.\frac{d^{\gamma} C(t)}{dt^{\gamma}}\right|_{t=0} = 0 \tag{12}$$

In Eq. (6) τ is the relaxation time, γ is the order of the differential operator known as the anomalous diffusion coefficient (for sub-diffusion process: $0 < \gamma < 1$; while that for super-diffusion process: $1 < \gamma < 2$), l is the prompt-neutron lifetime for finite media, the other parameters were defined previously.

For estimating the anomalous diffusion coefficient (γ), the Detrended Fluctuation Analysis (DFA) method can be applied to the neutronic signal of the average power range monitor of the Nuclear Power Plant (Espinosa-Paredes et al., 2006).

3.1. Fractional numerical solution

The numerical solution of the FNPK used in this work is presented in detailed form in the work of Espinosa-Paredes et al. (2011b). The idea of this numerical solution is propose a set of linear multi-term fractional differential equations for the system of equations as was given by Edwards et al. (2002).

The reactivity perturbation as a function of the time is introduced using the Eq. (3), which is consistent with the fractional numerical solution, presented in this work.

4. Simulations

In order to analyze the effect of the anomalous diffusion coefficient (γ) and relaxation time (τ) (FNPK approximation) on the behavior of the neutron density during start-up reactor, we applied the same study problem given by Zhang et al. (2008) and Palma et al. (2009), i.e., inserted reactivity velocity (r), sub-critical reactivity (ρ_i) and the duration of each lifting control rods (t_0).

The FNPK numerical model was compared with analytical solution of the Zhang et al. (2008). The numerical models presented in this work (fractional, and analytical solution) were implemented in a commercial computer program MATLAB®.

4.1. Nuclear parameters

The nuclear parameters used in this work were obtained from Palma et al. (2009) which are $\lambda = 0.001\ s^{-1}$, $\beta = 0.0075$, $\Lambda = 0.0015$ s and $q = 10^6\ n's/cm^3$ s, and the value of the parameter $l = 0.00024$ s was obtained from Glasstone and Sesonske (1981). The sub-criticality values used are −6 and −10 pcm, we considered two kinds of velocity of lifting control rods, that are 10 pcm/s and 40 pcm/s. The durations of the lifting control rods are two values, 5 s and 10 s. The anomalous relaxation time is $\tau^{\gamma} = 0.00001$; the anomalous diffusion order take the values $\gamma = 0.99, 0.9, 0.8, 0.6, 0.3$.

4.2. Numerical experiments

Figs. 1–4 show the results obtained of the numerical experimental (NE). The cases analyzed were:

4.2.1. NE 1

Comparison with analytical solution (Zhang et al., 2008) using $\rho_i = -6$ pcm, $r = 10$ pcm/s and $t_0 = 5$ s (Fig. 1).

4.2.2. NE 2

Effects of the velocity of lifting control rods ($r = 10$ pcm/s and $r = 40$ pcm/s) using a duration of lifting control rods ($t_0 = 5$ s) and sub-critical reactivity $\rho_i = -6$ pcm at the nuclear density response, for $\gamma = 0.99, 0.9, 0.6, 0.3$ (Fig. 2).

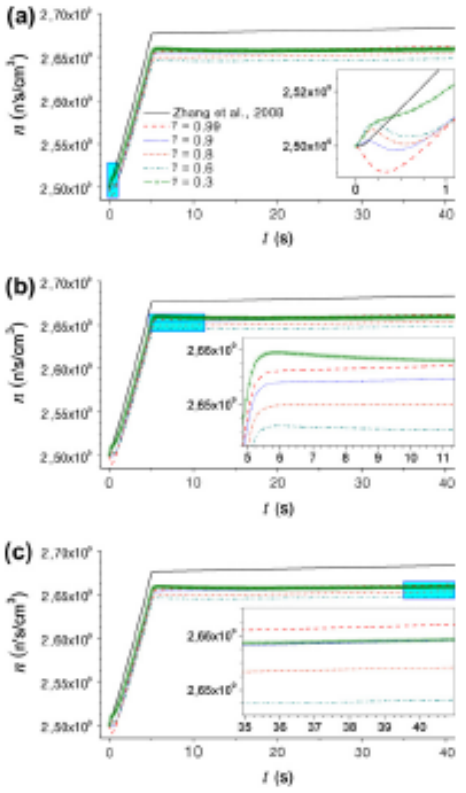

Fig. 1. Comparison of the neutron density response between CNPK and FNPK approximation, with $r = 10$ pcm/s, $\rho_c = -6$ pcm and $t_0 = 5$ s. The shaded area represents different approaches to small time scales: (a) initial startup, (b) after having raised the control rods and (c) long time of simulation.

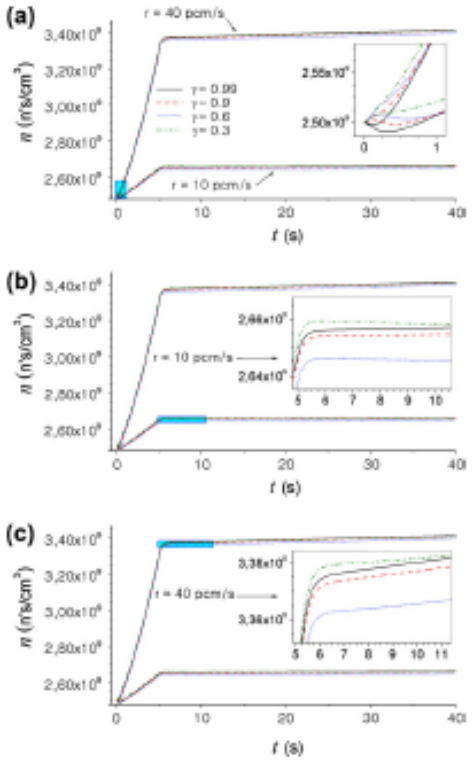

Fig. 2. Effects in the neutron density response when duration of lifting control rods ($t_0 = 5$ s) is same and the velocity of lifting control rods is different. The sub-critical reactivity value is $\rho_c = -6$ pcm. The shaded area represents different approaches to small time scales: (a) initial startup for $r = 10$ pcm/s and $r = 40$ pcm/s, (b) after having raised the control rods for $r = 10$ pcm/s and (c) after having raised the control rods for $r = 40$ pcm/s.

4.2.3. NE 3

Effects of the duration of lifting control rods ($t_0 = 5$ s and $t_0 = 10$ s) using a velocity of lifting control rods ($r = 10$ pcm/s) and sub-critical reactivity $\rho_c = -6$ pcm at nuclear density response, for $\gamma = 0.99, 0.9, 0.6, 0.3$ (Fig. 3).

4.2.4. NE 4

Effects at the nuclear density when reactivity sub-critical is $\rho_c = -10$ pcm, the duration of lifting control rods values are $t_0 = 1$ s and $t_0 = 4$ s and the velocity of lifting control rods values $r = 40$ pcm/s and $r = 10$ pcm/s, respectively, for $\gamma = 0.99, 0.9, 0.6, 0.3$ (Fig. 4).

4.3. Results and discussions

4.3.1. NE 1

The results are shown in Fig. 1. For the FNPK the solution numerical developed by Espinosa-Paredes et al. (2011b) with different anomalous diffusion order values (γ) was used. The transient behavior was analyzed considering three small time scales: (a) when start-up is begging, (b) after having raised the control rods and (c) at the end of the simulation time.

The results show that the behavior, in general terms described by the FNPK sub-predicts the behavior described by the CNPK after lifting the control rods, whose difference between these approximations is of the order of 2.4×10^7 n/s/cm³ practically for different values of γ (Fig. 1).

For small time scale the following delayed behavior due to relaxation time (which is different for each values of γ) are observed:

- When $\gamma = 0.99$ the FNPK approximation describes the following behavior: Fig. 1a shows a zoom (shaded area) at the range time 0–1 s. In this range the neutron density decreases, due to the existence of sub-diffusive processes which prevent the neutron moving freely, so that the neutron movement is delayed and neutron density consequently decreases. Physically this behavior is due to that the control rods are not extracted enough, therefore most of the neutrons generated in the fission process are absorbed where the minimum local of neutron density is reached at 0.25 s, and this is greater that the initial value of the neutron density ($n_0 = 2.5 \times 10^9$ n/s/cm³ s). After at $t = 1$ s the neutron density begins to increase, due to that the absorbed

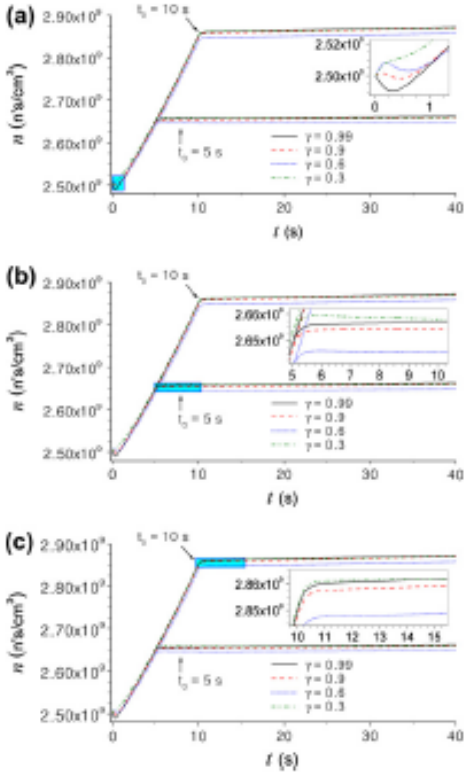

Fig. 3. Effects in the neutron density response when duration of lifting control rods is different and the velocity of lifting control rods is same ($r = 10$ pcm/s), with $\rho_0 = -6$ pcm. The shaded area represents different approaches to small time scales: (a) initial startup; the zoom include $t_0 = 5$ s and $t_0 = 10$ s (b) after having raised the control rods; the zoom only include $t_0 = 5$ s and (c) after having raised the control rods; the zoom include only $t_0 = 10$ s.

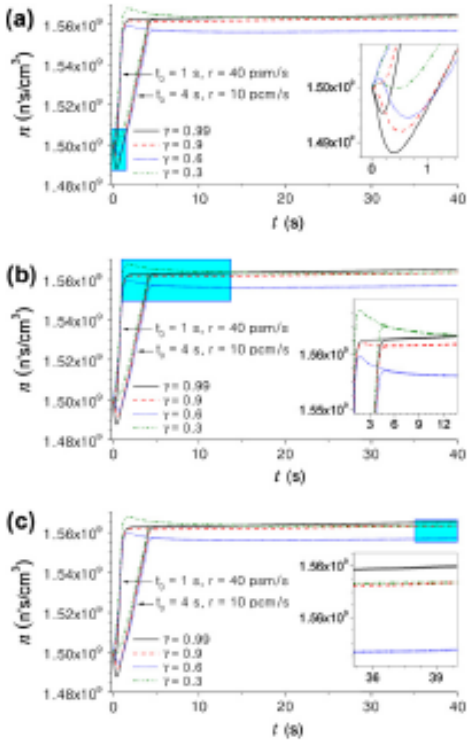

Fig. 4. Effects in the neutron density response when reactivity subcritical is $\rho_0 = -10$ pcm, the duration of lifting control rods values are $t_0 = 1$ s and $t_0 = 4$ s, and the velocity of lifting control rods values are $r = 40$ pcm/s and $r = 10$ pcm/s, respectively. The shaded area represents different approaches to small time scales: (a) initial startup, (b) after having raised the control rods and (c) long time of simulation.

neutrons by the control rods are much lower that the generated. After having raised the control rods, around of 5 s (zoom in Fig. 1b) the relaxant time effects on the behavior on the neutron density still are important respect to CNPK description. Is interesting observe the effect when the control rods were stopped (the vertical dot line indicate the moment, zoom Fig. 1b) the neutron density continues to increase slightly. Finally, in Fig. 1c shows the apparently steady state of FNPK which is smaller than CNPK, as was previously mentioned.

- For $\gamma = 0.9, 0.8$, and 0.6, the neutron density behavior described by the FPNK is shown in the zoom of the Fig. 1a–c. In the first instants (less to 0.2 s, in Fig. 1a) the neutron density increases, observing over-prediction regarding to CNPK equations. While raising the control rods the neutron density behavior has a local maximum at approximately at 0.2 s, and after the change in the trends is observed, whose magnitude is due to γ value, i.e. when decrease γ, the delayed effects in the neutron density are less. The physical interpretation is that when increase the γ value, the absorption effects are also greater, but it is not less than the initial value of the neutron density ($n_0 = 2.5 \times 10^9$ n's/cm^3 s). Is import to note that this behavior is due to that the production of neutron of external source ($q = 10^6$ n's/cm^3 s) and lifting control rods begin at same time, then the neutron density increase but the absorption capacity of control rods is greater than the capacity of the neutron multiplication and the neutron density decrease slightly. However, when the control rods is enough lifting the neutron density begins to increase. For $\gamma = 0.8$, and 0.6 (zoom in Fig. 1b and c) the behavior is similar for $\gamma = 0.99$, however, the neutron density is smaller. This behavior is not observed in CNPK due to that the absorbing delayed effects by the presence of the control rods are not considered.
- For $\gamma = 0.3$ (zoom in Fig. 1a), can be see that the neutron density increases continuously until that the behaviors described by FNPK and CNPK intersect approximately at $n = 2.51 \times 10^9$ n's/cm^3 which indicate that under this conditions, both approximations has the same predictions, before of this point the behavior of FNPK over-predict the behavior of CNPK, and after of this point can be observed a sub-predict. As was discussed previously; before that point the multiplication of neutrons is greater than the absorption effects, and after the relation time slow the neutron generation (change in the trends), but follow but still greater than the absorption effects. Fig. 1b shows that at approximately 5.5 s the absorption effects

are less respect other γ values. For long times (Fig. 1c) the neutron density have the same value of the neutron density than $\gamma = 0.9$.

In general terms, the results shows that the effect of relaxation time is that the neutronic reached after of lifting the control rods is less, and the effect of the anomalous diffusion coefficient has relevance at beginning and end of the lifting control rods.

4.3.2. NE 2

The results are shown in Fig. 2. The transient behavior was analyzed considering three small time scales: (a) when start-up is begging, (b) after having raised the control rods for $r = 10$ pcm/s, and (c) after having raised the control rods for $r = 40$ pcm/s.

The results show that the behavior for slower speed of lifting control rods $r = 10$ pcm/s was described above in NE 1. However, for $r = 40$ pcm/s, we can observe (zoom in Fig. 2a) that the anomalous diffusion values $\gamma = 0.9, 0.6, 0.3$ the neutron density behavior is similar that for $r = 10$ pcm/s but the magnitudes are greater, i.e., presents the same physical effects on absorbing and dispersion. At zoom in Fig. 2b, we can observed that the neutron density for $r = 10$ pcm/s ends to increase until $t = 5.5$ s and it apparently reached the steady values for all value of the γ, while at zoom in Fig. 2c we can observed that the increased in neutron density for $r = 40$ pcm/s ends at $t = 6.5$ s and continues increase slowly.

In general terms for scale small times we can observe that with slower speed of lifting control rods, the effects of the anomalous diffusion are greater that for faster speed of lifting control. This is because with a faster speed of lifting control rods the medium, loses quickly the property of being highly absorbent.

4.3.3. NE 3

The results are shown in Fig. 3. The transient behavior was analyzed considering three small time scales: (a) when start-up is begging, (b) after of duration of lifting control rods $t_0 = 5$ s, and (c) after of duration of lifting control rods $t_0 = 10$ s.

The behavior for the speed of lifting control rods $r = 10$ pcm/s was described above at Fig. 1 for $t_0 = 5$ s. In this NE (Fig. 3) we can observe the difference when that the duration of lifting control rods $t_0 = 10$ s has not any effect over the neutron density behavior for scale small time (zoom in Fig. 1a), i.e., the neutron density response of the short duration of lifting control rods $t_0 = 5$ s and the behavior of the long duration of lifting control rods $t_0 = 10$ s. Regarding the zoom in Fig. 3b and c are very similar, where the steady state behavior was reached to difference of the results in NE 2.

According with the results of the NE 1 and NE 2, the sub-diffusive effects are government by the velocity control rods, and do not by duration of lifting control rods.

4.3.4. NE 4

The results are shown in Fig. 4. The transient behavior was analyzed considering three small time scales: (a) when start-up is begging, (b) after having raised the control rods, and (c) long time of simulation.

This NE was realized with $\rho_i = -10$ pcm instead of $\rho_i = -6$ pcm, whit the idea of observing the sub-diffusive effects due to velocity and duration of lifting control rods.

In this NE for $r = 10$ pcm/s the duration of lifting control rods is greater than $r = 40$ pcm/s, but finally in both case the total reactivity inserted is same. According with that, we can observe at zoom in Fig. 4a that, for $r = 40$ pcm/s and $t_0 = 1$ s with the anomalous diffusion values $\gamma = 0.9, 0.9, 0.6, 0.3$ present neutron density behavior similar that for $r = 10$ pcm/s and $t_0 = 4$ s but the magnitudes are greater, i.e., presents the same physical effects of absorbing and dispersion (as was observed at NE 2, zoom in Fig. 2a). Fig. 4b (zoom), we can see than the neutron density behavior with $r = 40$ pcm/s and $t_0 = 1$ s reached values for each γ value, greater than neutronic density for $r = 10$ pcm/s and $t_0 = 4$ s. Fig. 4c, we observe that for large time scales, an apparently steady state is reached, whose differences are due to the different γ values. This behavior (Fig. 4c) is similar to results presented in Fig. 1c (see zoom) discussed above.

In general terms, for large time scales we can see that when the control rods was lifting the increasing of neutronic density is not equal to the values of steady state (apparently) obtained with CNPK regarding to FNPK. For short time scales the FNPK exhibits process sub-diffusive characterized by absorptions and dispersions whose magnitude depend of the γ.

The classical point neutron kinetics equations (Eqs. (1) and (2)), also were solved using the numerical approximation with explicit temporal integration method, i.e.:

$$\frac{n_{i+1} - n_i}{\Delta t} = \frac{\rho_i - \beta}{\Lambda} n_i + \lambda C_i + q \tag{13}$$

$$\frac{C_{i+1} - C_i}{\Delta t} = \frac{\beta}{\Lambda} n_i - \lambda C_i \tag{14}$$

where $\Delta t = t_{i+1} - t_i$, $n_i = n(t_i)$, $C_i = C(t_i)$, $\rho_i = \rho(t_i)$ and t_i is time lapsed at i-th iteration. The comparison of the results between Zhang et al. (2008), and numerical approximation of the classical neutronic point kinetics, show that are very similar. These, comparisons are not include in the previous figures, but is importantly mention in the context of this discussion.

5. Conclusion

The main results obtained in this work are:

- For large times scale (Fig. 1), the results shows that the classical equation of the neutron point kinetics (CNPK) over predicted the neutron density, regarding to fractional neutron point kinetics (FNPK).
- The results obtained shown that the effects of the anomalous diffusion (FNPK approximation) when nuclear reactor is start-up are more relevant for short times scale (Figs. 2–4).
- According with the results of the numerical experiments NE1 and NE2, the sub-diffusive effects are government by the velocity of control rods, and do not by the duration of lifting control rods.
- For the short times scales during lifting control rods and fast insertion of reactivity the FNPK model predicted greater neutron multiplication that can cause a trip of the reactor. This effect is not predicted by CNPK.

Acknowledgments

First Author is grateful for the financial support through a scholarship from the Consejo Nacional de Ciencia y Tecnología (CONACyT) for the Master's Graduate Studies in Engineering Program of the Universidad Nacional Autónoma de México, and special thanks to Laboratory of the Severe Accidents in Nuclear Reactors of the Universidad Autónoma Metropolitana-Iztapalapa, which was conducted this research.

References

Duderstadt, J.J., Hamilton, L.J., 1976. Nuclear Reactor Analysis. Jhon Wiley and Sons, New York, United States of America.

Edwards, J.T., Ford, N.J., Simpson, A.C., 2002. The numerical solution of linear multiterm fractional differential equations. J. Comput. Appl. Math. 148, 401–418.

Espinosa-Paredes, G., Álvarez-Ramírez, J., Vázquez, A., 2006. Detecting long-range correlation with detrended fluctuation analysis: application to BWR stability. Ann. Nucl. Energy. 33, 1308–1313.
Espinosa-Paredes, G., Polo-Labarrios, M.A., 2011. Time-Fractional Telegrapher's Equation (P1) Approximation for the Transport Equation. Nucl. Sci. Eng., in press.
Espinosa-Paredes, G., Polo-Labarrios, M.-A., Díaz-González, L., Vázquez-Rodríguez, A., Espinosa-Martínez, E.-G., 2011a. Sensitivity and Uncertainty Analysis of the Fractional Neutron Point Kinetics Equations. Ann. Nucl. Energy 42, 169–174.
Espinosa-Paredes, G., Polo-Labarrios, M.A., Espinosa-Martínez, E.G., del Valle-Gallegos, E., 2011b. Fractional neutron point kinetics equations for nuclear reactor dynamics. Ann. Nucl. Energy 38, 307–330.
Glasstone, S., Sesonske, A., 1981. Nucl. React. Eng., Third ed. VNR, New York, United States of America.
Palma, D.A.P., Martinez, A.S., Gonçalves, A.C., 2009. Analytical solution of point kinetics equations for linear reactivity variation during the start-up of a nuclear reactor. Ann. Nucl. Energy 36, 1469–1471.
Stacey, W.M., 2001. Nuclear Reactor Physics. John Wiley and Sons, Inc., New York, United States of America.
Zhang, F., Chen, W.Z., Gui, X.W., 2008. Analytic method study of point-reactor kinetic equation when cold start-up. Ann. Nucl. Energy 35, 748–749.

Anexo 5

Sensitivity and uncertainty analysis of the fractional neutron point kinetics equations

Annals of Nuclear Energy 42 (2012) 169–174

Contents lists available at SciVerse ScienceDirect

Annals of Nuclear Energy

journal homepage: www.elsevier.com/locate/anucene

Technical note

Sensitivity and uncertainty analysis of the fractional neutron point kinetics equations

G. Espinosa-Paredes [a,*], M.-A. Polo-Labarrios [a,b], L. Díaz-González [c], A. Vázquez-Rodríguez [a], E.-G. Espinosa-Martínez [d]

[a] Área de Ingeniería en Recursos Energéticos, Universidad Autónoma Metropolitana-Iztapalapa, Av. San Rafael Atlixco, 186, Col. Vicentina, México D.F. 09340, Mexico
[b] Departamento de Sistemas Energéticos, Facultad de Ingeniería, Universidad Autónoma de México, Av. Universidad 3000, México D.F. 04510, Mexico
[c] Facultad de Ciencias, Universidad Autónoma del Estado de Morelos, Av. Universidad 1001, Chamilpa, Cuernavaca 62209, Mexico

ARTICLE INFO

Article history:
Received 9 November 2011
Accepted 30 November 2011
Available online 9 January 2012

Keywords:
Telegrapher's equation
Anomalous diffusion exponent
Sensitivity analysis
Monte Carlo simulation

ABSTRACT

The aim of the present work is to evaluate the sensitivity and uncertainty of the anomalous diffusion coefficient in the Fractional Neutron Point Kinetics (FNPK) equations. This analysis was carried out through Monte Carlo simulations of sizes up to 65,000; the size of 50,000 was considered as valid for routine applications. The sensitivity was evaluated in terms of 99% confidence intervals of the mean to understand the range of mean values that may represent the entire statistical population of performance variables. The regression analysis with anomalous diffusion coefficient as the predictor variable showed statistically valid quadratic relationship for neutronic density and the delayed neutron precursor concentration. The uncertainties were propagated as follows: in a 1% change in the anomalous diffusion exponent the responses for neutron density, and precursor density changed by 0.017% and 0.000125% for short times, and for long times by 0.012% and 0.000267%, respectively.

1. Introduction

Recently a reduced model of neutron kinetics based on the neutron diffusion theory with a fractional constitutive law was proposed by Espinosa-Paredes et al. (2008, 2011). This work results in a fractional point neutron kinetics (FPNK) model based on the diffusion theory using all known theoretical arguments. The scope of the FPNK is to describe the neutron transient behavior in a highly heterogeneous configuration in nuclear reactors, in presence of strong neutron absorbers in the fuel, control rods and chemical shim in the coolant. In summary, there are many interesting problems to consider from the point of view of the fractional differential equations (FDEs), the challenge is the modeling and simulation of the new generation of nuclear reactors, as well as advanced molten salt reactor (e.g., Zhang et al., 2009), where the old paradigms can no longer be valid.

The main problem of the FPNK is a method for determination the fractional order (called as anomalous diffusion coefficient, ADC) of the ordinary differential equation. However, with the statistical treatment of the neutronic data of the nuclear power plant, the ADC can be estimated (Espinosa-Paredes et al., 2008). However, the lack of knowledge on the ADC limits the use of the FPNK.

The aim of this work is to present an anomalous diffusion coefficient sensitivity and uncertainty analysis of the FPNK from Monte Carlo simulations for sizes up to 50,000. The Monte Carlo simulation method was previously applied to mass flow rate sensitivity and uncertainty analysis in a natural circulation boiling water reactor (Espinosa-Paredes et al., 2010).

2. Monte Carlo method

The Monte Carlo method is based on sampling the vector of the input parameters in a random sequence, running the system model computer code for each sample of that vector to get a corresponding statistical sample of the vector of the output variables, and then estimating the characteristics of these output variables using the output samples. One of the benefits of the Monte Carlo method is that all standard statistical methods and tests can be used to estimate distributions of the output variables as well as to evaluate any hypothesis. This makes it the most straightforward and powerful method available in the scientific literature to deal with sensitivity analysis and uncertainty propagation in complex models. Although there exist equations for such error propagation processes (Bevington and Robinson, 2003), these equations are, in fact, approximate, and their use in the evaluation of complex models is highly cumbersome. These considerations make the Monte Carlo approach much more adequate for the present simulation study.

* Corresponding author.
E-mail address: gepe@xanum.uam.mx (G. Espinosa-Paredes).

0306-4549/$ - see front matter © 2011 Elsevier Ltd. All rights reserved.
doi:10.1016/j.anucene.2011.11.023

3. Methodology

As stated above, the aim of this work is to investigate the anomalous diffusion coefficient (ADC) effect in the fractional neutron point kinetic (FNPK). This is done by estimating the transient behavior during a reactor start-up. The approach used to compute sensitivity and uncertainty analysis is the Monte Carlo simulation. The Monte Carlo simulation methodology can be implemented according with the following steps (Espinosa-Paredes et al., 2010):

Step 1: Generating random numbers uniformly distributed in space (0, 1), i.e., samples from a uniform $U(0,1)$ distribution: The Marsenne Twister algorithm of Matsumoto and Nishimura (1998) was employed, which is a widely used generator with a very long $(2^{19937}-1)$ period. This is a highly desirable property for such applications (Law and Kelton, 2000). Thus, the necessary streams of independent and identically distributed random numbers (IID $U(0,1)$) of 64 bits were generated.

Step 2: Testing of the random numbers if they resemble independent and identically distributed IID $U(0,1)$ random variants: Each stream was tested for randomness using Marsaglia (1968) two- and three-dimensional plot method (Law and Kelton, 2000). The simulated data clearly filled the (0, 1) space as required by this randomness test in both two- and three-dimensions. Another test for randomness was also applied, which checks how many individual numbers are actually repeated in a given stream of random numbers, and if such repeated-numbers are few, the simulated random numbers can be safely used for further applications. On the average, only around 1 number out of 100,000 numbers in individual streams of IID $U(0,1)$ was repeated. Because the simulations sizes were only up to 40,000, practically no repeated numbers were encountered in the entire chain, which made the Monte Carlo method fully valid for this application.

Step 3: Converting the random numbers to continuous random variants for a normal distribution $N(0,1)$: The polar method of Marsaglia and Bray (1964) was chosen for the present application. Two parallel streams of random numbers (R_1 and R_2) were used for generating one set of IID $N(0,1)$ normal random variants. The simulated data were graphically examined for normality. Practically no repeated-numbers were found in tests with 100,000 numbers in these sets of random normal variants. Therefore, the data was considered as high quality to represent a normal distribution and could, therefore, be safely used for further applications. We have used them here for understanding the sensitivity and uncertainty analysis of the anomalous diffusion coefficient in the FNPK equations.

Step 4: Sensitivity and uncertainty analysis of anomalous diffusion coefficient in the FNPK equations: These IID $N(0,1)$ normal random variants for the evaluation of the sensitivity relationships of anomalous diffusion coefficient with neutron density and delayed neutron precursor density were used.

4. FNPK equations for nuclear reactor dynamics

The fractional model used in this work with a single-group delayed neutron precursors, is given by Espinosa-Paredes et al. (2011)

$$\tau^{\gamma}\frac{d^{\gamma+1}n}{dt^{\gamma+1}}+\tau^{\alpha}\left[\frac{1}{l}+\frac{(1-\beta)}{\Lambda}\right]\frac{d^{\gamma}n}{dt^{\gamma}}+\frac{dn}{dt}-\frac{\rho-\beta}{\Lambda}n+\lambda C+\tau^{\gamma}\lambda\frac{d^{\gamma}C}{dt^{\gamma}},\quad 0<\gamma<1 \tag{1}$$

where τ is the relaxation time, γ is the ADC of the fractional ordinary differential equation, n is the neutron density, C is the delayed neutron precursor density, l is the prompt-neutron lifetime for a finite media, Λ is the neutron generation time, β is the fraction of delayed neutrons, and ρ is the reactivity. When $\tau^{\gamma}\to 0$, the classic neutron point kinetics equation is recovered. The fractional model includes three additional terms with respect to the classic equation containing fractional derivatives: (1) $\frac{d^{\gamma+1}n}{dt^{\gamma+1}}$, (2) $\frac{d^{\gamma}n}{dt^{\gamma}}$, and (3) $\frac{d^{\gamma}C}{dt^{\gamma}}$. The physical interpretation of these terms suggest that for sub-diffusion processes, the first term has an important contribution for rapid changes in the neutron density, while the second term represents an important contribution when the change in the neutron density is relatively slow; e.g., during a start-up in a typical nuclear power plant that involves operational maneuvers due to the movement of the control rod drive. The third term becomes more important when the reactor is in shutdown process, also it could be important to understand the processes in the accelerator-driven system (ADS), which is a subcritical system characterized by a low fraction of delayed neutrons and by a small Doppler reactivity coefficient.

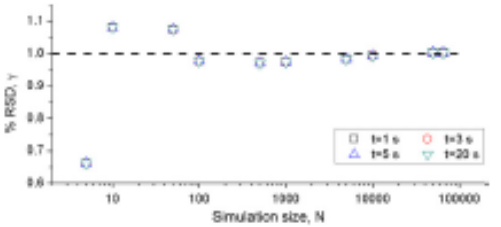

Fig. 1. Relative standard deviation (RSD) for γ as a function of the simulation size N. The horizontal dashed line at 1% is the reference line for γ.

The net rate of formation of the precursor of delayed neutrons corresponding to single-group is given by

$$\frac{dC}{dt}=\frac{\beta}{\Lambda}n-\lambda C \tag{2}$$

The first and second terms on the right side of this equation are the rate of formation of the precursors and radioactive decay, respectively.

Remarking, Eqs. (1) and (2) represent the fractional mathematical model to describe the neutron dynamic process in a nuclear reactor.

4.1. Fractional numerical solution

The numerical approximation of the solution of the FNPK model is presented in Espinosa-Paredes et al. (2011). These authors applied the numerical solution of linear multi-term fractional differential equations for the system of equations (Edwards et al., 2002).

5. Implementation of the Monte Carlo simulation

To analyse the effect of γ on the FNPK behavior, the Monte Carlo simulation was implemented in the numerical solution of the FNPK through the following expression:

$$\gamma_i=\gamma_0+b\times x_i,\quad i=1,2,3,\ldots,N \tag{3}$$

where γ_i is the ith value of the anomalous diffusion coefficient, γ_0 is an initial value less than one and greater than zero, b is a constant and x_i is the number related to the Monte Carlo method. Then, γ_i is calculated for each x_i value (with $i=1,2,3,\ldots,N$), which is used as the input data for the FNPK numerical model to run the dynamic simulation.

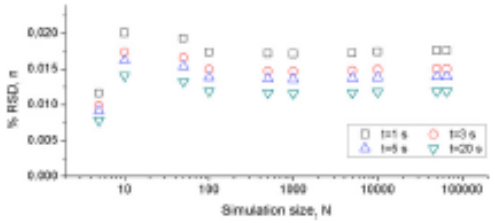

Fig. 2. Relative standard deviation (RSD) for n as a function of the simulation size *N*. The simulation time correspond to very short times ($t = 1$ s), short times ($t = 3$ s), medium-times ($t = 5$ s) and long times ($t = 20$ s).

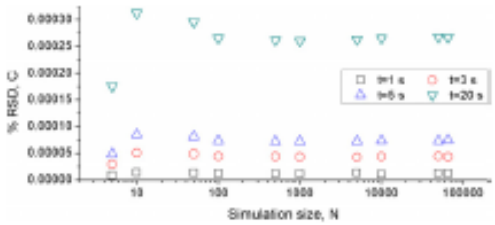

Fig. 3. Relative standard deviation (RSD) for *C* as a function of the simulation size *N*. The simulation time correspond to very short times ($t = 1$ s), short times ($t = 3$ s), medium-times ($t = 5$ s) and long times ($t = 20$ s).

To analyze the diffusion coefficient dynamic, numerical experiments are necessary where variations of the neutron density and concentration of the delayed neutron precursor are important with respect to time. Therefore, it is proposed a reactor startup considering insertion of linear reactivity (Zhang et al., 2008). During the reactor start-up different simulations times were considered for the sensitivity and uncertainty analysis. The times considered are 1 s, 3 s, 5 s and 20 s, and for each time results are presented.

Relevant parameters to sensitivity and uncertainty analysis according to their relative contribution on the overall FNPK behavior used in this study are: neutron density (*n*) and delayed neutrons precursor density (*C*), considering a single-group.

6. Results and discussions

6.1. Relative standard deviation (RSD)

The aim of this section is to determine the optimal sample size (*N*) where RSD is practically constant and independent from the simulation size.

Figs. 1–3 present a schematic plot showing RSD values expressed in percentages of the main operational parameters of the FNPK equations (γ, *n*, and *C*) for 1 s, 3 s, 5 s and 20 s elapsed time of the reactor startup. The RSD was calculated according to the following expression:

$$\mathrm{RSD} = \frac{s}{\bar{x}} \times 100 \tag{4}$$

where *s* is the standard deviation and $\bar{x}$ is the mean value. Consideration of the RSD allows to establish the optimal simulation size *N*. The optimal value of *N* is obtained when the value of RSD becomes invariable with respect to the simulation size *N*. It can be observed that for a simulation size *N* smaller than 5000, the RSD varies considerably and unpredictably; for $N = 10{,}000$ the variations in the values of RSD tend to decrease. For *N* greater than 50,000 (and up to 65,000), the values of RSD become practically constant and

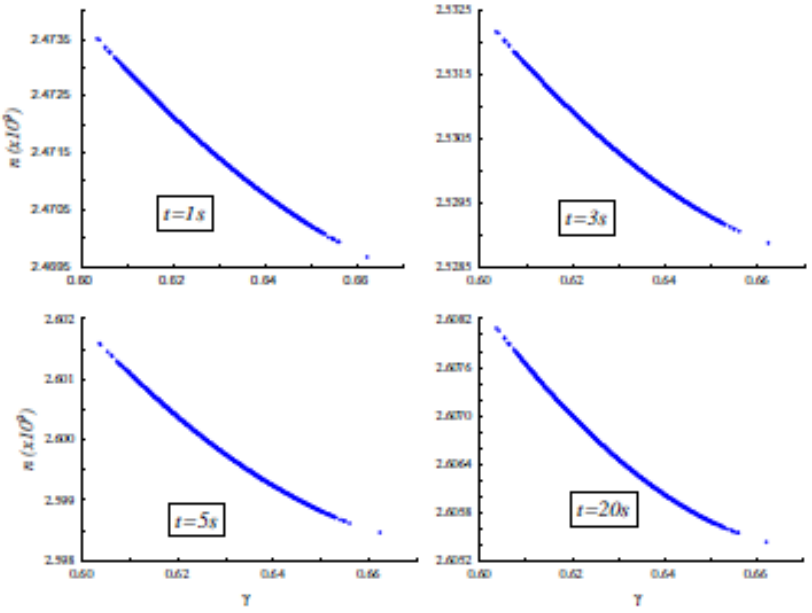

Fig. 4. Influence of anomalous diffusion coefficient (γ) on neutron density (*n*). Note a statistically significant negative correlation between these two parameters.

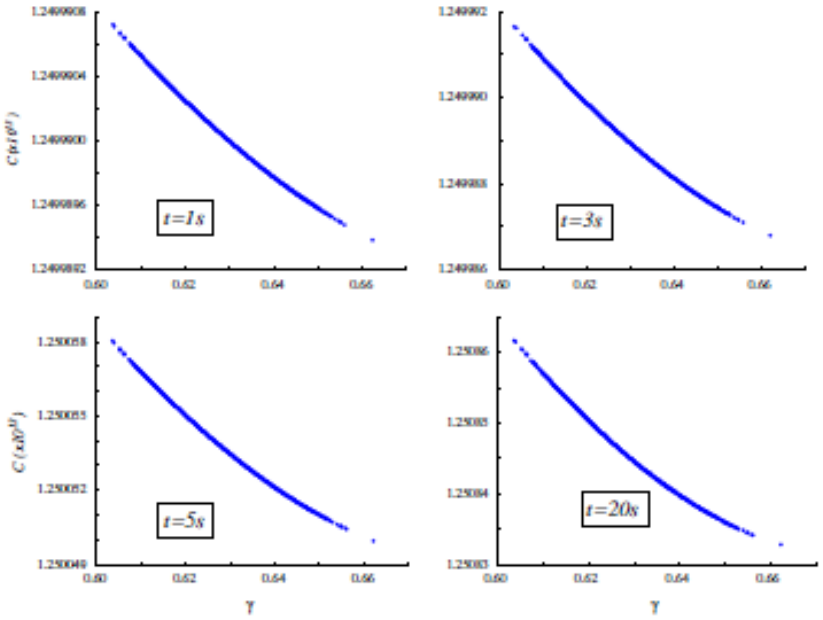

Fig. 5. Influence of anomalous diffusion coefficient (γ) on delayed neutron precursor concentration (C). Note a statistically significant negative correlation between these two parameters.

Table 1
Sensitivity analysis through 99% confidence intervals of the mean (CI99).

γ	n (10^8 neutron/cm^3)	C (10^{13} neutron/cm^3)
$t=1$		
0.629–0.630	2.471425–2.471430	1.24988000–1.24989000 02
$t=3$		
	2.530287–2.530292	1.24988869–1.24988875
$t=5$		
	2.599775–2.599780	1.25005350 0–1.25005351 1
$t=20$		
	2.606476–2.606480	1.25084 47–1.25084 48

independent of the simulation size. Therefore, the optimal simulation size N used in this work was 50,000 (Figs. 1–3).

It can be observed that the values of RSD for γ are the same for each time simulation as expected (Fig. 1), due that for each time the correspondent random numbers are the same.

On the other hand, the RSD for n and C present four different values for each simulation time as it can be observed in Figs. 2 and 3, respectively. The physical interpretation of these different values is the multiplicative neutron effects due to the insertion of positive reactivity by lifting the control rods, thus increasing neutronic power. When the neutron density increases the concentration of the delayed neutron precursor also increases. In these figures it can be observed that when both n and C with a value of $N \geq 50{,}000$, the RSD decreases with the increasing of the simulation time, i.e., when the neutron density increases.

6.2. Anomalous diffusion coefficient on the FNPK behavior

The results of the influence of ADC on the FNPK response characteristics evaluated from the Monte Carlo simulation are shown in Figs. 4 and 5 which were obtained with the simulation size of 50,000, for each simulation time.

The response of the neutron density with respect to the anomalous diffusion coefficient is depicted in Fig. 4. As it can be observed, the behavior of the neutron power is approximately quadratic with respect to the anomalous diffusion coefficient. However, the results in Fig. 4 show that the quadratic range is among 2.47201×10^9 and 2.46967×10^9 at 1 s, 2.53080×10^9 and 2.52886×10^9 at 3 s, 2.60027×10^9 and 2.59846×10^9 at 5 s, and 2.60690×10^9 and 2.60544×10^9 at 20 s for the neutron density, which corresponds to approximately 0.62–0.66 for the anomalous diffusion coefficient. It also can be observed that when the anomalous diffusion coefficient increases, the neutron density decreases and vice versa.

Fig. 5 shows the concentration of the delayed neutron precursor behavior as a function of the ADC, of which mathematical behavior is approximately of second order. The trend of the concentration of the delayed neutron precursor with the ADC is similar that the neutron density, i.e., when the anomalous diffusion coefficient increases, the concentration of the delayed neutron precursor decreases and vice versa.

6.3. Sensitivity analysis

We used the 99% confidence limits (CI99) or 99% confidence intervals (CI99) of the mean to understand the sensitivity of the system to changes in the ADC (γ). These were calculated using the standard formulae as follows:

$$CI99 = t_{(n-1)} \cdot \frac{s}{\sqrt{n}} \tag{5}$$

$$CI99 = \bar{x} \pm t_{(n-1)} \cdot \frac{s}{\sqrt{n}} \tag{6}$$

Table 2
Regression analysis of simulated data (γ as the predictor variable).

Dependent variable	Quadratic regression quality parameter (R^2)	Quadratic regression equation
$t = 1$		
n	0.999998	$n = 2.6831 \times 10^8 (\pm 1.83 \times 10^4) - 6.0332 \times 10^8 (\pm 5.80 \times 10^4)\gamma + 4.243 \times 10^8 (\pm 4.60 \times 10^4)\gamma^2$
C	0.999998	$C = 1.250 \times 10^{13} (\pm 6.26 \times 10^4) - 1.9975 \times 10^8 (\pm 1.99 \times 10^9)\gamma + 1.3969 \times 10^8 (\pm 1.58 \times 10^9)\gamma^2$
$t = 3$		
n	0.999998	$n = 2.757 \times 10^8 (\pm 1.87 \times 10^4) - 6.596 \times 10^8 (\pm 5.94 \times 10^4)\gamma + 4.7585 \times 10^8 (\pm 4.72 \times 10^4)\gamma^2$
C	0.999998	$C = 1.2503 \times 10^{13} (\pm 2.48 \times 10^9) - 8.4018 \times 10^8 (\pm 7.88 \times 10^9)\gamma + 5.9753 \times 10^8 (\pm 6.25 \times 10^9)\gamma^2$
$t = 5$		
n	0.999997	$n = 2.8321 \times 10^8 (\pm 1.91 \times 10^4) - 6.8044 \times 10^8 (\pm 6.06 \times 10^4)\gamma + 4.9468 \times 10^8 (\pm 4.81 \times 10^4)\gamma^2$
C	0.999998	$C = 1.2506 \times 10^{13} (\pm 4.36 \times 10^9) - 1.5082 \times 10^{10} (\pm 1.39 \times 10^9)\gamma + 1.0816 \times 10^{10} (\pm 1.10 \times 10^9)\gamma^2$
$t = 20$		
n	0.999996	$n = 2.8369 \times 10^8 (\pm 1.91 \times 10^4) - 6.8286 \times 10^8 (\pm 6.06 \times 10^4)\gamma + 5.0319 \times 10^8 (\pm 4.81 \times 10^4)\gamma^2$
C	0.999997	$C = 1.2531 \times 10^{13} (\pm 1.85 \times 10^6) - 6.5648 \times 10^{10} (\pm 5.87 \times 10^6)\gamma + 4.7914 \times 10^{10} (\pm 4.66 \times 10^6)\gamma^2$

R^2: Coefficient of multiple determination (squared correlation coefficient for a polynomial regression).
The quality of these fits is shown by the parameter (R^2) called the multiple-correlation coefficient (Bevington and Robinson, 2003).

Table 3
Uncertainty estimates on important parameters evaluated in terms of the RSD.

t (s)	γ (%)	n (%)	C (%)
1	1	0.017	1.25×10^{-4}
2	1	0.015	4.41×10^{-4}
5	1	0.014	7.32×10^{-4}
20	1	0.012	2.67×10^{-4}

where s is the standard deviation, $\bar{x}$ is the mean value, n is the simulation size used and t is the Student t critical value for the required degrees of freedom.

The results (Table 1) show how the statistical population mean values of the parameters in FNPK would be located (at 99% confidence or at 1% significance) within these respective intervals of 99% confidence level, starting, of course, with the sample mean values of $\gamma_0 = 0.63$, $n = 2.5 \times 10^8$ neutron/cm^3 and $C = 1.25 \times 10^{13}$ neutron/cm^3. Thus, there is 99% confidence that if the ADC (γ) were anywhere between the interval of 0.629–0.630, the concentration of the delayed neutron precursor (C) would be between $[1.249990001–1.249990002] \times 10^{13}$ neutron/cm^3, and the neutron density (n) between $[2.471425–2.471430] \times 10^8$ at $t = 1$ s; C would be between $[1.249988969–1.249988975] \times 10^{13}$, and n between $[2.530287–2.530292] \times 10^8$ at $t = 3$ s; C would be between $[1.250053500–1.250053511] \times 10^{13}$, and n between $[2.599775–2.599780] \times 10^8$ at $t = 5$ s; C would be between $[1.2508447–1.2508448] \times 10^{13}$, and n between $[2.606476–2.606480] \times 10^8$ at $t = 20$ s. Sensitivity analysis was also carried out through linear and polynomial regressions on the simulated data (Table 2) using the anomalous diffusion coefficient (γ) as the predictor variable. The results showed statistically valid quadratic correlations for neutron density and precursor concentration.

6.4. Uncertainty analysis

For this analysis, the results are summarized in Table 3. For 1% variation in the anomalous diffusion coefficient (γ), the neutron density (n) has a variation about 0.017% for very short times, 0.015% for short times, 0.14% for medium-times, and 0.012% for long times, which correspond to the least variation. Regarding to precursor concentration (C) that showed changes of about 0.0000125%, 0.0000441%, 0.0000732%, and 0.000267% for very short times, short times, medium-times and long times, respectively.

7. Conclusions

The sensitivity and uncertainty analysis of the fractional order of differential equation (anomalous diffusion coefficient, γ) in the fractional point neutron kinetic (FPNK) equations was performed with the Monte Carlo simulations. The following results were obtained:

- The optimal simulation size N found in this work was 50,000 when the RSD values were practically constant and independent of the simulation (Figs. 1–3).
- The influence of anomalous diffusion coefficient (γ) on neutron power (n), and concentration of the delay neutron precursor (C) evaluated from the Monte Carlo simulation were graphically obtained (Figs. 4 and 5).
- The sensitivity was evaluated in terms of 99% confidence intervals of the mean to understand the range of mean values that may represent the entire statistical population of performance variables (Table 1). The regression analysis with the γ as the predictor variable showed statistically valid quadratic correlations for both neutron density and concentration of the delayed neutron precursor (Table 2). The uncertainties were propagated as follows: for 1% change in the anomalous diffusion coefficient, the responses for the neutron density, and concentration of the delayed neutron precursor changed by 0.017% and 0.0000125% for short times, and for long times by 0.012% and 0.000267%, respectively (Table 3).

Acknowledgements

Second Author is grateful for the financial support through a scholarship from the Consejo Nacional de Ciencia y Tecnología (CONACyT) for the Master's Graduate Studies in Engineering Program of the Universidad Nacional Autónoma de México, and special thanks to Laboratory of the Severe Accidents in Nuclear Reactors of the Universidad Autónoma Metropolitana-Iztapalapa, which was conducted this research.

References

Bevington, P.R., Robinson, D.K., 2003. Data Reduction and Error Analysis for the Physical Sciences. McGraw Hill, Boston.
Edwards, J.T., Ford, N.J., Simpson, A.C., 2002. The numerical solution of linear multi-term fractional differential equations: systems of equations. Journal of Computational and Applied Mathematics 148, 401–418.

Espinosa-Paredes, G., Morales-Sandoval, J.B., Vázquez-Rodríguez, R., Espinosa-Martínez, E.-G., 2008. Constitutive laws for the neutron density current. Annals of Nuclear Energy 35, 1963–1967.

Espinosa-Paredes, G., Polo-Labarrios, M.-A., Espinosa-Martínez, E.-G., del Valle-Gallegos, E., 2011. Fractional neutron point kinetics equations for nuclear reactor dynamics. Annals of Nuclear Energy 38, 307–330.

Espinosa-Paredes, G., Verma, S.P., Vázquez-Rodríguez, A., Nuñez-Carrera, A., 2010. Mass flow rate sensitivity and uncertainty analysis in natural circulation boiling water reactor core from Monte Carlo simulations. Nuclear Engineering and Design 240, 1050–1062.

Law, A.M., Kelton, W.D., 2000. Simulation Modeling and Analysis, third ed. McGraw Hill, Boston.

Marsaglia, G., 1968. Random numbers fall mainly in the planes. Proceedings of the National Academy of Sciences of the United States of America 61, 25–28.

Marsaglia, G., Bray, T.A., 1964. A convenient method for generating normal variables. SIAM Review 6, 260–264.

Matsumoto, M., Nishimura, T., 1998. Mersenne Twister: a 623-dimensionally equidistributed uniform pseudo-random number generator. ACM Transactions on Modelling and Computer Simulation 8, 3–30.

Zhang, F., Chen, W.Z., Gui, X.W., 2008. Analytic method study of point-reactor kinetic equation when cold start-up. Annals of Nuclear Energy 35, 746–749.

Zhang, D.L., Qiu, S.Z., Su, G.H., Liu, C.L., Qian, L.B., 2009. Analysis on the neutron kinetics for a molten salt reactor. Progress in Nuclear Energy 51, 624–636.

Anexo 6

Sensitivity and uncertainty analysis of the fractional neutron point kinetics equations

Annals of Nuclear Energy 38 (2011) 307–330

Contents lists available at ScienceDirect

Annals of Nuclear Energy

journal homepage: www.elsevier.com/locate/anucene

Fractional neutron point kinetics equations for nuclear reactor dynamics

Gilberto Espinosa-Paredes [a,*], Marco-A. Polo-Labarrios [a], Erick-G. Espinosa-Martínez [b], Edmundo del Valle-Gallegos [c,1]

[a] Área de Ingeniería en Recursos Energéticos, Universidad Autónoma Metropolitana-Iztapalapa, Av. San Rafael Atlixco 186, Col. Vicentina, México, D.F. 09340, Mexico
[b] Retorno Québec 6, Col. Burgos de Cuernavaca 62580, Temixco, Mor., Mexico
[c] Escuela Superior de Física y Matemáticas, Instituto Politécnico Nacional, Av. Instituto Politécnico Nacional s/n, Col. San Pedro Zacatenco, México, D.F. 07738, Mexico

ARTICLE INFO

Article history:
Received 30 July 2010
Received in revised form 8 October 2010
Accepted 15 October 2010
Available online 13 November 2010

Keywords:
Neutron point kinetics
Non-Fickian approximation
Diffusion equation
Stability analysis
Reactivity changes

ABSTRACT

The fractional point-neutron kinetics model for the dynamic behavior in a nuclear reactor is derived and analyzed in this paper. The fractional model retains the main dynamic characteristics of the neutron motion in which the relaxation time associated with a rapid variation in the neutron flux contains a fractional order, acting as exponent of the relaxation time, to obtain the best representation of a nuclear reactor dynamics. The physical interpretation of the fractional order is related with non-Fickian effects from the neutron diffusion equation point of view. The numerical approximation to the solution of the fractional neutron point kinetics model, which can be represented as a multi-term high-order linear fractional differential equation, is calculated by reducing the problem to a system of ordinary and fractional differential equations. The numerical stability of the fractional scheme is investigated in this work. Results for neutron dynamic behavior for both positive and negative reactivity and for different values of fractional order are shown and compared with the classic neutron point kinetic equations. Additionally, a related review with the neutron point kinetics equations is presented, which encompasses papers written in English about this research topic (as well as some books and technical reports) published since 1940 up to 2010.

Contents

* Corresponding author. Fax: +52 55 5804 4900.
E-mail address: gepe@xanum.uam.mx (G. Espinosa-Paredes).
[1] COFAA-IPN fellowship.

0306-4549/$ - see front matter © 2010 Elsevier Ltd. All rights reserved.
doi:10.1016/j.anucene.2010.10.012

1. Introduction

The neutron point kinetics (NPK) equations are one of the most important reduced models of nuclear engineering, and they have been the subject of countless studies and applications to understand the neutron dynamics and its effects.

Nowadays, the neutron diffusion concept is a tool commonly used to understand the complex behavior of the averaged neutron motion. Most reactor studies treat the neutron motion as a diffusion process, wherein it is assumed that neutrons tend in the average to be diffused from regions of high to low neutron density. The treatment of the neutron transport as a diffusion process has only limited validation because neutrons tend to stream at relatively large distances between interactions. For example, in a Light Water Reactor (LWR) the mean free path of thermal neutrons is typically around 1 cm, comparable to the fuel pin diameter; and around a few centimeters for fast neutrons. Then the diffusion model fails to predict the neutron distribution in a fuel pin, where the transport equation should be used.

The process of neutron diffusion takes place in a highly heterogeneous hierarchical configuration (see Fig. 1.1). Fig. 1.1a represents the cross section of a nuclear reactor core, Fig. 1.1b represents the fuel assembly which is an array of fuel cells (each ensemble consists in four assemblies for most Boiling Water Reactors (BWR)), Fig. 1.1c shows an array of fuel pins. Normally these arrays (assemblies, cells and pins) are periodic with an anisotropy characterized by the nominal geometry array (Todreas and Kazimi, 1990a,b).

In this paper, to correct some *anomalous diffusion* phenomena due to highly heterogeneous configuration in nuclear reactors, we propose a fractional diffusion model as a constitutive equation of the neutron current density. The fractional diffusion model developed in this work can be applied where large variations of neutron cross sections normally preclude the use of the classical neutron diffusion equation, specifically, the presence of strong neutron absorbers in the fuel, control rods, and the coolant when injected boron forces the reactor to shutdown.

The fractional model derived in this work for the NPK equations with m groups of neutron delayed precursors, is given by

$$\tau^{\kappa}\frac{d^{\kappa+1}n}{dt^{\kappa+1}}+\tau^{\kappa}\left[\frac{1}{l}+\frac{(1-\beta)}{\Lambda}\right]\frac{d^{\kappa}n}{dt^{\kappa}}+\frac{dn}{dt}-\frac{\rho-\beta}{\Lambda}n+\sum_{i=1}^{m}\lambda_i C_i+\tau^{\kappa}\sum_{i=1}^{m}\left(\lambda_i\frac{d^{\kappa}C_i}{dt^{\kappa}}\right),\quad 0<\kappa\leq 2 \tag{1.1}$$

where τ is the relaxation time, κ is the anomalous diffusion order (for sub-diffusion process: $0<\kappa<1$; while that for super-diffusion process: $1<\kappa<2$), n is the neutron density, C_i is the concentration of the ith neutron delayed precursor, l is the prompt-neutron

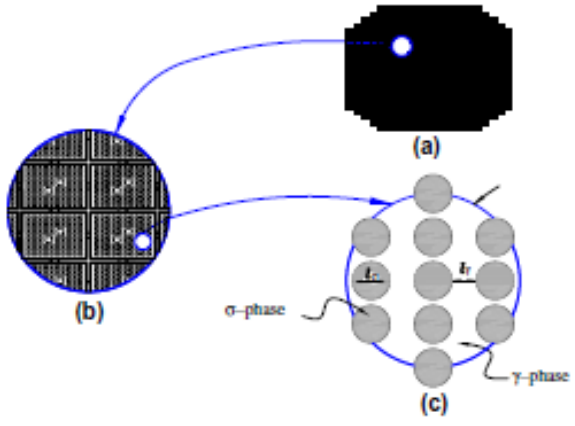

Fig. 1.1. Characteristic lengths of the system. (a) Nuclear reactor core; (b) Scale I: fuel assembly; (c) Scale II: array of fuel rods.

lifetime for finite media (defined by Eq. (6.9)), Λ is the neutron generation time (defined by Eq. (6.10)), β is the fraction of delayed neutrons, and ρ is the reactivity. When $\tau^{\kappa} \to 0$, the classic NPK equation is recovered. The fractional model includes three additional terms with respect to the classic equation containing fractional derivatives: (1) $\frac{d^{\alpha-1}n}{dt^{\alpha-1}}$, (2) $\frac{d^{\alpha}n}{dt^{\alpha}}$, and (3) $\frac{d^{\alpha}c_i}{dt^{\alpha}}$. The physical meaning of these terms suggests that for sub-diffusion processes, the first term has an important contribution for rapid changes in the neutron density (for example in the turbine trip in a BWR nuclear power plant (NPP)), while the second term represents an important contribution when the change in the neutron density is relatively slow, for example during start-up in a NPP that involves operational maneuvers due to the movement of the control rod drive. The third term becomes more important for example when the reactor is in shutdown process, also it could be important to understand the processes in the accelerator-driven system (ADS), which is a subcritical system characterized by a low fraction of delayed neutrons and by a small Doppler reactivity coefficient.

The modified constitutive laws proposed in this work allow to extend the scope and to improve the classical diffusion theory. Respect to the scope (as was mentioned above) to describe the neutron transient behavior in highly heterogeneous configuration in nuclear reactors, in presence of strong neutron absorbers in the fuel, control rods and chemical shim in the coolant. In order to improving the classical diffusion theory, we mean that the fractional model for neutron diffusion can improve predictions and presumably in some cases must be similar to the complicated theory of transport. However, the main objective of this work is to obtain a reduced model of neutron kinetics based on the theory of neutron diffusion with a fractional constitutive law. This model results in a fractional point-neutron kinetics obtained based on diffusion theory using all known theoretical arguments.

In summary, there are many interesting problems to consider under the point of view of fractional differential equations (FDEs), the challenge is there, now is the time to compare new with old paradigms to apply the best ones in the modeling and simulation of the new generation of nuclear reactors.

The numerical approximation of the solution of the fractional NPK model was obtained applying the numerical solution of linear multi-term fractional differential equations for the system of equations given by Edwards et al. (2002). The fractional kinetics model can be represented as a multi-term high-order linear fractional differential equation, which is in turn written as a system of ordinary and fractional differential equations, each one of the order (at the most) of the unity (Edwards et al., 2002). Results for neutron dynamics behavior for both positive and negative reactivity steps and for different values of fractional orders are presented and compared with the classic NPK equations. Additionally, a related review with NPK equations is presented, which encompasses the papers written in english about this research topic (as well as some books and technical reports) published since 1940 up to 2010.

2. Review on neutron point kinetics (NPK) equations

In this paper a review of works related with analytical and numerical solution of NPK equations is presented, which encompasses the papers written in English language about this research topic published since 1940 up to 2010. Besides, reviewing the journal articles, we also briefly mention some important technical reports and books. However, discussion regarding papers in conferences and meetings is not included.

2.1. NPK equations with feedback effects

The presence of temperature feedback is useful to provide an estimate of the transient behavior of a reactor and other variables in reactor cores which are tightly coupled; in this sense some works were developed to solve analytically the NPK equations (e.g., Fuchs, 1946; Chernick, 1951; Hansen, 1952; Frohlich and Johnson, 1969; Russel and Duncan, 1982; Gupta and Trasi, 1986; Chen et al., 2006; Li et al., 2007). Fuchs (1946) and Hansen (1952) tried to obtain the solution in a closed form for a large reactivity step using an adiabatic fuel heat-up model in which heat losses were neglected, since the power excursions occurring in the region of prompt criticality are extremely short in duration; Chernick (1951) has adopted a phase diagram approach for a qualitative study and a special perturbation method for an analytical treatment in a Newtonian feedback model. Frohlich and Johnson (1969) obtained the solution using a constant heat removal model for a ramp reactivity, while Russel and Duncan (1982) have recently used a similar model to investigate non-adiabatic excursions for a large step reactivity. On the other hand Gupta and Trasi (1986) solved analytically the NPK equations including delayed neutrons with Newtonian feedback for a reactivity step using perturbation theory, obtained an asymptotically stable solution for the neutron density for a given reactivity step. They showed that the asymptotic power level is independent of perturbation modes higher than the fundamental one and that the change in the steady power level is inversely proportional to the magnitude of the (negative) fuel temperature reactivity coefficient. Aboanber and Hamada (2002, 2003a,b) developed the power series solution (PWS) to solve the NPK equations with Newtonian temperature feedback in a simple matrix form very convenient for an explicit power series solution involving no approximation beyond the usual space-independent assumption. Also, the rational Padé approximation technique is applied to the non-linear system including temperature feedback via an analytical inversion method (Aboanber and Nahla, 2002a,b). However, if equations have constant coefficients, exact analytical solutions are easily established (Aboanber, 2003a,b), but they are elusive when the coefficients vary with time. Basilen and Lewins (1996) have introduced the solution of the NPK equations by a power series with time varying reactivity.

Based on the Nordheim–Fuchs model, Chen et al. (2006) tried to find the solution for the prompt supercritical transient process of a nuclear reactor with temperature feedback and a large reactivity step, and they extended the valid limits of initial power to any level. In some early literatures (e.g., Hetrick, 1993; Glasstone and Sesonske, 1994), the delayed supercritical transient process with a small reactivity step and temperature feedback was analyzed. It is the consensus of most authors that the analytical expression for the delayed supercritical process with temperature feedback could not be derived. Chen et al. (2007) presented a new analysis for the prompt supercritical process of a nuclear reactor with temperature feedback and initial power while inserting large and small reactivity steps.

The delayed supercritical process in a nuclear reactor, with temperature feedback while inserting a small reactivity step is also analyzed by Li et al. (2007). The relation between reactivity and time is derived and the effects of the small reactivity step and initial power on the delayed supercritical process are analyzed and discussed. To test the developed solution and to prove the validity of the method for application purposes, a comparison with other methods indicates the superiority of temperature prompt jump approximation. Some useful new conclusions are drawn, which can provide an important theory for the safety analysis and operating management of the nuclear reactor.

Recently, the NPK equations with one-group delayed neutrons and an adiabatic feedback model were solved analytically by Nahla (2009). The analytical solution is based on an expansion of the neutron density in powers of a small parameter, the prompt neutron generation time, into the second order differential equation in

the neutron density. The relations of reactivity, neutron density and temperature with time are calculated and compared with the analytic method of Chen et al. (2007), where Nahlás results are in general sub-predicted regarding Chens results.

Previous works have been restricted to the adiabatic feedback model (e.g., Kohler, 1969; Gupta and Trasi, 1986; Chen, 1990; Dam, 1996; Chen et al., 2006, 2007). Kohler (1969) has presented analytical expressions based on the point reactor model for the increase in peak power, temperature and energy release in prompt supercritical excursions. Chen (1990) studied a non-linear time dependent point power reactor problem with delayed temperature feedback on reactivity. Dam (1996) has analyzed the NPK equations in combination with linear temperature feedback for the reactivity and an adiabatic core heating of the core after loss of cooling. Damen and Kloosterman (2001) used a simple reactor model with one-group of delayed neutrons and first order fuel and temperature feedback mechanisms to calculate the linear transfer function from reactivity to reactor power that was subsequently used in a root-locus analysis.

2.2. NPK equations with stochastic approximation

Some exotic techniques as well as stochastic approximation have been proposed to solve (stochastically) and study non-linear effects of the NPK equations (e.g., Akcasu and Karasulu, 1976; Quabili and Karasulu, 1979; Saito, 1979; Behringer et al., 1990; Hayes and Allen, 2005).

The NPK equations are deterministic and can only be used to estimate average values of the neutron density, the neutron delayed precursor concentrations, and power level. However, the actual dynamical process is stochastic in nature and the neutron density and neutron delayed precursor concentrations vary randomly with time. At high power levels, the random behavior is negligible but at low power levels, such as at start-up (Hurwitz et al., 1963a,b; MacMillian and Storm, 1963), random fluctuations in the neutron density and neutron precursor concentrations may be significant.

Akcasu and Karasulu (1976) studied the statistical properties of the power response of a point reactor to a stochastic reactivity insertion and a stochastic external neutron source, in the absence of feedback effects. These authors showed that the autocorrelation function and spectral density of the power response of a point reactor can be determined exactly through the Fokker–Planck theory when the source and reactivity noise are white Gaussian processes. Other main result of these authors is that when delayed neutrons are taken into account, there is no exact solution when the reactivity noise is non-white.

Regarding the stochastic theory, the work by Quabili and Karasulu (1979) constitutes a comprehensive study of the statistical properties of non-linear responses of a point reactor to stochastic non-white reactivity inputs. These authors present the usefulness and limitation in Bourret's approximation as well as in logarithmic linearization for solving stochastic NPK equations with a non-Gaussian, non-white parametric noise, inasmuch as the Fokker–Planck theory is effectively applicable to Gaussian-white cases. The work of Saito (1979), points out the importance and usefulness of the Novikov–Furutsu formula in treating with a Gaussian colored parametric noise source.

The Wiener–Hermite functional (WHF) method was applied by Behringer et al. (1990) to the NPK equations excited by Gaussian random reactivity noise under stationary conditions, also the neutron steady-state value and the power spectral density (PSD) of the neutron flux was calculated in a second-order (WHF-2) approximation. They found that the WHF method is a powerful tool for studying the non-linear effects in the stochastic differential equation. Behringer and Piñeyro (1994) studied the stability criterion in the NPK equation when it includes delayed neutrons and is excited by a white noise Gaussian reactivity. The stability criterion was established by Behringer (1991) where the WHF and Fokker–Planck (FP) methods were applied; the stability parameters with WHF and FP are numerically equivalent.

Hayes and Allen (2005) derived stochastic differential equations for the dynamics of the neutron density and precursor concentrations of delayed neutrons in a point nuclear reactor, where the stochastic model is tested against Monte Carlo calculations and experimental data. The results demonstrated that the stochastic differential equation model accurately describes the random behavior of the neutron density and the precursor concentrations in a point reactor. In this investigation, the NPK equations are shown to model a system of interacting populations (the populations of neutrons and precursors of delayed neutrons). According with these authors the stochastic system of differential equations generalizes the deterministic NPK equations; computational solution of these stochastic equations is performed applying a modified form of the numerical method developed in Kinard and Allen (2004). The stochastic model is tested against Monte Carlo calculations and experimental data and results indicated that the stochastic model and computational method are accurate.

2.3. NPK equations with reactivity oscillations

Other line of investigation related to the point kinetics model is for example the work of Peinetti et al. (2006), who analyzed the kinetics induced by reactivity oscillations in a subcritical reactor in the framework of the point kinetics approximation, where sinusoidal reactivity oscillations were considered. These authors found that if a single group of precursors is taken into account, the system behaves like a strongly-damped linear oscillator with periodically-varying coefficients; however, in the point kinetics limit, reactivity oscillations in a nuclear reactor could be regarded as parametric excitations of a linear oscillator.

The study of the kinetics induced by reactivity oscillations in a subcritical nuclear has been previously studied (e.g., Hetrick, 1993; Ravetto, 1997; Dulla et al., 2006a,b). This problem is particularly important because, as shown by Ravetto (1997) and by Dulla et al. (2006), reactivity oscillations in a multiplying system could destabilize its response and lead to exponentially-diverging power transients. An important case is represented by molten salt reactors, where reactivity oscillations can be observed when lumps of precipitated fissile material spontaneously form inside the system; other case is the kinetics induced by reactivity oscillations by vibrating control rods in nuclear reactors. The previous work of Akcasu (1958) solved the problem the oscillations of reactivity without feedback by means of a functional series in powers of oscillatory amplitude. On the other hand, Lewins (1995) takes into account the higher-order effects of the reactivity oscillations with delayed neutrons.

2.4. NPK equations as a stiff problem

Point kinetics equations in their standard form are stiff; meaning that there exists in the system a response time which is very short compared with the overall time scale of the process, i.e., the difference in magnitude orders between the prompt and delayed neutron lifetimes, which results in the restriction of very small time steps in numerical solutions of the kinetic equations. The stiff problem of this model has been the inspiration for several works focused on analytical and numerical solutions of the point kinetics equations (e.g., Hetrick, 1971; Mitchell, 1977; Chao and Attard, 1985; Sánchez, 1989), and there are several methods especially adapted for solving initial value problems for stiff systems of ordinary differential equations. Specifically, among such methods

are the following: numerical integration using Simpson's rule (Keepin and Cox, 1960), finite element method (Kang and Hansen, 1973), Runge–Kutta procedures (Allerd and Carter, 1968; Sánchez, 1989), quasi-static method (Ott and Meneley, 1969; Koclas et al., 1996), piecewise polynomial approach (Hennart, 1977), singular perturbation method (Hendry and Bell, 1969; Goldstein and Shotkin, 1969; Biensld et al., 1978), finite difference method (Brown, 1957) and other methods which are based on integral equation formulations with the slowly varying factor in each integrand represented by an assumed functional form (Adelr, 1961; Hansen et al., 1965; Porsching, 1966). Most of these methods are successful in some specific problems, but still suffer, more or less, from disadvantages, as well as limitations on the maximum permissible time-step size to ensure computational stability, and inability to handle NPK equations in their full generality (Vigil, 1967).

Mitchell (1977) proposed the Taylor series methods for the solution of the NPK equations. This author applies two transformations whereby the system of equations may be solved using Taylor's series with a considerable increase in efficiency. The first method rests on a transformation of the independent variable and may be used for neutron generation times (Λ) down to approximately 10^{-5} s. The second method involves an expansion of the system of equations into a larger system in which the generation time is absent; and when the Λ value is smaller, the method becomes more efficient. Previous applications respect the Mitchells work of Taylor's series to the reactor kinetics equations were reported by various authors (Vigil, 1967; Mennig and Auerbach, 1967; Dubois and Grossman, 1972 and MacMillan, 1972).

With the idea of overcoming the stiffness problem in reactor kinetics, Chao and Attard (1985) applied stiffness confinement method (SCM) for solving the kinetics equations. This method consists in the stiffness decoupling from the differential equations for precursors and confined to the one for the prompt neutrons, which can be analytically solved. Devooght and Mund (1985) presented an excellent study on numerical solution of neutron kinetics equations using A-stable algorithms; they showed that the implicit Rosenbrock's Runge–Kutta method (Rosenbrock, 1963) is a candidate for nuclear kinetics analysis. Years later, also to avoid the problem of stiffness, Sánchez (1989) implemented an A-stable Runge–Kutta Method. Others schemes have been implemented (e.g. Porsching, 1966; da Nobrega, 1971; Aboanber and Nahla, 2002a,b, 2004). Porsching (1966) developed a numerical solution of the reactor kinetics equations in terms of a difference equation involving an exponential matrix. Da Nobrega (1971) introduced a technique based on the Padé (1, 1) and Padé (2, 0) approximations for the solution of the NPK equation, while Aboanber and Nahla (2002b) have introduced a method based on the analytical inversion of polynomials in the point kinetics matrix which was applied to different cases of Padé approximation for the solution of the point kinetics equation. These authors subsequently (Aboanber and Nahla, 2004) developed a new analytical method based on the Padé approximation which can not only employ much larger time steps due to the stiffness confinement. The idea of the Padé approximation as a rational approximation to the exponential function and their applications to the point kinetics equations can be traced back to two fundamental papers (Porsching, 1966; Da Nobrega, 1971).

In a recent technical note, a numerical procedure to efficiently calculate the solution to the point kinetics equation in nuclear reactor dynamics is described and investigated by Kinard and Allen (2004), where they considered that piecewise constant reactivity and source functions were made, which led to a system of linear differential equations. The piecewise constant assumption allows to solve the point kinetics equations exactly, and the problem of stiffness disappears.

Buzano et al. (1995) proposed a technique based on a hybrid technique that relies on an exact analytic integration of the reactor power equation, associated to an iterative procedure, leading to a self-consistent estimate of the best parabolic interpolation of the precursor concentrations. This approach allows time steps as large as several tens of seconds, provided that the reactivity curve, inside each one of them, being best fitted linearly to an acceptable accuracy. It may be observed that the Buzanós et al. method is similar to the method previously adopted by Chao and Attard (1985).

The power series method to solve the neutron and precursor equations was proposed by Basken and Lewins (1996), they found that a fundamental solution in a thermal reactor can be computed with high accuracy over time steps of approximately 0.25 s, which represents 25 times the shortest time constant of these stiff equations.

2.5. NPK equations: pedagogical aspect

From a pedagogical point of view, Ruby (1991) pointed out the importance of a neutron source in the teaching of reactor kinetics, he noted that source effects were commonly neglected in reactor theory courses and texts (e.g., Murray, 1957). However, the reactor kinetics model with source was presented by Toppel (1959) and Isbin (1963) without proof. Then, Murray (1994) presented the solution of the point kinetics equations with a neutron source, considering that the solution can be expressed in terms of the solution without source by a simple scaling, involving reactivity with an added constant term. On the other hand, Lewins (1995) presented a simple example for didactic use, which considers oscillations of reactivity and stability with delayed neutrons.

The special case is presented by Iwanaga and Sekimoto (2005), where they proposed a new calculation technique for the kinetics of the subcritical system, in which the neutrons are calculated by using steady state equation at each time point, and the neutron delayed precursors are calculated using time dependent equation. This work is applied to accelerator-driven system (ADS) that is a subcritical system which is characterized by a low fraction of delayed neutrons and by a low Doppler reactivity coefficient.

2.6. NPK equations: recent works

Van Den Eynde (2006) provided a correction to reactor kinetics solution of the Chao and Attard (1985). However, Ganapol (2007) analyzed the importance of the relatively sophisticated computer algebra combined with an efficient Rosenbrock type differencing, which is the base of the Van Den Eyndés work, while Chao and Attardś work represents a basic application of a standard finite difference algorithm. In one way or other, the accuracy to accelerate the convergence was analyzed in Chao (2006) and Lewins (2006).

The analytical solution was derived by Zhang et al. (2008), for reactor cold start-up whose process is the reactivity insertion by lifting control rod discontinuously. The analytical solution was derived considering that the reactivity is introduced linearly and discontinuously. It is therefore very important to understand the rule of neutron density variation and to find out the relationships among the speed of lifting control rod and the duration and speed of neutron density response. It is also helpful for the operators to grasp the rule in order to avoid a start-up accident. Recently, Palma et al. (2009) derived an analytical solution of point kinetics equations, but unlike the Zhang et al. work's, considered linear reactivity variation during the start-up due to control rods withdrawal of a nuclear reactor. The formulation proposed by Palma et al. (2009) consists in the solution of the point kinetics equations for one-group of neutron precursors without using the prompt jump approximation, i.e., the approximation consists of disregarding the term of the second derivative for neutron density in relation

to time. To validate the analytical approximation, Palma et al. (2009) applied the method of finite difference (Hashimoto et al., 2000) to obtain its numerical solution.

A numerical algorithm called CORE (which signifies constant reactivity) to solve the point kinetics equations of nuclear reactors was developed by Quintero-Leyva (2008). It generates results consistent with relatively recent numerical methods and shows better accuracy and less sensitivity regarding time step than the standard Runge–Kutta (4th order) method.

A new mathematical formula of the period-reactivity inhour equation is presented by Nahla (2008). This formula is represented in a polynomial form with degree $i+j+1$ for i-group of delayed neutrons and j-group of photoneutrons. Specifically, the generalization of analytical exponential model (GAEM) was proposed and applied by this author to solve the point kinetics equations of Be- and D_2O-moderated reactors. Results of GAEM were compared with Padé approximation found that the GAEM provides a fast and accurate computational technique for the NPK equations of delayed neutrons and photoneutrons with step, ramp, sinusoidal, and feedback reactivities.

The power series solution (PWS) method was applied by Sathiyasheela (2009) for solving the point kinetics equations for a typical Liquid Metal Fast Breeder Reactor (LMFBR) with a lumped model of temperature feedback. Although there are other numerical methods available that are faster than PWS method, there was a convergence problem for higher reactivity addition rates but the method worked for smaller time steps. With the available fast computers at this time, the PWS is an efficient method for reactor dynamics studies.

A numerical integral method that efficiently provides the solution of the point kinetics equations by using the better basis function (BBF) for the approximation of the neutron density in one time step integration is described and investigated by Li et al. (2009). The approach is based on an exact analytic integration of the neutron density equation, where the stiffness of the equations is overcome by the fully implicit formulation. The procedure is tested by using a variety of reactivity functions, including step, ramp, and oscillatory reactivity changes. The solution of the better basis function method is compared to other analytical and numerical solutions of the NPK equations. The results show that selecting a better basis function can improve the efficiency and accuracy of this integral method. According with this author the computational method is more accurate and efficient than the methods in some earlier references (Yeh, 1978; Chao and Attard, 1985; Sánchez, 1989; Aboanber and Hamada, 2002; Kinard and Allen, 2004).

The integro-differential equation of the point kinetics of nuclear reactor was solved by Quintero-Leyva (2009), approximating the neutron density with piecewise polynomial and exponential functions. In the Quintero-Leyvás work, the differential equation for the precursor concentrations of delayed neutrons was integrated with a general production term, which then was used to obtain an integral–differential equation of the neutron density for the point reactor kinetics. According with this author integral–differential equation could provide advantages over the ordinary differential system of equations when numerical solutions are needed.

Aboanber and El Mhlawy (2009) solved the two-point kinetics equations for reflected reactors using an analytical inversion method (AIM), which was previously adopted by Aboander and Nahla (2002a,b). A new version of the reflected core inhour equation was derived and analyzed previously by Aboanber and El Mhlawy (2008).

Due to that the basic neutronic problem is unstable by nature, no let to be important mentioned the work of Theler and Bonetto (2010), who proposed a method to analyze the stability of the reactor point kinetics equations, in order to grasp the general behavior of the system and to generate some conceptual design maps. These authors, linear non-feedback case are studied and differences between Lyapunov and bounded-input bounded-output (BIBO) stability are presented.

A numerical approach for the solution of reactor point kinetics equations by including the fuel burn-up and temperature feedback is presented by Tashakor et al. (2010). In contrast with previous works (Kohler, 1969; Dam, 1996; Aboanber and Nahla, 2002a,b; Chen et al., 2007; Nahla, 2009), Tashakor's et al., method considers delayed neutrons fraction as a function of time which can be used for the core evaluation in transient state.

The analytical solution for solving the NPK equations with several groups of delayed neutrons is presented by Nahla (2010). This solution is based on the roots of the inhour equation, actually matrix eigenvalues, whose analytical solution represents the exact analytical solution for the point kinetics equations of several groups of delayed neutrons with constant reactivity, and with ramp and temperature feedback reactivities.

2.7. Remarks and discussions

According to the previous review the NPK approximation is approximately 80 years old. Research about NPK equations mainly covers a wide number of formal aspects going from seeking for an analytical solution (or exact solution) up to obtain at least a numerical solution, with linear and no-linear approximations. These solutions include cases with and without feedback effects taking or not into account delayed neutrons. Specifically, in the years 1940–1970 it seems that the efforts of researchers were in the search of procedures to get analytic solutions covering many physical situations. However, presently and in spite of the technological development of computers it still remains an intellectual challenge to propose methods to obtain analytical solutions for more general problems. The main standard characteristic of the NPK equations, from the mathematical and numerical analysis point of view is that they are stiff and non-linear. The combination of stiffness and non-linearity has generated a great deal of research as was seen in Section 2.4. Other line of research is the stochastic approach that began in the 1970s (according to our information), which has been accepted until now by a selected group of researchers, this is because it allows the study of non-linear effects of the NPK equations, that is another aspect of the statistical properties of the power response of a point reactor. In the early 2000s to 2010 there arose new proposals to get analytical and also numerical solutions of the NPK equations and according with this tendency there will be more research in this direction in the coming years.

In this research the main goal is not to provide a new method nor a technique or approach to solve the NPK equations. Instead of doing that the contribution goes in the sense of providing to the interested community with a fractional NPK model that reproduces the classic NPK model under certain conditions but that takes into account length and time scaling allowing to capture non-Fickian effects. The fractional NPK model here developed was analyzed and numerically solved in this work and represents a novel proposal whose framework could be the beginning of an extensive research both experimental and theoretical for applications in the nuclear science.

3. Phenomenological analysis

Consider the processes of collision and reaction in a reactor core with characteristic length scales in Fig. 1.1, where the fuel material is dispersed in lumps within the moderator. Then it can be considered only "two materials" shown in the system; namely, the fuel (σ) and the moderator (γ) where all neutrons in the reactor have

the same speed and that the angular flux is only linearly anisotropic. Then, the conservation equation for the neutron collision and reaction processes in this system, as well as the initial and boundaries conditions at interfaces are given by (Duderstadt and Hamilton, 1976):

$$\frac{1}{v}\frac{\partial\phi_\ell(\mathbf{r},t)}{\partial t}+\nabla\cdot\mathbf{J}_\ell(\mathbf{r},t)+\Sigma_{a\ell}(\mathbf{r},t)\phi_\ell(\mathbf{r},t)=S_\ell(\mathbf{r},t) \tag{3.1}$$

$$\frac{1}{v}\frac{\partial\mathbf{J}_\ell(\mathbf{r},t)}{\partial t}+\frac{1}{3}\nabla\phi_\ell(\mathbf{r},t)+\Sigma_{tr\ell}(\mathbf{r},t)\mathbf{J}_\ell(\mathbf{r},t)=0, \tag{3.2}$$

3.1. Initial conditions

$$\phi_\ell(\mathbf{r},0)=\phi_{\ell 0}(\mathbf{r}) \tag{3.3}$$

where sub-index ℓ is allowed to play the role of materials γ or σ, i.e. moderator or fuel respectively.

3.2. Inner boundary conditions

$$-\mathbf{n}_{\gamma\sigma}\cdot D_\gamma\nabla\phi_\gamma=-\mathbf{n}_{\gamma\sigma}\cdot D_\sigma\nabla\phi_\sigma \quad \text{at} \quad \gamma\sigma-\text{interface} \tag{3.4}$$

$$\phi_\gamma=\phi_\sigma, \qquad \text{at} \quad \gamma\sigma-\text{interface} \tag{3.5}$$

where for material ℓ, ϕ_ℓ is the neutron flux, $\mathbf{J}_\ell$ is the neutron current density, $\Sigma_{a\ell}$ is the absorption cross section, S_ℓ is the neutron source, D_ℓ is the neutron diffusion coefficient and $\mathbf{n}_{\gamma\sigma}$ is the unit normal vector directed from material γ towards material σ. In these equations

$$\Sigma_{a\ell}(\mathbf{r},t)=\Sigma_t(\mathbf{r},t)-\Sigma_{s\ell}(\mathbf{r},t) \tag{3.6}$$

$$\Sigma_{tr}(\mathbf{r},t)=\Sigma_t(\mathbf{r},t)-\mu_0\Sigma_s(\mathbf{r},t) \tag{3.7}$$

where μ_0 is the average of the scattering cosine angle and, $\Sigma_t(\mathbf{r},t)$, $\Sigma_{s\ell}(\mathbf{r},t)$, and $\Sigma_{tr\ell}(\mathbf{r},t)$ are, respectively, the total, scattering and transport cross sections for material ℓ.

4. Constitutive laws for the neutron current density

The typical consideration is to neglect the time derivative $v^{-1}\partial\mathbf{J}_\ell/\partial t$ in Eq. (3.2). If the time variation rate of the neutron current density is much slower than the collision frequency ($v\Sigma_{a\ell}$), i.e.

$$\frac{1}{|\mathbf{J}_\ell|}\frac{\partial|\mathbf{J}_\ell|}{\partial t}<<v\Sigma_{a\ell} \tag{4.1}$$

4.1. Fickian approximation

Since $v\Sigma_t$ is typically of order $10^6\,s^{-1}$ or larger (Duderstadt and Hamilton, 1976), Eq. (3.2) simplifies to

$$\mathbf{J}_\ell(\mathbf{r},t)=-D_\ell(\mathbf{r},t)\nabla\phi_\ell(\mathbf{r},t), \tag{4.2}$$

In many engineering areas, Eq. (4.2) is widely known as the Fick's law, where $D_\ell(\mathbf{r},t)$ is the neutron diffusion coefficient given by

$$D_\ell(\mathbf{r},t)=\frac{1}{3\Sigma_{tr\ell}(\mathbf{r},t)}=\frac{1}{3[\Sigma_{s\ell}(\mathbf{r},t)-\mu_0\Sigma_{s\ell}(\mathbf{r},t)]} \tag{4.3}$$

The diffusion theory provides a strictly valid mathematical description of the neutron flux when the assumptions made in its derivation are satisfied (Stacey, 2004):

A1. Absorption much less likely than scattering
A2. Linear spatial variation of the neutron distribution
A3. Isotropic scattering

The first assumption is satisfied for most of the moderating and structural materials found in a nuclear reactor, but not for the fuel and control elements. The second condition is satisfied a few mean free paths away from the boundary of large homogeneous media with relatively uniform source distribution. The third condition is satisfied for scattering from heavy atomic mass nuclei. However, the Fickian diffusion processes exhibit some *anomalous diffusion* phenomena due to the highly heterogeneous configuration in nuclear reactors, specifically, the presence of strong neutron absorbers in the fuel, control rods and chemical shim in the coolant. The dynamics of these absorbers radically change the local energy generation and turn the re-distribution of the same absorber, frequently requiring a more accurate treatment, for example the neutron transport, than that provided by the classical diffusion theory.

The non-fulfillment of any of these assumptions represents clear evidence that the standard Fick's law, needs to be modified.

4.2. Non-Fickian approximation

The restriction given by Eq. (4.1) is not valid for time scales in which the neutron flux has rapid variations and under these circumstances Eq. (3.2) recovers relevance. Then Eq. (3.2) can be rewritten using the neutron diffusion coefficient (Eq. (4.3)):

$$\tau_\ell\frac{\partial\mathbf{J}_\ell(\mathbf{r},t)}{\partial t}+\mathbf{J}_\ell(\mathbf{r},t)=-D_\ell(\mathbf{r})\nabla\phi_\ell(\mathbf{r},t) \tag{4.4}$$

where

$$\tau_\ell=\frac{1}{v\Sigma_{tr}}=\frac{3D_\ell}{v} \tag{4.5}$$

Eq. (4.4) corresponds to non-Ficks law, whose mathematical structure is identical to the Cattaneo (1958) and Vernotte (1958) constitutive equation, where τ_ℓ is a relaxation time. It is important to note that the Cattaneo's equation is suitable for time scales such that $t\lesssim\tau_\ell$. Combining Eqs. (3.1) and (4.4), we obtain a one-speed neutron wave equation

$$\frac{\partial^2\phi_\ell(\mathbf{r},t)}{\partial t^2}+\left(v\Sigma_{a\ell}(\mathbf{r},t)+\frac{1}{\tau_\ell}\right)\frac{\partial\phi_\ell(\mathbf{r},t)}{\partial t}-a_\ell^2\nabla^2\phi_\ell(\mathbf{r},t)-\frac{v}{\tau_\ell}[S_\ell(\mathbf{r},t)-\Sigma_{a\ell}(\mathbf{r},t)\phi_\ell(\mathbf{r},t)]+v\frac{\partial S_\ell(\mathbf{r},t)}{\partial t} \tag{4.6}$$

where a_ℓ is the propagation speed of "neutron wave", which is given by

$$a_{\ell\pm}=\pm\sqrt{\frac{v}{\tau_\ell}D_\ell} \tag{4.7}$$

Here $a_{\ell\pm}$ represents that the neutrons wave has two-propagation speeds, whose magnitude is the same but moving on opposite directions. $a_{\ell\pm}=\pm\sqrt{vD_\ell/\tau_\ell}$. This proposal is just enough to realize that the wave propagation speed corresponding to the physical problem is not infinite. However, the classical P_1 approximation which gives rise to the Telegraphel's equation has a finite velocity but with the wrong value, of $v/\sqrt{3}$ (Heizler, 2010), which can be limited for many physical effects related with the neutron processes.

When time scale given by Eq. (4.1) is satisfied, the Ficks equation $\mathbf{J}_\ell=-D_\ell\nabla\varphi_\ell$ is recovered and the above equation simplifies to

$$\frac{1}{v}\frac{\partial\phi_\ell}{\partial t}+\Sigma_{a\ell}(\mathbf{r},t)\phi_\ell(\mathbf{r},t)=\nabla\cdot D_\ell(\mathbf{r},t)\nabla\phi_\ell(\mathbf{r},t) \tag{4.8}$$

As it is well known, the Ficks equation yields a parabolic differential equation for the neutron field, and as a consequence, the propagation speed of the wave is infinite. It is proposed that the neutron flux $\phi_\ell(\mathbf{r},t)$ is a potential field, with a neutron current density $\mathbf{J}_\ell$ given by the Ficks law (Eq. (4.2)). In the field of neutron distribution there exists *equipotential surfaces*, i.e., $\phi_\ell[\mathbf{r}(t),t]=$ *constant*. In many works (e.g., Cattaneo, 1958; Vernotte, 1958; Sadler and Dhaler,

1964; Lulkov, 1966; Kadaifar, 1976; Bubnov, 1976; Sieniutycz, 1979; Kaminski, 1990; Ozisik and Tzou, 1994; Barletta and Zanchini, 1994), it was emphasized that parabolic equation implies infinite speed propagation. In order to take into account finite speed propagation, the model should be replaced by an adequate hyperbolic equation obtained by combining the phenomenological relationship of the non-Fickian type and the neutron balance as well as Eq. (4.6).

In the following section these ideas are extended using the fractional model concept.

5. Anomalous diffusion

In previous section we have analyzed the neutron equation based on the constitutive Fick's law (Eq. (4.8)) and the corresponding to the non-Fick's law (Eq. (4.6)). However, these ideas can be extended by applying a fractional constitutive law.

In many natural systems, diffusion processes that do not follow the Ficks diffusion law have been observed. Such phenomena are referred to as anomalous diffusion. Specifically, in the case of the system described in Fig. 1.1, some anomalous diffusion phenomena occur due to the highly heterogeneous configuration. Contrary to a Fickian diffusion process, the presence of very highly absorbing control elements can induce spatially constrained neutron motion. The result is an anomalous diffusion process that cannot be accurately described as a Fickian diffusion process.

Recently, Nec and Nepomnyashchy (2007) have proposed fractional modifications to Cattaneo's constitutive equation as a phenomenological model to describe anomalous diffusion processes. It has been realized recently that in many physical processes the concept of normal diffusion, with its inherent temporal scaling of the average square displacement $\langle r^2(t)\rangle \sim t$, is suitable. A more general relation $\langle r^2(t)\rangle \sim t^{\kappa}$, is characteristic for sub-diffusion ($0<\kappa<1$) or super-diffusion ($\kappa>1$). The properties concerning these equations have been intensively researched (Schneider and Wyss, 1989; Metzler and Klafter, 2000; Mainardi and Pagnini, 2003; Lenzy et al., 2005).

According with these ideas Espinosa-Paredes et al. (2008) derived a fractional model for neutron balance given by

$$\tau_\gamma^\kappa \frac{1}{v}\frac{\partial^{\kappa+1}\phi_\gamma}{\partial t^{\kappa+1}} + \tau_\gamma^\kappa \Sigma_{a\gamma}\frac{\partial^\kappa \phi_\gamma}{\partial t^\kappa} + \frac{1}{v}\frac{\partial \phi_\gamma}{\partial t} + \Sigma_{a\gamma}\phi_\gamma - D_\gamma \nabla^2 \phi_\gamma \tag{5.1}$$

where a version of the fractional constitutive equation of the neutron current density is

$$\tau_\gamma^\kappa \frac{\partial^\kappa \mathbf{J}_\gamma}{\partial t^\kappa} + \mathbf{J}_\gamma = -D_\gamma \nabla \phi_\gamma \tag{5.2}$$

Strictly speaking this equation is the constitutive law of the non-Fickian law; however we call it fractional constitutive equation. It can be observed that the fractional approximation given by Eq. (5.1) does not include the source term, but in this work it will be considered (see Section 6).

This approximation gives rise to the fractional Telegrapher's equation given by Eq. (5.1). The initial conditions for fractional model are presented in Appendix A.

The suitable interfacial condition between moderator and fuel regions is obtained by combining Eqs. (3.4) and (5.2):

$$\tau_\gamma^\kappa \frac{\partial^\kappa J_\gamma}{\partial t^\kappa} + \mathbf{n}_{\gamma_\sigma}\cdot D_\gamma \nabla \phi_\gamma = \tau_\sigma^\kappa \frac{\partial^\kappa J_\sigma}{\partial t^\kappa} + \mathbf{n}_{\sigma\gamma}\cdot D_\sigma \nabla \phi_\sigma, \quad \text{at the } \gamma\sigma-\text{interface} \tag{5.3}$$

where

$$J_\gamma = \mathbf{n}_{\gamma_\sigma}\cdot \mathbf{J}_\gamma \tag{5.4}$$

$$J_\sigma = \mathbf{n}_{\sigma\gamma}\cdot \mathbf{J}_\sigma \tag{5.5}$$

Here, $\mathbf{n}_{\gamma_\sigma}$ is the unit vector, normal at the interface, which is directed from the γ-moderator towards the σ-fuel; a similar meaning for $\mathbf{n}_{\sigma\gamma}$ where $\mathbf{n}_{\gamma_\sigma} = -\mathbf{n}_{\sigma\gamma}$.

In these equations, the fractional derivative operator $\partial^\kappa/\partial t^\kappa$ is defined in the Riemann–Liouvillés sense (Oldham and Spanier, 1974) and κ is the anomalous diffusion order. The fractional wave model, Eq. (5.3), retains the main dynamic characteristics of the neutron motion.

When $\tau_\gamma^\kappa \to 0$ in Eq. (5.1), the equation based on Ficks law is recovered and when $\kappa \to 1$, the wave equation is obtained (based on the non-Fickian's law or Cattaneo's constitutive equation), which was defined by Chen et al. (2008) as normal diffusion.

The conservation of the Eq. (5.1) is guaranteed because the classical diffusion equation (Eq. (4.8)) represents an equation of balance to be met categorically and in this work it is not proposed a modification of this equation. The neutron current law was modified (Eq. (5.2)) which considers the fractional relaxation time. The time relaxation may stem from possible "obstacles and traps" (in a general interpretation) that delay the particles move and thus introduce memory effects into the motion, without affecting the particle conservation. It is important to note that a change in current law such as $\mathbf{J}^\kappa \propto -D_\kappa \nabla^\kappa \varphi_\gamma$ mean a justification related to the particle conservation and further explored, but this is not the case because in this work only shows the memory effect is introduced through time relaxation.

The anomalous diffusion order κ can be obtained by NPP data using Detrended Fluctuation Analysis (DFA) which is a method based on the random walk theory and was applied to a neutron power signal of the Forsmark stability benchmark (Espinosa-Paredes et al., 2008). DFA is a scaling method commonly used for detecting long-range correlation in non-stationary time series.

So far we have based our study considering that all neutrons in the reactor have the same speed. However, the neutrons in a reactor have energies spanning the energy range from 10 MeV down to less than 0.01 eV and neutron-nuclear cross sections depending on the incident neutron energy (Dudeastadt and Hamilton, 1976). Then, a more realistic treatment of the neutron energy dependence, the multi-group diffusion fractional equations was proposed by Espinosa-Paredes et al. (2008).

Fractional calculus deals with the study of the fractional order of the integral and derivative operators over real or complex domains and their applications in various fields of science and engineering (e.g., Oldham and Spanier, 1974; Miller and Ross, 1993; Samko et al., 1993; Podlubny, 1999; Hilfer, 2000; Kilbas et al., 2006; Magin, 2006).

In general terms the anomalous diffusion conditions of neutron process are: highly heterogeneous systems, extremely high neutron flux gradient, extremely large neutron current density, or an extremely short transient duration.

The physical problems were mentioned in Section 4.1. However, it is important to note that according with a recent publication (Reyes-Ramirez et al., 2010) the results of infinite multiplication factor as a function of the irradiation time for heterogeneous and homogeneous configuration is similar. This result is revealing because the consideration of the highly heterogeneous system may not be a sufficient condition for use the fractional model in fast reactor. However, the condition of a highly heterogeneous system with a thermal reactor is less restrictive, i.e. the heterogeneous effect of a system with fast neutrons, according to these results, are less sensitive than in a heterogeneous system with thermal neutrons due to the free mean path of the neutrons.

The Eq. (5.1) can be considered as the fractional Telegrapher's equation. The classical P_1 equations have several shortcomings, connected to its limitation in the physical description of the neutron field. Recent works have, for instance, showed its limitation in the description of sharp wave front propagation (e.g., Heitzler, 2010).

Nonetheless that the P_1 equations have several shortcomings it is undoubtedly that since the Hayasaka and Takeda (1968) study on the neutron wave propagation up to more recent researches on the same topic (Dulla et al., 2006; Dulla and Ravetto, 2008; Heizler 2010) is a very important approach yet, particularly in the analysis of neutron pulsed experiments and the arising of Accelerator Driven Sources nowadays under study. With the exception of the Dulla et al. (2006) research, the three remaining publications have as the subject of study the Telegrapher's equation as it is part of the present contribution. However Dulla and Ravetto (2008) go beyond by considering numerical aspects of the time and space discretization based on the Diamond Difference (DD) and Linear Discontinuous (LD) methods without limiting the angular discretization of the angular neutron flux to S_2 and P_1 approximations but also treating up to S_N and P_{N-1} approximations.

By doing so, a natural question arises: are such approximations of high-order? Firstly, if energy is not involved, one may approximate the neutron transport equation in angle, space, and time, but the shortcomings of the angle approximation are inherited to the resulting space and time discretizations if nothing is done to take into account not only highly anisotropic behavior due to highly heterogeneous media but also to capture the right asymptotic behavior of the neutron flux when such heterogeneities are present. The present work starts, as a first approach, from the P_1 equations, but it shall be generalized to higher-order angle approximations, either from S_N and/or P_{N-1} approximations.

A further contribution is the study of a neutron propagation problem and analyze the wave front motion with the fractional (P_1 equations) Telegrapher's equation given by Eq. (5.1).

In summary, there are many interesting problems to consider under the point of view of fractional differential equations (FDEs), the challenge is there, now is the time to compare new with old paradigms to apply the best ones in the modeling and simulation of the new generation of nuclear reactors.

5.1. Restrictions of length and time scales

The behavior of φ_γ is affected by complex processes, as was discussed previously and it can be best estimated with the fractional model for one energy-group (Eq. (5.1)) (for multi-group energy see Espinosa-Paredes et al., 2008), which is more complex than the traditional model given by Eq. (4.8). However the scope of the fractional model must be determined. Then, in this section we will discuss the scope of the fractional model through an analysis of order of magnitude of the length and time scales.

We assumed that the diffusion processes are carried out exclusively in the moderator, which has a characteristic length ℓ_γ (e.g., the distance between two fuel rods as is illustrated in Fig. 1.1.) and the characteristic length of the system is L_c (e.g. fuel assembly); then the approximations given by the Fickian and non-Fickian diffusion theory are valid as long as length scale restrictions are met

$$\ell_\gamma << L_c \tag{5.6}$$

For example, in a LWR the mean free path of thermal neutrons is around 1 cm, comparable to the fuel pin diameter and on the order of centimeters for fast neutrons. The relaxation time is given by Eq. (4.5) ($\tau = 3v^{-1}D_\gamma$) and the order of magnitude of diffusion characteristic time constant can be defined as

$$t_d - O\left(\frac{L_\varphi^2}{vD_\gamma}\right) \tag{5.7}$$

where L_φ^2 is the characteristic length associated with changes in the neutron flux. It can be observed that

$$\frac{L_\varphi^2}{vD_\gamma t_d} << 1 \tag{5.8}$$

The relation between Eqs. (4.5) and (5.7) is given by

$$\frac{\tau_\gamma}{t_d} - O\left(\frac{3D_\gamma^2}{L_\varphi^2}\right) \tag{5.9}$$

Since D_γ^2/L_φ^2 is much less than one, the scale time restriction is given then by

$$\frac{\tau_\gamma}{t_d} << 1 \tag{5.10}$$

The fractional form of this restriction is given by

$$\left(\frac{\tau_\gamma}{t_d}\right)^\kappa << 1 \tag{5.11}$$

If constraints of the length and time scales given by Eqs. (5.8) and (5.11) respectively are satisfied the fractional approach to describe diffusion process in nuclear reactors can be applied.

6. Derivation of the fractional NPK equations

In order to derive the fractional equation for a point reactor, we consider the source term. Then, Eq. (5.1) takes the following form, where sub-index γ has been removed to simplify the notation

$$\frac{\tau^\kappa}{v}\frac{\partial^{\kappa+1}\phi}{\partial t^{\kappa+1}} + \tau^\kappa \Sigma_a \frac{\partial^\kappa \phi}{\partial t^\kappa} + \frac{1}{v}\frac{\partial \phi}{\partial t} = S - \Sigma_a \phi + D\nabla^2\phi + \tau^\kappa \frac{\partial^\kappa S}{\partial t^\kappa} \tag{6.1}$$

which was obtained following the procedure of Espinosa-Paredes et al. (2008), i.e., the operator divergence is applied to fractional constitutive law for the neutron density current (Eq. (5.2)) and the result is combined with the diffusion equation (Eq. (3.1)). It is important to note that $\varphi = \varphi(\mathbf{r}, t)$ and $S = S(\mathbf{r}, t)$.

The one-group source term S is given by (Glasstone and Sesonske, 1981)

$$S = (1-\beta)k_\infty \Sigma_a \phi + \sum_{i=1}^{m} \lambda_i \hat{C}_i \tag{6.2}$$

where the first term on the right side represents the rate of production of prompt neutrons, while the second term is the total rate of formation of delayed neutrons. The density numbers of these $\hat{C}_i$ precursors are also a function of position and time, i.e. $\hat{C}_i = \hat{C}_i(\mathbf{r}, t)$.

Substituting Eq. (6.2) into Eq. (6.1), we obtain

$$\frac{\tau^\kappa}{v}\frac{\partial^{\kappa+1}\phi}{\partial t^{\kappa+1}} + \tau^\kappa[\Sigma_a + (1-\beta)k_\infty \Sigma_a]\frac{\partial^\kappa \phi}{\partial t^\kappa} + \frac{1}{v}\frac{\partial \phi}{\partial t} - [(1-\beta)k_\infty \Sigma_a - \Sigma_a]\phi + D\nabla^2\phi + \sum_{i=1}^{m}\lambda \hat{C}_i + \tau^\kappa \sum_{i=1}^{m}\left(\lambda_i \frac{\partial^\kappa \hat{C}_i}{\partial t^\kappa}\right) \tag{6.3}$$

According to Glasstone and Sesonske (1981) $\nabla^2\varphi$ can be replaced by $-B_g^2\phi$, where B_g^2 is the geometric buckling. Then, the previous equation can be written as:

$$\frac{\tau^\kappa}{v}\frac{\partial^{\kappa+1}\phi}{\partial t^{\kappa+1}} + \tau^\kappa[\Sigma_a + (1-\beta)k_\infty \Sigma_a]\frac{\partial^\kappa \phi}{\partial t^\kappa} + \frac{1}{v}\frac{\partial \phi}{\partial t} - [(1-\beta)k_\infty \Sigma_a - \Sigma_a - DB_g^2]\phi + \sum_{i=1}^{m}\lambda_i \hat{C}_i + \tau^\kappa \sum_{i=1}^{m}\left(\lambda_i \frac{\partial^\kappa \hat{C}_i}{\partial t^\kappa}\right) \tag{6.4}$$

In this equation φ and $\hat{C}_i$ are functions of both space and time in a finite reactor; then we write φ and $\hat{C}_i$ as a product of two functions (variables separation),

$$\phi = \varphi(t)\psi(\mathbf{r}) \tag{6.5}$$

$$\hat{C}_i = C_i(t)\psi(\mathbf{r}) \tag{6.6}$$

where $\psi(\mathbf{r})$ is the fundamental mode of the corresponding steady state condition of the neutron diffusion equation. Substituting these expressions into Eq. (6.4), leads to

$$\tau^{\kappa}\frac{d^{\kappa+1}n(t)}{dt^{\kappa+1}}+\tau^{\kappa}[\Sigma_a+(1-\beta)k_\infty\Sigma_a]v\frac{d^{\kappa}n(t)}{dt^{\kappa}}+\frac{dn(t)}{dt}$$
$$-[(1-\beta)k_\infty\Sigma_a-\Sigma_a-DB_g^2]vn(t)+\sum_{i=1}^{m}\lambda_iC_i+\tau^{\kappa}\sum_{i=1}^{m}\left(\lambda_i\frac{d^{\kappa}C_i}{dt^{\kappa}}\right) \tag{6.7}$$

where $\phi(t)=vn(t)$. In order to simplify the above equation we used the following definitions (Glasstone and Sesonske, 1981; Lamarsh and Baratta, 2001) for diffusion area, neutron lifetime, neutron generation time, effective multiplication factor, and reactivity, respectively:

$$L^2=\frac{D}{\Sigma_a} \tag{6.8}$$

$$l=\frac{1}{v\Sigma_a\left(1+L^2B_g^2\right)} \tag{6.9}$$

$$\Lambda=\frac{1}{k_\infty\Sigma_a v} \tag{6.10}$$

$$k_{eff}=\frac{k_\infty}{1+L^2B_g^2} \tag{6.11}$$

$$\rho=\frac{k_{eff}-1}{k_{eff}} \tag{6.12}$$

Then, finally the fractional equation for NPK equations is given by

$$\tau^{\kappa}\frac{d^{\kappa+1}n}{dt^{\kappa+1}}+\tau^{\kappa}\left[\frac{1}{l}+\frac{(1-\beta)}{\Lambda}\right]\frac{d^{\kappa}n}{dt^{\kappa}}+\frac{dn}{dt}$$
$$-\frac{\rho-\beta}{\Lambda}n+\sum_{i=1}^{m}\lambda_iC_i+\tau^{\kappa}\sum_{i=1}^{m}\left(\lambda_i\frac{d^{\kappa}C_i}{dt^{\kappa}}\right) \tag{6.13}$$

When $\tau^{\kappa}\to 0$, the classic equation is recovered, i.e.,

$$\frac{dn}{dt}=\frac{\rho-\beta}{\Lambda}n+\sum_{i=1}^{m}\lambda_iC_i \tag{6.14}$$

6.1. Comparison between fractional and classical equations

A quick comparison of Eqs. (6.13) and (6.14), shows that Eq. (6.13) includes three additional terms with respect to the classic equation containing fractional derivatives:

(1) $\frac{d^{\kappa+1}n}{dt^{\kappa+1}}$,
(2) $\frac{d^{\kappa}n}{dt^{\kappa}}$ and
(3) $\frac{d^{\kappa}C_i}{dt^{\kappa}}$.

The physical meaning of these terms suggests that for sub-diffusion process ($\kappa<1$), the first term has an important contribution for rapid changes in the neutron density (for example in a turbine trip in a BWR nuclear power plant (NPP)), while the second term represents an important contribution when changes in the neutron density are relatively slow, for example during the start-up in a NPP involving operational maneuvers due to movement of the control rod drive. The third term becomes more important in some cases, for example when the reactor is in shutdown process, also it could be important to understand the processes in accelerator-driven system (ADS), which is a subcritical system characterized by a small fraction of delayed neutrons and by a small Doppler reactivity coefficient (Iwanaga and Sekimoto, 2005).

The net rate of formation of the precursor of delayed neutrons corresponding to the ith group is given by

$$\frac{dC_i}{dt}=\frac{\beta_i}{\Lambda}n-\lambda_iC_i \tag{6.15}$$

where this equation was derived considering that

$$\frac{d\hat{C}_i}{dt}=\beta_ik_\infty\Sigma_a\phi-\lambda_i\hat{C}_i \tag{6.16}$$

along with Eqs. (6.5) and (6.6). The first and second terms on right side of this equation are the rate of formation of the precursors and radioactive decay of the ith group, respectively. In these equations β represents the total fraction of delayed neutrons.

Remarking, Eqs. (6.13) and (6.15) represent the fractional mathematical model to describe the neutron dynamics process in nuclear reactor and the delayed-neutrons precursor of the ith group, respectively.

7. Solution procedures of the fractional equation

The numerical approximation of the solution of the fractional NPK model was obtained applying the numerical solution of linear multi-term fractional differential equations for systems of equations (Edwards et al., 2002). The fractional kinetics model can be represented as a multi-term high-order linear fractional differential equation, which is calculated by writing the problem as a system of ordinary and fractional differential equations (OFDE).

Considering one-group of delayed neutrons the fractional point equation and initial conditions are given by:

Fractional point kinetics

$$\tau^{\kappa}\frac{d^{\kappa+1}n}{dt^{\kappa+1}}+\tau^{\kappa}\left[\frac{1}{l}+\frac{(1-\beta)}{\Lambda}\right]\frac{d^{\kappa}n}{dt^{\kappa}}+\frac{dn}{dt}=\frac{\rho-\beta}{\Lambda}n+\lambda C+\tau^{\kappa}\lambda\frac{d^{\kappa}C}{dt^{\kappa}} \tag{7.1}$$

$$n(0)=n_0, \tag{7.2}$$

Precursor concentration

$$\frac{dC}{dt}=\frac{\beta}{\Lambda}n-\lambda C \tag{7.3}$$

$$C(0)=C_0=\frac{\beta}{\Lambda\lambda}n_0, \tag{7.4}$$

The initial conditions for fractional model are presented in Appendix A.

For estimating the anomalous diffusion order (κ), the Detrended Fluctuation Analysis (DFA) method can be applied to the neutronic signal of the average power range monitor of the NPP (Espinosa-Paredes et al., 2006).

7.1. Preliminaries on fractional calculus

In this section, we introduce notations, definitions, and preliminary facts which are used in the OFDE problem.

The topic of the fractional calculus has gained considerable importance during the past two decades, mainly due to its applications in diverse fields of science and engineering (e.g., Schneider and Wyss, 1989; Miller and Ross, 1993; Samko et al., 1993; Benson et al., 2000; Metzler and Klafter, 2000; Baeumer et al., 2000; Hilfer, 2000; Kilbas et al., 2006). The advantage of the fractional calculus is that fractional derivatives provide a description of memory and hereditary properties of various materials and processes.

The fractional calculus involves different definitions of the fractional operator as well as the Riemann-Liouville fractional derivative, Caputo derivative, amount others, such as Grünwald–Letnikov derivative and Riesz derivative (Oldham and Spanier, 1974; Podlubny, 1999).

The Riemann–Liouville definition of fractional derivatives, is defined as

$${}^{\kappa}D^{\kappa}\varphi(t)=\frac{\partial^{\kappa}\varphi(t)}{\partial t^{\kappa}}=\frac{1}{\Gamma(m-\kappa)}\frac{\partial^m}{\partial t^m}\int_a^t\frac{\varphi(\xi)}{(t-\xi)^{\kappa+1-m}}d\xi,\quad m-1<\kappa<m \tag{7.5}$$

where m is a positive integer and $\Gamma(m-\kappa)$ is the gamma function whose argument is $m-\kappa$. The Caputo's derivative is defined (Podlubny, 1999)

$$ {}_C D^{\kappa}\varphi(t) = \frac{\partial^{\kappa}\varphi(t)}{\partial t^{\kappa}} = \frac{1}{\Gamma(m-\kappa)}\int_0^t \frac{\varphi^{(m)}(\xi)}{(t-\xi)^{\kappa+1-m}}d\xi, \quad m-1<\kappa<m \tag{7.6} $$

where $\varphi^{(m)} = \partial^m\varphi/\partial t^m$.

The difference between both definitions is given by the equation (Podlubny, 1999; Hilfer, 2000)

$$ {}_C D^{\kappa}\varphi(t) = {}^{RL}D^{\kappa}\varphi(t) - \sum_{m=0}^{m-1}\frac{t^{\alpha-\kappa}}{\Gamma(\alpha-\kappa+1)}\varphi^{(\kappa)}, \quad m-1<\kappa<m \tag{7.7} $$

In this work we utilize the Caputo version of the fractional derivative given by Eq. (7.6) which enables the initial conditions in the same form as for differential equations of integer order, which allows the OFDE system to have a unique solution (Edwards et al., 2002). Furthermore, the initial condition required by the Caputo definition coincides with an identifiable physical state.

Regarding the Riemann–Liouville definition of fractional derivatives, the initial conditions and their derivatives must be specified in terms of fractional integrals, which is more complex to determine respect Caputo version.

For more details on fractional derivative concepts, definitions and properties, see (e.g., Oldham and Spanier, 1974; Miller and Ross, 1993; Samko et al., 1993; Podlubny, 1999; Hilfer, 2000; Leszczynski and Ciesielski, 2001).

7.2. Numerical algorithm

In order to solve the fractional equation we use the numerical algorithm given by Edwards et al. (2002).

In order to simplify the notation, the differential operator D is used instead of d/dt. Then, the system of equations can be written in a linear multi-term fractional form as follows:

Fractional point kinetics

$$ D^{\kappa+1}n + a_1 Dn + a_2 D^{\kappa}n + a_3 n - b_2 D^{\kappa}C + b_3 C, \quad 0<\kappa\leq 1 \tag{7.8} $$

Precursor concentration

$$ DC + b_3 C - a_0 n \tag{7.9} $$

where the coefficients of the above equations are:

$$ a_0 = \frac{\beta}{\Lambda} \tag{7.10} $$

$$ a_1 = -\frac{1}{\tau^{\kappa}}\left(\frac{\rho-\beta}{\Lambda}\right) \tag{7.11} $$

$$ a_2 = -\left[\frac{1}{l}+\frac{(1-\beta)}{\Lambda}\right] \tag{7.12} $$

$$ a_3 = \frac{1}{\tau^{\kappa}} \tag{7.13} $$

$$ b_1 = \frac{\lambda}{\tau^{\kappa}} \tag{7.14} $$

$$ b_2 = \lambda \tag{7.15} $$

It is important to consider that the fractional operators $D^{\kappa+1}$ and D^{κ} are defined by Eq. (7.5).

7.3. Reduction of the problem to an OFDE system

In this section we convert the problem into an OFDE system, each one with an order at the most of the unity.

Following the procedure given by Edwards et al. (2002), we define a change of variables regarding the original problem:

Fractional point kinetics

$$ x_1(t) = n(t) \tag{7.16} $$

$$ x_2(t) = D^{\kappa}n(t) = D^{\kappa}x_1 \tag{7.17} $$

$$ x_3(t) = Dn(t) = Dx_1 \tag{7.18} $$

$$ x_4(t) = D^{\kappa}Dn(t) = D^{\kappa+1}n(t) = D^{\kappa}x_3 \tag{7.19} $$

Precursor concentration

$$ y_1(t) = C(t) \tag{7.20} $$

$$ y_2(t) = D^{\kappa}C(t) = D^{\kappa}y_1 \tag{7.21} $$

$$ y_3(t) = DC(t) = Dy_1 \tag{7.22} $$

The mathematical expressions given by Eqs (7.16)–(7.22), can be expressed in a matrix form as follows:

$$ \begin{pmatrix} D^{\kappa} & 0 & 0 & 0 & 0 \\ D & 0 & 0 & 0 & 0 \\ 0 & 0 & D^{\kappa} & 0 & 0 \\ 0 & 0 & 0 & D^{\kappa} & 0 \\ 0 & 0 & 0 & D & 0 \end{pmatrix} \begin{pmatrix} x_1 \\ x_2 \\ x_3 \\ y_1 \\ y_2 \end{pmatrix} = \begin{pmatrix} x_2 \\ x_3 \\ x_4 \\ y_2 \\ y_3 \end{pmatrix} \tag{7.23} $$

where

$$ x_4 = -\sum_{j=1}^{3} a_j x_j + \sum_{j=1}^{2} b_j y_j \tag{7.24} $$

$$ y_3 = a_0 x_1 - b_2 y_1 \tag{7.25} $$

The term x_4 is obtained by substituting Eqs. (7.16)–(7.18) into Eq. (7.19), while y_3 was obtained by substituting Eqs. (7.16) and (7.20) into Eq. (7.22).

7.4. Discretization of the fractional derivatives

In order to discretize the fractional derivative, Edwards et al. (2002) used the Diethelm's method (Diethelm, 1997a,b), which is defined as:

$$ D^{\kappa}x = \frac{1}{{}_{\kappa}\gamma_i}\left(\sum_{j=0}^{i} {}_{\kappa}\omega_{j,i}x_{i-p} + \frac{x_0}{\kappa}\right) \tag{7.26} $$

here

$$ {}_{\kappa}\gamma_i = (ih)^{\kappa}\Gamma(-\kappa) \tag{7.27} $$

where h is the time-step size, $\Gamma(-\kappa)$ is the gamma function whose argument is $-\kappa$; x_0 is the initial condition, and ${}_{\kappa}\omega_{j,0}, \ldots, {}_{\kappa}\omega_{j,i}$ are convolution weights defined as:

$$ {}_{\kappa}\omega_{j,i} = \begin{cases} -1, & \text{for } p=0 \\ 2p^{1-\kappa} - (\kappa-1)^{1-\kappa} - (\kappa+1)^{1-\kappa}, & \text{for } p=1,2,\cdots,i-1 \\ (\kappa-1)p^{\kappa} - (p-1)^{1-\kappa} + p^{1-\kappa}, & \text{for } p=i \end{cases} \tag{7.28} $$

In order to discretize Eq. (7.17), we apply Eq. (7.26) with $x = x_1$:

$$ D^{\kappa}x_{1,i} = \frac{1}{{}_{\kappa}\gamma_i}\left(\sum_{j=0}^{i} {}_{\kappa}\omega_{j,i}x_{1,i-p} + \frac{x_{1,0}}{\kappa}\right) \tag{7.29} $$

The method given by Edwards et al. (2002) considers that

$$ S_{1,i} = \sum_{j=1}^{i} {}_{\kappa}\omega_{j,i}x_{1,i-p} + \frac{x_{1,0}}{\kappa} \tag{7.30} $$

Now, substituting Eq. (7.30) into Eq. (7.29)

$$ D^{\kappa}x_{1,i} = \frac{1}{{}_{\kappa}\gamma_i}({}_{\kappa}\omega_{0,i}x_{1,i} + S_{1,i}) \tag{7.31} $$

In this equation it can be observed that

$$\sum_{p=0}^{i} {}^{\kappa}\omega_{p} x_{1,i-p} - \sum_{p=1}^{i} {}^{\kappa}\omega_{p} x_{1,i-p} = {}^{\kappa}\omega_{0} x_{1,i} \tag{7.32}$$

As $D^{\kappa} x_{1,i} = x_{2,i}$ (Eq. (7.17)), we finally get:

$$x_{2,i} = \frac{1}{{}^{\kappa}\gamma_{1}} ({}^{\kappa}\omega_{0} x_{1,i} + S_{1,i}) \tag{7.33}$$

Now, solving for $S_{1,i}$:

$$S_{1,i} = {}^{\kappa}\gamma_{1} x_{2,i} - {}^{\kappa}\omega_{0} x_{1,i} \tag{7.34}$$

Combining Eqs. (7.34) and (7.30), we obtain

$${}^{\kappa}\gamma_{1} x_{2,i} - {}^{\kappa}\omega_{0} x_{1,i} - \sum_{p=1}^{i} {}^{\kappa}\omega_{p} x_{1,i-p} + \frac{x_{1,0}}{\kappa} \tag{7.35}$$

To discretize Eq. (7.18) we use the trapezium rule

$$x_{1,i} = x_{1,i-1} + \frac{h}{2}(x_{2,i} + x_{2,i-1}) \tag{7.36}$$

Now, we proceed in similar form with respect to the procedure used in Eq. (7.17), i.e.

$$S_{2,i} = x_{1,i-1} + \frac{h}{2} x_{2,i-1} \tag{7.37}$$

Substituting Eq. (7.37) into Eq. (7.36), we have

$$x_{1,i} = S_{2,i} + \frac{h}{2} x_{2,i} \tag{7.38}$$

here, solving for $S_{2,i}$

$$S_{2,i} = x_{1,i} - \frac{h}{2} x_{2,i} \tag{7.39}$$

Now, combining Eqs. (7.36) and (7.39), we have

$$x_{1,i} - \frac{h}{2} x_{2,i} = x_{1,i-1} + \frac{h}{2} x_{2,i-1} \tag{7.40}$$

Then, the discretized forms of Eqs. (7.19), (7.21), and (7.22) are given by:

$${}^{\kappa}\gamma_{1}(b_{1} y_{1,i} + b_{2} y_{2,i}) - {}^{\kappa}\gamma_{1}(a_{1} x_{1,i} + a_{2} x_{2,i}) - ({}^{\kappa}\gamma_{1} a_{1} + {}^{\kappa}\omega_{0,i}) x_{1,i} - \sum_{p=1}^{i} {}^{\kappa}\omega_{p} x_{1,i-p} + \frac{x_{1,0}}{\kappa} \tag{7.41}$$

$$({}^{\kappa}\gamma_{1}) y_{2,i} - {}^{\kappa}\omega_{0} y_{1,i} - \sum_{p=1}^{i} {}^{\kappa}\omega_{p,i} y_{1,i-p} + \frac{y_{1,0}}{\kappa} \tag{7.42}$$

$$y_{1,i}\left(1 - \frac{b_{2} h}{2}\right) - \frac{a_{0} h}{2} x_{1,i} = y_{1,i-1} + \frac{h}{2}(a_{0} x_{1,i-1} - b_{1} y_{1,i-1}] \tag{7.43}$$

Eqs. (7.35), (7.49), (7.41), (7.42), and (7.43) represent the discretized form of the OFDE set for fractional point kinetics and precursor concentration, respectively. These equations in matrix form are:

$$\begin{pmatrix} -{}^{\kappa}\omega_{0} & {}^{\kappa}\gamma_{1} & 0 & 0 & 0 \\ 1 & 0 & -h/2 & 0 & 0 \\ -{}^{\kappa}\gamma_{1} a_{1} & -{}^{\kappa}\gamma_{1} a_{2} & -({}^{\kappa}\gamma_{1} a_{2} + {}^{\kappa}\omega_{0,i}) & {}^{\kappa}\gamma_{1} b_{1} & {}^{\kappa}\gamma_{1} b_{2} \\ 0 & 0 & 0 & -{}^{\kappa}\omega_{0,i} & {}^{\kappa}\gamma_{i} \\ -(a_{0} h)/2 & 0 & 0 & 1 - (b_{1} h)/2 & 0 \end{pmatrix} \begin{pmatrix} x_{1,i} \\ x_{2,i} \\ x_{3,i} \\ y_{1,i} \\ y_{2,i} \end{pmatrix} - \begin{pmatrix} S_{1,i} \\ S_{2,i} \\ S_{3,i} \\ R_{1,i} \\ R_{2,i} \end{pmatrix} \tag{7.44}$$

where

$$S_{1,i} = \sum_{p=1}^{i} {}^{\kappa}\omega_{p} x_{1,i-p} + \frac{x_{1,0}}{\kappa} \tag{7.45}$$

$$S_{2,i} = x_{1,i-1} + \frac{h}{2} x_{2,i-1} \tag{7.46}$$

$$S_{3,i} = \sum_{p=1}^{i} {}^{\kappa}\omega_{p} x_{3,i-p} + \frac{x_{3,0}}{\kappa} \tag{7.47}$$

$$R_{1,i} = \sum_{p=1}^{i} {}^{\kappa}\omega_{p} y_{1,i-p} + \frac{y_{1,0}}{\kappa} \tag{7.48}$$

$$R_{2,i} = y_{1,i-1} + \frac{h}{2}(a_{0} x_{1,i-1} - b_{2} y_{1,i-1}] \tag{7.49}$$

8. Simulations

8.1. Implementation

In order to analyze the effect of the anomalous diffusion order (κ) and the relaxation time (τ) on the behavior of the neutron density, the numerical model (Eqs. (7.35), (7.49) and (7.41)–(7.43)) was implemented for the solution and simulation in a commercial computer program MATLAB®. The Gaussian elimination method was applied to invert the matrix given by Eq. (7.44).

8.2. Nuclear parameters and initial conditions

The nuclear parameters used in this study were obtained from Kinard and Allen (2004):

$$\beta = \sum_{i=1}^{6} \beta_{i} = 0.007$$

$$\lambda = \frac{\beta}{\sum_{i=1}^{6} \frac{\beta_{i}}{\lambda_{i}}} = 0.0810958\, s^{-1}$$

$$\Lambda = 0.002\, s$$

$$l = 0.00024\, s$$

where β_i and λ_i are presented in Table 8.1, and the value of parameter l was obtained from Glasstone and Sesonske (1981).

The initial conditions are:

$$x_{1,0} = n_{0} = 1$$

$$x_{2,0} = 0$$

$$x_{3,0} = 0$$

$$y_{1,0} = C_{0} = 43.1588$$

$$y_{2,0} = 0$$

where $C_0 = \frac{\beta_0}{\lambda_0 \Lambda}$.

In these initial conditions, units have been omitted intentionally for simplicity purposes.

Table 8.1
Neutron delayed fractions and decay constants (Kinard and Allen, 2004).

	β_i	$\lambda_i\ (s^{-1})$
Group 1	0.000266	0.0127
Group 2	0.001491	0.0317
Group 3	0.001316	0.1550
Group 4	0.002849	0.3110
Group 5	0.000960	1.4000
Group 6	0.000182	3.8700

8.3. Stability criteria and numerical experiments

In order to discretize the fractional derivative of the NPK model, the method of Diethelm (1997a,b) was applied. The numerical stability of the discretized fractional equation is not yet clarified, especially its application in nuclear science. Then, the stability of the fractional NPK model by the Diethelm scheme is investigated. The stability of the numerical scheme is estimated and the stability limit of the time-step size (h) is determined for different values of the anomalous diffusion order (κ) and of the relaxation time (τ). In order to obtain a stable solution, a set of time-step sizes were chosen by trial-and-error for different values of κ and τ^{κ}.

A series of numerical experiments were carried out in order to gain a better understanding of the dynamics of the fractional NPK model. We considered three cases for τ^{κ}, specifically $\tau^{\kappa} = 10^{-4}s^{\kappa}$, $10^{-5}s^{\kappa}$, and $10^{-6}s^{\kappa}$. For each τ^{κ} we considered four values of κ, namely 0.99, 0.98, 0.97 and 0.96, and for each value of κ, we established 22 values of the time-step size (h) such that $0.001 \leq h \leq 0.25$ s. The simulation time considered was 1 s.

In the numerical experiments the initial conditions given in Section 8.2 are assumed, i.e.: $x_{1,0} = n_0 = 1$, $y_{1,0} = C_0 = 43.1588$, $x_{2,0} = 0$, $x_{3,0} = 0$ and $y_{2,0} = 0$.

The stability criteria considered in this work is related with 2% of the relative error to $n_0 = 1$ at 1 s of the simulation:

$$2\% \leq \left| \frac{n_f - n_0}{n_0} \right| \times 100 \tag{8.1}$$

where n_f is the neutron density calculated from the fractional model.

8.4. Stability results

Fig. 8.1 shows the neutron density behavior with $\tau^{\kappa} = 10^{-4}s^{\kappa}$ and $\kappa = 0.99$, for h in the interval [0.001 s, 0.25 s], where each graphic corresponds to a value of h.

It can be observed in Fig. 8.1 that for some of the values of h neutron density converges to a value equal to 1 (dashed line) and for some other values of h it diverges moving away from the expected value $n_0 = 1$. Then, qualitatively, we can say that the numerical scheme for the solution of the fractional NPK model for $\tau^{\kappa} = 10^{-4}s^{\kappa}$ and $\kappa = 0.99$ at 1 s of the simulation it is stable to time-step sizes less than 0.0125 s, because the neutron density behavior tends to converge to the expected value (from a conservative point of view). However, according with the stability criteria, the relative error is 0.79% for a time-step size of 0.00625 s and 2.33% for a time-step size of 0.0125 s.

If the value of h is less than 0.0125 s, the neutron density behavior converges in a damped form. A more detailed analysis shows the following: taking as a reference the curve given by $h = 0.001$ s, we can observe that the oscillatory behavior of the neutron density is damped and the amplitude of the oscillation is decreasing with a determined frequency and therefore its period. Now if we focus our attention in a different curve, h less than 0.02 s (e.g., $h = 0.00125$ s), we can observe that the oscillation amplitude is the least than the one that corresponds for $h = 0.001$ s, while the period increases. In general it can be observed that for time-step sizes over 0.001 s the oscillation amplitude decreases and the period of oscillation increases.

Fig. 8.2 shows the neutron density behavior with $\tau^{\kappa} = 10^{-4}s^{\kappa}$ and $\kappa = 0.98$, for h in [0.001 s, 0.25 s]. We observe that the behavior

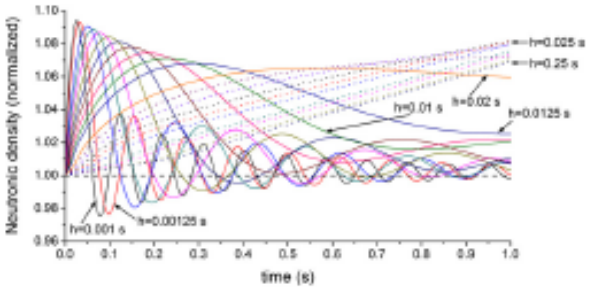

Fig. 8.1. Neutron density behavior for $\tau^{\kappa} = 10^{-4}s^{\kappa}$ and $\kappa = 0.99$, for different values of a time-step size (h between 0.001 s and 0.25 s).

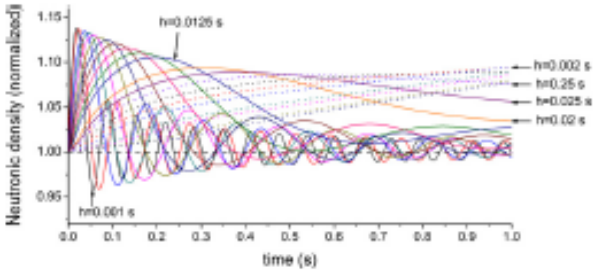

Fig. 8.2. Neutron density behavior for $\tau^{\kappa} = 10^{-4}s^{\kappa}$ and $\kappa = 0.98$, for different values of a time-step size (h between 0.001 s and 0.25 s).

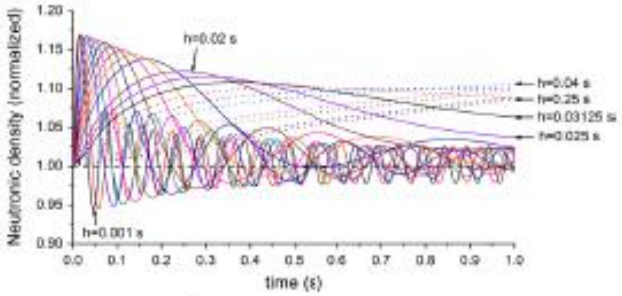

Fig. 8.3. Neutron density behavior for $\tau^{\kappa} = 10^{-4}s^{\kappa}$ and $\kappa = 0.97$, for different values of the time-step size (h between 0.001 s and 0.25 s).

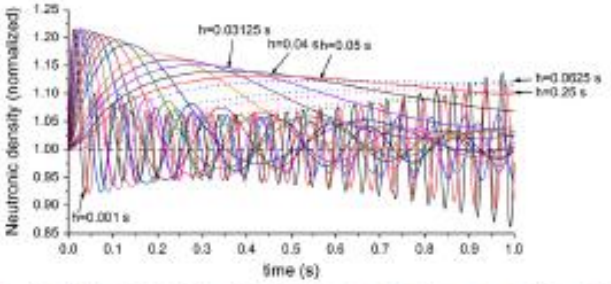

Fig. 8.4a. Neutron density behavior for $\tau^{\kappa} = 10^{-4}s^{\kappa}$ and $\kappa = 0.96$, for different values of the time-step size (h between 0.001 and 0.25).

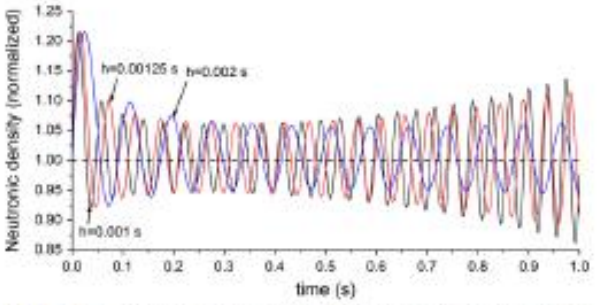

Fig. 8.4b. Neutron density behavior for $\tau^{\kappa} = 10^{-4}s^{\kappa}$ and $\kappa = 0.96$, for $h = 0.001$ s, 0.00125 s, and 0.002 s.

of the curves are very similar to the curves shown in Fig. 8.1 for $\kappa = 0.99$. However, we identify that the numerical scheme for $\tau^{\kappa} = 10^{-4}s^{\kappa}$ and $\kappa = 0.98$ is stable to time-step sizes less than or equal to 0.01s, whose relative error is 1.9%. Thus for $\kappa = 0.98$, the numerical experiment allows a time-step size higher with respect to the case for $\kappa = 0.99$.

Fig. 8.3 shows the neutron density behavior with $\tau^{\kappa} = 10^{-4}s^{\kappa}$ and $\kappa = 0.97$, for h in [0.001 s, 0.25 s]. We observe that the behavior of the curves are very similar to the curves shown in Figs. 8.1 and 8.2 for $\kappa = 0.99$ and $\kappa = 0.98$, respectively. For this case ($\tau^{\kappa} = 10^{-4}s^{\kappa}$ and $\kappa = 0.97$) the numerical scheme is stable for time-step sizes less than or equal to 0.01 s whose relative error is 0.32%. The same result was obtained with $\kappa = 0.98$ but with a relative error equal to 1.9%.

For the case $\tau^{\kappa} = 10^{-4}s^{\kappa}$ and $\kappa = 0.96$, for h in the time interval [0.001 s, 0.25 s] the analysis is very complex as shown in Fig. 8.4a. Then, in order to determine the time-step limit where the numerical scheme is stable, we analyze separately some curves of this figure as illustrated in Figs. 8.4b and 8.4c.

Fig. 8.4b shows the neutron flux behavior for $h = 0.001$ s, 0.00125 s, and 0.002 s. In this figure for $h = 0.001$ s and 0.00125 s, we can observe that the oscillations exhibit a divergent behavior. For $h = 0.002$ s the oscillation apparently maintains a constant amplitude, but a detailed analysis shows that slowly diverges.

Therefore, we establish in good approximation that the numerical scheme is not stable if 0.001 s ≤ h ≤ 0.002 s.

Fig. 8.4c shows the neutron density behavior for $\tau^* = 10^{-5}s^*$, $\kappa = 0.96$ and $h = 0.025$ s. In this figure it can be observed that the oscillation amplitude is constant for an elapsed time greater than 0.6 s. Despite of the oscillatory behavior, which remains constant around the 5% peak to peak, under this conditions it can be established that the numerical scheme is stable for $h = 0.025$ s with $\tau^* = 10^{-5}s^*$ and $\kappa = 0.96$.

According with this analysis the numeric scheme for $\tau^* = 10^{-5}s^*$ and $\kappa = 0.96$, is stable if 0.0025 s ≤ h ≤ 0.008 s. The relative error is 0.91% for $h = 0.025$ s and 0.39% for $h = 0.008$ s.

Figs. 8.5–8.8 show the neutron density behavior with $\tau^* = 10^{-5}s^*$ for $\kappa = 0.99$, $\kappa = 0.98$, $\kappa = 0.97$, and $\kappa = 0.96$, respectively. The results show that the amplitude of the oscillation for the curves when $\tau^* = 10^{-5}s^*$ are smaller than the ones with the results obtained when $\tau^* = 10^{-4}s^*$ (see Figs. 8.1–8.4). The stability results are presented in Table 8.2.

Figs. 8.9–8.12 show the neutron density behavior with $\tau^* = 10^{-5}s^*$ and for $\kappa = 0.99$, $\kappa = 0.98$, $\kappa = 0.97$, and $\kappa = 0.96$. These figures show that the oscillatory behavior practically disappeared. Other characteristics of the results obtained with these numerical experiments is that the solution converges (continuous line) very slowly decaying.

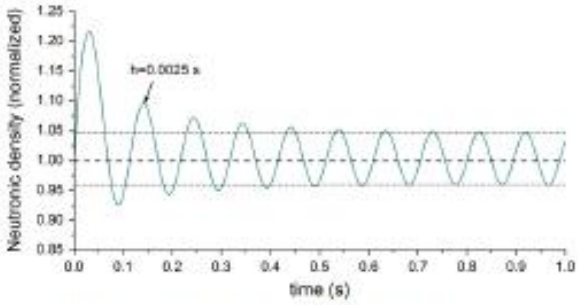

Fig. 8.4c. Neutron density behavior for $\tau^* = 10^{-4}s^*$ and $\kappa = 0.96$, with $h = 0.0025$ s.

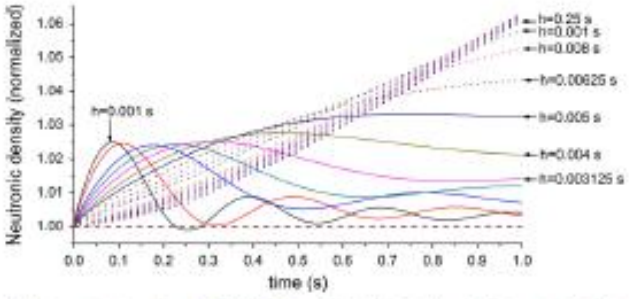

Fig. 8.5. Neutron density behavior as a function of time for $\tau^* = 10^{-5}s^*$ and $\kappa = 0.99$, for different values of the time-step size (h between 0.001 s and 0.25 s).

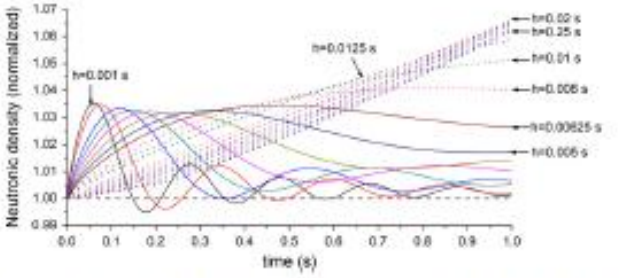

Fig. 8.6. Neutron density behavior as a function of time for $\tau^* = 10^{-5}s^*$ and $\kappa = 0.98$, for different values of the time-step size (h between 0.001 s and 0.25 s).

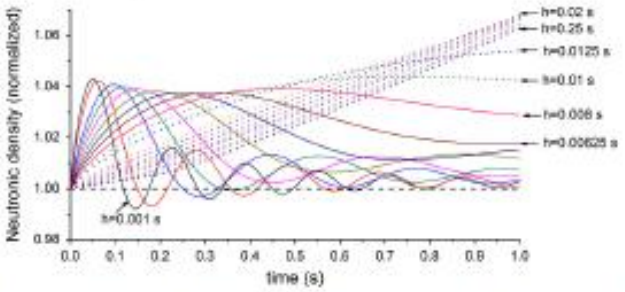

Fig. 8.7. Neutron density behavior as a function of time for $\tau^* = 10^{-5}s^*$ and $\kappa = 0.97$, for different values of the time-step size (h between 0.001 s and 0.25 s).

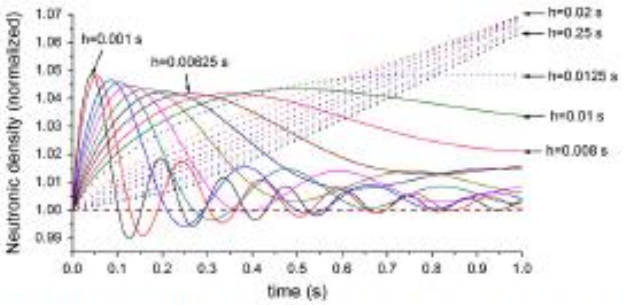

Fig. 8.8. Neutron density behavior as a function of time for $\tau^* = 10^{-5}s^*$ and $\kappa = 0.96$, for different values of the time-step size (h between 0.001 s and 0.25 s).

Table 8.2
Estimation of the time-step size limit for a stable behavior of the numerical scheme.

κ	Time-step size (s), $\tau^* = 1.0^{-5}s^*$	Relative error (%)	Time-step size (s), $\tau^* = 1.0^{-6}s^*$	Relative error (%)	Time-step size (s), $\tau^* = 1.0^{-7}s^*$	Relative error (%)
0.99	$h \leq 0.00625$	0.79	$h \leq 0.003125$	1.42	$h \leq 0.00125$	1.9
0.98	$h \leq 0.0100$	1.9	$h \leq 0.0050$	1.71	$h \leq 0.00125$	1.05
0.97	$h \leq 0.0100$	0.32	$h \leq 0.00625$	1.76	$h \leq 0.0020$	1.52
0.96	$0.0025 \leq h$	0.91	$h \leq 0.00625$	1.76	$h \leq 0.0025$	1.73
	$h \leq 0.008$	0.39				

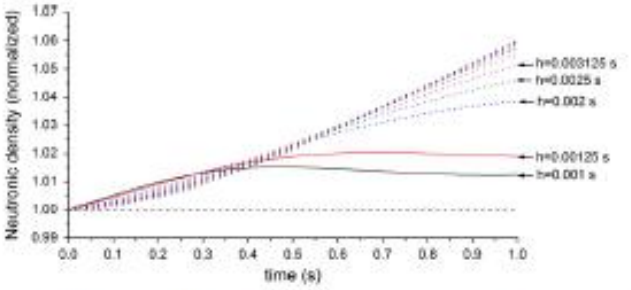

Fig. 8.9. Neutron density behavior as a function of time for $\tau^* = 10^{-6}s^*$ and $\kappa = 0.99$, for different values of the time-step size (h between 0.001 s and 0.25 s).

According with the numerical experiments and results, we present a summary for the limit, the stability and the relative error of the numerical scheme for $\tau^* = 10^{-5}s^*$, $\tau^* = 10^{-6}s^*$, and $\tau^* = 10^{-7}s^*$ (Table 8.2). It is important to mention again that this limit is obtained applying a 2% error calculated at 1 s simulation (Eq. (8.2)).

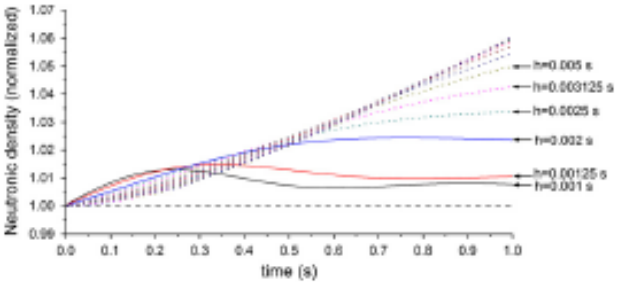

Fig. 8.10. Neutron density behavior as a function of time for $\tau^{\kappa} = 10^{-6}s^{\kappa}$ and $\kappa = 0.98$, for different values of a time-step size (h between 0.001 s and 0.25 s).

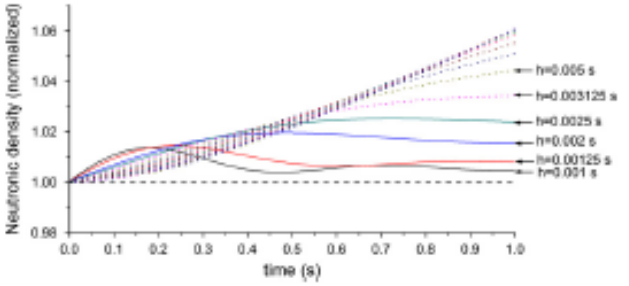

Fig. 8.11. Neutron density behavior as a function of time for $\tau^{\kappa} = 10^{-6}s^{\kappa}$ and $\kappa = 0.98$, for different values of the time-step size (h between 0.001 s and 0.25 s).

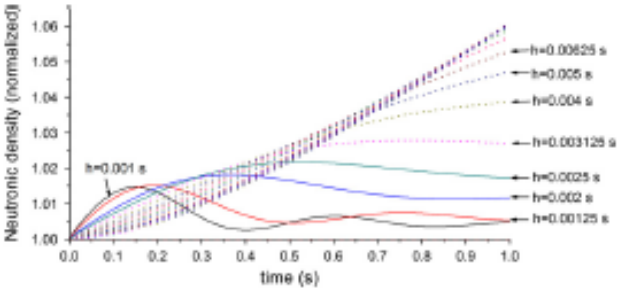

Fig. 8.12. Neutron density behavior as a function of time for $\tau^{\kappa} = 10^{-6}s^{\kappa}$ and $\kappa = 0.96$, for different values of the time-step size (h between 0.001 s and 0.25 s).

For example, Fig. 8.13 shows the behavior of the neutron density taking into account the influence of the anomalous diffusion order κ for $\tau^{\kappa} = 10^{-5}s^{\kappa}$ with $h = 0.005$ s. As observed in this figure, for $\kappa = 0.96$ the neutron density reaches a higher value (or peak) with respect to other values of κ greater than 0.96. However, for $\kappa = 0.99$ the decay is slower with respect to other values of κ less than 0.99, with reference to the 0.5 s of simulation. The physical interpretation of the results indicates that the sub-diffusion process of the neutron is "slower" for values of κ greater than 0.96.

Figs. 8.14–8.17 show the behavior of the neutron density for various values of τ^{κ} considering κ as a constant. The time-step size used for these numerical experiment is $h = 0.00125$ s.

Fig. 8.14 shows an oscillatory behavior of the neutron density for $\tau^{\kappa} = 10^{-4}s^{\kappa}$ with $\kappa = 0.99$, which is damped with the elapsed time. If we compare this behavior with respect to $\tau^{\kappa} = 10^{-5}s^{\kappa}$ and $\tau^{\kappa} = 10^{-6}s^{\kappa}$, we observe the following features: (1) for $\tau^{\kappa} = 10^{-5}s^{\kappa}$ the behavior is oscillatory but with values smaller than $\tau^{\kappa} = 10^{-4}s^{\kappa}$, (2) for $\tau^{\kappa} = 10^{-6}s^{\kappa}$ the oscillatory behavior practically disappears, (3) The amplitude of the first wave is greater than the one corresponding to $\tau^{\kappa} = 10^{-5}s^{\kappa}$ and $\tau^{\kappa} = 10^{-6}s^{\kappa}$.

Figs. 8.15–8.17 (for $\kappa = 0.96$, 0.97, and 0.98, respectively), exhibit behaviors similar to that previously described (Fig. 8.14). However, it can be observed that (for $\tau^{\kappa} = 10^{-4}s^{\kappa}$ and $\tau^{\kappa} = 10^{-5}s^{\kappa}$) have higher frequencies of oscillation and higher amplitudes respect to results obtained with $\kappa = 0.99$. For values of $\tau^{\kappa} = 10^{-6}s^{\kappa}$ for all

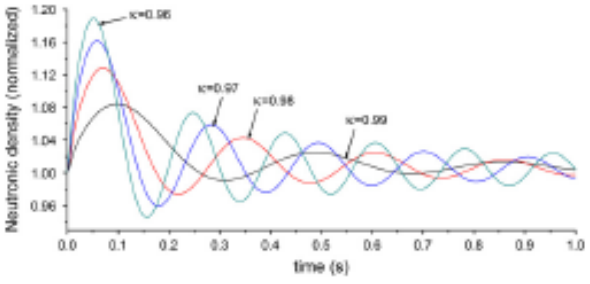

Fig. 8.13. Neutron density behavior as a function of time for $h = 0.004$ s and $\tau^{\kappa} = 10^{-4}s^{\kappa}$, with $\kappa = 0.99, 0.98, 0.97$, and 0.96.

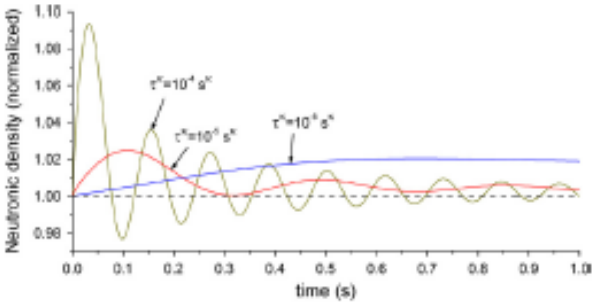

Fig. 8.14. Neutron density behavior as a function of time for $h = 0.00125$ s and $\tau^{\kappa} = 10^{-4}s^{\kappa}$, $10^{-5}s^{\kappa}$, $10^{-6}s^{\kappa}$, with $\kappa = 0.99$.

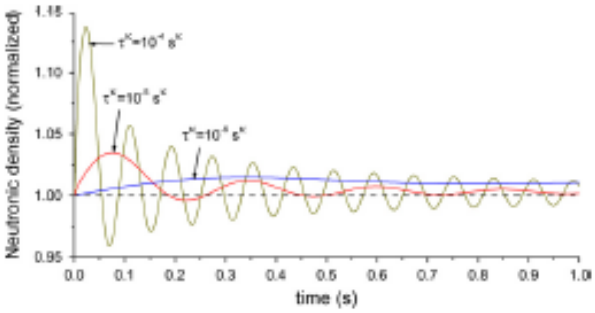

Fig. 8.15. Neutron density behavior as a function of time for $h = 0.00125$ s and $\tau^{\kappa} = 10^{-4}s^{\kappa}$, $10^{-5}s^{\kappa}$, and $10^{-6}s^{\kappa}$, with $\kappa = 0.98$.

cases ($\kappa = 0.96$, 0.97, 0.98 and 0.99) behavior is unchanged. Then, for very small values of τ^{κ} the fractional effects no contribute to the behavior of the neutron density, i.e., are neglected.

8.5. Numerical experiments with reactivity changes

The behavior of the fractional model with reactivity changes is presented in this section. The numerical experiments consider the insertion of two reactivity steps:

- Case 1: $\rho = 0.003$
- Case 2: $\rho = -0.003$

In each of these cases the neutron density is analyzed by different values of the anomalous diffusion order, namely $\kappa = 0.96, 0.97, 0.98, 0.99$. The model is perturbed at time $t = 0$. The fractional relaxation times considered for this numerical experiment are $\tau^{\kappa} = 10^{-4}s^{\kappa}$, $10^{-5}s^{\kappa}$, $10^{-6}s^{\kappa}$. The relaxation time is given by $\tau = (10^{-5})^{1/\kappa}s$ and thus it increases when κ increases.

The fractional model was compared with an analytical solution given by Glasstone and Sesonske (1981):

$$n(t) = n_0\left[\frac{\beta}{\beta-\rho}e^{(\rho/(\beta-\rho))t} - \frac{\rho}{\beta-\rho}e^{-(\beta-\rho/\Lambda)t}\right] \tag{8.2}$$

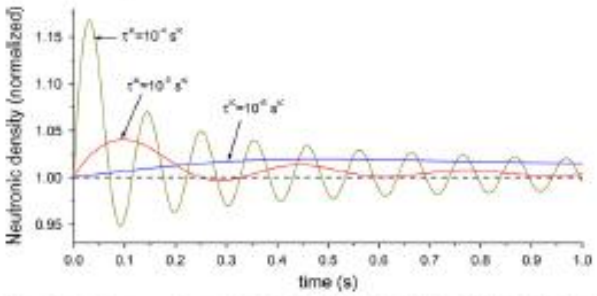

Fig. 8.16. Neutron density behavior as a function of time for $h = 0.00125$ s and $\tau^{\kappa} = 10^{-4}s^{\kappa}$, $10^{-5}s^{\kappa}$, and $10^{-6}s^{\kappa}$, with $\kappa = 0.97$.

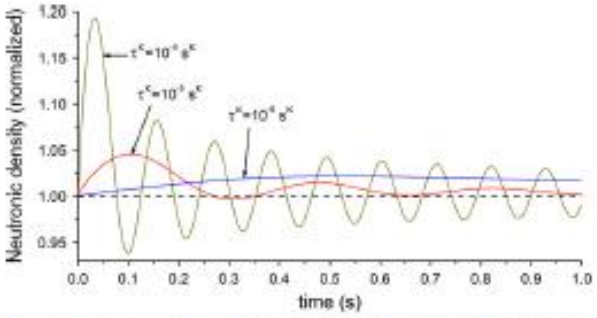

Fig. 8.17. Neutron density behavior as a function of time for $h = 0.00125$ s and $\tau^{\kappa} = 10^{-4}s^{\kappa}$, $10^{-5}s^{\kappa}$, and $10^{-6}s^{\kappa}$, with $\kappa = 0.96$.

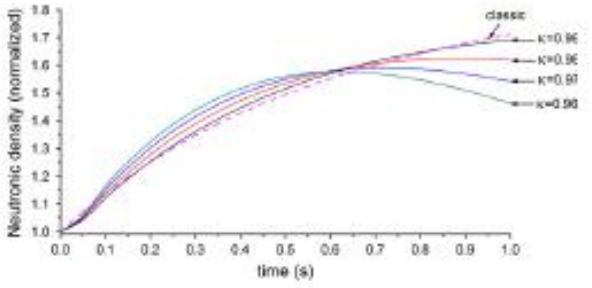

Fig. 8.18. Insertion of positive reactivity ($\rho = 0.003$) for $h = 0.00125$ s and $\tau^{\kappa} = 1.0^{-4}s^{\kappa}$, with $\kappa = 0.99, 0.98, 0.97, 0.96$.

The comparison of the fractional model with this analytical solution allows to establishing the importance of the fractional terms.

Results for $\rho = 0.003$

Figs. 8.18–8.20 show the neutron density behavior in an insertion of positive reactivity, $\rho = 0.003$, for $\tau^{\kappa} = 10^{-4}s^{\kappa}$, $10^{-5}s^{\kappa}$, and $10^{-6}s^{\kappa}$, respectively. Each of these figures is plotted for different κ values, and the analytical classic solution given by Eq. (8.2) is also plotted (the dotted line corresponds to the classic NPK equations where $\tau^{\kappa} = 0$), in order to establish the sub-diffusion effects of the fractional model.

It can be observed in Fig. 8.18 that for $\tau^{\kappa} = 10^{-5}s^{\kappa}$ the sub-diffusion effects are important for $\kappa = 0.96$, which can be inferred because it shows more difference with respect to the analytical solution. When $\kappa \to 1$ the sub-diffusion effects are practically neglected, specifically for $\kappa = 0.99$ the trend is very similar to the classic analytical solution. This means that the terms of the differential operators of fractional order do not contribute to the dynamic description of the neutron density. In this figure at approximately 0.06 s it can be observed an inflexion point and at 0.6 s a critical point. At 0.6 s the fractional model changes the trend

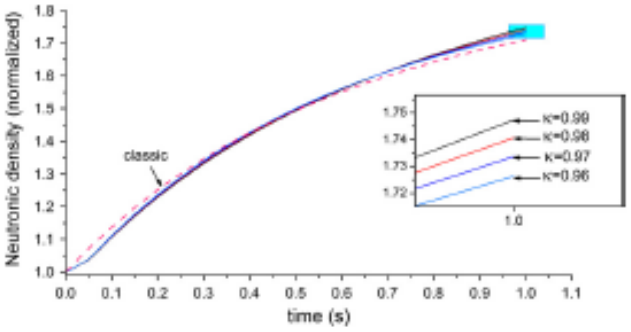

Fig. 8.19. Insertion of positive reactivity ($\rho = 0.003$) for $h = 0.00125$ s and $\tau^{\kappa} = 10^{-5}s^{\kappa}$, with $\kappa = 0.99, 0.98, 0.97, 0.96$.

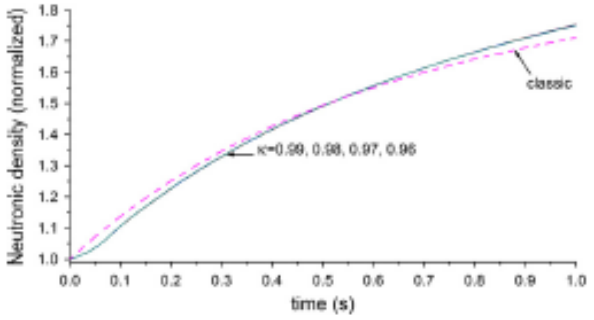

Fig. 8.20. Insertion of positive reactivity ($\rho = 0.003$), for $h = 0.00125$ s and $\tau^{\kappa} = 10^{-5}s^{\kappa}$, with $\kappa = 0.99, 0.98, 0.97, 0.96$.

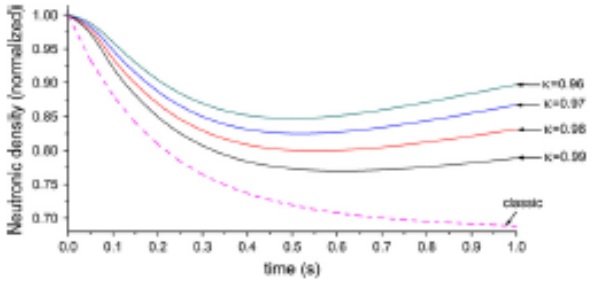

Fig. 8.21. Insertion of negative reactivity ($\rho = -0.003$), for $h = 0.00125$ s and $\tau^{\kappa} = 10^{-5}s^{\kappa}$ with $\kappa = 0.99, 0.98, 0.97, 0.96$.

presenting in some cases slow growth ($\kappa = 0.98$ and 0.99) and a slow decline in other ($\kappa = 0.96$ and 0.97).

For $\tau^{\kappa} = 10^{-5}s^{\kappa}$ and $\tau^{\kappa} = 10^{-6}s^{\kappa}$ (Figs. 8.19 and 8.20 respectively) it can be observed that the sub-diffusion effects are small, inclusive for $\tau^{\kappa} = 10^{-5}s^{\kappa}$. In order to show the effect of κ it was necessary to plot a small scale graphic (Fig. 8.19). Now, for $\tau^{\kappa} = 10^{-6}s^{\kappa}$, the sub-diffusion effects are neglected for all values of κ, as shown in Fig. 8.20.

Result for $\rho = -0.003$

Figs. 8.21–8.23 show the neutron density behavior in an insertion of the negative reactivity, $\rho = -0.003$, for $\tau^{\kappa} = 10^{-5}s^{\kappa}$, $10^{-5}s^{\kappa}$, and $10^{-6}s^{\kappa}$, respectively. Each of these figures is plotted for different values of κ, and the classic analytical solution given by Eq. (8.2) is also plotted (the dotted line corresponds to the classic point-neutron kinetic equation where $\tau^{\kappa} = 0$).

In Fig. 8.21 it can be observed that for $\tau^{\kappa} = 10^{-4}s^{\kappa}$ the sub-diffusion effects are important for all of κ values, which shows appreciable differences with respect to the analytical solution. At

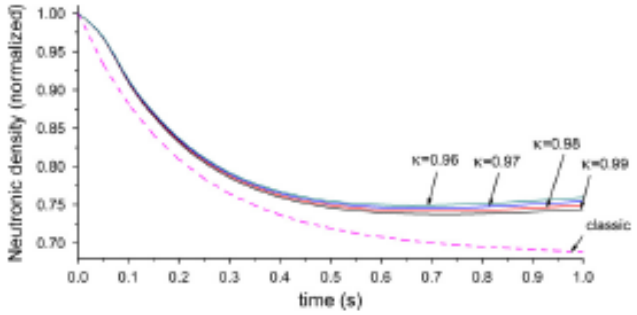

Fig. 8.22. Insertion of negative reactivity ($\rho = -0.003$), for $h = 0.00125$ s and $\tau^{\kappa} = 10^{-5}s^{\kappa}$, with $\kappa = 0.99, 0.98, 0.97, 0.96$.

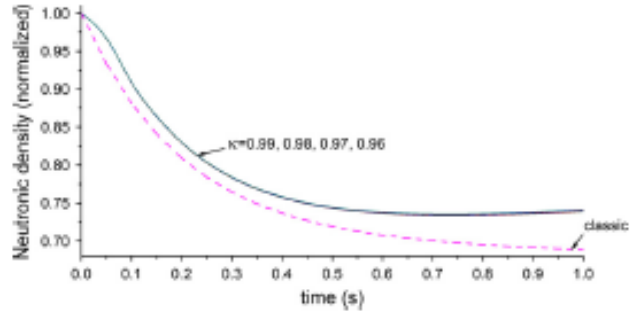

Fig. 8.23. Insertion of negative reactivity ($\rho = -0.003$), for $h = 0.00125$ s and $\tau^{\kappa} = 10^{-5}s^{\kappa}$, with $\kappa = 0.99, 0.98, 0.97, 0.96$.

approximately 0.45 s the behavior of the neutron density of the fractional model changes from a minimum value to a very slow increment. For $\tau^{\kappa} = 10^{-5}s^{\kappa}$ (Fig. 8.22) the sub-diffusion effects still prevalent, although its effect is less respect to case for $\tau^{\kappa} = 10^{-5}s^{\kappa}$.

Finally, for $\tau^{\kappa} = 10^{-6}s^{\kappa}$, the sub-diffusion effects are neglected for all values of κ (Fig. 8.23). However, in the classic analytical solution the neutron density decays very slow, while that the fractional model practically maintains a constant value from 0.7 s to the rest of the simulation time.

9. Conclusions and remarks

The fractional NPK model, Eq. (1.1), for the dynamic behavior in a nuclear reactor was derived from the fractional diffusion equation, Eq. (5.1), whose fractional constitutive equation, Eq. (5.2), was considered. The fractional model retains the main dynamic characteristics of the neutron motion in which the relaxation time associated with a rapid variation in the neutron flux contains a fractional exponent to obtain the best representation of the nuclear reactor dynamics. This mathematical representation covers the full spectrum of the collision behavior from a neutron diffusion equation point of view, i.e., classic diffusion (Fickian approximation) and sub-diffusion effects (non-Fickian approximation or fractional model). The scope of the fractional diffusion equation was obtained through a length and time scales order of magnitude analysis, Eqs. (5.8) and (5.11).

The fractional NPK model contains three additional terms regarding the classical model containing fractional derivatives: (1) $\frac{\partial^{\kappa-1}n}{\partial t^{\kappa-1}}$, (2) $\frac{\partial^{\kappa}n}{\partial t^{\kappa}}$ and (3) $\frac{\partial^{\kappa}c_i}{\partial t^{\kappa}}$. These terms may be important when the fractional relaxation time τ^{κ} is of the order of $10^{-5}s^{\kappa}$, as was demonstrated with numerical experiments in this work.

The procedure of the numerical approximation to the solution of the fractional NPK model is presented, which was based in the work of Edwards et al. (2002). The numerical stability for the fractional method was researched and several numerical experiments were made to confirm the validity of the numerical scheme given by Diethelm (1997a,b). The limit of time-step size of the fractional numerical scheme for different values of κ was obtained (see Table 8.1). The stability criterion obtained is limited to 2% of the relative error at 1 s of the elapsed time of simulation. For example for $\tau^{\kappa} = 10^{-6}s^{\kappa}$ with $\kappa = 0.99$ the limit of stability was found to be $h \leq 0.00625$ s with a relative error 0.79%, and for $\tau^{\kappa} = 10^{-5}s^{\kappa}$ the time-step size found was $h \leq 0.003125$ s with a relative error 1.42%.

The numerical experiments and comparison with the classic analytical solution for both positive and negative reactivity steps were carried out for different values of the fractional order κ. The results obtained for the positive reactivity step shown that the fractional effects or the sub-diffusive behavior are important for $\tau^{\kappa} > 10^{-5}s^{\kappa}$ (Fig. 8.18), while that for $\tau^{\kappa} = 10^{-6}s^{\kappa}$ the effects of the fractional behavior are neglected for $\kappa = 0.96$, 0.97, 0.98, and 0.99 (Fig 8.20). For $\tau^{\kappa} > 10^{-5}s^{\kappa}$ appreciable differences can be observed with respect to the classic analytical solution, and for $\tau^{\kappa} = 10^{-6}s^{\kappa}$ the trend is similar to the classic solution.

The results for the negative reactivity step for $\tau^{\kappa} = 10^{-6}s^{\kappa}$ shown that the sub-diffusion effects are important for all values

of κ, which shows appreciable differences regarding the classic analytical solution. Also we found that for $\tau^{\kappa} = 10^{-6}s^{\kappa}$ the effects of the fractional behavior are neglected for κ.

In this work we presented a detailed picture of the NPK equations, through papers published since 1940 up to 2010. This review shows that the fractional NPK model developed and studied in this work, represents a novel proposal whose framework could be the beginning of an extensive research both experimental and theoretical for applications in the nuclear science.

The concluding remarks are:

- The assumptions related with the classical diffusion model represents a clear evidence that the standard Fick's law, needs to be modified. In this work the non-Fickian law based in the fractional model was proposed in this work (Eq. (5.2)).
- The physical implications of the fractional model is based in that the fractional derivatives are hereditary functional possessing a total memory of past states.
- The modified constitutive laws proposed in this work allow to extend the scope and to improve the classical diffusion theory, particularly to describe the neutron transient behavior in highly heterogeneous configuration in nuclear reactors, in presence of strong neutron absorbers in the fuel, control rods and chemical shim in the coolant. Now, respect to improving the classical diffusion theory, i.e., we mean that the fractional model for neutron diffusion can improve predictions of the classical diffusion model and presumably in some cases must be similar to the complicated theory of transport.
- The main objective of this work is to obtain a reduced model of neutron kinetics based on the theory of neutron diffusion with a fractional constitutive law. This model results in a fractional point-neutron kinetics obtained based on diffusion theory using all known theoretical arguments.
- The Eq. (5.1) can be considered as the fractional Telegrapher's equation. The classical P_1 equations have several shortcomings, connected to its limitation in the physical description of the neutron field. Nonetheless that the P_1 equations have several shortcomings it is undoubtedly that since the Hayasaka and Takeda (1968) study on the neutron wave propagation up to more recent researches on the same topic (Dulla et al., 2006; Dulla and Ravetto, 2008; Heitzler, 2010) is a very important approach yet, particularly inthe analysis of neutron pulsed experiments and the attsing of Accelerator Driven Sources nowadays under study.

In summary, there are many interesting problems to consider under the point of view of FDEs, the challenge is there, now is the time to compare new with old paradigms to apply the best ones in the modeling and simulation of the new generation of nuclear reactors. For example. A further contribution is the study of a neutron propagation problem and analyze the wave front motion with the fractional (P_1 equations) Telegrapher's equation given by Eq. (5.1).

Acknowledgements

The authors are grateful for the referee's comments on this work, which allowed to establish with more clarity the physical interpretation of the new paradigm presented in this work. Special thanks to Dr. Rodolfo Vazquez-Rodríguez and Dr. Francisco Valdés-Parada for their personal comments related with the fractional constitutive law and its implications. Finally, the first author wishes to thank the Safeguard and Nuclear Security National Commission (CNSNS by its Spanish acronym) of México due to their financial support along the last ten years through different grants for research projects.

Appendix A. Initial conditions for FDEs

In this work, we used fractional differential equations (FDEs) in terms of Caputo definition (Podlubny, 1999). A typical feature of differential equations both classical and fractional is the need to specify additional conditions in order to produce a unique solution. The initial conditions required by the Caputo definition coincide with identifiable physical states (Edwards et al., 2002). For the case of Caputo FDEs, these additional conditions are just the static initial conditions, which are akin to those of classical ODEs, and are therefore familiar to us (Diethelm et al., 2005).

With this idea, we have conservation equation for the collision neutron and reaction processes in this system, given by

$$\frac{1}{v}\frac{\partial\phi_g(\mathbf{r},t)}{\partial t}+\nabla\cdot\mathbf{J}_g(\mathbf{r},t)+\Sigma_{ag}(\mathbf{r},t)\phi_g(\mathbf{r},t)=S_g(\mathbf{r},t) \tag{A.1}$$

$$\frac{1}{v}\frac{\partial\mathbf{J}_g(\mathbf{r},t)}{\partial t}+\frac{1}{3}\nabla\phi_g(\mathbf{r},t)+\Sigma_{tr,g}(\mathbf{r},t)\mathbf{J}_g(\mathbf{r},t)=0, \tag{A.2}$$

The Eq. (3.2) can be rewritten as

$$\tau\frac{\partial\mathbf{J}_g(\mathbf{r},t)}{\partial t}+\mathbf{J}_g(\mathbf{r},t)=-D_g(\mathbf{r})\nabla\phi_g(\mathbf{r},t) \tag{A.3}$$

where D_g is the neutron diffusion coefficient and τ is the relaxation time.

The initial conditions of these equations can be given in terms of the flux and the current

$$\phi_g(\mathbf{r},0)=\phi_{g0}(\mathbf{r}) \tag{A.4}$$

$$\mathbf{J}_g(\mathbf{r},0)=\mathbf{J}_{g0}(\mathbf{r}) \tag{A.5}$$

The FDEs and initial values are given by

$$\frac{1}{v}\frac{\partial\phi_g(\mathbf{r},t)}{\partial t}+\nabla\cdot\mathbf{J}_g(\mathbf{r},t)+\Sigma_{ag}(\mathbf{r},t)\phi_g(\mathbf{r},t)=S_g(\mathbf{r},t) \tag{A.6}$$

$$\tau_g^{\kappa}\frac{\partial^{\kappa}\mathbf{J}_g(\mathbf{r},t)}{\partial t^{\kappa}}+\mathbf{J}_g(\mathbf{r},t)=-D_g(\mathbf{r})\nabla\phi_g(\mathbf{r},t) \tag{A.7}$$

$$\phi_g(\mathbf{r},0)=\phi_{g0}(\mathbf{r}) \tag{A.8}$$

$$\mathbf{J}_g(\mathbf{r},0)=\mathbf{J}_{g0}(\mathbf{r}) \tag{A.9}$$

$$\frac{\partial^{\kappa}\mathbf{J}_g(\mathbf{r},t)}{\partial t^{\kappa}}=0. \tag{A.10}$$

In order to comply with the static initial conditions (Diethelm et al., 2005), it is necessary to impose the initial condition given by Eq. (A.10).

Applying again the principle of the static initial condition, the fractional equations for a point reactor and the corresponding initials conditions are given:

$$\tau^{\kappa}\frac{d^{\kappa+1}n(t)}{dt^{\kappa+1}}+\tau^{\kappa}\left[\frac{1}{l}-\frac{(1-\beta)}{\Lambda}\right]\frac{d^{\kappa}n(t)}{dt^{\kappa}}+\frac{dn(t)}{dt}-\frac{\rho-\beta}{\Lambda}n(t)+\lambda C(t)+\tau^{\kappa}\lambda\frac{d^{\kappa}C(t)}{dt^{\kappa}} \tag{A.11}$$

where the initial conditions are

$$n(0)=n_0 \tag{A.12}$$

$$\left.\frac{d^{\kappa+1}n}{dt^{\kappa+1}}\right|_{t=0}=0 \tag{A.13}$$

$$\left.\frac{d^{\kappa}n}{dt^{\kappa}}\right|_{t=0}=0 \tag{A.14}$$

It can be observed that these initial conditions satisfy the static initial condition, provided $\frac{dn(0)}{dt}=0$.

The physical implications are based in the difference between ordinary derivatives and fractional derivatives, i.e., the ordinary derivatives are point functionals, while that of fractional

derivatives are hereditary functional possessing a total memory of past states (Diethelm et al., 2005).

References

Ahoanber, A.E., 2003a. Analytical solution of the point kinetics equations by exponential mode analysis. Progress in Nuclear Energy 42 (2), 179–197.

Ahoanber, A.E., 2003b. An efficient analytical form for the period-reactivity relation of beryllium and heavy-water moderated reactors. Nuclear Engineering and Design 224, 279–292.

Ahoanber, A.E., El Mhlawy, A.M., 2008. A new version of the reflected core inhour equation and its solution. Nuclear Engineering and Design 238, 1670–1680.

Ahoanber, A.E., El Mhlawy, A.M., 2009. Solution of two-point kinetics equations for reflected reactors using analytical inversion method (AIM). Progress in Nuclear Energy 51, 155–162.

Ahoanber, A.E., Hamada, Y.M., 2002. PWS: an efficient code system for solving space-independent nuclear reactor dynamics. Annals of Nuclear Energy 29, 2159–2172.

Ahoanber, A.E., Hamada, Y.M., 2003a. Power Series Solution (PWS) of nuclear reactor dynamics with Newtonian temperature feedback. Annals of Nuclear Energy 30, 1111–1122.

Ahoanber, A.E., Hamada, Y.M., 2003b. Power series solution (PWS) of nuclear reactor dynamics with Newtonian temperature feedback. Annals of Nuclear Energy 30, 1111–1122.

Ahoanber, A.E., Nahla, A.A., 2002a. Solution of the point kinetics equations in the presence of Newtonian temperature feedback by Padé approximations via analytical inversion method. Journal of Physics A – Mathematical and General 35, 9609–9627.

Ahoanber, A.E., Nahla, A.A., 2002b. Generalization of the analytical inversion method for the solution of the point kinetics equations. Journal of Physics A – Mathematical and General 35, 3245–3263.

Ahoanber, A.E., Nahla, A.A., 2004. On Padé approximations to the exponential function and application to the point kinetics equations. Progress in Nuclear Energy 44, 347–368.

Adelr, F.T., 1961. Reactor kinetics: integral equation formulation. Journal of Nuclear Energy, Part A & B 15, 81.

Akcasu, Z., 1958. General solution of the reactor kinetic equations without feedback. Nuclear Science and Engineering 3, 456–467.

Akcasu, Z.A., Karasulu, M., 1976. Non-linear response of point-reactors to stochastic inputs. Annals of Nuclear Energy 3, 11–18.

Allard, J.C., Carter, D.S., 1958. Kinetics of homogeneous power reactors of the IAPRE type. Nuclear Science and Engineering 3, 482–503.

Barletta, A, Zanchini, E., 1994. Hyperbolic heat conduction and local equilibrium: a second law analysis. International Journal of Heat and Mass Transfer 40, 1007–1016.

Barlow, J., Lawins, J., 1996. Power series of the reactor kinetics equations. Nuclear Science and Engineering 122, 407–416.

Baumer, B., Benson, D.A., Meerschaer, M.M., Wheatcraft, S.W., 2000. Subordinated advection-dispersion equation for contaminant transport. Water Resources Research 37, 1543–1550.

Behringer, K., 1991. Generalized treatment of point reactor kinetics driven by random reactivity fluctuations via the Wiener–Hermite functional method. Annals of Nuclear Energy 18, 397–412.

Behringer, K., Pifeyro, J., 1994. Concerning the stability parameter in point reactor kinetics driven by random reactivity noise. Annals of Nuclear Energy 21, 787–791.

Behringer, K., Pifeyro, J., Mennig, J., 1990. Application of the Wiener-Hermite functional method to point reactor kinetics driven by random reactivity fluctuations. Annals of Nuclear Energy 17, 643–656.

Benson, D.A., Wheatcraft, S.W., Meerschaer, M.M., 2000. Application of a fractional advection-dispersion equation. Water Resources Research 36, 1403–1412.

Bienski, T., Cadarnski, A., Mika, J., 1978. Higher order prompt-jump approximation in reactor kinetics. Nuclear Science and Engineering 66, 277–283.

Brown, H.D., 1957. A general treatment of flux transients. Nuclear Science and Engineering 2, 687–693.

Bubnov, V.A., 1976. Wave concepts in theory of heat. International Journal of Heat and Mass Transfer 19, 175–195.

Bustano, M.L., Corno, S.E., Cravero, I., 1995. A new procedure for integrating the point kinetic equations for fission reactors. Computers & Mathematics with Applications 29, 5–19.

Cattaneo, C., 1958. A form of heat conduction equation which eliminates the paradox of instantaneous propagation. Compte Rendus 247, 431–433.

Chao, Y.A., 2006. Reply to comments on a resolution of the stiffness problem of reactor kinetics. Nuclear Science and Engineering 153, 200–202.

Chao, Y.A., Attard, A., 1985. A resolution of the stiffness problem of reactor kinetics. Nuclear Science and Engineering 90, 40–46.

Chen, G.S., 1990. A nonlinear study in a reactor with delayed temperature feedback. Progress in Nuclear Energy 23 (1), 81–91.

Chen, W.Z., Kuang, B., Guo, L.P., Chen, Z.Y., Zhu, B., 2006. New analysis of prompt supercritical process with temperature feedback. Nuclear Engineering and Design 236, 1326–1329.

Chen, W.Z., Guo, L.P., Zhu, B., Li, H., 2007. Accuracy of analytical methods for obtaining supercritical transients with temperature feedback. Progress in Nuclear Energy 49, 290–302.

Chen, W.R., Wang, J., Qiu, W.-Y., Ren, F.Y., 2008. Solutions for time-fractional diffusion equation with absorption: influence of different diffusion coefficients and external forces. Journal of Physics A: Mathematical and Theoretical 41 (045003), 10.

Chernick, J., 1951. The dependence of the reactor kinetics on temperature, BNL-173.

da Nobrega, J.A.W., 1971. A new solution of the point kinetics equations. Nuclear Science and Engineering 46, 369–375.

Dam, V.H., 1996. Dynamics of passive reactor shutdown. Progress in Nuclear Energy 30 (3), 255–264.

Damen, P.M.G., Kloosterman, J.L., 2001. Dynamics aspects of plutonium burning in an inert matrix. Progress in Nuclear Energy 38 (3–4), 371–374.

Devooght, J., Mund, E., 1985. Numerical solution of neutron kinetics equations using A-stable algorithms. Progress in Nuclear Energy 16, 97–126.

Diethelm, K., 1997a. An algorithm for the numerical solution of differential equations of fractional order. Electronic Transactions on Numerical Analysis 5, 1–6.

Diethelm, K., 1997b. Numerical approximation of finite-part integrals with generalized compound quadrature formulae. IMA Journal of Numerical Analysis 17, 479–493.

Diethelm, K., Ford, N.J., Freed, A.D., Luchko, Y., 2005. Algorithms for the fractional calculus: a selection of numerical methods. Computer Methods in Applied Mechanics and Engineering 194, 743–773.

Dubois, C., Grossman, M., 1972. Optimized Taylor series method in point kinetics calculations. Transactions of the American Nuclear Society 15, 288–289.

Duderstadt, J.J., Hamilton, L.J., 1976. Nuclear Reactor Analysis. John Wiley & Sons, USA.

Dulla, S., Ravetto, P., 2008. Numerical aspects in the study of neutron propagation. Annals of Nuclear Energy 35, 656–664.

Dulla, S., Garaopol, B.D., Ravetto, P., 2006a. Space asymptotic method for the study of neutron propagation. Annals of Nuclear Energy 33, 932–940.

Dulla, S., Nicolino, C., Ravetto, P., 2006b. Reactivity oscillation in source driven systems. Nuclear Engineering and Technology 38, 657–664.

Edwards, J.T., Ford, N.J., Simpson, A.C., 2002. The numerical solution of linear multi-term fractional differential equations. Journal of Computational and Applied Mathematics 148, 401–418.

Espinosa-Paredes, G., Álvarez-Ramírez, J., Vázquez, A., 2006. Detecting long-range correlation with detrended fluctuation analysis: Application to BWR stability. Annals of Nuclear Energy 33, 1308–1313.

Espinosa-Paredes, G., Morales-Sandoval, J., Vázquez-Rodríguez, R., Espinosa-Martínez, E.-G., 2008. Constitutive laws for the neutron density current. Annals of Nuclear Energy 35, 1963–1967.

Fröhlich, R., Johnson, S.R., 1969. Exact solution of the non-linear prompt kinetics equations. Nucleonik 12, 93–96.

Fuchs, K., 1946. Efficiency for Very Slow Assembly. LASL LA-596.

Garaopol, B., 2007. A further comment on a resolution of the stiffness problem of reactor kinetics or life all about nothing? (Letter to the Editor). Nuclear Science and Engineering 157, 245–247.

Glasstone, S., Sesonske, A., 1981. Nuclear Reactor Engineering, Third ed. VNR, New York, United States of America.

Glasstone, S., Sesonske, A., 1994. Nuclear Reactor Engineering. Chapman & Hall Inc., pp. 296–299.

Goldstein, R., Shotkin, L.M., 1969. Use of the prompt-jump approximation in fast reactor kinetics. Nuclear Science and Engineering 38, 94–103.

Gupta, H.P., Trasi, M.S., 1986. Asymptotically stable solutions of point-reactor kinetics equations in the presence of Newtonian temperature feedback. Annals of Nuclear Energy 4, 203–207.

Hansen, G.E., 1952. Burst Characteristics Associated with the Slow Assembly of Fissionable Material. LASL LA-1441.

Hansen, K.F., Koen, B.V., Little, W.W., 1965. Stable numerical solutions of the reactor kinetics equations. Nuclear Science and Engineering 22, 51–59.

Hashimoto, K., Ikeda, H., Takeda, T., 2000. Numerical instability of time-discretized one-point kinetic equations. Annals of Nuclear Energy 27, 791–803.

Hayanaka, H., Takeda, S., 1968. Study of neutron wave propagation. Journal of Nuclear Science and Technology 5, 564–571.

Hayes, J.G., Allen, E.J., 2005. Stochastic point-kinetics equations in nuclear reactor dynamics. Annals of Nuclear Energy 32, 572–587.

Heitzler, S.J., 2010. Asymptotic telegrapher's equation (P1) approximation for the transport equation. Nuclear Science and Engineering 166, 17–35.

Hendry, W.L., Bell, G.I., 1969. An analysis of the time-dependent neutron transport equation with delayed neutrons by the method of matched asymptotic expansions. Nuclear Science and Engineering 35, 240–248.

Hennart, J.P., 1977. Piecewise polynomial approximations for nuclear reactor point and space kinetics. Nuclear Science and Engineering 64, 875–901.

Hetrick, D.L., 1971. Dynamics of Nuclear Reactors. The University of Chicago Press.

Hetrick, D.L., 1993. Dynamics of Nuclear Reactors. American Nuclear Society, La Grange Park, IL.

Hilfer, R., 2000. Applications of Fractional Calculus in Physics. World Scientific, Singapore.

Hurwitz Jr., H., MacMillan, D.B., Smith, J.H., Storm, M.L., 1963a. Kinetics of low source reactor startups. Part I. Nuclear Science and Engineering 15, 156–186.

Hurwitz Jr., H., MacMillan, D.B., Smith, J.H., Storm, M.L., 1963b. Kinetics of low source reactor startups. Part II. Nuclear Science and Engineering 15, 187–196.

Isbin, H.S., 1963. Introductory Nuclear Reactor Theory. Van Nostrand Reinhold Company, New York.

Iwanuga, K., Sekimoto, H., 2005. Study on kinetics of subcritical system contribution of delayed neutrons to the transient after a reactivity insertion. Annals of Nuclear Energy 32, 1953–1962.

Kadaller, Chill., 1976. On propagation speed of heat in materials without memory. International Journal of Engineering Science 14, 1161–1164.

Kaminski, W., 1990. Hyperbolic heat conduction for materials with a nonhomogeneous inner structure. ASME Journal of Heat Transfer 112, 555–560.

Kang, C.M., Hansen, K.F., 1973. Finite element methods for reactor analysis. Nuclear Science and Engineering 51, 456–495.

Keepin, G.R., Cox, C.W., 1960. General solution of the reactor kinetic equations. Nuclear Science and Engineering 8, 670–690.

Kilbas, A.A., Srivastava, H.M., Trujillo, J.J., 2006. Theory and Applications of Fractional Differential Equations. Begell House, Connecticut.

Kinard, M., Allen, K.E.J., 2004. Efficient numerical solution of the point kinetics equations in nuclear reactor dynamics. Annals of Nuclear Energy 31, 1039–1051.

Kodat, J., Sinaoui, M.T., Hébert, A., 1996. Solution of the improved and generalized quasistatic methods using an analytic calculation or a semi-implicit scheme to compute the precursor equations. Annals of Nuclear Energy 23 (14), 1127–1142.

Kohler, W.H., 1969. Reactivity feedback with short delayed times. Journal of Nuclear Energy 23, 569–574.

Lamarsh, J.R., Baratta, A.J., 2001. Introduction to Nuclear Engineering, third ed. Prentice-Hall Inc, New Jersey.

Lenzy, E.K., Mendes, R.S., Andrade, J.S., da Silva, L.R., Lucena, L., 2005. N-dimensional fractional diffusion equation and Green function approach: spatially dependent diffusion coefficient and external force. Physical Review E 71 (052101), 4.

Leszczynski, J., Ciesielski, M., 2001. A Numerical Method for Solution of Ordinary Differential Equations of fractional Order, LNCS, vol. 2328. Springer Verlag.

Lewins, J.D., 1995. Reactivity oscillations and stability with delayed neutrons. Annals of Nuclear Energy 22, 411–414.

Lewins, J.D., 2006. Reply to comments on a resolution of the stiffness problem of reactor kinetics. Nuclear Science and Engineering 153, 200–202.

Li, H., Chen, W., Zhang, F., Luo, Z., 2007. Approximate solutions of point kinetics equations with one delayed neutron group and temperature feedback during delayed supercritical process. Annals of Nuclear Energy 34, 521–526.

Li, H., Chen, W., Luo, L., Zhu, Q., 2009. A new integral method for solving the point reactor neutron kinetics equations. Annals of Nuclear Energy 36, 427–432.

Lulkov, A.V., 1966. Application of irreversible thermodynamics methods to investigation of heat and mass transfer. International Journal of Heat and Mass Transfer 9, 138–152.

MacMillan, D.B., 1972. Dynamics of Nuclear Systems. In: Herrick, D.L. (Ed.). University of Arizona Press.

MacMillan, D.B., Storm, M.L., 1963. Kinetics of low source reactor startups. Part III. Nuclear Science and Engineering 16, 369–380.

Magin, R.L., 2006. Fractional Calculus in Bioengineering. Begell House, Connecticut.

Mainardi, F., Pagnini, G., 2003. The Weight functions as solutions of the time-fractional diffusion equation. Applied Mathematics and Computation 141, 51–62.

Mennig, J., Auerbach, T., 1987. The application of Lie series to reactor theory. Nuclear Science and Engineering 28, 159–165.

Metzler, R., Klafter, J., 2000. Boundary value problems for fractional diffusion equations. Physica A: Statistical Mechanics and its Applications 278, 107–125.

Miller, K.S., Ross, B., 1993. An Introduction to the Fractional Integrals and Derivatives: Theory and Applications. Wiley, New York.

Mitchell, B., 1977. Taylor series methods for the solution of the point reactor kinetics equations. Annals of Nuclear Energy 4, 169–176.

Murray, R.L., 1957. Nuclear Reactor Physics. Prentice-Hall, Englewood Cliffs, New Jersey.

Murray, R.L., 1994. Reactor kinetics pedagogical insight. Nuclear Science Engineering 118, 268–271.

Nahla, A.A., 2008. Generalization of the analytical model to solve the point kinetics equations of Be- and D$_2$O-moderated reactors. Nuclear Engineering and Design 238, 2648–2653.

Nahla, A.A., 2009. An analytical solution for the point reactor kinetics equations with one group of delayed neutrons and the adiabatic feedback model. Progress in Nuclear Energy 51, 124–128.

Nahla, A.A., 2010. Analytical solution to solve the point reactor kinetics equations. Nuclear Engineering and Design 240, 1622–1629.

Nec, Y., Nepomnyashchy, A.A., 2007. Turing instability in sub-diffusive reaction-diffusion system. Journal of Physics A: Mathematical and Theoretical 40, 14687–14702.

Oldham, K.B., Spanier, J., 1974. The Fractional Calculus. Academic Press.

Orr, K.O., Meneley, D.A., 1969. Accuracy of the quasistatic treatment of spatial reactor kinetics. Nuclear Science and Engineering 36, 402–411.

Ozisik, M.N., Tzou, D.Y., 1994. On the wave theory in heat conduction. ASME Journal of Heat Transfer 116, 526–535.

Palma, D.A.P., Martinez, A.S., Gonçalves, A.C., 2009. Analytical solution of point kinetics equations for linear reactivity variation during the start-up of a nuclear reactor. Annals of Nuclear Energy 36, 1469–1471.

Peinetti, F., Nicolino, C., Ravetto, P., 2005. Kinetics of a point reactor in the presence of reactivity oscillations. Annals of Nuclear Energy 33, 1189–1195.

Podlubny, I., 1999. Fractional Differential Equations. Academic, New York.

Poreching, T.A., 1966. Numerical solution of the reactor kinetics by approximate exponentials. Nuclear Science and Engineering 25, 188–193.

Quabili, E.R., Karanaila, M., 1979. Methods for solving the stochastic point reactor kinetic equations. Annals of Nuclear Energy 6, 133.

Quintero-Leyva, B., 2008. CORE: a numerical algorithm to solve the point kinetics equations. Annals of Nuclear Energy 35, 2136–2138.

Quintero-Leyva, B., 2009. On the numerical solution of the integro-differential equation of the point kinetics of nuclear reactors. Annals of Nuclear Energy 36, 1280–1284.

Ravetto, P., 1997. Reactivity oscillations in a point reactor. Annals of Nuclear Energy 24, 303–314.

Reyes-Ramírez, R., Martín-del-Campo, C., François, J.L., Brun, E., Diamontid, E., Malvagi, F., 2010. Comparison of MCNPX-CSG and TRIPOLI-4-D the fuel depletion calculations of a gas-cooled fast reactor. Annals of Nuclear Energy 37, 1101–1106.

Rosenbrock, H.H., 1963. Some general implicit processes for the numerical solution of differential equations. The Computer Journal 5, 329–330.

Ruby, L., 1991. A problem in the teaching of reactor kinetics. Nuclear Science and Engineering 107, 394–396.

Russel, V.K., Duncan, D.L., 1982. Analytical model for non-adiabatic reactor excursion. Transactions of the American Nuclear Society 43, 714–715.

Sadler, S.J., Dhaler, J.S., 1964. Nonstationary diffusion. Physics of Fluids 2, 1743–1746.

Saito, K., 1979. An application of Novikov–Furutsu formula to solving stochastic point reactor kinetics having a Gaussian parametric noise with an arbitrary spectral profile. Annals of Nuclear Energy 6, 591–593.

Samko, S.G., Kilbar, A.A, Marichev, O.I., 1993. Fractional Integrals and Derivatives: Theory and Applications. Gordon and Breach, Linghorne, PA.

Sánchez, J., 1989. On the numerical solution of the point reactor kinetics equations by generalized Runge-Kutta methods. Nuclear Science and Engineering 103, 94–99.

Sathiyasheela, T., 2009. Power series solution method for solving point kinetics equations with lumped model temperature and feedback. Annals of Nuclear Energy 36, 246–250.

Schneider, W.R., Wyss, W., 1989. Fractional diffusion and wave equations. Journal of Mathematical Physics 30, 134–144.

Sieniutycz, S., 1979. The wave equation for simultaneous heat and mass transfer in moving media-structure testing, time–space transformations and variational approach. International Journal of Heat and Mass Transfer 22, 585–599.

Stacey, W.M., 2004. Nuclear Reactor Physics. Wiley-VCH.

Tashakor, S., Jahanfarnia, G., Hashemi-Tilehnoee, M., 2010. Numerical solution of the point reactor kinetics equations with fuel burn-up and temperature feedback. Annals of Nuclear Energy 37, 265–269.

Theler, G.C., Bonetto, F.J., 2010. On the stability of the point reactor kinetics equations. Nuclear Engineering and Design 240, 1443–1449.

Todreas, N.E., Kazimi, M.S., 1990a. Nuclear System. II: Elements of Thermal Hydraulic Design. Hemisphere Publishing Corporation, USA.

Todreas, N.E., Kazimi, M.S., 1990b. Nuclear System. I: Thermal Fundamentals. Hemisphere Publishing Corporation, USA.

Toppel, B.J., 1959. Sources of error in reactivity determinations by means of asymptotic period measurements. Nuclear Science and Engineering 5, 88–98.

Van Den Eynde, G., 2006. Comments on a resolution of the stiffness problem reactor kinetics. Nuclear Science and Engineering 153, 200–202.

Vernotte, P., 1958. Les paradoxes de la théorie continue de l'équation de la chaleur. Compte Rendus 246, 3154–3155.

Vigil, J.C., 1967. Solution of the reactor kinetics equations by analytic continuation. Nuclear Science and Engineering 29, 392–401.

Yeh, K., 1978. Polynomial approach to reactor kinetic equations. Nuclear Science and Engineering 66, 235–242.

Zhang, F., Chen, W.Z., Cui, X.W., 2008. Analytic method study of point-reactor kinetic equation when cold start-up. Annals of Nuclear Energy 35, 746–749.

Referencias

Aboanber, A.E., Analytical solution of the point kinetics equations by exponential mode analysis, Progress in Nuclear Energy 42 (2), 179–197 (2003).

Anderson, P.L., Meerschaert, M.M., Modeling river flows with heavy tails, Water Resources Res. 34, 2271-2280 (1998).

Badar, A.M., Zubair, M.S., Sheiki, A., Uncertainty analysis of heat-exchanger thermal design using the Monte Carlo simulation technique, Energy 18, 859-866 (1993).

Bartumeus, F., da Luz, M., Viswanathan, G., Catalan, J., Animal search strategies: a quantitative random-walk analysis. Ecology 86: 3078-3087 (2005).

Bell, G.I., Gladstone, S., Nuclear Reactor Theory, Van Nostrand-Reinhold (1971).

Bell, G.I., Hansen, G.E., Sandmeier, H.A., "Multitable Treatments of Anisotropic Scattering in SN Multigroup Transport Calculations," Nucl. Sci. Eng., 28, 376 (1967).

ben-Avraham D., Havlin, S., Diffusion and Reactions in Fractals and Disordered Systems (Cambridge University Press, 2000).

Bevington, P.R., Robinson, D.K., 2003. Data Reduction and Error Analysis for the Physical Sciences. McGraw-Hill, Boston.

Bouchaud, J-P, Georges, A., Anomalous diffusion in disordered media. Statistical mechanisms, models and physical applications. Phys. Rep. 195, 127-293 (1990).

Brockmann, D., Hufnagel, L., Geisel, T., The scaling laws of human travel, Nature 439, 462-65 (2006).

Brown, R., London and Edinburgh philosophical magazine and journal of science 4, 161 (1828).

Cai, X., Liu, F., Numerical simulation of the fractional-order control system, J. Appl. Math. & Computing 23, 229-241 (2007).

Caputo, M., Linear models of dissipation whose Q is almost frequency independent II, Geophys. J. Royal Astron. Soc. 13, p. 529-539 (1976).

Cattaneo, Sulla conduzione del calore, Atti Sem. Mat. Fis. Univ. Modena 3, 83-101 (1948).

Chao, Y.A., Reply to comments on a resolution of the stiffness problem of reactor kinetics, Nuclear Science and Engineering 153, 200–202 (2006).

Chen, W.Z., Kuang, B., Guo, L.F., Chen, Z.Y., Zhu, B., 2006. New analysis of prompt supercritical process with temperature feedback. Nuclear Engineering and Design 236, 1326–1329.

Casas-Vázquez, D. Jou, Lebon, Extended Irreversible Thermodynamics (Berlin: Springer) 1996.

Case, K. M., De Hoffmann, F., Placzek, G., Carlson, B., and Goldstein, M. (1953), Introduction to the Theory of Neutron Diffusion-Volume I, Los Alamos Scientific Laboratory.

Chen, X.Y., Divergence phenomena of critical extrapolation curve of control rods rising during physical start-up of PWR: the cause and mechanism, Nuclear Power Engineering 18 (6), 496–499 (1997) (in Chinese).

Compte, A., Metzler, R., The generalized Cattaneo equation for the description of anomalous transport process, Journal of Physics A: Mathematical and General 30, 7277-7289 (1997).

Crank, J., The Mathematics of Diffusion, Clarendon Press, Oxford, 1970.

Datta, S., Electronic transport in mesoscopic systems (Cambridge University Press, 1995).
Davis, A., Marshak, A., Lévy kinetic in slab geometric: scaling of transmission probability, in Fractal Frontiers, edited by M. M. Novak and T. G. Dewey (World Scientific, 1997).

Davison, B., Sykes, J.B., Neutron Transport Theory, Oxford University Press (1958).

Diethelm, K., Ford, N.J., Analysis of fractional differential equation", J. Math. Anal. Appl., 265, p. 229-248 (2002a).

Diethelm, K., Ford, N.J., Numerical solution of the Bagley-Trovik equation", BIT, 42, p. 490-507 (2002b).

Diethelm, K., Ford, N.J., The numerical solution of linear and non-linear fractional differential equation involving fractional derivatives of several orders", Numerical Analysis Report, Manchester Centre for Computational Mathematics, 379 (2001).

Duderstadt, J. J., Hamilton, L. J., 1976, Nuclear reactor analysis, John Wiley and Sons, USA.

Edwards, J.T., Ford, N.J., Simpson, A.C., The numerical solution of linear multiterm fractional differential equations, Journal of Computational and Applied Mathematics 148, 401–418 (2002).

Einstein, A., English translation; Investigations on the Theory of Brownian Movement, Ann. Phys. (Leipzig) 17, 549 (1905). (Dover, New York, 1956).

Álvarez-Ramírez, J., Espinosa-Paredes, G., Vázquez, A., Detrended fluctuation analysis of the neutronic power from a nuclear reactor, Physica A 351, 227-240 (2005).

Espinosa-Paredes, G., Morales-Sandoval, J.B., Vázquez-Rodríguez, R., Espinosa-Martínez, E-G., Constitutive laws for the neutron density current, Annals of Nuclear Energy 35, p. 1963-1967 (2008).

Espinosa-Paredes, G., Polo-Labarrios, M.-A., Espinosa-Martínez, E.-G., Del Valle-Gallegos, E., Fractional neutron point kinetics equations for nuclear reactor dynamics, Annals of Nuclear Energy31, 1039-1051 (2011).

Espinosa-Paredes, G., Polo-Labarrios, M.-A., Time-fractional telegrapher equation (P1) approximation for the transport equation, Nuclear Science and Engineering 171 (2012a). En prensa.

Espinosa-Paredes, G., Polo-Labarrios, M.-A., Numerical Analysis of Start-up PWR with Fractional Neutron Point Kinetic Equation, Progress in Nuclear Energy (2012b). Articulo sometido.

Espinosa-Paredes, G., Polo-Labarrios, M.-A., Application of the fractional neutron point kinetic equation: Start-up, Annals of Nuclear Energy 46, 37-42 (2012c).

Espinosa-Paredes, G., Polo-Labarrios, M.-A., Díaz-González, L., Vázquez-Rodríguez, A., Espinosa-Martínez, E.-G., Sensitivity and uncertainty analysis of the fractional neutron point kinetics equations, Annals of Nuclear Energy 42, 169-174 (2012a).

Espinosa-Paredes, G., Polo-Labarrios, Vázquez-Rodríguez, A., Sensitivity and uncertainty analysis of the time fractional telegrapher's equation for neutron motion, Progress in Nuclear Energy (2012b), Articulo sometido.

Espinosa-Paredes, G., Verma, S.P, Vázquez-Rodrígueza, A., Nuñez-Carrera, Mass flow rate sensitivity and uncertainty analysis in natural circulation boiling water reactor core from Monte Carlo simulations Nuclear, Engineering and Design 240, 1050–1062 (2010).

Fellah, M., Fellah, Z., Depollier, C., Generalized hyperbolic fractional equation for transient-wave propagation in layered rigid-frame porous materials, Physical Review E - Statistical, Nonlinear and Soft Matter Physics 77, (2008).

García-Colín, L., Goldstein, P., La física de los procesos irreversibles, Tomo 2, El Colegio Nacional, México (2003).

Glasstone, S., Sesonske, A., 1968, Nuclear Reactor Engineering, Reverté, Madrid, España.

Godoy, S., García-Colín S., L., From the quantum random walk to classical mesoscopic diffusion in crystalline solids, Physical Review E53, 5779-5785 (1996).

Gorenfo, R., Mainardi, F., Fractional calculus: integral and diferential equations of fractional order, in: A. Carpinteri, F. Mainardi (Eds), Fractals and fractional calculus in continnum mechanics, Springer, pp. 223-276, Berlin (1997).

Gorenflo, R., Mainardi, F., Moretti, D., Time fractional diffusion: a discrete random walk approach, Journal of Nonlinear Dynamics 29, 129-143 (2000).

Guanhua, H., Quanzhong, H., Hongbin, Z., Jing, C., Yunwu, X., Shaoyuan, F., Modeling contaminant transport in homogeneous porous media with fractional advection-dispersion equation, Science in China Ser. D Earth Sciences 48, 295-302 (2005).

Grmela, M., Teichmann, J., Lagrangian formulation of the Maxwell-Cattaneo hydrodynamics, International Journal of Engineering Science 21, 297-313 (1983).

Havlin, S., Ben-Avraham, Diffusion in disordered media, Advances in Physics D 36,187-292 (1987).

Heizler, S.I., Asymptotic Telegrapher's Equation (P1) Approximation for the Transport Equation, Nuclear Science and Engineering 166, 17–35 (2010).

Hetrick, D.L., 1993. Dynamics of Nuclear Reactor. American Nuclear Society, Jbc., Illinois, USA, ISBN 0-89448-453-2, pp. 164–167.

Hilfer, R., 2000. Applications of Fractional Calculus in Physics. World Scientific, Singapore.

Joseph D.-D., Preziosi L., Heat waves, Reviews of Modern Physics 61, 41-73 (1989).

Kaminski, W., Hyperbolic heat conduction equation for materials with a nonhomogenous inner structure, Journal of Heat Transfer-Transactions of the ASME 112(3), 555-560 (1990).

Katarzyna D. Lewandowska, Hyperbolic subdiffusion in a membrane system, ActaPhysical Polonica B 40, 1991-1500 (2009).

Kinard, M., Allen, E.J., Efficient numerical solution of the point kinetics equations in nuclear reactor dynamics, Annals of Nuclear Energy 31, 1039-1051 (2004).

Lamarsh, J.R., Baratta, A.J., 2001. Introduction to Nuclear Engineering, third ed. Prentice-Hall Inc, New Jersey.

Law, A.M., Kelton, W.D., 2000, Simulation Modeling and Analysis: Boston, McGraw Hill, Third edition.

Leszczynski, J., Ciesielski, M., 2001. A Numerical Method for Solution of Ordinary Differential Equations of Fractional Order, LNCS, vol. 2328. Springer Verlag.

Li, H., Chen, W., Zhang, F., Luo, Z., Approximate solutions of point kinetics equations with one delayed neutron group and temperature feedback during delayed supercritical process, Annals of Nuclear Energy 34, 521–526 (2007).

Li, H., Chen, W., Zhang, F., Chen, Z., A new formula of neutron multiplication during startup of PWR, Progress in Nuclear Energy 52, 321-326 (2010).

Lewis, E.E., Miller, W.F., Computational Methods of Neutron Transport, American Nuclear Society, La Grange Park, Illinois (1993).

Marsaglia, G., 1968, Random numbers fall mainly in the planes: National Academy of Science Proceedings, 61(1), 25–28.

Marsaglia, G., Bray, T.A., 1964, A convenient method for generating normal variables: Society for Industrial and Applied Mathematics, SIAM Review, 6(3), 260–264.

McTaggart, C.L., Lindsay, K.A., Nonclassical effects in the B6nard problem, SIAM Journal on Applied Mathematics 45, 70-92 (1985).

Meerschaert, M.M., and Tadjeran, C., Finite difference approximations for fractional advection–dispersion flow equations, J. Comput. Appl. Math. 172, 65–77 (2003).

Miller, K.S., Ross, B., 1993. An Introduction to the Fractional Integrals and Derivatives: Theory and Applications. Wiley, New York.

Nonnenmacher, T.F., On the derivation of second order hydrodynamic equation, Journal of Non-Equilibrium Thermodynamics 5, 361-378 (1980).

Nonnenmacher, T.F., Derivation of Exact Non-Linear Constitutive Equations: A Simple Model for a Non-Linear Diffusion Theory, Journal of Non-Equilibrium Thermodynamics 9, 171-176 (1984).

Oldham, K.B., Spanier, J., 1974. The Fractional Calculus. Academic Press.

Palma, D.A.P., Martinez, A.S., Gonçalves, A.C. 2009. Analytical solution of point kinetics equations for linear reactivity variation during the start-up of a nuclear reactor. Annals of Nuclear Energy 36, 1469-1471.

Pearson, K., A mathematical theory of random migration (Dulau and co., London, 1906).

Podlubny, I., 1999. Fractional Differential Equations. Academic, New York.

Pomraning, G.C., The Equations of Radiation Hydrodynamics, Pergamon Press (1973).

Rochman, D., Koning, A.J., van der Marck, S.C., Hogenbirk, A., Sciolla, C.M., Nuclear data uncertainty propagation: Perturbation vs. Monte Carlo, Annals of Nuclear Energy 38, 942-952 (2011).

Ruggeri, T., Muracchini, A., Seccia, L., Shock waves and second sound in a rigid heat conductor: A critical temperature for NaF and Bi, Physical Review Letters 64, 2640-2643 (1990).

Samko, S.G., Kilbas, A.A., Marichev, O.I., 1993. Fractional Integrals and Derivatives: Theory and Applications. Gordon and Breach, Linghorne, PA.

Scher, H., Montroll, E.W., Anomalous transit-time dispersion in amorphous solids, Phys. Rev. B12, 2455-2477 (1975).

Scher, H., Margolin, G., Metzler, R., Klafter, J., Berkowitz, B., The dynamical foundation of fractal stream chemistry: The origin of extremely long retention times, Geophysical Research Letters 29, 1061 (2002).

Stacey, W.M., 2001. Nuclear Reactor Physics. John Wiley and Sons, INC, New York, United States of America.

Straughan, B., Franchi, F., Bénard convection and the Cattaneo law of heat conduction, Proceedings of the Royal Society A 96, 175–178 (1984).

Ter Verkrijging Van., Anomalous Diffusion of Dirac fermions, Casimir PhD Series, Delft-Leiden 30, (2080).

Valdés-Parada, F.J., Ochoa-Tapia, J.A., Alvarez-Ramirez, J., Effective medium equation for fractional Cattaneo´s diffusion and heterogeneous reaction in disordered porous media, Physics A 369, 318-328 (2006).

Vázquez-Rodríguez, R., Espinosa-Paredes, G., Morales-Sandoval, J., Vázquez-Rodríguez, A., Espinosa-Martínez, E.-G., Averaging the neutron diffusion equation. Progress in Nuclear Energy, vol. 51, 474-484 (2009).

Velasco, R.M., Garcia Colin S., L., Kinetic approach to generalized hydrodynamics, Physical Review A 44, 4961 (1991).

Verma, S.P., 2005. Estadística básica para el manejo de datos experimentales: Aplicación en la geoquímica (geoquimiometría). Universidad Nacional Autónoma de México, México, D.F..

Weeks, E.R., Urbach, J.S., Swinney, H. L., Physica D 97, 291 (1996).

Wu, J., Berland, K.M., Propagators and time-dependent diffusion coefficients for anomalous diffusion, Biophysical journal 95-(4), 2049-52 (2008).

Yang, Qianqian, Turner, Ian, Liu, Fawang. "Analytical and numerical solutions for the time and space-symmetric fractional diffusion equation". In: ANZIAM Journal: Proceedings of the 4th Biennial Computational Techniques and Applications Conference (CTAC2008), Australian National University, Canberra, 13- 16 July (2008).

Zakari, M., Jou, D., Equations of State and Transport-equations In Viscous Cosmological Models, Physical Review D. 48, 1597–1601 1993).

Zhang, D.L., Qiu S.Z., Su G.H., Liu C.L., Qian L.B., Analysis on the neutron kinetics for a molten salt reactor, Progress in Nuclear Energy 51, 624–636 (2009).

Zhang, F., Chen, W.Z., Gui, X.W., Analytic method study of point-reactor kinetic equation when cold start-up, Annals of Nuclear Energy 35, 746-749 (2008).